Univerzita Karlova v Praze

Přírodovědecká fakulta

Studijní program: Geografie

Studijní obor: Kartografie, geoinformatika a dálkový průzkum Země

Mgr. Veronika Kopačková

Environmentální aplikace obrazové spektroskopie

Hyperspectral Remote Sensing for Environmental Mapping and Monitoring

Disertační práce

Vedoucí závěrečné práce/Školitel: Doc. Jan Kolář

Praha, 2013

Prohlášení:

Prohlašuji, že jsem závěrečnou práci zpracoval/a samostatně a že jsem uvedl/a všechny použité informační zdroje a literaturu. Tato práce ani její podstatná část nebyla předložena k získání jiného nebo stejného akademického titulu.

V Praze, 18. 6. 2013

In memory of my mother and father
Jiřina kopačková and Josef Kopačka

Abstract

Although the principles of spectroscopy are well known and methods for analysis have been widely developed, particularly for spectra collected in laboratory environments, the heterogeneity of landscapes and earth surface features in extensive environmental studies still presents new challenges and opportunities for analysis of hyperspectral (HS) imagery. Image spectroscopy is potentially the best approach for assessing diverse environmental issues, however very little research has been performed on a regional scale and on long-term monitoring, mainly because of the rather high costs related to HS data acquisition and the expert knowledge which is still required for HS data pre-processing and processing. The main purpose of this thesis is to use Image Spectroscopy as a tool to monitor the environmental conditions in a region affected by anthropogenic activities via estimating both geochemical and biochemical parameters on a regional scale. The research has been carried on the Sokolov lignite mine, NW Bohemia, a region affected by long-term extensive mining.

The thesis is divided into two thematic parts. First part is devoted to applications of Image Spectroscopy into Acid Mine Drainage mapping and its related issues (chapters 2 and 3). Initially, high-altitude spectroradiometry (ASTER - Advanced Spaceborne Thermal Emission and Reflection Radiometer satellite data) together with ground-based spectroradiometry are employed in order to identify the locations of the most significant sources of Acid Mine Drainage (AMD) discharge at the Sokolov lignite open-pit mines. The equivalent mineral end-members are successfully derived from the ASTER image data and a sub-pixel method (Linear Spectral Unmixing, LSU) is employed to relatively estimate the selected end-member abundances and to identify low-pH zones (*chapter 2*).

Next, a geochemical conceptual model of the site is defined. It is found that pH <3.0 characterize material with the presence of pyrite, jarosite or lignite. Jarosite in association with goethite indicate increased pH (3.0-6.5) and goethite alone indicate nearly neutral or higher pH (>6.5). The spectral properties of these minerals or their mineral associations are further analyzed. These minerals have absorption feature parameters which are common for both forms, individual minerals as well as parts of the mixtures, while the shift to longer wavelengths of the absorption maximum centered between 0.9-1.0 µm is one of the main parameters that allows differentiation among the secondary minerals. The multi Range Spectral Feature Fitting (MRSFF) technique is employed to map the defined mineral end-members indicating certain pH ranges in the HS image datasets (HyMap data acquired 07/2009). This technique is found to be sensitive enough to assess the desired spectral parameters (e.g., absorption maximum wavelength position, symmetry, absorption depth). Furthermore, the multiple regression model using the fit images, the results of MRSFF, as inputs is constructed to estimate the surface pH and high accuracy is attained (R^2: 0.61, Rv^2: 0.76). This is one of the very first approaches employing image spectroscopy for quantitative pH modeling in a mining environment and the achieved results demonstrate the potential application of hyperspectral remote sensing as an efficient method for environmental monitoring (*chapter 3*).

In the second thematic part (chapters 4-6) Image Spectroscopy is applied into monitoring of vegetation stress. The studied forest stands surround the lignite open pit mines in Sokolov, but have not been directly affected by the mining activities. The model based on the derivative indices (D_{718}/D_{708}) attaining the greatest accuracy (RMSE: 0.21 mg/g, Rv^2: 0.94) is selected to produce a map of foliar chlorophyll concentrations (Cab). The Cab values retrieved from the image reflectance (HyMap data acquired 07/2009) are tested together with other non-quantitative vegetation indicators to create a statistical method allowing assessment of the condition of Norway spruce. As a result, the following HyMap derived parameters (Cab, REP: Red Edge Position, SIPI: Structure Insensitive Pigment Index, PRI: Photosynthetic Reflectance Index) are integrated together to assess the subtle changes in physiological status of the macroscopically undamaged foliage of Norway spruce (*chapter 4*).

In the following study the same method described above is employed and validated while using additional temporal HS image data set (08/2010). The classification results are validated by ground truth data (total chlorophyll - Cab, carotenoids - Car and carotenoid to chlorophyll ratio - Car/Cab) and are associated with the geochemical conditions of the forest stands. Both biochemical analysis of the sampled foliage and classification of 2009 and 2010 hyperspectral images identified the same sites affected by vegetation stress. In addition to higher Car/Cab, which enabled detection of the stressed trees using hyperspectral image data, these sites showed critically low pH and lower values for the macronutrient parameters in both organic horizons and, in addition, both sites exhibit critically low base cation to aluminum ratios (Bc/Al) for lower organic and top mineral (0-20 cm) soil horizons. The results of this study demonstrate the added value of multi-temporal approaches for hyperspectral data and its further potential for monitoring forest ecosystems (*chapter 5*).

Lastly, the potential of diverse foliar biochemical parameters used as stress indicators is assessed to suggest the most sensitive once having the biggest potential for future HS Remote Sensing forest monitoring. The relationship between soil and spruce needle contents of macronutrients and potentially toxic elements and tested whether the soil parameters and their vertical distribution within a soil profile (two organic and two mineral horizons) affect foliage biochemical parameters (contents of photosynthetic pigments, phenolic compounds and lignin). Factor analysis is used to identify underlying variables that explain the pattern of correlations within and between the biochemical and geochemical datasets. The correlations between two toxic element contents in needles (aluminum (Al) and arsenic (As)) and the contents of soluble phenolic compounds and total carotenoid to chlorophyll (Car/Cab) ratio suggest that these latter two biochemical parameters, which both proved to be sensitive to the soil geochemical conditions, can serve as suitable non-specific stress markers, thus should be further considered for vegetation stress monitoring while employing the methods of Image Spectroscopy (*chapter 6*).

Key words: *Image spectroscopy; multi-date hyperspectral data; mining impacts; Acid Mine Drainage (AMD); pH modeling; vegetation stress; non-specific stress markers; heavy metal stress*

Abstrakt

Přestože je obrazová spektroskopie (také nazývané jako hyperspektrální dálkový průzkum Země) metodou používanou po několik dekád a její principy jsou známy a aplikovány, heterogenita a vysoká komplexnost přírodního prostředí stále brání její přímé a rychlé aplikaci do oblasti monitoringu životního prostředí. Tento specifický druh distančních dat nabízí široký potenciál pro celou řadu environmentálních aplikací, avšak pouze omezený počet studií využívá metody obrazové spektroskopie pro analýzu plošně rozsáhlejších oblastí (regionů), či pro studium dynamiky prostředí s využitím časové řady hyperspektrálních dat. Toto lze přičíst poměrně vysokým finančním nákladům, které je nutno vynaložit na pořízení těchto dat (většinou pořizována letecky). Dalším faktorem jsou pak vysoké nároky kladené na znalosti a zkušenosti experta, který tato data zpracovává a analyzuje. Proto i v současné době chybí obecně uchopitelné metody pro rychlé a spolehlivé získávání informací na podkladě hyperspektálních dat pokrývajících rozsáhlejší území/regiony, či analyzující dynamické změny v rámci definovaného časového období. Předložená disertační práce se věnuje aplikaci metod obrazové spektroskopie jako moderního nástroje pro environmentální monitoring, přičemž se zaměřuje na modelování vybraných geochemických a biochemických parametrů. Metody jsou testovány na území Sokolovské hnědouhelná pánve a jejím blízkém okolí, regionu zasaženém dlouhodobou povrchovou těžbou hnědého uhlí. Disertační práce je členěna do dvou tematických celků. První z nich (kapitoly 2 a 3) je věnován aplikaci minerální a obrazové spektroskopie pro vymezení plošného výskytu povrchové acidifikace (anglický termín: AMD – Acid Mine Drainage) a modelování povrchového pH. Druhá tematická část (kapitoly 4, 5 a 6) se věnuje zhodnocení fyziologického stavu smrkových porostů.

V kapitole 2 jsou s využitím satelitních dat ASTER (Advanced Spaceborne Thermal Emission and Reflection Radiometer satellite data) pomocí metody LSU (Linear Spectral Unmixing; algoritmus zohledňující vícesložkový/směsný obsah pixelu v lineárním poměru) plošně vymezeny kyselé zvětralinové povrchy (pH<4), jež charakterizuje výskyt jarositu a lignitu (hnědé uhlí). Tento druh aplikace ukazuje, že i satelitní data, která jsou v porovnání s leteckými hyperspektrálními daty velmi levná a rychle dostupná, mohou přinést dobré výsledky pro detekci kyselých povrchů.

Kapitola 3 se věnuje vytvoření modelu pro odhad povrchového pH odkrytých substrátů s využitím leteckých hyperspektrálních dat HyMap (07/2009). Nejdříve je nadefinován konceptuální model řešící vztah mezi pH a výskytem tzv. indikativních minerálů, které jsou stabilní v určitém rozsahu pH a mohou být proto využity jako jeho indikátory. Bylo zjištěno, že velmi kyselé prostředí (pH <3) charakterizuje výskyt jarositu a lignitu. V případě, že se jarosit vyskytuje v asociaci s goethitem, pH substrátu se pohybuje v rozsahu 3-6.5. Přítomnost samotného goethitu pak indikuje prostředí blízké neutrálnímu až mírně zásaditému (6.5<pH<8.0). U těchto indikativních minerálů jsou analyzovány jejich optické vlastnosti a nalezeny takové parametry absorpčních příznaků, jež jsou společné jak pro „čisté“ minerály, tak i pro jejich směsi. Je zjištěno, že posun absorpčního maxima v rozmezí 0.9-1.0 µm směrem do delších vlnových délek umožňuje vzájemně rozlišit zkoumané sekundární Fe^{3+} minerály (jarosit a goethit). Tohoto trendu je dále využito i pro jejich prostorové mapování a relativní kvantifikaci. S využitím metody „Multi Range Spectral Feature Fitting” (MRSFF), jež pomocí výpočtu nejmenších čtverců určuje míru podobnosti sledovaných absorpčních příznaků mezi typologickým spektrem (anglický termín: end-member) a obrazovým spektrem, byly identifikovány nadefinované indikativní minerály, které se v prostředí hnědouhelné pánve vyskytují převážně ve formě minerálních směsí. Dále byl pomocí vícenásobné regrese sestrojen validní model pro kvantitativní odhad povrchového pH (R^2: 0.61, Rv^2: 0.76). Tato studie je jednou z prvních, jež aplikuje metody obrazové spektroskopie pro kvantitativní modelování pH v prostředí povrchových dolů vyznačující se vysokou heterogenitou.

V druhé tematické části je obrazová spektroskopie aplikována do oblasti monitoringu zdravotního stavu lesních smrkových porostů, které se vyskytují v bezprostředním okolí Sokolovské pánve, avšak

nejsou přímo zasaženy vlastní těžbou. Za účelem zhodnocení zdravotního stavu těchto porostů je sestrojena kvantitativní mapa obsahu celkového chlorofylu (Cab), jež je konstruována na základě vegetačního indexu odvozeného z derivovaného spektra (D_{718}/D_{708}) obrazových dat HyMap (07/2009). Pro odhad Cab bylo touto metodou dosaženo relativně vysoké přesnosti (RMSE: 0.21 mg/g, R^2=0.91, Rv^2: 0.94). Dále jsou z obrazových dat derivovány a analyzovány další indexy indikující vegetační stres (REP: Red Edge Position, SIPI: Structure Insensitive Pigment Index, PRI: Photosynthetic Reflectance Index). Výsledně je vytvořen statistický model integrující obsah chlorofylu (Cab) s vegetačními indexy REP a SIPI, jež umožňuje vyhodnotit fyziologický stav smrkových porostů a identifikovat případný stress i u takových porostů, jež ještě nevykazují viditelné symptomy poškození (kapitola 4).

V kapitole 5 je výše popsaná metoda aplikována na další sadu hyperspektrálních dat HyMap, jež byly pořízeny v následujícím roce (08/2010). Výsledky klasifikace jsou dále validovány s biochemickými parametry smrkového jehličí a asociovány s geochemickými podmínkami půdního prostředí. Klasifikací obou hyperspektrálních datových sad (HyMap 07/2009 a 08/2010), stejně jako statistickým vyhodnocením biochemických a geochemických parametrů, bylo identifikováno zatížení a vegetační stres u stejných lokalit. Půdní prostředí těchto lokalit vykazuje kriticky nízké pH, nízké hodnoty makro-nutričních parametrů, a navíc i nízký poměr množství bazických kationtů vztažených k volně dostupnému hliníku (Bc/Al). Výsledky této části prokazují validitu modelu navrženého v kapitole 4 a dále demonstrují přidanou hodnotu hyperspektrálních dat, jež jsou pořizována ve více časových horizontech.

V poslední kapitole je statisticky vyhodnocena široká škála biochemických parametrů za účelem vytipování jejich potenciálního využití jako nespecifických indikátorů vegetačního stresu. Faktorová analýza je aplikována pro statistické testování vztahu mezi biochemickými parametry jehličí a vertikální distribucí půdních makro-nutričních parametrů a potenciálně toxických prvků. Je nalezen vztah mezi koncentracemi arzenu (As) a hliníku (Al) v jehličí a v půdním profilu. Kromě toho byl nalezen také vztah mezi koncentracemi As a Al, obsahem fenolických látek v jehlicích a poměrem fotosyntetických pigmentů Car/Cab (karotenoidy/chlorofyl: Car/Cab). Tyto výsledky demonstrují, že vedle poměru Car/Cab je i obsah fenolických látek významným indikátorem vegetačního stresu. Oba tyto parametry je proto vhodné využít pro detekci vegetačního stresu. Vývoj nových modelů/postupů pro jejich přesnější stanovení pomocí obrazové spektroskopie tak přinese nové možnosti pro monitoring fyziologického stavu lesních porostů.

Klíčová slova: *obrazová spektroskopie, hyperspektrální data, acidifikace, multi-temporální analýza, modelování pH, vegetační stress, nespecifické stresové ukazatele, těžké kovy*

Acknowledgement

I express my sincere gratitude to my supervisor Doc. Jan Kolář for his guidance and great support especially during the time when this thesis has been finalized. Firstly, I thank Dr. Stephane Chevrel and Dr. Anne Bourguignon (both BRGM) for their enthusiasm and willingness to bring the ASD and to start systematically collecting the field spectra in Sokolov. I extend my sincere thanks to Prof. Jana Albrechtová and Dr. Zuzana Lhotáková, both from the Department of Experimental Plant Biology – Charles University in Prague, for their invaluable collaboration and for providing me with the necessary expertise on the "tree issues". I express my great thanks to the EO-MINER fellows, Prof. Eyal Ben-Dor (TAU), Dr. Christian Fisher and Christoph Ehrler (both DLR) for their great help with the atmospheric correction. Many thanks are due to Dr. Petr Rojík (Sokolovská uhelná a.s.) for his substantial assistance with the field campaigns in Sokolov, I know it was not easy with us not sometimes but many times. I would like to thank my colleagues for the Czech Geological Surve who are also my friends; Jan Mišurec, Jan Jelének and Lucie Koucká; for their great help in the field as well as at the office. I especially thank to my son Lukáš for being so patient and just great.

The present research is being undertaken within the framework of Grants No. 205/09/1989 (HypSo: grant funded by the Czech Science Foundation) and No. 244242 (EO-MINERS: FP7 grant funded by the EC).

Contents

List of figures

List of tables

List of acronyms

A0-10 Mineral horizon (0-10 cm)

A10-20 Mineral horizon (10-20 cm)

AAS Atomic Absorption Spectrometry

ANOVA Analysis of Variance

AMD Acid Mine Drainage

AOT Aerosol Optical Thickness

BD Band Depth

BRDF Bi-directional Reflectance Distribution Function

Cab Total Chlorophyll Content

$CADAC_{543-760}$ Chlorophyll Absorption Depth Normalized Area under Curve between 543-760 nm

Car Total Carotenoid Content

Car/Cab Carotenoid to Chlorophyll Ratio

CEST Central European Summer Time

C:N Carbon to Nitrogen Ratio

CR Continuum Removal

D_{718}/D_{704} 1st derivative ratio at 718 and 704 nm

D_{718}/D_{747} 1st derivative ratio at 718 and 747 nm

DW Dry Weight

DEM Digital Elevation Model

DMF Dimethylforamide

expSIPI Exponentially transformed SIPI index

FWHM Full-Width Half-Maximum

FW Fresh Weight

GPS Global Positioning System

HCRF Hemispherical-Conical Reflectance Factor

HS Hyperspectral

ICP International Co-operation Programme

IMU Inertial Measurement Unit

IS Imaging Spectroscopy

K-S Kolmogorov-Smirnov test

LAI Leaf Area index

LSU Linear Spectral Unmixing

Lig Lignin

MLC Maximum Likelihood Classification

MNF Minimum Noise Fraction

MRSFF Multi Range Spectral Feature Fitting

N_{690} Reflectance at 690 nm normalized to the reflectance at 675 and 744 nm

N_{704} Reflectance at 704 nm normalized to the reflectance at 675 and 744 nm

N_{718} Reflectance at 718 nm normalized to the reflectance at 675 and 744 nm

N_{733} Reflectance at 733 nm normalized to the reflectance at 675 and 744 nm

NDVI Normalized Difference Vegetation Index

Oa Second organic horizon

Ol+Of Top organic horizon

PLSR Partial Least Square Regression

PCA Principal Component Analysis

PPI Pixel Purity Index

PRI Photochemical Reflectance Index

r_{xy} Pearson's correlation coefficient

R^2 Coefficient of determination (training dataset)

Rv^2 Coefficient of determination (validation dataset)

REP Red-Edge Position

RMSE Root Mean Square Error

ROI Region of Interest

RT Radiative Transfer

SAM Spectral Angle Mapper

SFF Spectral Feature Fitting

SIPI Structure Insensitive Pigment Index

SMA Spectral Mixture Analysis

SMR Stepwise Multiple Regression

SNR Signal-to-Noise Ratio

SWIR Short-Wave Infrared

TEA Total Exchangeable Acidity

TOC Total Organic Carbon

VNIR Visible Near Infrared

VOG Vogelmann Red-edge Index

HCRF Hemispherical-Conical Reflectance Factor

XRD X-Ray Diffraction

1. Introduction

1.1 Environmental issues in coal mining and current monitoring methods

Coal mining generates a number of significant environmental impacts, such as increased acidity of the soil/water environment, called mineral Acid Mine Drainage (AMD). AMD is produced when sulfide-bearing material is exposed to oxygen and water. Characterized by low pH and high concentrations of heavy metals and other toxic elements (Kabata-Pendias, 2004), AMD can severely contaminate surface waters and groundwater, as well as soils, and stresses the surrounding vegetation. The typical AMD pattern leads to accumulation of Fe sulfates, oxy-hydroxides, and oxides in a spatial and temporal sequence that represents the buffering of an acidic solution as it moves away from its source (Montero et al., 2005; Swayze et al., 2000). AMD can then be mapped by identifying these typical spatial sequences of indicative minerals.

Low substrate pH and heavy metal contamination are stress factors for vegetation and lead to changes in the contents of important leaf/foliage compounds (e.g., photosynthetic pigments, phenolic compounds and lignin), which can be used as non-specific indicators of plant stress. Particularly the contents of photosynthetic pigments are closely related to photosynthetic performance and can serve as early-warning symptoms of plant stress, before macroscopic changes are detected (e.g. Lepedus et al., 2005). The chlorophyll content of needles generally decreases under stress conditions, which can include nutrient deficiency and the presence of heavy metals (Ivanov et al., 2011; Maestri et al., 2010).

From this point of view, a mining environment with high acidity, high heavy metal concentrations and extreme heterogeneity represents a complex system that needs to be assessed in a multidisciplinary way. Conventionally used laboratory analyses can be very accurate, but they are costly and extremely labor and time intensive, and even destructive when used for vegetation. In addition, they can hardly be extended to cover large regions/areas.

However, estimates of physical and chemical parameters over large areas can be obtained using remote sensing data acquired from an air or space platform (Gao et al., 2008; Heiskanen et al., 2008; Kokaly et al., 2003; Sirikulchayanon et al., 2008,). Modern remote sensing has become a novel tool not only for detecting target materials but also for monitoring dynamic processes and induced changes in physical/chemical properties. The use of multispectral imagery has been demonstrated to effectively map the distribution of ecosystem types and vegetative systems (Everitt et al., 2002; Lamb and Brown, 2001), as well as for monitoring diverse environmental impacts caused by human

activities (He et al., 2009; Matějíček and Kopačková, 2010; Rathore et al., 1993). However, the low spectral resolution of multispectral imagery is a major limitation.

On the other hand imagery with higher spectral resolution (e.g., hyperspectral) provides sufficient spectral resolution to describe diagnostic absorption signatures (Clark et al., 1990; Ustin et al., 2004; Vane & Goetz, 1993). Data with very high spectral resolution – hereafter referred to as imaging spectroscopy (IS) data, which is also known in the remote sensing community as hyperspectral (HS) data, has been successfully used in earlier studies to detect environmental factors, such as oil contamination (Li et al., 2005), hazardous mining materials (Kemper and Sommer, 2002) or vegetation stress and damage (Hamzeh et al., 2013).

1.2 Image spectroscopy and its environmental applications

Specific chemical bonds in materials, whether solid, liquid or gas, determine the surface reflectance and emittance, as variations in material composition often cause shifts in the position and shape of absorption bands in the spectrum. Spectroscopy has the advantage of being sensitive to both crystalline and amorphous materials, unlike some diagnostic methods, such as X-ray diffraction (Clark et al., 1999). Basically, the wavelength position of the absorption maxima allows material identification while the absorption depth reflects the material quantity.

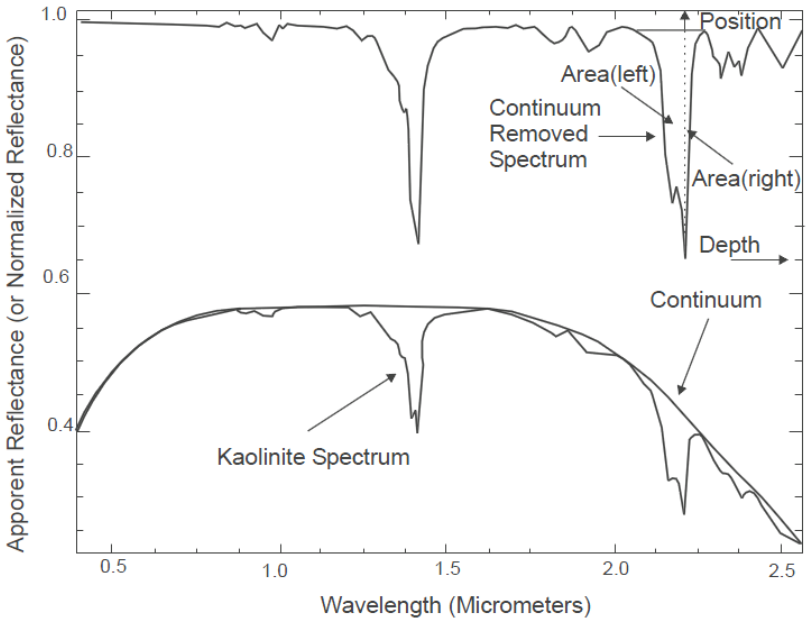

Figure 1.1: *Definition of the continuum and continuum removal and subsequent definition of absorption feature characteristics (adopted from Van Der Meer 2004).*

Imaging spectroscopy is a relatively new field that has rapidly grown during the last two decades, however, high spatial resolution hyperspectral (HSRH) data is still a relatively novel data source for analysis of large -scale aspects in the environment and earth sciences. The term hyperspectral is used to indicate a very large number of narrow spectral channels (usually about two hundred) in comparison with multispectral sensing that is represented typically by 4-10 spectral channels at much wider intervals. The main aim in hyperspectral sensing is to create an image of a scene in a large number of discrete continuous narrow spectral bands, so that an almost continuous spectrum can be generated for each pixel. Imaging spectrometry possesses the capability to identify and map the distribution of real spatial features with specific physical-chemical properties (minerals, solid solution series, contamination in surface waters and so on).

The image spectral data, after adequate pre-processing, can be interpreted using a field and laboratory spectral library of indicative end-members (minerals used to generate mineral maps). The visible-near infrared (VNIR) portion of the spectrum is a source of information about absorption in transition metals, particularly iron, allowing for instance mapping surfaces with a high concentration of hematite and goethite (Hunt et al., 1972) and also detecting chlorophyll absorption by photosynthesizing plants (Knipling, 1970). The short wave infrared (SWIR) portion of the spectrum is useful in detecting such minerals as carbonates, hydrates, and hydroxides (Boardman and Kruse, 1994; Clark et al., 1990). On the other hand, the VNIR and SWIR portions of the electromagnetic spectrum are not useful in detecting the main constituents of igneous rocks, quartz and feldspars, due to their lack of absorption features in the VNIR and SWIR wavelengths. These can be mapped using the thermal infrared region (TIR, 8-12 µm) (Gillespie, 1986). The reflectance/emittance can be measured by spectrometers used in the laboratory, in the field, in aircraft and on satellites.

The following sections give a detailed description of the spectroscopic basis for studying environmental issues typically present at mining sites.

1.2.1 Basis for spectral interpretation and mineral identification of Acid Mine Drainage

AMD is a biologically mediated oxidation process, which leads to the formation of a solution with low pH and high contents of Fe^{2+}, Fe^{3+} and SO_4. In waste piles, meteoric water is acidified by the process of sulfide oxidation (mainly microbial oxidation of pyrite) and is then partially neutralized by hydrolysis reactions of aluminosilicates and other minerals in the waste piles as the solution flows from active oxidation points. This leads to accumulation of Fe sulfates, oxyhydroxides and oxides in a

spatial and temporal sequence that represents the buffering by the acidic solution as it moves away from its source (Swayze et al, 2000).

Pyrite and (or) pyrrhotite are ubiquitous at all of the sites. Generalized possible reaction pathways from primary Fe-sulfide minerals to secondary sulfate minerals observed at a mining site are illustrated in Fig. 1.2. Ferric iron is the main oxidant of these minerals in natural systems, along with ferrous iron and sulfates, which can precipitate as early-formed efflorescent sulfate salts (Stoffregen et al., 2000). A variety of different oxidation pathways can operate in any given setting. Dissolved metals and sulfate can remain in solution or become incorporated in a variety of minerals (e.g., hydroxides, iron oxides and hydroxysulphates), depending on the local chemical and physical environment (Seal et al., 2000).

The pathways of FeS_2 oxidation can be controlled either chemically or organically by microorganisms. The kind of sulphate mineral formed is a function of the solution composition and local conditions, e.g. humidity, acidity and redox potential. The seasonal variations in AMD compositions are generally registered because, in dry periods, the pH is lower and the electrical conductivity (EC), SO_4 and, in consequence, the metal concentrations (e.g., Fe, Mn, Cu, Zn, Pb and Cd) are higher. Dilution decreases the metal concentrations and EC and increases the pH during the winter (Gomes et al., 2006).

1.2.1.1 Spectral properties of hydroxides, iron oxides and hydroxysulfates

Electrical processes involving orbital electrons in transition metals give rise to broad absorption features that are observed from 0.4 to 1.3 µm. Reflectance spectra of Fe minerals reflect single- and paired-electron transitions between the energy levels in unfilled 3d orbitals and metal-ligand electron transfers (Sherman and Waite, 1985). The wavelength and intensity of absorption features in this region depend on the nature of the crystal field around the Fe atom and on the kind of bonds around it because the nature of magnetic coupling between $Fe3^+$ ions (as influenced by the crystal field) facilitates the transition of electrons between energy states (Sherman and Waite, 1985). Thus, in $Fe3^+$ minerals, subtle differences in the shape and wavelength of the absorption features (Montero et al., 2005) reflect the crystal structure of the minerals and enable their identification (Fig. 1.3).

Hematite (Fe oxide) possesses the structure of closely packed face-sharing FeO_6 octahedra (Burns, 1993), and the strong antiferromagnetic interactions among the Fe3+ ions affect the electron transitions and electric charge transfers to create a very strong absorption (delineated by low reflectance) at wavelengths shorter than 0.55 µm (Taran and Rossman, 2002). The strong absorption

caused by Fe^{3+} electron transition is characteristic at 0.85–0.9 µm, with a concave downward inflection at 0.9–0.95 µm (Morris et al., 1985).

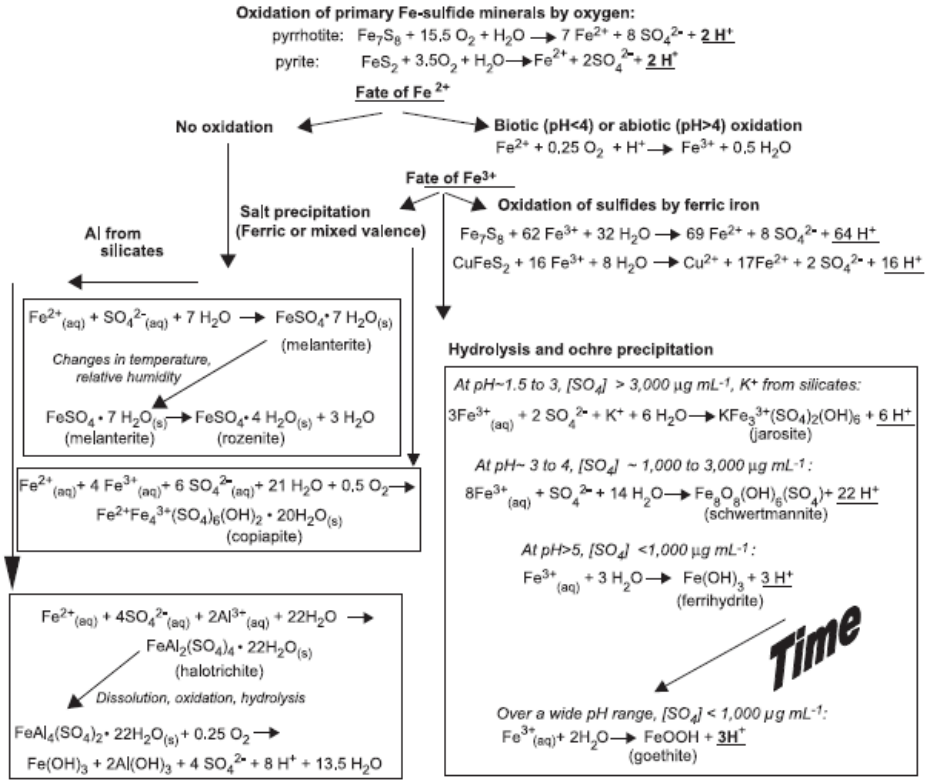

Figure 1.2: *Model of the accumulation of secondary Fe minerals in Fe sulfide-rich mine-waste environments according to pH values from field data. Modified by Montero et al. (2005) from model by Bigham (1994).*

The *ferrihydrite* structure has similarities to that of hematite except that some of the Fe sites are vacant and some oxygen sites are occupied by H_2O and OH^-(Sherman et al., 1982). Electron and paired-electron transitions in Fe^{3+} cause strong absorption centered at approximately 0.50 µm and broad absorption at wavelengths greater than 0.95 µm, respectively (Bishop et al., 1993). *Goethite* has edge-sharing FeO_6 octahedra; paired and single Fe^{3+} electron transitions (Sherman et al., 1982) cause strong absorption at 0.45 µm (edge at 0.55 µm) and broad asymmetric absorption between 0.90 and 1.00 µm (Morris et al., 1985).

In *schwertmannite* [$Fe_8O_8(OH)_6SO_4$], the presence of SO_4^{2-} bridges between some edge-sharing $FeO_3(OH)_3$ octahedra creates two sites for Fe^{3+} (Bishop et al., 1993), which are reflected in a very broad asymmetric absorption feature at 0.9 µm and strong absorption with a steep edge at wavelengths of less than 0.5 µm (Bishop et al., 1993).

Jarosite has edge-sharing FeO_6 octahedra bridged by hydroxyl and sulfate groups that form sheets separated by K^+ ions (Rossman, 1976). Bridging of Fe by both OH^- and SO_4^{2-} gives rise to four electron and paired-electron transitions observed in the spectrum of well-crystallized jarosite (Morris, 1998). Spectral features diagnostic of jarosite include a narrow absorption feature near 0.43 µm and a broad feature near 0.92 µm. An inflection past 1.0 µm affects the symmetry of the broad absorption feature.

In *copiapite*, Fe^{3+} octahedra are linked by corner-sharing OH^- and SO_4 molecules to form chains, and Fe^{2+} occupies the center of an isolated and weakly connected $Fe(H_2O)_6$ octahedron at the origin of the unit cell (Fanfani et al., 1973). The strong magnetic interaction of ferric ions through the hydroxyl bridge gives rise to intense, narrow and symmetric absorption features at approximately 0.43 and 0.87 µm (Rossman, 1975).

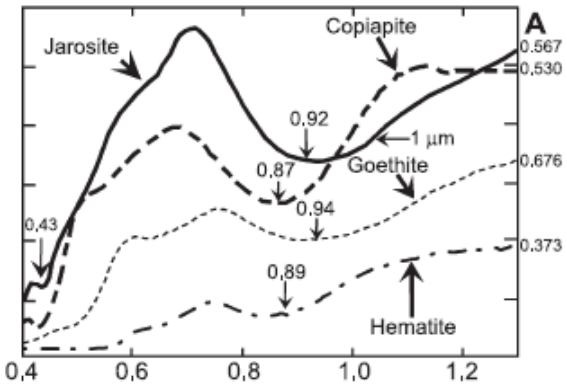

Figure 1.3: *Laboratory reflectance spectra of selected secondary Fe minerals reference minerals (Montero et al., 2005). Spectra are offset vertically for clarity. Light arrows indicate absorption features used in the identification of spectra, and the center of that feature (in µm) obtained by the continuum removal method of Clark et al. (1990).*

1.2.1.2 Mineral identification and mixing problem

The real world is a complex mixture of materials on any possible scale. In general, there are four types of mixtures (Clark et al., 1999):

- Linear Mixture. The materials in the field of view are optically separated so there is no multiple scattering between components. The combined signal is simply the sum of the fractional area times the spectrum of each component. This is also called an areal mixture.
- Intimate Mixture. An intimate mixture occurs when different materials are in intimate contact in a scattering surface, such as the mineral grains in a soil or rock. Depending on the optical properties of each component, the resulting signal is a highly non-linear combination of the end-member spectra.

- Coatings. Coatings occur when one material coats another. Each coating is a scattering/transmitting layer whose optical thickness varies with the material properties and wavelength.
- Molecular Mixtures. Molecular mixtures occur on a molecular level, such as two liquids, or a liquid and a solid mixed together (e.g., water adsorbed on a mineral; gasoline spilled onto soil). The close contact of the mixture components can cause band shifts in the adsorbate, such as the interlayer water in montmorillonite, or the water in plants.

In spite of being weak absorbers by themselves, many minerals can dominate the final signal if present as submicrometer coatings on a substrate that is a strong absorber (Montero et al., 2005; Sherman et al., 1982). This particular example illustrates the difficulty in identifying minerals in the spectra of geological materials, many of which are intimate mixtures of fine-grained to amorphous minerals. In addition, natural geologic surfaces are often partially covered with non-geological materials (e.g., vegetation). The reflectance spectra of mixtures are a nonlinear expression of the combined spectra of the pure mineral end-members and their abundances, in a way that reflects the accessibility of light to each mineral grain, the complexity of inter-grain and intra-grain light reflection and scattering, and the optical properties of each type of mineral grain (Adams and Filice, 1967). While studying secondary minerals, variations in grain size that affect the relative intensities of overlapping absorption features must be considered because small secondary minerals commonly coat larger particles and dominate the reflectance spectra (Gaffey et al., 1993; Montero et al., 2005).

Mixing can exist on various scales and also affects the measured infrared spectral properties of an area (Clark, 1999). Even high-spatial-resolution (2-m pixel) images can have contributions from multiple sub-pixel-scale components. Based on these findings, the most efficient and valid methods are those taking in account the spectral mixture models, where the end members (set of reference spectra for known materials) must first be defined. Proper end-member selection as an input to un-mixing is crucial if we want to avoid singularity and orthogonality problems with matrix inversion of linear systems (Van der Meer and De Jong, 2000).

1.2.2 Spectral response of vegetation to environmental stress

Absorption of light in the visible spectrum by plant pigments produces a unique spectral reflectance signature. Leaf pigments absorb strongly across the visible region from 0.35 to 0.70 µm. (Kokaly et al., 2009) (Fig. 1.4). Light is captured in the process of photosynthesis (Govindjee and Krogmann, 2004) and the light energy is stored as carbohydrates, through a series of electron transfers that

occur on the thylakoid membranes in chloroplasts. In the intact chloroplast, pigment–protein complexes are organized in two photosystems that harvest light and transfer energy to the reaction centers. In addition to chlorophyll a and b, the photosynthetic antenna (the organized association of pigments that capture photons and transfer energy to the reaction centers) contain other membrane-bound accessory pigments that include β-carotene, lutein and xanthophyll cycle pigments (Lichtenthaler, 1987).

The spectral responses of plants exhibit significant changes as the leaves transform from actively photosynthetic to total senescence and as the stress agents influence this process. The spectral response of healthy plants to solar radiation is, in general, similar though differences exist between plants due to their morphology and physiology, background soil types, and the climate. Healthy plants have diagnostic high reflectance in the near-infrared region of solar radiation because of strong internal scattering of incident light from cell walls and intercellular spaces. An example of the mean spectral response of healthy vegetation in the visible and NIR region of the electromagnetic spectrum is shown in Fig.1.4.

When plants become senescent or stressed, however, the mesophyll tissue begins to desiccate and cell walls collapse, which results in substantially reduced intercellular surface area and air space. Senescent and stressed plants thus reflect more red light, but much less in the near-infrared region compared to healthy green plants. Greater reflection of red light is due to the loss of photosynthetic pigments, resulting in less absorption (Fig. 1.4).

Better knowledge of pigment distributions and estimation of their concentrations could provide a basis for monitoring physiological and ecological processes (Ustin et al., 2009). Currently, a variety of techniques have been used for detecting early-stage vegetation stress in airborne and satellite imagery. These techniques frequently include “red-edge” detection.

The “red edge” explicitly refers to the wavelength of the “red-edge” inflection point (REIP), the sharp reflectance change observed in the spectrum of green plants in the 680–740-nm wavelength range (Ustin et al., 1999). It is the long-wavelength edge of the chlorophyll absorption feature, sensitive to the amount of chlorophyll or leaf area visible to the sensor, and thus has been used as an indicator of stress and senescence of vegetation (Dawson and Curran, 1998; Ustin et al., 1999), where it was applied to variation within one vegetation type. Chlorosis increases reflectance across the visible spectrum and causes a shift to shorter wavelengths (blue-shift) of the red edge, due to narrowing of the chlorophyll absorption feature and a reduction in depth (Ustin and Curtiss, 1990). Gates et al.

(1965) and Collins (1978) described early observations of a blue shift of the red edge, which was attributed to the loss of chlorophyll. In contrast, with increased chlorophyll content, the chlorophyll absorption feature deepens and broadens (e.g., Buschmann and Nagel, 1993) causing a red shift (Collins, 1978).

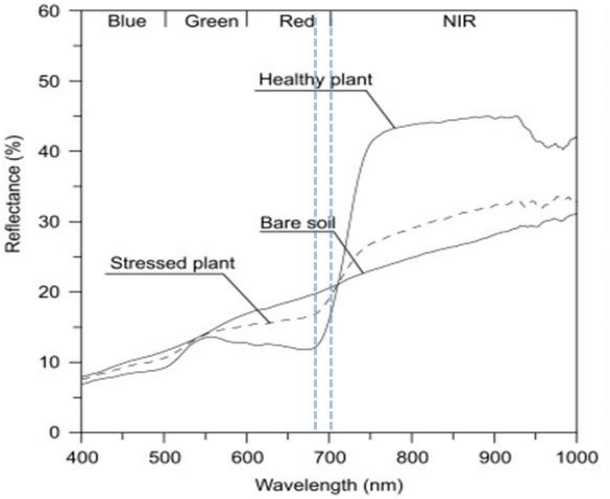

Fig. 1.4: *Representative reflectance spectra for healthy and stressed plants and bare soil in the visible (400–700 nm) to NIR (700–1000 nm) regions of the spectrum. Bars indicate the primary chlorophyll band at 680 nm and the region of the red-edge inflection point (Modified from Yang et al., 2008).*

In addition to chlorophyll, the carotenoid content (carotenoids represent different chemical compounds such as xanthophylls and anthocyanis) is also an indicator of vegetation stress. The Photochemical Reflectance Index (PRI) (Gamon et al., 1997) is frequently used to detect foliar stress (Ustin et al., 2009) and the basis for the PRI is that short-term changes in reflectance response to the light are observed at 531 nm, reflecting reversible changes in the distribution of xanthophyll cycle pigments (Demming-Adams, 1990). The relationship between the PRI and photosynthetic light-use efficiency has been explored on multiple scales (leaf to stand-level) (Gamon, 2001; Drolet et al., 2005; Nakaji et al., 2005). In addition, carotenoids and anthocyanis are pigments that are not associated with the chloroplast but are often observed during environmental stresses and during senescence (Schaberg et al., 2008). These pigments have a single absorption maximum around 529 nm and can be detected by reflectance changes in the green region (Ustin et al., 2009). Various empirical approaches have been used to estimate carotenoids; the spectral indexes used as chlorophyll and carotenoid indicators were summarized by Ustin et al. (2009).

In addition to the empirical methods described above, radiative transfer (RT) modeling has proven to be a powerful tool in understanding the interaction of light with plant canopies and in inferring the biochemical and biophysical characteristics from the reflectance spectra of vegetation. This

understanding leads to the development of more reliable remotely sensed information about vegetation health (Ganapol et al., 1998; Jacquemoud and Baret 1998; van de Tol, 2009; Verhoef, 1984). However, these models are computationally demanding and require a large number of leaf and canopy variables, which are often difficult to estimate (Fang et al., 2003). Furthermore, physical models can suffer from ill-posed problems or can lead to a bias in the retrieved biophysical parameters and all these limitations make them difficult to use on a regional scale.

1.3 Purpose of this study

Although the principles of spectroscopy are well known and methods for analysis have been widely developed, particularly for spectra collected in laboratory environments, the heterogeneity of landscapes and earth surface features in extensive environmental studies still presents new challenges and opportunities for analysis of HS imagery. Image spectroscopy (HS remote sensing) is potentially the best approach for assessing diverse environmental issues; however very little research has been performed on a regional scale and on long-term monitoring, mainly because of the rather high costs related to HS data acquisition and the expert knowledge which is still required for HS data pre-processing and processing. Therefore, even today there is still a lack of multi-stripe and/or time-series HS data and reliable methods for extracting the required information for these datasets. Based on the concept described in the chapter 1.2 the following hypothesis was formulated:

Hypothesis

1. Image spectroscopy has been used for modeling the physical and chemical properties of targeting surfaces. Therefore, these methods can be used as a tool to monitor the environmental conditions in regions affected by mining activities via estimating both geochemical and biochemical parameters over large areas.
2. At mining sites, Acid Mine Drainage (AMD) is a common environmental problem resulting in the discharge of acid solutions from the pyritic waste piles and the subsequent accumulation of secondary precipitates by hydrolysis reactions. Mineral spectroscopy, both high and low altitude, allows identification of the minerals that serve as indicators of sub-aerial oxidation of pyrite (‘hot spots’) and the subsequent formation of AMD. Furthermore, the surface pH can be modeled using image spectroscopy while identifying indicative minerals and estimating their abundances.

3. At mining sites, negative physio-chemical changes under soil conditions (e.g., heavy metal contamination and low pH) are stress factors that lead to changes in the contents of important leaf/foliage compounds, which can be used as non-specific indicators of plant stress. These indicators can be estimated by means of image spectroscopy and can detect vegetation stress before these phenomena can be observed visually. From this point of view, these novel methods can give early warning information, especially if multi-date hyperspectral image datasets are processed.

Objectives

Accordingly, to investigate the hypothesis, the main purpose of this thesis is to use airborne hyperspectral (HS) data for estimation of parameters which can be further used for environmental monitoring. The specific thesis objectives are as follows:

(i) To formulate mineral spectroscopy-based techniques allowing identification of acidity sources and surface pH estimation for exposed surfaces in extremely heterogeneous environments characteristic for mining sites.

(ii) To formulate a HS remote sensing technique allowing early detection of vegetation stress on a regional scale.

(iii) To validate one of the latter techniques using an additional temporal HS image dataset.

(iv) To assess the applicability of using diverse needle biochemical parameters as biological indicators of adverse soil condition parameters and select the most sensitive ones with the greatest potential for future HS Remote Sensing monitoring.

1.4 Thesis structure

The thesis is divided into two major parts. Chapters 2 and 3 are both thematically devoted to applications of Image Spectroscopy to Acid Mine Drainage mapping and its related issues. Chapter 2 deals with the ability to identify sources of acidity using ASTER satellite data, as this represents an easily accessible and low-cost data source. Chapter three focuses on the development of a new technique to quantitatively estimate the pH for exposed surfaces in mining and post mining environments.

In chapters 4-5, Image Spectroscopy is employed to monitor vegetation stress. Chapter 4 describes a novel monitoring technique integrating selected spectral indexes to assess subtle changes in the physiological status of macroscopically undamaged Norway spruce foliage. This technique is validated using an additional temporal HyMap dataset and forest stand specific geochemical parameters (chapter 5).

In chapter 6, the potential of diverse foliar biochemical parameters used as stress indicators is assessed and the most sensitive ones with the greatest potential for future HS Remote Sensing monitoring are suggested.

References

ADAMS, J. B. & FILICE, A. L. (1967), 'Spectral Reflectance 0.4 To 2.0 Microns of Silicate Rock Powders', *Journal of Geophysical Research* **72**(22), 5705-.

BIGHAM, J. M.; CARLSON, L. & MURAD, E. (1994), 'Schwertmannite, A New Iron Oxyhydroxysulphate From Pyhasalmi, Finland, and Other Localities', *Mineralogical Magazine* **58**(393), 641-648.

BISHOP, J. L.; PIETERS, C. M. & BURNS, R. G. (1993), 'Reflectance and Mossbauer-spectroscopy of Ferrihydrite-montmorillonite Assemblages As Mars Soil Analog Materials', *Geochimica Et Cosmochimica Acta* **57**(19), 4583-4595.

BISHOP, J. L.; PIETERS, C. M.; BURNS, R. G.; EDWARDS, J. O.; MANCINELLI, R. L. & FROSCHL, H. (1995), 'Reflectance Spectroscopy of Ferric Sulfate-bearing Montmorillonites As Mars Soil Analog Materials', *Icarus* **117**(1), 101-119.

Boardman, J. W. & Kruse, F. A. (1994), 'Automated Spectral Analysis - A Geological Example Using Aviris Data, North Grapevine Mountains, Nevada', *Proceedings of the Tenth Thematic Conference On Geologic Remote Sensing - Exploration, Environment, and Engineering, Vol I*, I407-I418.

BURNS, R. G. (1994), 'Mineral Mossbauer-spectroscopy - Correlations Between Chemical-shift and Quadrupole Splitting Parameters', *Hyperfine Interactions* **91**(1-4), 739-745.

BUSCHMANN, C. & NAGEL, E. (1993), 'Invivo Spectroscopy and Internal Optics of Leaves As Basis For Remote-sensing of Vegetation', *International Journal of Remote Sensing* **14**(4), 711-722.

Clark, R.Rencz, A., ed., (1999), *Manual of Remote Sensing, Remote Sensing for the Earth SciencesSciences, vol. 3.*, Wiley, New York, chapter Spectroscopy of rocks and minerals and principles of spectroscopy., pp. 3-58.

Clark, R. N.; King, T. V. V.; Klejwa, M.; Swayze, G. A. & Vergo, N. (1990), 'High Spectral Resolution Reflectance Spectroscopy of Minerals', *Journal of Geophysical Research-solid Earth and Planets* **95**(B8), 12653-12680.

COLLINS, W. (1978), 'Remote-sensing of Crop Type and Maturity', *Photogrammetric Engineering and Remote Sensing* **44**(1), 43-55.

Daughtry, C. S. T.; Walthall, C. L.; Kim, M. S.; de Colstoun, E. B. & McMurtrey, J. E. (2000), 'Estimating corn leaf chlorophyll concentration from leaf and canopy reflectance', *Remote Sensing of Environment* **74**(2), 229-239.

Dawson, T. P. & Curran, P. J. (1998), 'A new technique for interpolating the reflectance red edge position', *International Journal of Remote Sensing* **19**(11), 2133-2139.

DEMMIGADAMS, B. (1990), 'Carotenoids and Photoprotection In Plants - A Role For the Xanthophyll Zeaxanthin', *Biochimica Et Biophysica Acta* **1020**(1), 1-24.

Drolet, G. G.; Huemmrich, K. F.; Hall, F. G.; Middleton, E. M.; Black, T. A.; Barr, A. G. & Margolis, H. A. (2005), 'A MODIS-derived photochemical reflectance index to detect inter-annual variations in the photosynthetic light-use efficiency of a boreal deciduous forest', *Remote Sensing of Environment* **98**(2-3), 212-224.

FANFANI, L.; NUNZI, A.; ZANAZZI, P. F. & ZANZARI, A. R. (1973), 'Copiapite Problem - Crystal-structure of A Ferrian Copiapite', *American Mineralogist* **58**(3-4), 314-322.

Fang, H. L.; Liang, S. L. & Kuusk, A. (2003), 'Retrieving leaf area index using a genetic algorithm with a canopy radiative transfer model', *Remote Sensing of Environment* **85**(3), 257-270.

GAFFEY, M. J.; BELL, J. F.; BROWN, R. H.; BURBINE, T. H.; PIATEK, J. L.; REED, K. L. & CHAKY, D. A. (1993), 'Mineralogical Variations Within the S-type Asteroid Class', *Icarus* **106**(2), 573-602.

Gamon, J. A.; Field, C. B.; Fredeen, A. L. & Thayer, S. (2001), 'Assessing photosynthetic downregulation in sunflower stands with an optically-based model', *Photosynthesis Research* **67**(1-2), 113-125.

Gamon, J. A.; Serrano, L. & Surfus, J. S. (1997), 'The photochemical reflectance index: an optical indicator of photosynthetic radiation use efficiency across species, functional types, and nutrient levels', *Oecologia* **112**(4), 492-501.

Ganapol, B. D.; Johnson, L. F.; Hammer, P. D.; Hlavka, C. A. & Peterson, D. L. (1998), 'LEAFMOD: A new within-leaf radiative transfer model', *Remote Sensing of Environment* **63**(2), 182-193.

Gao, J. & Liu, Y. S. (2008), 'Mapping of land degradation from space: a comparative study of Landsat ETM+ and ASTER data', *International Journal of Remote Sensing* **29**(14), 4029-4043.

GATES, D. M.; KEEGAN, H. J.; SCHLETER, J. C. & WEIDNER, V. R. (1965), 'Spectral Properties of Plants', *Applied Optics* **4**(1), 11-.

Gomes, M. E. P. & Favas, P. J. C. (2006), 'Mineralogical controls on mine drainage of the abandoned Ervedosa tin mine in north-eastern Portugal', *Applied Geochemistry* **21**(8), 1322-1334.

Govindjee & Krogmann, D. (2004), 'Discoveries in oxygenic photosynthesis (1727-2003): a perspective', *Photosynthesis Research* **80**(1-3), 15-26.

Hamzeh, S.; Naseri, A. A.; AlaviPanah, S. K.; Mojaradi, B.; Bartholomeus, H. M.; Clevers, J. G. P. W. & Behzad, M. (2013), 'Estimating salinity stress in sugarcane fields with spaceborne hyperspectral vegetation indices', *International Journal of Applied Earth Observation and Geoinformation* **21**, 282-290.

He, B.; Oki, K.; Wang, Y. & Oki, T. (2009), 'Using remotely sensed imagery to estimate potential annual pollutant loads in river basins', *Water Science and Technology* **60**(8), 2009-2015.

Heiskanen, J. (2008), 'Evaluation of global land cover data sets over the tundra-taiga transition zone in northernmost Finland', *International Journal of Remote Sensing* **29**(13), 3727-3751.

Hunt, G.R.and Salisbury, J. & Lenhoff, C. (1971), 'Visible and nearinfrared spectra of minerals and rocks: III. Oxides and hydroxides', *Mod. Geol.* **2**, 195– 205.

Ivanov, Y. V.; Savochkin, Y. V. & Kuznetsov, V. V. (2011), 'Scots pine as a model plant for studying the mechanisms of conifers adaptation to heavy metal action: 1. Effects of continuous zinc presence on morphometric and physiological characteristics of developing pine seedlings', *Russian Journal of Plant Physiology* **58**(5), 871-878.

Kabata-Pendias, A. (2004), 'Soil-plant transfer of trace elements - an environmental issue', *Geoderma* **122**(2-4), 143-149.

Kemper, T. & Sommer, S. (2002), 'Estimate of heavy metal contamination in soils after a mining accident using reflectance spectroscopy', *Environmental Science & Technology* **36**(12), 2742-2747.

Kokaly, R. F.; Asner, G. P.; Ollinger, S. V.; Martin, M. E. & Wessman, C. A. (2009), 'Characterizing canopy biochemistry from imaging spectroscopy and its application to ecosystem studies', *Remote Sensing of Environment* **113**, S78-S91.

Kokaly, R. F.; Despain, D. G.; Clark, R. N. & Livo, K. E. (2003), 'Mapping vegetation in Yellowstone National Park using spectral feature analysis of AVIRIS data', *Remote Sensing of Environment* **84**(3), 437-456.

Lamb, D. W.; Steyn-Ross, M.; Schaare, P.; Hanna, M. M.; Silvester, W. & Steyn-Ross, A. (2002), 'Estimating leaf nitrogen concentration in ryegrass (Lolium spp.) pasture using the chlorophyll red-edge: theoretical modelling and experimental observations', *International Journal of Remote Sensing* **23**(18), 3619-3648.

Lepedus, H.; Viljevac, M.; Cesar, V. & Ljubesic, N. (2005), 'Functioning of the photosynthetic apparatus under

low and high light conditions in chlorotic spruce needles as evaluated by in vivo chlorophyll fluorescence', *Russian Journal of Plant Physiology* **52**(2), 165-170.

Li, L.; Ustin, S. L. & Lay, M. (2005), 'Application of AVIRIS data in detection of oil-induced vegetation stress and cover change at Jornada, New Mexico', *Remote Sensing of Environment* **94**(1), 1-16.

LICHTENTHALER, H. K. (1987), 'Chlorophylls and Carotenoids - Pigments of Photosynthetic Biomembranes', *Methods In Enzymology* **148**, 350-382.

Maestri, E.; Marmiroli, M.; Visioli, G. & Marmiroli, N. (2010), 'Metal tolerance and hyperaccumulation: Costs and trade-offs between traits and environment', *Environmental and Experimental Botany* **68**(1), 1-13.

Montero, I. C.; Brimhall, G. H.; Alpers, C. N. & Swayze, G. A. (2005), 'Characterization of waste rock associated with acid drainage at the Penn Mine, California, by ground-based visible to short-wave infrared reflectance spectroscopy assisted by digital mapping', *Chemical Geology* **215**(1-4), 453-472.

Morris, R. V. (1998), 'Goldenrod pigments and the occurrence of hematite and possibly goethite in the Olympus-Amazonis region of Mars', *Icarus* **134**(1), 1-10.

MORRIS, R. V.; LAUER, H. V.; LAWSON, C. A.; GIBSON, E. K.; NACE, G. A. & STEWART, C. (1985), 'Spectral and Other Physicochemical Properties of Submicron Powders of Hematite (alpha-Fe_2o_3), Maghemite (gamma-fe2o3), Magnetite (fe3o4), Goethite (alpha-feooh), and Lepidocrocite (gamma-feooh)', *Journal of Geophysical Research-solid Earth and Planets* **90**(NB4), 3126-3144.

Nakaji, T.; Takeda, T.; Fujinuma, Y. & Oguma, H. (2005), 'Effect of autumn senescence on the relationship hetween the PRI and LUE of young Japanese larch trees', *Phyton-annales Rei Botanicae* **45**(4), 535-542.

RATHORE, C. S. & WRIGHT, R. (1993), 'Monitoring Environmental Impacts of Surface Coal-mining', *International Journal of Remote Sensing* **14**(6), 1021-1042.

ROSSMAN, G. R. (1976), 'Spectroscopic and Magnetic Studies of Ferric Iron Hydroxy Sulfates - Series Fe(oh)so4.nh2o and Jarosites', *American Mineralogist* **61**(5-6), 398-404.

ROSSMAN, G. R. (1975), 'Spectroscopic and Magnetic Studies of Ferric Iron Hydroxy Sulfates - Intensification of Color In Ferric Iron Clusters Bridged By A Single Hydroxide Ion', *American Mineralogist* **60**(7-8), 698-704.

Schaberg, P. G.; Murakami, P. F.; Turner, M. R.; Heitz, H. K. & Hawley, G. J. (2008), 'Association of red coloration with senescence of sugar maple leaves in autumn', *Trees-structure and Function* **22**(4), 573-578.

Seal, R. R.; Hammarstrom, J. M.; Foley, N. K. & Alpers, C. N. (2000), 'Geoenvironmental models for seafloor base- and precious-metal massive sulfide deposits', *Icard 2000, Vols I and Ii, Proceedings*, 151-160.

SHERMAN, D. M.; BURNS, R. G. & BURNS, V. M. (1982), 'Spectral Characteristics of the Iron-oxides With Application To the Martian Bright Region Mineralogy', *Journal of Geophysical Research* **87**(NB12), 169-180.

Sherman, D. M. & Waite, T. D. (1985), 'Electronic-spectra of Fe^{3+} Oxides and Oxide Hydroxides In the Near Ir To Near Uv', *American Mineralogist* **70**(11-12), 1262-1269.

Sirikulchayanon, P.; Sun, W. X. & Oyana, T. J. (2008), 'Assessing the impact of the 2004 tsunami on mangroves using remote sensing and GIS techniques', *International Journal of Remote Sensing* **29**(12), 3553-3576.

Stoffregen, R. E.; Alpers, C. N. & Jambor, J. L. (2000), 'Alunite-jarosite crystallography, thermodynamics, and geochronology', *Sulfate Minerals - Crystallography, Geochemistry and Environmental Significance* **40**, 453-479.

Swayze, G. A.; Smith, K. S.; Clark, R. N.; Sutley, S. J.; Pearson, R. M.; Vance, J. S.; Hageman, P. L.; Briggs, P. H.; Meier, A. L.; Singleton, M. J. & Roth, S. (2000), 'Using imaging spectroscopy to map acidic mine waste', *Environmental Science & Technology* **34**(1), 47-54.

Taran, M. N. & Rossman, G. R. (2002), 'High-temperature, high-pressure optical spectroscopic study of ferric-iron-bearing tourmaline', *American Mineralogist* **87**(8-9), 1148-1153.

van der Tol, C.; Verhoef, W.; Timmermans, J.; Verhoef, A. & Su, Z. (2009), 'An integrated model of soil-canopy spectral radiances, photosynthesis, fluorescence, temperature and energy balance', *Biogeosciences* **6**(12), 3109-3129.

USTIN, S. L. & CURTISS, B. (1990), 'Spectral Characteristics of Ozone-treated Conifers', *Environmental and Experimental Botany* **30**(3), 293-308.

Ustin, S. L.; Gitelson, A. A.; Jacquemoud, S.; Schaepman, M.; Asner, G. P.; Gamon, J. A. & Zarco-Tejada, P. (2009), 'Retrieval of foliar information about plant pigment systems from high resolution spectroscopy', *Remote Sensing of Environment* **113**, S67-S77.

Ustin, S. L.; Roberts, D. A.; Gamon, J. A.; Asner, G. P. & Green, R. O. (2004), 'Using imaging spectroscopy to study ecosystem processes and properties', *Bioscience* **54**(6), 523-534.

Van der Meer, F. & De Jong, S. M. (2000), 'Improving the results of spectral unmixing of Landsat Thematic Mapper imagery by enhancing the orthogonality of end-members', *International Journal of Remote Sensing* **21**(15), 2781-2797.

VANE, G. & GOETZ, A. F. H. (1993), 'Terrestrial Imaging Spectrometry - Current Status, Future-trends', *Remote Sensing of Environment* **44**(2-3), 117-126.

VERHOEF, W. (1984), 'Light-scattering By Leaf Layers With Application To Canopy Reflectance Modeling - the Sail Model', *Remote Sensing of Environment* **16**(2), 125-141.

Yang, X. H.; Huang, J. F.; Wang, X. Z. & Wang, F. M. (2008), 'The estimation model of rice leaf area index using hyperspectral data based on support vector machine', *Spectroscopy and Spectral Analysis* **28**(8), 1837-1841.

2. Application of high altitude and ground-based spectroradiometry to mapping hazardous low-pH materiál

Kopačková, V., Chevrel, S., Bourguignon, A., & Rojík, P., (2012): Application of high altitude and ground-based spectroradiometry to mapping hazardous low-pH material derived from the Sokolov open-pit mine, Journal of Maps, DOI:10.1080/17445647.2012.705544.

Abstract

Mineral spectroradiometry, both from airborne/spaceborne sensors and ground measurements, represents an alternative to conventional methods and an efficient way to characterize mines and assess the potential for AMD (Acid Mine Drainage) discharge. High-altitude spectroradiometry (ASTER - Advanced Spaceborne Thermal Emission and Reflection Radiometer satellite data) together with ground and laboratory-based spectroradiometry (ASD Filedspec spectroradiometer) were employed in order to identify the locations of the most significant sources of AMD discharge at the Sokolov lignite open-pit mines, Czech Republic. As a result, a map with delineated low-pH zones was created and validated by the ground truth data.

Key words: Acid Mine Drainage (AMD), spectroradiometry, ASTER, mining waste, Sokolov open-pit mine, mineral spectroscopy

2.1 Introduction

Mines (abandoned, still-active) are one of the most challenging environmental problems faced by governments, communities and the mining industry worldwide. The typical mineral acid mine drainage (AMD)/acid rock drainage (ARD) results in acid solutions discharged from the pyritic waste piles and the subsequent accumulation of secondary precipitates by hydrolysis reactions. Those processes lead to the accumulation of Fe minerals, where centres of such low-pH forming minerals as copiapite and jarosite (pH< 3) are surrounded successively by goethite and hematite, the minerals marking progressive increases in the pH (Swayze et al., 2000). Because of the lack of uniform legislative and economic strategies for management of mine waste, inadequate characterization of AMD, is a major obstacle to remediation of post-mining sites and complete inventorization and assessment of their environmental impacts are far from complete.

Numerous studies have demonstrated the high potential of the use of Hyperspectral (HS) data for diverse geological applications, such as mineral exploration (Rowan et al. 2000, Bedini et al. 2009), drill core analysis (Kruse et al. 1996, Bolin & Moon, 2003), hydrothermal alteration (Gersman et al., 2008) and geological mapping (Dadon et al., 2011). Mineral spectroscopy, both high and low altitude, represents an alternative to conventional methods (chemical analyses-based assessment tools, Gomes & Favas, 2006) and an efficient way to characterize mines and assess the potential for AMD discharge while focusing on minerals that serve as indicators of subaerial oxidation of pyrite ("hot spots") and the subsequent formation of AMD. HS data, both field and image data sets, were successfully utilized to identify AMD sources (Swayze et al., 2000, Montero et al., 2005) and to quantify heavy metal concentrations in acid surfaces (Choe et al., 2008; Kemper & Sommer, 2002; Kopačková et al., 2011; Pandit et al. 2010).

Nonetheless, valuable results can still be achieved using multispectral data (Robins et al., 2000). ASTER (Advanced Spaceborne Thermal Emission and Reflection Radiometer) (Abrams, 2000) is a spaceborn sensor that has frequently been used by the geologic remote sensing community because of its unique design. ASTER is designed with three bands in the visible/near-infra red (VNIR, a 15 m spatial resolution) and six bands in the short-wave infrared (SWIR, 30 m spatial resolution) spectral range, and it also has five thermal bands (TIR, 90 m spatial resolution). Although the ASTER data don't provide users with hundreds of narrow and contiguous spectral bands, the main advantage of hyperspectral remote sensing that allows quantitative analysis of surface components, this data still has a high potential to identify diverse minerals and map relative abundances (Van Der Meer at el.,

2012). The VNIR bands have been shown to be capable of mapping the relative abundances of iron oxides/hydroxides (Vicente & de Souza Filho, 2011), and SWIR bands can be used to separate advanced mineral groups including argillic minerals (kaolinite, alunite, dickite), phyllic alteration minerals (sericite) and propylitic minerals (calcite, epidote, chlorite) (Mars & Rowan, 2010).

In this study, we tested the ability to indentify sources of acidity using satellite ASTER data, as they represent an easily accessible and incomparably cheaper data source. In addition to conventionally used laboratory analyses, we utilized ground-based spectrometry and imaging spectroscopy, to assess the capability of these two techniques in mapping areas of high acidity in the Sokolov basin, as the pH is a predominant factor in heavy metal mobilization and distribution. More specifically, we investigated how the pH indicating minerals/components can be identified using ASTER optical (VNIR and SWIR) bands and how sub-pixel abundances can be spatially mapped.

2.2 Site description

The study was performed in the Sokolov basin in the western part of the Czech Republic (Fig. 2.1), in a region affected by long-term extensive lignite mining. The Sokolov basin, containing rocks of Oligocene to Miocene age, is 8 – 9 km wide and up to 36 km long, with a total area of about 200 km^2. The basin is limited by the Krušné Hory Fault (NNE-SSW trending) and is also characterized by a system of minor parallel faults, forming a significant tectonic zone of lithospheric extent (Ziegler, 1990). Another significant fault system of the Ohře Rift consists in the faults running in the NNW-SSE to NW-SE direction (Rajchl et al., 2009).

The basement of the Sokolov Basin is formed of Variscan and pre-Variscan metamorphic complexes of the Eger, Erzgebirge, Slavkov Forest, Thuring-Vogtland Crystalline Units and granitoids of the Karlovy Vary Pluton. The upper portions of these rocks are frequently weathered to kaolinitic residue. The basal late Eocene Staré-Sedlo-Formation is formed of well-sorted fluvial sandstones and conglomerates and is overlain by a volcano-sedimentary complex up to 350 m thick, which contains three lignite seams: the Josef seam (up to 20 m thick), the Anežka seam (5-12 m thick) and Antonín seam (20-30 m thick, reaching up to 62 m) (Rojík, 2004). The brown coal (lignite) contains 5 to 8% sulfur (S), and belongs among coal seams enriched in As (Yudovich and Ketreis, 2005) and other heavy metals, such as Cd, Ni, Cu, Zn, Pb (Bouška and Pešek, 1999).

Dumped material consists mostly of Cypris clays, which can be characterized as well-laminated clays with different varieties of mineralogical composition: kaolinite, montmorillonite, illite with

admixtures of Ca-Mg-Fe carbonates, sulphates, sulphides, analcite, Mg-micas and bitumen (Rojík, 2004). Due to the presence of S in the coal, the lignite mines both still active and abandoned, are largely affected by acid mine drainage (AMD) (Kopačkova et al., 2011).

2.3 Data

2.3.1 Material sampling and analysis

Over 60 points (Fig. 2.1) distributed in still-active (Jiří, Medard and Družba) and abandoned (Lítov, Lomnice, Sylvestr and PVS - Podkrušnohorská výsypka) open-pit mines were documented in the field. Particular attention was paid to the abandoned mines with significant AMD-affected areas. At the sampling points spectroradiometric measurements were collected in natural illumination conditions using an ASD FieldSpec 3® portable spectroradiometer (in situ spectroscopy measurements). The ASD instrument uses three separate spectrometers to measure the radiance between wavelengths of 0.350 µm and 2.500 µm. Radiance spectra were normalized against a 99% Spectralon® white reference to produce relative reflectance spectra for each measurement. The spectra for each point represented an average calculated from at least three point measurements distributed within petrologically homogenous material.

Samples of the surface material (0-1 cm depth) reflecting all the major mineral varieties were collected at selected points (in total 57 samples). They were dried and sieved to < 2 mm, and the abundance of trace elements including major heavy metals was measured using a portable Innov-x Alpha RFA spectrometer. Furthermore, the samples were subjected to selected X-Ray Diffraction analysis and determination of laboratory pH, sulphur (S total wt %), and Total Organic Carbon (TOC_%).

In the Laboratory, further spectra were obtained by measuring the samples of all the facies encountered in the Sokolov basin in artificial illumination conditions, using the spectroradiometer's contact probe (laboratory spectroscopy measurements).

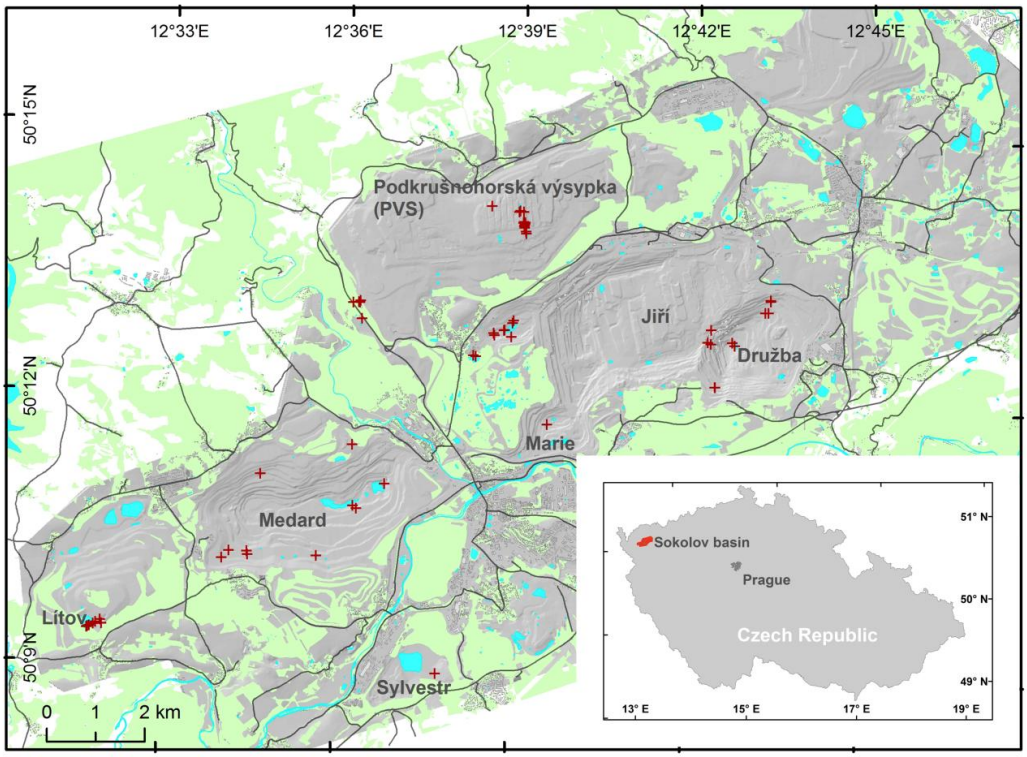

Figure 2.1: *Topographic scheme of the Sokolov mining area, Czech Republic, showing main pit lakes, dump areas, and sampling points (green – vegetation based on the 1: 10,000 topographic map).*

2.3.2 ASTER image data

ASTER covers a wide spectral region with 14 bands from the visible to the thermal infrared. In our study, we worked with 9 bands covering the visible (VIS), near infrared (NIR) and short wave infrared (SWIR) spectral regions. The available cloudless ASTER image (acquisition date 2004-09-19, 1B processing level) has been corrected for atmospheric effects using ATCOR 2 software. The best result was achieved using the following setting:

- Middle latitude summer rural type of atmosphere was chosen
- Aster metafile was used to set up the calibration coefficients (Bias [c0] and Gain [c1]) for each band
- The in-flight calibration method was employed using the tuff spectrum

Conversion of data from radiance to reflectance enabled comparison of the image spectra with the reference spectral libraries, once the latter were resampled to the ASTER spectral range and bands.

For the further analysis, the water bodies and vegetated areas were masked out by calculating the NDVI and thresholding the NDVI image values. The following analysis was performed only on the surface with no or sparse vegetation cover and outside of water bodies (0.0 <NDVI <0.4).

2.4 Methods

2.4.1 Spectral libraries

Spectra conducted with the ASD spectrometer during the field campaign and in the laboratory were re-sampled to the ASTER band wavelength. For these spectra, we obtained XRD analysis to elucidate the mineralogy. It was then possible to study the spectral absorption features of the variables (AMD indicating minerals, lignite abundance, clay minerals) and the feasibility of detecting them using an ASTER satellite image.

2.4.2 ASTER end-member definition and image unmixing

In the Sokolov basin, the anthropogenic materials exhibited extreme heterogeneity (Kopačková et al., 2009), especially jarosite was present in the site material as a secondary or accessory mineral. Lignite was found to have major abundances and was also found in all the possible forms of mixtures with other minerals.

In the case of the ASTER satellite data (spatial resolution of 15 and 30 m in the VNIR and SWIR region, respectively), the majority of the pixels were spectral mixtures of diverse minerals. Therefore, prior to material mapping, it was necessary to derive the pure end members for the fundamental physical components (mineral/organic constituents).

Pure end-member spectra can be extracted either directly from image pixels of known target materials or from spectral libraries measured in the field. The use of reflectance end members from spectral libraries can be problematic because they can suffer mainly from spatial and temporal variability in the reflectance properties of the cover types (Asner & Heidebrecht, 2002). The second approach is more realistic, as end-member spectra are derived directly from the image by extracting the reflectance from relatively pure pixels. Taking in account the spatial resolution of the ASTER data (15-30 m) and the fact that the ASTER image and spectral libraries were not acquired simultaneously, we decided to use the image-derived end members for further image processing. The method consisting of the Minimum Noise Fraction transformation (MNF) (Boardman & Kruse, 1994; Green et al., 1988) and Pixel Purity Index (PPI) (Boardman et al., 1995) procedures was employed to select the

"pure" image end members. In this routine, the image data are subjected to spectral and spatial reduction in order to identify the end members of spectrally unique pixels which are assumed to be the most pure pixels.

The MNF uses two opposite orthogonal linear transformations based on Principal Components Analysis (PCA) to reduce the inter-band correlation and isolate noise. The MNF transformation allows not only reduction of the data dimensionality which is required mainly for hyperspectral image datasets, but also estimation of the noise level in the data. Similarly to Vincente and de Souza Filho (2011), we used the MNF transformation to reduce possible sets of end members that can be separated and expressed in the set of MNF images (9 MNF bands can be calculated in case of using the ASTER VNIR-SWIR bands).

The PPI procedure randomly and repeatedly reprojects a pixel's array into an n-dimensional scatter plot arrangement using a vector unit. The pixels in the extreme position in each projection are recorded. These pixels are assumed to be spectrally unique and „pure" and are therefore called end members, and their reflectance property is used for further material mapping in the image data.

After inspection of the image-derived end members and their comparison with the measured spectra of the samples with known mineralogy (identified by XRD), we were able to identify the image end members that characterized the fundamental mineral components of the Sokolov mining dump surfaces (Fig. 2.4): lignite, clay, jarosite and goethite.

To relatively estimate the selected end-member abundances it was highly desirable to use a sub-pixel method rather than hard classifier (e.g., Spectral Angle Mapper (SAM); Kruse et al., 1993) while taking into account the extreme heterogeneity of the Sokolov surfaces and diverse material mixing level present in the ASTER pixels. Therefore we took advantage of the linear spectral unmixing (LSU) (Settle and Drake, 1993) method, as it allows identification of sub-components of the spectrum and determination of the abundance of different materials for each pixel.

Although this method was designed primarily for hyperspectral image data analysis, it has frequently been used even for mapping sub-pixel abundances using multispectral data (Dawelbait & Morari, 2012; Parente et al., 2009; Pacheco & McNairn, 2010; Shanmugam et al., 2006; Vicente & de Souza Filho, 2011). The only condition is that the number of derived fractions (end members) is equal to or less than the number of bands. Spectral mixture analysis is also based on the principle that the reflectance recorded for each pixel within an image is a combination of the reflectance from all the

pure end members found in that image. This condition cannot be fulfilled in work with multispectral images. However, our analysis is based on the assumption that linear mixing is a sufficient first order approximation to constrain the mineralogy but not the absolute abundances of the selected indicative minerals discussed here. To derive abundance images constrained linear unmixing was computed in the ENVI software. Constrained unmixing assumes that the sum of the fractions is one and that each fraction is greater than or equal to zero (Bateson & Curtiss, 1996; Dennison & Roberts, 2003). The output is a fraction image, with coefficients lying between 0 and 1 and summing to 1, for each end member along with an image containing an error of fit.

2.5 Results

2.5.1 Linking sample' pH and mineralogy

The typical AMD pattern leads to accumulation of Fe sulfates, oxy-hydroxides and oxides in a spatial and temporal sequence that represents the buffering of an acidic solution as it moves away from its source (Swayze et al., 2000). Spectroscopic AMD approaches are based on the mapping of those minerals that occur on the surface of waste-rock piles and their surroundings, focusing on minerals that serve as indicators of sub-aerial oxidation of pyrite ("hot spots") and the subsequent formation of AMD (Montenero et al., 2005; Swayze et al., 2000).

Studying the results of the chemical/mineral analysis, two AMD scenarios were found (Fig.2). Very low to low pH characterized (i) material rich in lignite (2.5 <pH <3.9) and (ii) material with the presence of jarosite as a part of a mixture (1.8 <pH <2.8). Montero et al. (2005) obtained similar results and found that jarosite is present near the source of the acidity and that it is formed at pH values <3. On the other hand, Montero et al. (2005) found that goethite is formed at pH values generally less than 6. In our case goethite was present as part of a mixture throughout a wide pH range (3.0 <pH <8.5) and thus this mineral, by itself, did not indicate any specific pH value (Fig. 2.2). Based on these findings, we selected lignite and jarosite, the constituents present in the material with very low to low pH, to be indicators of the material that needs closer examination and should thus be spatially mapped.

2.5.2 Spectral characteristics of the selected minerals/constituents

Clay minerals (e.g., kaolinite,illite) display combinations of an Al–OH bend overtone and an OH stretch (Clark et al., 1990) that arise within an edge-sharing $Al(OH)_6$ octahedral layer (gibbsite layer) linked to sheets of SiO_4 tetrahedra. In case of kaolinite, the most common clay mineral found in the

surface material of the Sokolov basin, the vibration of the Al–OH molecule create double absorption features around 2.1 and 2.2 µm. The strong absorption feature at 2.206 µm can be detected using ASTER band 6 (Fig 3). Additionally, OH vibration stretch overtones create another doublet near 1.4 µm, but ASTER spectral resolution does not allow detection of this absorption (Fig. 2.3).

In accordance with other studies (Montero et al., 2005), *iron oxy-hydroxides (e.g., goethite, hematite, ferrihydrite)* exhibited diagnostic absorption before 1.000 µm. The wavelengths and intensities of the absorption features in this region depend on the nature of the crystal field around the Fe atom and on the nature of the bonds around it, because the nature of the magnetic coupling between the $Fe3^{+}$ ions (as influenced by the crystal field) facilitates the transition of electrons between energy states (Sherman & Waite, 1985). Thus, in $Fe3^{+}$ minerals, subtle differences in the shapes and wavelengths of the absorption features reflect the crystal structure of the minerals and allow their identification (Montero et al., 2005). Goethite was found to be the most frequent iron oxy-hydroxide identified in the samples and exhibited strong absorption around 0.500 µm, but this absorption cannot be detected using the ASTER data. However, ASTER spectral resolution allows detection of the other absorption features – less distinctive absorption around 0.660 µm (ASTER band 2) and a broad asymmetric absorption between 0.90 and 1.00 µm (ASTER band 3).

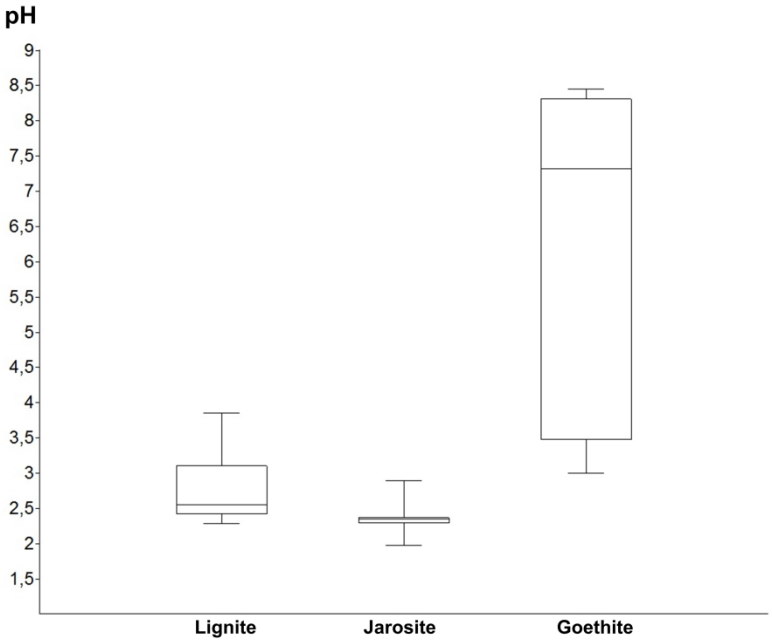

Figure 2.2: *Box plots of the pH values of the material with the presence of lignite, jarosite and goethite.*

Jarosite, similar to other *hydroxysulfates (e.g., schwertmannite, copiapite)* and iron *oxy-hydroxides*, exhibits diagnostic absorption before 1.000 µm (Montero et al., 2005), and additionally exhibits an absorption feature between 2.2 -2.3 µm (Fig. 2.3). After resampling the spectra to ASTER band resolution, jarosite and the associated mineral spectra still exhibit diagnostic absorption round 0.90 µm (ASTER band 3) and a supplementary typical absorption feature at 2.262 µm (ASTER band 7) (Fig. 2.3).

As already mentioned above, *goethite* and *jarosite* both exhibit a diagnostic absorption feature before 1.000 µm. However, jarosite has an absorption maximum at shorter wavelengths (at approximately 0.910 µm, Fig. 2.3) than goethite (approximately at 0.950 µm). After resampling the spectra of these two minerals to ASTER spectral resolution, we can see different trends between bands 2 (central wavelength at 0.661 µm) and 3 (central wavelength at 0.807 µm). As goethite has its absorption maximum shifted to longer wavelengths, there is still a steep increasing slope between bands numbers 2 and 3. On the other hand, jarosite, which has an absorption maximum close to the central wavelength of band 3, exhibits a rather flat or decreasing trend between these two bands (Fig. 2.3).

Material with high *lignite* content (> 5 %) exhibited a characteristic, very small slope of the spectral curve between 0.800 – 1.200 µm (Fig. 2.3) with an absorption maximum at approximately 0.640 µm. This trend can also be observed after resampling to ASTER spectral resolution, as the slope between ASTER bands 1, 2, 3 and 4 is similarly very small. In addition, absorption was identified at 2.309 µm, indicating humic acid (Ben-Dor & Chen, 1997). In ASTER resolution, the humic acid content affects the slope between bands 7 and 8 (Fig. 2.3).

2.5.3 End-member mapping using ASTER image data

By inspecting the spectral libraries, both low-pH indicators, jarosite and lignite, were clearly identified as part of the AMD material, which is generally formed at pH below 4.0. Furthermore, their equivalent end members were successfully derived from the ASTER image data (image end-members, Fig. 2.4). In accordance with the lab/field spectral libraries, image-derived end-members exhibited the opposite trends between ASTER bands 2 and 3 for goethite (steep and increasing trend) and jarosite (decreasing trend). Lignite exhibited the typical low reflectance and characteristic small slope between bands 1 and 2. Clay exhibited a distinct absorption feature at 2.206 µm (ASTER band 6). In the SWIR2 region, all the image-derived end¨members had clay (2.206 µm) absorption predominating over the other less prominent absorptions (jarosite: 2.263 µm and lignite: 2.309 µm).

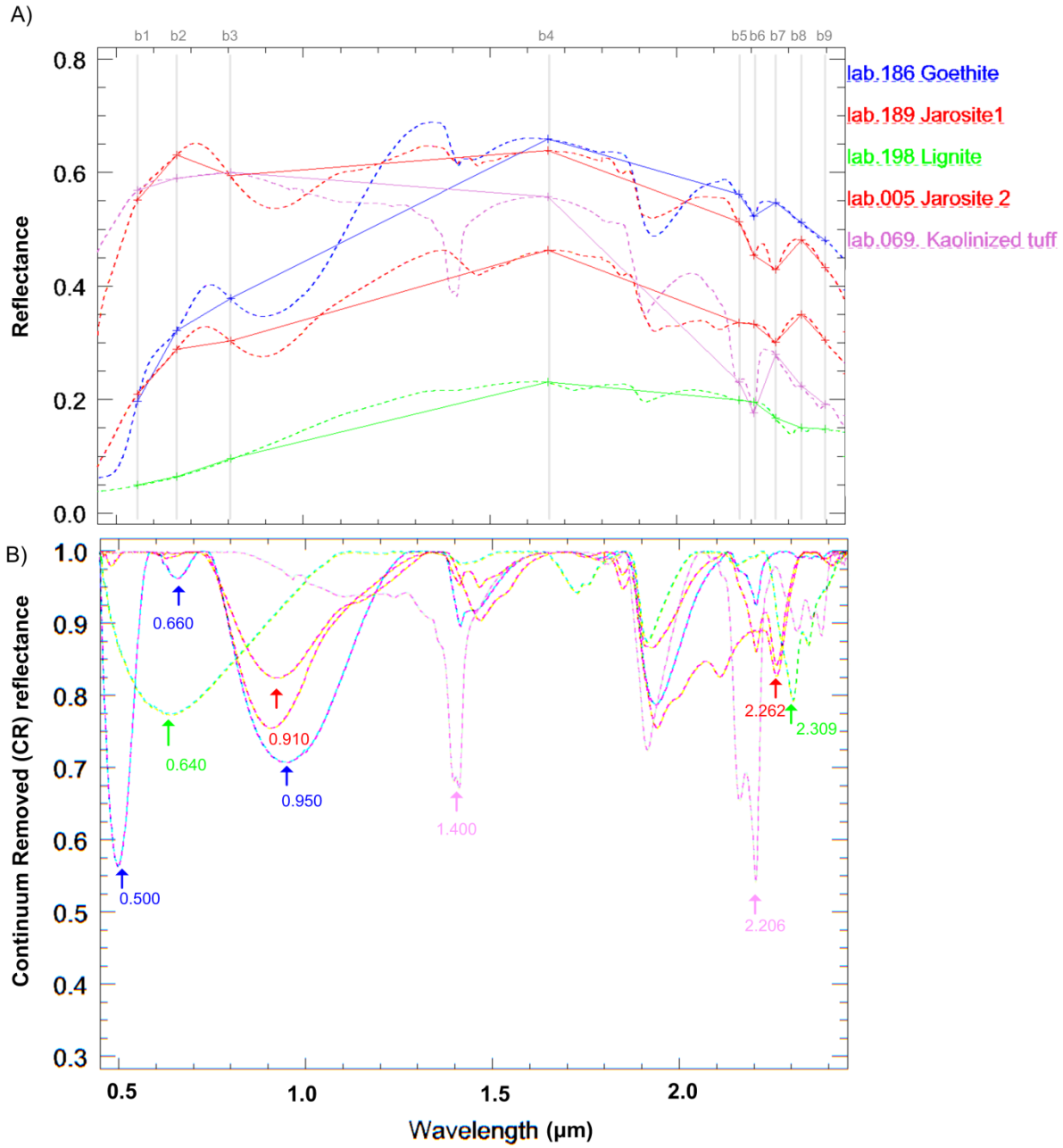

Figure 2.3: *A) Diagnostic absorption features of jarosite-rich material compared to the material rich in iron oxy-hydroxides, kaolinite and lignite. ASTER resampled spectra are plotted together with the full spectra acquired with the ASD FieldSpec 3® spectroradiometer. B) Laboratory continuum-removed (CR, Clark & Roush 1984, Kruse et al. 1993) spectra of the selected end members.*

This can be explained by rather coarse spatial resolution of ASTER data and a high degree of material heterogeneity. Clays (mainly kaolinite) were identified as minerals with major abundances in most of the samples collected in the field; thus the other, less distinctive SWIR absorptions indicating jarosite or lignite could not be identified using ASTER image data. However, all four image end members exhibited large enough differences in the spectral range between 0.5 and 1.5 µm (Fig. 2.4).

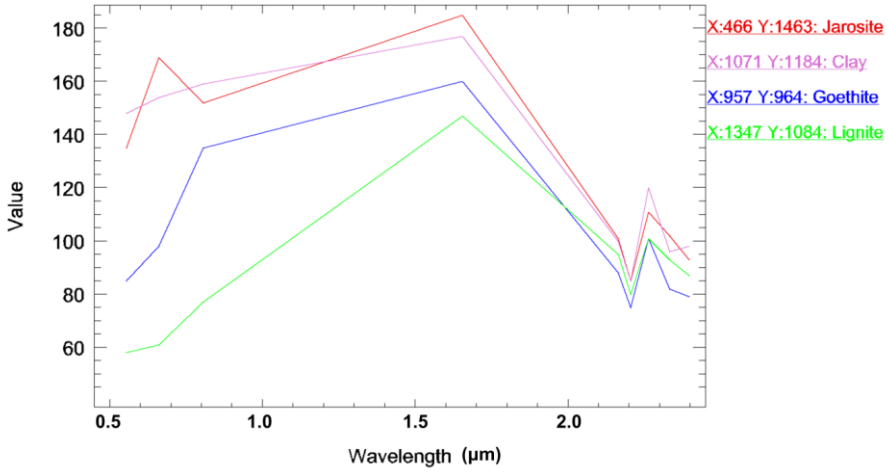

Figure 2.4: *Image-derived end-members used for further unmixing.*

The relative abundance maps of the major end-members (jarosite, clay, goethite and lignite) were calculated via applying linear unmixing. However, as only two of them can clearly indicate low pH, the jarosite and lignite abundance maps were further statistically classified using the standard deviation classification system after image unmixing. Generally, this classification expresses how much the particular value varies from the mean, respectively how far from the mean the particular value is in terms of the standard deviations (σ). The mean values and the standard deviations from the mean (σ) were calculated for the jarosite and lignite abundance maps. As a result, the low pH zones from both abundance maps were delineated as the mean + 1 σ. Matrix analysis was employed to create a single map from these two datasets. Matrix analysis yielded a new thematic map that contained separate classes for (i) a low pH zone with an abundance of jarosite, (ii) a low pH zone with an abundance of lignite, and (iii) a low pH zone with an abundance of jarosite and lignite (Fig. 2.5).

2.5.4 Map validation

The map associated with this article was validated using the ground truth (57 pH measurements). As it was not possible to derive a pH map from the ASTER image, we could not validate the map by comparing the pH pixel values directly with the pH in situ measurements. Our goal was to identify the low-pH zones and therefore the validation was performed in the following way. The in-situ pH measurements were classified into two classes: class 1 (pH< 4.0) and class 2 (pH>4.0) and the ground truth Regions of Interest (ROI's) were then created. Similarly, the map was reclassified into two classes: class 1 (delineated low pH zones) and class 2 (the other pixels). The confusion matrix

(Congalton, 1991) was then calculated to show how well the pixels of the final map with delineated low pH zones match the ground truth data.

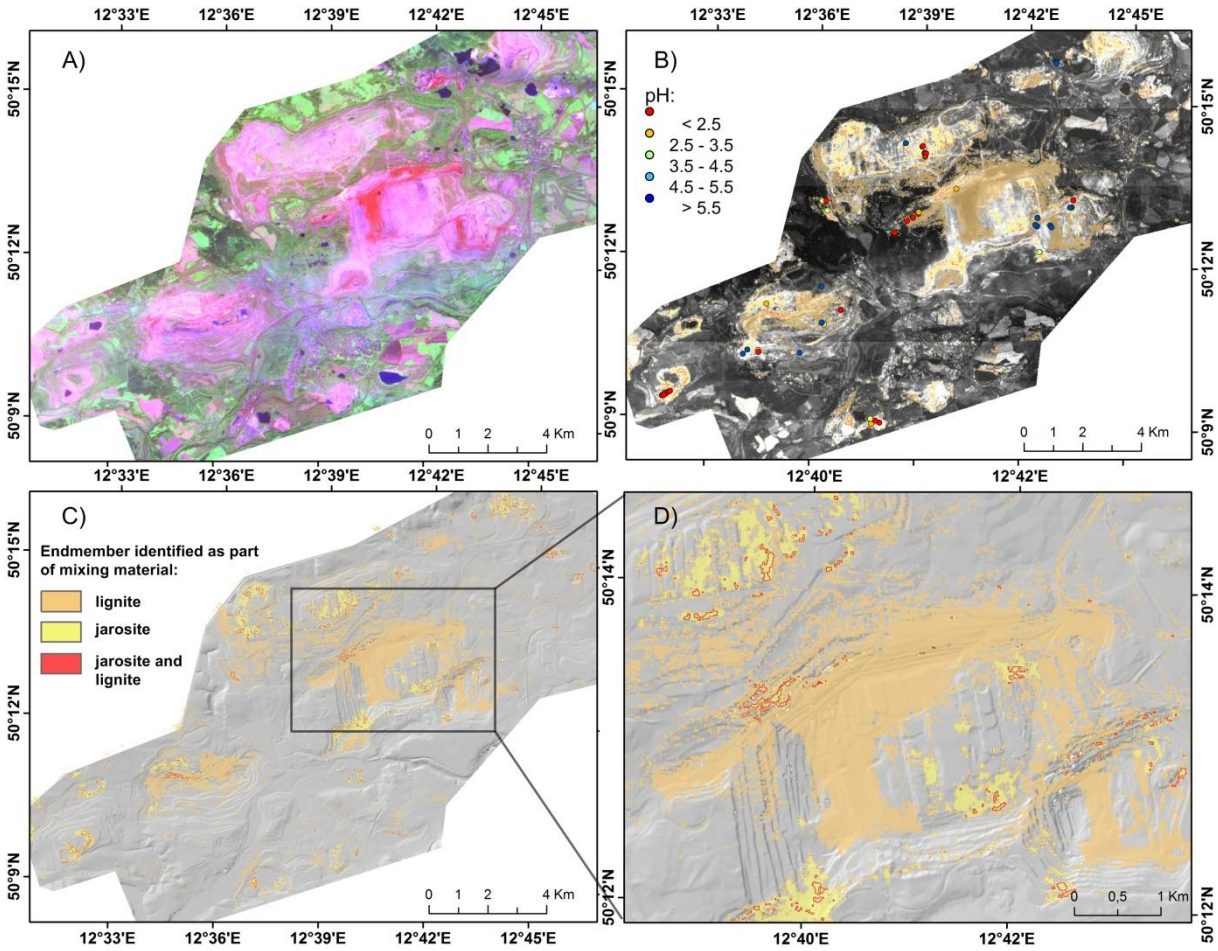

Figure 2.5: *A): Aster image, bands 6, 3, 1 as RGB. B): pH sampling points used for validation. C, D): Result of the spectral unmixing.*

Table 2.1: *Confusion matrix statistics*

Class	Producer accuracy (%)	User accuracy (%)	Producer accuracy (Pixels)	User accuracy (Pixels)
Class1 (pH< 4.0)	70.83	70.83	17/24	17/24
Class2 (pH>4.0)	78.13	78.13	25/32	25/32
Overall Accuracy	(42/56) 75.00%			
Kappa Coefficient	0.45			

2.6 Conclusions

The VNIR-SWIR spectral region provides valuable information on diverse material properties, which cannot be acquired using any other conventional field/laboratory method. The spectral property of both constituents, jarosite (AMD indicating mineral) and lignite (the organic component) occurring as part of mixtures, can be identified using ground/laboratory-based and imaging spectroscopy (ASTER). The map with the low pH zones delineated, the result of ASTER image unmixing, achieved sufficient overall accuracy (75%), especially if we take in account the high dynamics of the mining environment and the fact that the ASTER data were acquired in 2004 and the ground truth data were collected in 2009. Our study shows the high potential of multispectral data such as ASTER in the field of mapping and monitoring the hazardous wastes from mining activities. This kind of maps, especially if the method is applied as multi-temporal approach, could be useful for land-use planners and local authorities, as well as for the mining company itself, as the company is responsible for successful reclaiming of abandoned mines and environmental monitoring of mines in general.

Acknowledgements

The present research is being undertaken within the framework of Grant No. 205/09/1989. The authors would like to thank Sokolovská uhelná mining company for its strong support for this project, in particular in organizing field visits and providing the technical assistance of several specialists and logistics during these visits, including authorizations to access mine sites. We are also grateful for the comments of Dr. Berg, Dr. Slonecker and Prof. Deroin, whose reviews helped improve the quality of the manuscript and Dr. Siegel for his suggestions on how to improve the cartographic design.

References

Abrams, M. (2000), 'The Advanced Spaceborne Thermal Emission and Reflection Radiometer (ASTER): Data products for the high spatial resolution imager on NASA's Terra platform', *International Journal of Remote Sensing* **21**(5), 847-859.

Asner, G. P. & Heidebrecht, K. B. (2002), 'Spectral unmixing of vegetation, soil and dry carbon cover in arid regions: comparing multispectral and hyperspectral observations', *International Journal of Remote Sensing* **23**(19), 3939-3958.

Bateson, A. & Curtiss, B. (1996), 'A method for manual endmember selection and spectral unmixing', *Remote Sensing of Environment* **55**(3), 229-243.

Bedini, E.; van der Meer, F. & van Ruitenbeek, F. (2009), 'Use of HyMap imaging spectrometer data to map mineralogy in the Rodalquilar caldera, southeast Spain', *International Journal of Remote Sensing* **30**(2), 327-348.

Ben-Dor, E.; Inbar, Y. & Chen, Y. (1997), 'The reflectance spectra of organic matter in the visible near-infrared and short wave infrared region (400–2500 nm) during a controlled decomposition process', *Remote Sensing of Environment* **61**(1), 1-15.

Boardman, J. W. (1995), 'Analysis, understanding and visualization of hyperspectral data as convex sets in n-space', *Imaging Spectrometry* **2480**, 14-22.

Boardman, J. W. & Kruse, F. A. (1994), 'Automated Spectral Analysis - A Geological Example Using Aviris Data, North Grapevine Mountains, Nevada', *Proceedings of the Tenth Thematic Conference On Geologic Remote Sensing - Exploration, Environment, and Engineering, Vol I*, I407-I418.

Bolin, B. J. & Moon, T. S. (2003), 'Sulfide detection in drill core from the Stillwater Complex using visible/near-infrared imaging spectroscopy', *Geophysics* **68**(5), 1561-1568.

Bouska, V. & Pesek, J. (1999), 'Quality parameters of lignite of the North Bohemian Basin in the Czech Republic in comparison with the world average lignite', *International Journal of Coal Geology* **40**(2-3), 211-235.

Chevrel, S.; Kopačková, V.; Bourguignon, A.; Rojik, P. & Metelka, V. (2008), 'Monitoring Hazardous Wastes Using Space-borne and Ground-based Spectroradiometry - Sokolov Lignite Mines (Czech Republic)', *in* Weiersbye I. Dye P. Fourrier A., Tibbet M., ed., 'Mine Closure 2008', Australian Centre for Geomechanics, 651-662.

Chevrel, S.; Kopačková, V.; Bourguignon, A.; Rojik, P. & Metelka, V. (2008), 'Application of High Altitude and Ground-based Spectroradiometry in the Monitoring of Hazardous Waste Derived from Sokolov Open-pit Mine', *Mine Water and the Environment, Proceedings*, 371-374.

Choe, E.; van der Meer, F.; van Ruitenbeek, F.; van der Werff, H.; de Smeth, B. & Kim, Y. W. (2008), 'Mapping of heavy metal pollution in stream sediments using combined geochemistry, field spectroscopy, and hyperspectral remote sensing: A case study of the Rodalquilar mining area, SE Spain', *Remote Sensing of Environment* **112**(7), 3222-3233.

Clark, R. N. & Roush, T. L. (1984), 'Reflectance Spectroscopy - Quantitative-analysis Techniques For Remote-sensing Applications', *Journal of Geophysical Research* **89**(NB7), 6329-6340.

Clark, R. N., R. N.; King, T. V. V.; Klejwa, M.; Swayze, G. A. & Vergo, N. (1990), 'High Spectral Resolution Reflectance Spectroscopy of Minerals', *Journal of Geophysical Research-solid Earth and Planets* **95**(B8), 12653-12680.

Congalton, R. G. (1991), 'A Review of Assessing the Accuracy of Classifications of Remotely Sensed Data',

Remote Sensing of Environment **37**(1), 35-46.

Dadon, A.; Ben-Dor, E.; Beyth, M. & Karnieli, A. (2011), 'Examination of spaceborne imaging spectroscopy data utility for stratigraphic and lithologic mapping', *Journal of Applied Remote Sensing* **5**, 053507.

Dawelbait, M. & Morari, F. (2012), 'Monitoring desertification in a Savannah region in Sudan using Landsat images and spectral mixture analysis', *Journal of Arid Environments* **80**, 45-55.

Dennison, P. E. & Roberts, D. A. (2003), 'The effects of vegetation phenology on endmember selection and species mapping in southern California chaparral', *Remote Sensing of Environment* **87**(2-3), 295-309.

Gersman, R.; Ben-Dor, E.; Beyth, M.; Avigad, D.; Abraha, M. & Kibreab, A. (2008), 'Mapping of hydrothermally altered rocks by the EO-1 Hyperion sensor, Northern Danakil Depression, Eritrea', *International Journal of Remote Sensing* **29**(13), 3911-3936.

Gomes, M. E. P. & Favas, P. J. C. (2006), 'Mineralogical controls on mine drainage of the abandoned Ervedosa tin mine in north-eastern Portugal', *Applied Geochemistry* **21**(8), 1322-1334.

Green, A. A.; Berman, M.; Switzer, P. & Craig, M. D. (1988), 'A Transformation For Ordering Multispectral Data In Terms of Image Quality With Implications For Noise Removal', *Ieee Transactions On Geoscience and Remote Sensing* **26**(1), 65-74.

Kemper, T. & Sommer, S. (2002), 'Estimate of heavy metal contamination in soils after a mining accident using reflectance spectroscopy', *Environmental Science & Technology* **36**(12), 2742-2747.

Kopačková, V.; Bourguignon, A.; Chevrel, S.and Koubová, M. & Rojík, P. (2009), 'Effect of mineralogical and geochemical properties on reflectance properties of waste from Sokolov open pit lignite mine, Czech Republic', *in* M. Tibbett A.B. Fourie, ed., 'Mine Closure 2009', Australian Centre for Geomechanics, 569-580.

Kopačková, V.; Chevrel, S. & Bourguignon, A. (2011), 'Spectroscopy as a tool for geochemical modeling', *Proc. SPIE* **8181**, 818106.

Kruse, F. A. (1996), 'Identification and mapping of minerals in drill core using hyperspectral image analysis of infrared reflectance spectra', *International Journal of Remote Sensing* **17**(9), 1623-1632.

Kruse, F. A.; Lefkoff, A. B.; Boardman, J. W.; Heidebrecht, K. B.; Shapiro, A. T.; Barloon, P. J. & Goetz, A. F. H. (1993), 'The Spectral Image-processing System (sips) - Interactive Visualization and Analysis of Imaging Spectrometer Data', *Remote Sensing of Environment* **44**(2-3), 145-163.

Mars, J. C. & Rowan, L. C. (2010), 'Spectral assessment of new ASTER SWIR surface reflectance data products for spectroscopic mapping of rocks and minerals', *Remote Sensing of Environment* **114**(9), 2011-2025.

Montero, I. C.; Brimhall, G. H.; Alpers, C. N. & Swayze, G. A. (2005), 'Characterization of waste rock associated with acid drainage at the Penn Mine, California, by ground-based visible to short-wave infrared reflectance spectroscopy assisted by digital mapping', *Chemical Geology* **215**(1-4), 453-472.

Murad, E. & Rojik, P. (2005), 'Iron mineralogy of mine-drainage precipitates as environmental indicators: review of current concepts and a case study from the Sokolov Basin, Czech Republic', *Clay Minerals* **40**(4), 427-440.

Pacheco, A. & McNairn, H. (2010), 'Evaluating multispectral remote sensing and spectral unmixing analysis for crop residue mapping', *Remote Sensing of Environment* **114**(10), 2219-2228.

Pandit, C. M.; Filippelli, G. M. & Li, L. (2010), 'Estimation of heavy-metal contamination in soil using reflectance spectroscopy and partial least-squares regression', *International Journal of Remote Sensing* **31**(15), 4111-4123.

Parente, M.; Bishop, J. L. & Bell, J. F. (2009), 'Spectral unmixing for mineral identification in pancam images of soils in Gusev crater, Mars', *Icarus* **203**(2), 421-436.

Rajchl, M.; Ulicny, D.; Grygar, R. & Mach, K. (2009), 'Evolution of basin architecture in an incipient continental rift: the Cenozoic Most Basin, Eger Graben (Central Europe)', *Basin Research* **21**(3), 269-294.

Robbins, E. I.; Anderson, J. E.; Cravotta, C. A.; Nord, G. L. & Slonecker, E. T. (2000), 'Remotely-sensed multispectral reflectance variations in acidic versus near-neutral contaminated coal mine drainage in Pennsylvania', *Icard 2000, Vols I and Ii, Proceedings*, 1551-1561.

Rojík, P. (2004), 'New stratigraphic subdivision of the Tertiary in the Sokolov Basin in Northwestern Bohemia', *Journal of the Czech Geological Society* **49/3-4**, 173-185.

Rowan, L. C.; Crowley, J. K.; Schmidt, R. G.; Ager, C. M. & Mars, J. C. (2000), 'Mapping hydrothermally altered rocks by analyzing hyperspectral image (AVLRIS) data of forested areas in the Southeastern United States', *Journal of Geochemical Exploration* **68**(3), 145-166.

Settle, J. J. & Drake, N. A. (1993), 'Linear Mixing and the Estimation of Ground Cover Proportions', *International Journal of Remote Sensing* **14**(6), 1159-1177.

Shanmugam, P.; Ahn, Y. H. & Sanjeevi, S. (2006), 'A comparison of the classification of wetland characteristics by linear spectral mixture modelling and traditional hard classifiers on multispectral remotely sensed imagery in southern India', *Ecological Modelling* **194**(4), 379-394.

Sherman, D. M. & Waite, T. D. (1985), 'Electronic-spectra of Fe-3+ Oxides and Oxide Hydroxides In the Near Ir To Near Uv', *American Mineralogist* **70**(11-12), 1262-1269.

Swayze, G. A.; Smith, K. S.; Clark, R. N.; Sutley, S. J.; Pearson, R. M.; Vance, J. S.; Hageman, P. L.; Briggs, P. H.; Meier, A. L.; Singleton, M. J. & Roth, S. (2000), 'Using imaging spectroscopy to map acidic mine waste', *Environmental Science & Technology* **34**(1), 47-54.

Van der Meer, F. D.; van der Werff, H. M. A.; van Ruitenbeek, F. J. A.; Hecker, C. A.; Bakker, W. H.; Noomen, M. F.; van der Meijde, M.; Carranza, E. J. M.; de Smeth, J. B. & Woldai, T. (2012), 'Multi- and hyperspectral geologic remote sensing: A review', *International Journal of Applied Earth Observation and Geoinformation* **14**(1), 112-128.

Van der Meer, F. (2004), 'Analysis of spectral absorption features in hyperspectral imagery', *International Journal of Applied Earth Observation and Geoinformation* **5**, 55-68.

Vicente, L. E. & de Souza Filho, C. R. (2011), 'Identification of mineral components in tropical soils using reflectance spectroscopy and advanced spaceborne thermal emission and reflection radiometer (ASTER) data', *Remote Sensing of Environment* **115**(8), 1824-1836.

Yamaguchi, Y. & Naito, C. (2003), 'Spectral indices for lithologic discrimination and mapping by using the ASTER SWIR bands', *International Journal of Remote Sensing* **24**(22), 4311-4323.

Yudovich, Y. E. & Ketris, M. P. (2005), 'Arsenic in coal: a review', *International Journal of Coal Geology* **61**(3-4), 141-196.

Ziegler, P. A. (1990), 'Collision Related Intra-plate Compression Deformations In Western and Central-europe', *Journal of Geodynamics* **11**(4), 357-388.

3. Using multiple spectral feature analysis for quantitative pH mapping in a mining environment

Kopačková, V., (submitted for International Journal of Applied Earth Observation and Geoinformation): Using multiple spectral feature analysis for quantitative pH mapping in a mining environment.

Abstract

The pH is one of the major chemical parameters affecting the results of remediation programs carried out at abandoned mines and dumps and one of the major parameters controlling heavy metal mobilization and speciation. This study is concerned with testing the feasibility of estimating surface pH on the basis of airborne hyperspectral (HS) data (HyMap). The work was carried on the Sokolov lignite mine, as it represents a site with extreme material heterogeneity and high pH gradients. First, a geochemical conceptual model of the site was defined. Pyrite, jarosite or lignite were the diagnostic minerals of very low pH (<3.0), jarosite in association with goethite indicated increased pH (3.0-6.5) and goethite alone characterized nearly neutral or higher pH (>6.5). It was found that these minerals have absorption feature parameters which are common for both forms, individual minerals as well as parts of the mixtures, while the shift to longer wavelengths of the absorption maximum centered between 0.90-1.00 µm is the main parameter that allows differentiation among the Fe^{3+} secondary minerals. The Multi Range Spectral Feature Fitting (MRSFF) technique was employed to map the defined end-members indicating certain pH ranges in the HS image datasets. This technique was found to be sensitive enough to assess differences in the desired spectral parameters (e.g., absorption maximum wavelength position, absorption depth). Furthermore, the regression model using the fit images, the results of MRSFF, as inputs was constructed to estimate the surface pH and statistical significant accuracy was attained (R^2=0.61, Rv^2=0.76). This study represents one of the very first approaches employing image spectroscopy for quantitative pH modeling in a mining environment and the achieved results demonstrate the potential application of hyperspectral remote sensing as an efficient method for environmental monitoring.

Key words: *Acid Mine Drainage (AMD), pH modeling, mineral spectroscopy, mining impacts, environmental monitoring, Multiple Spectral Feature Fitting*

3.1 Introduction

Mining activities, both underground and open cast mining, are still associated with many environmental problems such as Acid Mine Drainage (AMD) (Akcil et al., 2006), generation of large quantities of toxic substances (Kemper and Sommer, 2003) and consequent release of heavy metals into the environment (Gomes and Favas, 2006). As AMD can severely contaminate surface and groundwater, as well as soils, these anthropogenic activities can have serious human health and ecological implications (Grimalt et al., 1999a, 1999b) if the mines are not monitored and the necessary environmental treatment is not in place.

AMD release from mine waste rock, tailings and mine structures, such as pits and underground workings, is primarily a function of the mineralogy of local rock material (mainly secondary minerals associated with sulfide-bearing material) and the availability of water and oxygen. The typical AMD pattern leads to accumulation of Fe sulfates, oxy-hydroxides and oxides in a spatial and temporal sequence that represents the buffering of an acidic solution as it moves away from its source (Montero et al., 2005; Swayze et al., 2000). Therefore, these minerals can serve as pH indicators (indicative minerals). Because mineralogy and the other factors affecting AMD formation are highly variable within a site as well as from site-to-site, predicting the potential for AMD using conventional laboratory analysis can be exceedingly challenging and costly. However, modern remote sensing has become a novel tool, not only for detecting and quantifying geological materials (Plaza et al., 2009; Van der Meer, 2012), but also for monitoring dynamic processes and induced changes in physical/chemical properties (Ben-Dor et al., 2009; Chabrillat et al., 2002; Escribano et al., 2010; Haubrock et al., 2008; Kokaly et al., 2003).

In a mining environment, the use of multispectral imagery has been effectively used to monitor environmental impacts (De Marais et al.,2012; He et al., 2009; Kalifa and Arnous, 2012; Matějíček and Kopačková, 2010) as well as to detect AMD generating material (Kopačková et al., 2012a; Robins et al., 2000). However, the low spectral resolution of multispectral imagery is a major limitation. On the other hand, data with very high spectral resolution – hereafter referred to as imaging spectroscopy (IS) data, which is also known in the remote sensing community as hyperspectral (HS) data, has been successfully used in earlier studies to detect diverse mining environmental factors. Reflectance spectroscopy, both ground and image-based methods, has been successfully used to locate acid-generating minerals at mine sites (Kopačková et al., 2012b; Montero et al., 2005; Quental et al., 2013; Riaza et al., 2011a, 2011b; Richter et al., 2008, 2009; Swayze et al., 2000, 2006) and to determine heavy metal concentrations (Chloe et al., 2008, 2009; Kemper and Sommer, 2002;

Kopačková et al., 2011; Pandit et al., 2010). However, very few studies have been published on quantitative pH mapping in a mining environment. Particularly the extreme heterogeneity and the fact that the material is present in the form of mixtures rather than pure minerals (Montero et al., 2005; Riaza et al., 2011a) make these environments too complex and quantitative pH mapping still remains challenging. Therefore, the objectives of this paper are to:

- link the mineral, geochemical and spectral properties of the material at abandoned lignite mines and dumps
- find spectral parameters reflecting the pH conditions which remain even if the minerals are present in the form of mixtures
- employ a spectral mapping method that allows identification of the indicative minerals (based on the above considerations) even if present in mixtures and enable mapping of the pH spatial patterns using airborne multi-flight line hyperspectral data
- build a pH model and validate the estimated pH using ground truth data

3.2 Material and methods

3.2.1 Test site

General description on the test site is given in the chapter 2.2.

3.2.2 Data

3.2.2.1 Aerial HS image datasets

The hyperspectral image data was acquired in 2009 (July 27th) during the HyEUROPE 2009 flight campaign using the HyMap (HyVista Corp., Australia) airborne imaging spectrometer. The HyMap sensor records image data in 126 narrow spectral bands covering the entire spectral interval between 0.450-2.480 µm spectral range with Full Width Half Maximum (FWHM) of 15 nm and ground field of view of 4 m. The resulting ground pixel resolution of the image datasets was 5 m. In order to successfully pre-process the hyperspectral data, a supportive calibration and validation ground campaigns were organized simultaneously with the HyMap data acquisition in 2009 and 2010. At the selected homogenous targets the ground measurements were acquired by the ASD FielSpec-3 spectroradiometer to properly calibrate as well as validate the image data and to enable: (i) atmospheric correction of the airborne hyperspectral images and ii) retrieving at surface reflectance values for the further verification. The selected targes met the following conditions: (i) spatial homogeneity for a minimum area of 5x5 image pixels and (ii) natural or artificial nearly

Lambertian ground surfaces. The hemispherical-conical reflectance factor (HCRF) (Schaepman-Strub et al., 2006) was measured for each reference target. Raw spectroradiometric data were transformed into the HCRF using the calibrated white spectralon panel. In addition, Microtops II Sunphotometer (Solar Light Comp., USA) measurements were taken approximately every 30 seconds during the HyMap data acquisition. Data acquired by the Sunphotometer was used for estimation of the actual atmospheric conditions (AOT - aerosol optical thickness, WV- water vapor content).

Nine individual HyMap stripes covered the entire area of the Sokolov lignite basin (Fig. 3.1). The orientation and geometry of the HyMap strips followed the SW-NE orientation of the lignite basin. This setting represented an optimal solution from the economic point of view; on the other hand, this setting (relative solar azimuth at the acquisition hour was about 73 deg) caused that the data suffered from strong cross-track illumination and bi-directional reflectance distribution function effects (Verrelst et al., 2008). Therefore, prior to atmospheric correction, the data had to be preprocessed to minimize these effects. The specific pre-processing focused on correcting the cross track illumination effect via (i) calculating the polynomial coefficients for the gases located in different spectral regions (O_2 at 760 nm, H_2O at 930 nm), (ii) interpolating between the calculated polynomial coefficients for all the wavelengths (full spectral configuration), and (iii) using interpolated polynomial coefficients to correct differences across the image (for each image separately). After the preprocessing described above, radiometric rectification suggested by Brook and Ben-Dor (2011) was applied.

Final atmospheric correction was performed in the ATCOR-4 software package (Richter, 2009). This software was designed for atmospheric correction of airborne hyperspectral image data using the MODTRAN 4 physical model of the atmosphere (Adler-Golden et al., 1999). The data obtained during the supportive ground campaign were used to improve the results of the atmospheric correction. Direct ortho-georectification was performed using the PARGE software package (Schläpfer et al, 1998). Finally, the hyperspectral image data was georeferenced to the UTM 33N (WGS-84) coordinate system. To assess the final accuracy, the product was compared to the very high spatial resolution aerial orthophotos (pixel size = 0.5 m) and a resulting standard positional accuracy of 3.7 m was defined. Prior to image analysis, the water bodies and vegetated areas were masked out.

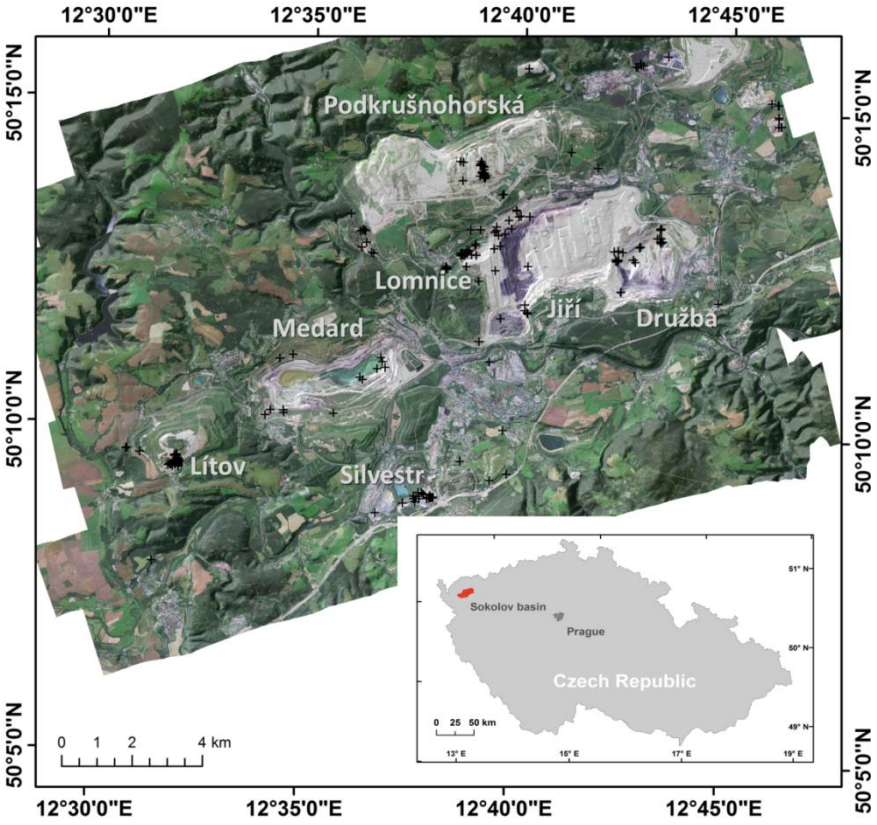

***Figure 3.1**: Test site: sampling/measuring points displayed on the HyMap 2009 data (corrected reflectance, true color coding).*

3.2.2.2 Field data: material sampling and analysis

Over 170 points (Fig. 3.1) distributed in still-active (Jiří, Medard and Družba) and abandoned (Lítov, Lomnice, Sylvestr and PVS - Podkrušnohorská výsypka) open-pit mines were documented in the field during the 2008 and 2009 field campaigns. Particular attention was paid to the abandoned mines with significant AMD-affected areas. At the sampling points spectroradiometric measurements were collected in natural illumination conditions using an ASD FieldSpec 3® portable spectroradiometer (*in situ spectroscopy measurements*). The ASD instrument uses three separate spectrometers to measure the radiance between wavelengths of 0.350 µm and 2.500 µm. Radiance spectra were normalized against a 99% Spectralon® white reference to produce relative reflectance spectra for each measurement.

Samples of the surface material (0-2 cm depth) were collected at 80 selected points. They were dried and sieved to < 2 mm and the abundance of trace elements including major heavy metals was measured using a portable Innov-x Alpha RFA spectrometer. Furthermore, the samples were

subjected to selected X-Ray Diffraction analysis and determination of laboratory pH, sulphur (S total wt %), and Total Organic Carbon (TOC_%).

Further spectra were obtained by measuring the sieved samples as well as the samples of all the minerals and facies encountered in the Sokolov basin (Rojík, 2004) in artificial illumination conditions, using the spectroradiometer's contact probe (*laboratory spectroscopy measurements*).

3.2.3 Methods

Firstly, the geochemical and mineral properties were linked with the reflectance spectra acquired in the field and laboratory as well as with the reflectance of the corresponding HyMap pixels. The obtained spectra were normalized employing the continuum removal (CR) method (Kruse et al., 1993). This method is a standard transformation in the field of spectroscopy (Van der Meer, 2006), as it removes the continuum contribution from the reflectance spectrum. Multiple absorption features within the VIS/NIR/SWIR region were enhanced after the normalization. Additionally, spectra were convolved to the HyMap spectral resolution using a Gaussian convolution and the FWHM value for each band. The effect of mineral mixtures and heterogeneity on the spectral properties was studied. It was then possible to identify the spectral ranges and parameters of the indicative minerals which remain the same either at the level of pure minerals (laboratory spectra) or at the level of mineral mixtures (field and image spectra).

Prior to material mapping using HS images, it is necessary to derive the pure end members for the fundamental physical components (mineral/organic constituents). Pure end-member spectra can be extracted either directly from the image pixels or from spectral libraries measured in the field. The use of reflectance end-members from spectral libraries can be problematic because they can suffer mainly from spatial and temporal variability in the reflectance properties of the cover types (Asner and Heidebrecht, 2002). On the other hand, using end-members from spectral libraries also has some benefits. Their composition is known, and in addition, the standard procedure used for deriving image end-members consists of several time consuming steps: the minimum noise fraction transformation (MNF) (Boardman and Kruse, 1994; Green at al., 1988) and pixel purity index (PPI) calculation (Boardman, 1995). Nonetheless, success still depends on individual skills and the experience of the expert. For the reasons described above, it was preferred to select representative field spectra end-members and to use these for further mapping using HyMap image data.

There are many commonly used analytical techniques for mapping the target material in hyperspectral images: the entire pixel method (called hard classifiers), such as spectral angle

mapping (SAM) (Kruse et al., 1993) and spectral feature fitting (SFF) (Clark et al., 1991); sub-pixel methods, such as spectral mixture analysis (SMA) (Adams et al., 1995) and mixture-tuned matched filtering (MTMF) (Boardman, 1998). However, in order to model the pH, it was necessary to identify the specific minerals typical for the AMD patterns (mainly Fe sulfates and iron oxy-hydroxides). All these minerals exhibit diagnostic absorptions before 1.000 µm. (Kopačková et al., 2012a; Montero et al., 2005; Murphy et al., 2013; Swayze et al., 2000, 2006). The wavelengths and intensities of the absorption features depend on the nature of the crystal field around the Fe atom and on the nature of the bonds around it, because the nature of the magnetic coupling between the $Fe3^{+}$ ions facilitates the transition of electrons between energy states (Sherman and Waite, 1985). Thus, in Fe^{3+} minerals, subtle differences in the shapes and wavelengths of the absorption features reflect the crystal structure of the minerals and allow their identification, such parameters should be used for the spectral mapping.

The HS image data differ from the field spectral measurements, as they have lower spectral resolution; moreover, the measured spatial domain is also different. Pixel reflectance in heterogeneous environment has a significant mixing problem as it is a result of spectral reflectance of different materials present within the pixel; on the other hand, filed spectra tend to represent rather point measurements. Therefore, it was necessary to select a mapping technique/method which is robust enough to identify the targeting minerals even if present as part of mixtures. Optimally, a desire technique should enable setting of specific spectral ranges where characteristic absorptions of target minerals are exhibited and it should be sensitive to subtle absorption features and their parameters (e.g., absorption maximum wavelength, depth).

The Spectral Feature Fitting (SFF) technique is a method that was successfully used to map minerals in multispectral/hyperspectral image data (Debba et al., 2005; Haest et al., 2012; Mars and Rowan, 2010). The advantage of SFF over other methods, such as spectral angle mapping (SAM), is that it is sensitive to subtle absorption features (Tangestani et al., 2011; Van der Meer, 2004) and also minimizes the influence of the effects of variations in mineral grain size and illumination (Kruse et al., 1993; Kruse and Lefkoff, 1993). This method is available in ENVI software and compares the fit of the image spectra to the reference spectra using a least-squares technique (Clark et al., 1991). The reference spectra (whether the laboratory or field measurements or extracted directly from the image) are scaled to match the image spectra after the continuum is removed from both data sets. A least-squares fit is calculated band-by-band between each reference (end-member) spectra and the unknown spectra of an image pixel (Clark et al., 1991; Van der Meer, 2004). The total root mean

square error (RMSE) is used to generate an RMS error image for each end-member. The output is represented by a "fit" image, which is a measure of how well the unknown spectrum matches the reference spectrum on a pixel-by-pixel basis (Van der Meer, 2004).

Figure 3.2: *Homogenous targets used for training and validation.*

An improved multiple feature-based technique, multi range spectral feature fitting (MRSFF), was employed in this study. MRSFF provides a promising classification technique as yielded higher accuracy than SAM (Judd and Steinberg, 2007) or than SAM and NDVI (Pan et al., 2013). The user can choose the Multi Range SFF function to define multiple and different wavelength ranges around each end-member's absorption features, which is very useful for mineral identification. From this point of view, such an approach is highly suitable for pH mapping, as specific mineral associations indicating certain pH ranges exhibit multiple absorptions.

The ground truth data, pH measured for the homogenous targets (3x3 pixel size: 15x15 m in extent), were used to build and validate a pH model. The data were divided into two different datasets (Fig. 3.2): (i) training (12 samples) and (ii) validation (14 samples). Both the calibration and validation targets were selected in the way to cover the high mineral variability characterizing the studied sites. To estimate the pH, a multiple regression model was constructed between the end-member fit images and the training dataset. The results were then statistically assessed using 14 validation targets/samples and the coefficients of determination (Rv^2) together with the Std. Error of the Estimate were defined (Fig. 3.7, Tab 3.3).

3.3 Results

3.3.1 Linking the pH with mineral and spectral properties

Spectroscopic AMD approaches are based on mapping of those minerals that occur on the surface of waste-rock piles and their surroundings, focusing on minerals that serve as indicators of subaerial oxidation of pyrite ('hot spots') and the subsequent formation of AMD (Fe sulfates, oxy-hydroxides, and oxides accumulating in a spatial and temporal sequences, Montero et al., 2005; Swayze et al., 2000). However, the concept is more complex at lignite open-pit mines, as low pH values also characterize organic material represented by lignite and its weathering products (Kopačkova et al., 2012a).

The results of the chemical/mineral analysis were studied in detail and a site-specific conceptual model describing the relationship between the mineral composition and the pH is presented in Fig. 3.3. The pH of the studied samples varied between 2.5 and 8.5. Low pH (<3.0) characterized the material containing pyrite, jarosite or lignite, which were present either individually or as a part of mixtures. When the pH increased (3.0<pH< 6.5), jarosite was always present in association with goethite. Once the pH exceeded 6.5, jarosite was no longer present in the material, and goethite was the most common ferric mineral. Unlike reported by Montero at al. (2005), goethite was present throughout a wide pH range (pH between 2.5 and 8.5); however if together with jarosite, this corresponded to acid to nearly neutral pH (pH between 3.0 and 6.5). Clays (mainly kaolinite) were the most frequent minerals present in all kind of abundances and mixtures throughout the whole pH and did not indicate any specific pH conditions. Based on these findings, further investigations were focused on minerals or mineral associations described above.

The most frequent mineral constituents typical for diverse material type sorted by pH are summarized in Tab. 3.1. Not all of the minerals identified by XRD exhibit diagnostic absorption within the VNIR-SWIR spectral region (e.g., feldspar, quarts) and can be mapped using optical data. Nevertheless, the fundamental pH-indicative minerals can be identified using their reflectance properties, except for pyrite. Pyrite is not stable and quickly oxidizes when it reaches the surface, where it is replaced by secondary minerals (e.g., hydroxysulfates and oxy-hydroxides). Consequently, this mineral would not be detectable by optical methods as they only allow analysis of the surface.

The spectral properties of selected mineral constituents are depicted in Fig. 3.4. Clearly, pure minerals measured in the lab (3.4A, 3.4B) exhibit multiple diagnostic absorption features throughout the whole spectral range (VNIR/SWIR). These absorptions have higher separability compared to the

spectra of the same mineral constituents present as mixtures (field spectra acquired in the field under natural conditions) (Figs. 4C and 4D).

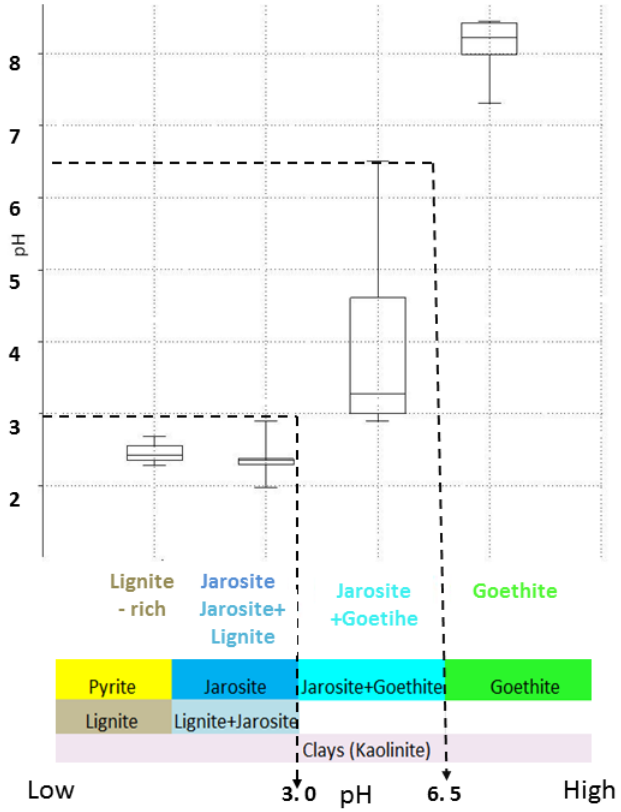

Figure 3.3: *Mineral conceptual model: Sokolov case study.*

Secondary minerals with Fe^{3+} (hydroxysulfates and oxy-hydroxides) exhibit absorption features around 0.45 µm and before 1.00 µm (Clark et al., 1990; Montero et al., 2005; Murthy et al., 2013). If present as pure minerals (Fig. 3.4A), goethite show a strong and rather wide absorption centered at around 0.500 µm, on the other hand the diagnostic absorption for jarosite is narrow and centered at slightly shorter wavelength (around 0.450 µm). The absorption feature centered between 0.900–1.000 µm differs for these two minerals as well. The absorption maximum is shifted, reflecting differences in crystal structure (Sherman and Waite, 1985), goethite absorption maximum is centered at longer wavelengths (closer to 1.000 µm) while jarosite exibit maximum absorption at shorter wavelengths (closer to 0.900 µm). The same trend in the shift of the absorption maximum wavelength remains for jarosite and goethite even if they are present as mixtures (Fig. 3.4C). Jarosite, if present in a pure form, exhibits an additional absorption feature around 2.260 µm in the SWIR

region (Fig. 3.4B). Material with high lignite content (>5%) exhibited a characteristic, very small slope of the spectral curve between 0.800 µm and 1.200 µm (Fig. 3.4A) with an absorption maximum at approximately 0.600 µm. Additionally, absorption at 1.700 and 2.309 µm indicating humic acid (Ben-Dor et al., 1997) can be identified (Fig.3.4B).

Table 3.1: *Most frequent mineral constituents typical for diverse material type sorted by pH (minerals detectable by the means of optical spectroscopy are in bold).*

Minerals	*quartz*	**muscovite**	**kaolinite**	**smektite**	*siderite*	*anatas*	*pyroxene*	*k-feldspar*	*pyrite*	**jarosite**	**goethite**	**lignite**
Material: lignite-rich, very low pH (< 3)	x	x	x	x	x	x		x	x	x		x
Material: without lignite, very low pH (< 3)	x	x	x		x	x	x	x	x	x		
Material: without lignite, pH between 3.0 and 6.5	x	x	x			x		x		x	x	
Material: without lignite, nearly neutral or higher pH (6.5-8.5)	x	x	x	x	x	x		x			x	

In terms of the predominant absorption in SWIR for mineral mixtures (Fig. 4D), the doublet between 2.100 and 2.200 µm caused by the vibration of the Al–OH molecule (Clark et al., 1990) indicates the presence of kaolinite. The jarosite absorption at 2.260 µm is not present if jarosite is part of mixtures. The absorptions at 1.700 and 2.309 typical for the lignite-rich material remained; however, the absorption depth is smaller and the shape is simplified.

The field spectra of the mineral constituents described above were compared to the reflectance spectra of the corresponding pixels of the HyMap images (Fig. 3.5). The same trend in the shift of the absorption maximum wavelengths before 1.000 µm could be seen even with the HyMap decreased spectral and spatial resolution; where the maximum is shifted even to the longer wavelengths.

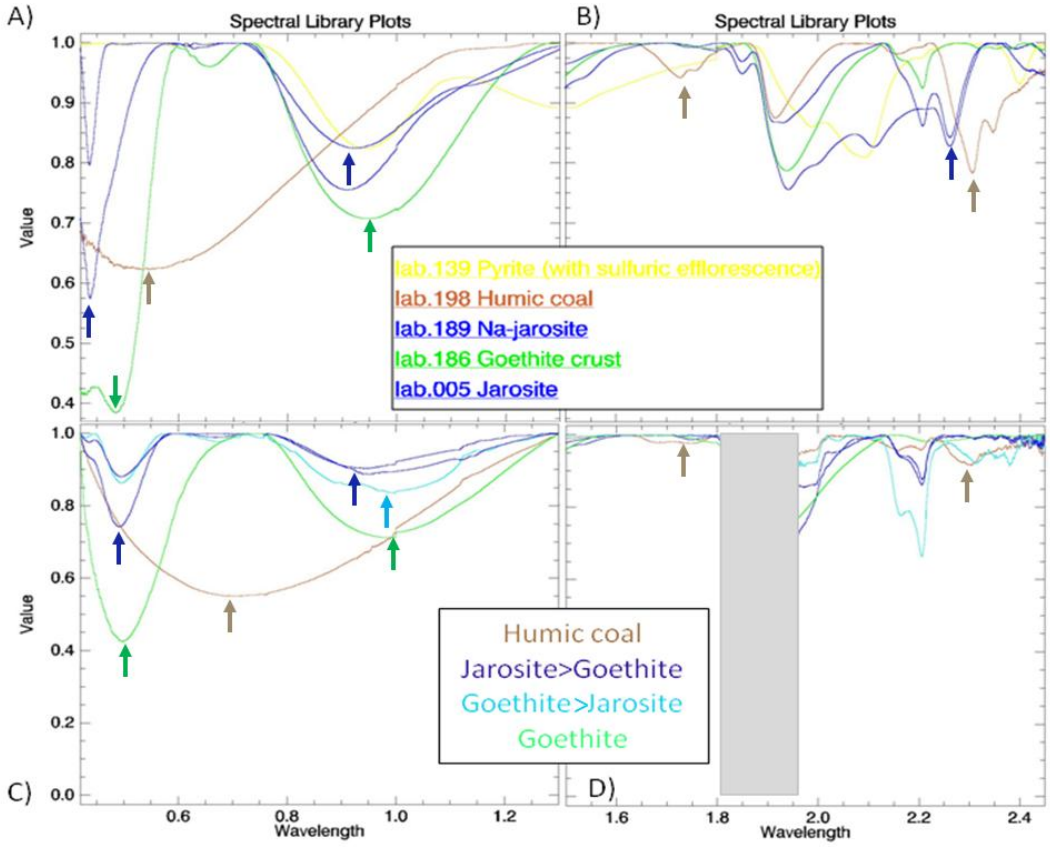

Figure 3.4: *Spectral plots for the typical mineral constituents (A, B: pure minerals; C, D: depicted minerals present in mixtures; arrows pointing at the absorption maximum wavelengths which are characteristic for the depicted minerals).*

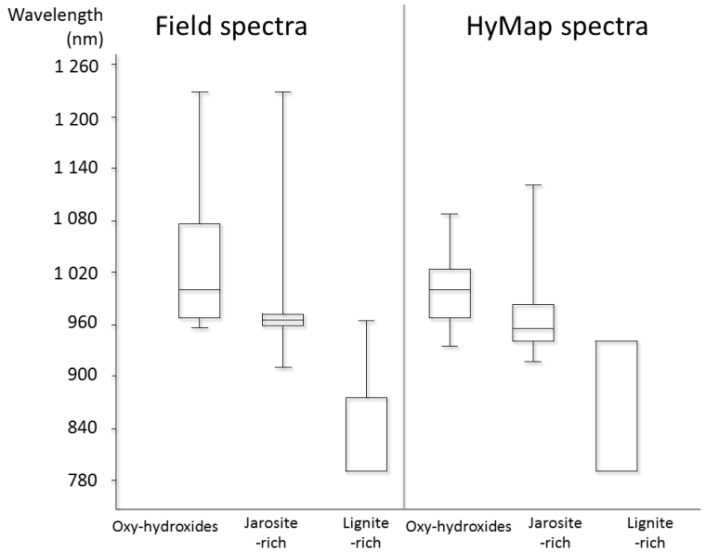

Figure 3.5*: Trend in the shift of the absorption maximum, the field spectra were compared to the reflectance spectra of the corresponding pixels of the HyMap images.*

3.3.2 Employing Multi Range Spectral Feature Fitting

To select the end-members for spectral mapping, the field spectral libraries were assessed together with the results of XRD analysis and grouped into (Fig. 3.6) (i) the spectral libraries of the fresh lignite which characterize the deep absorption at 0.640 µm (end-member 1); this material is characterized by very low pH values (<3.0), (ii) the spectral libraries of clays rich in lignite which still exhibit the typical absorption at 0.640 µm (end-member 2); this material is also characterized by very low pH values (<3.0), (iii) the spectra of the material where high abundance of jarosite was identified and the absorption maximum of the absorption feature centered between 0.900-1.000 µm was located at the shorter wavelengths (end-member 3); this material is characterized by very low pH (<3.0), (iv) the libraries of materials where a high abundance of goethite was identified and the maximum of the absorption feature centered between 0.900-1.000 µm was located at the longer wavelengths; this material is characterized by pH>6.5, Aside these, additional group was created containing (v) the material where the secondary Fe minerals represented a minimal fraction and where muscovite and chlorite were the major minerals present in the samples.

The spectral libraries were averaged to generate representative spectra for each mineral group defined above (Fig. 3.6). These represented the end/members further employed for spectral mapping using MRSFF. The end-member fit images were derived and further statistically assessed to test whether acceptable regression models can be obtained to model the surface pH. Different scenarios were tested including different numbers of end-members as well as setting different spectral ranges (Tab. 3.2).

The best result in identification of selected minerals as well as in predicting the surface pH (R^2=0.63, Rv^2=0.77) was achieved when all five end-members were included (scenario 6, Fig.3.7) and when the spectral ranges were defined separately for the diagnostic absorptions between 0.460-0.780 µm, 0.780-1.200 µm, 1.600-1.790 µm and 2.080-2.400 µm (Tab.3.2).

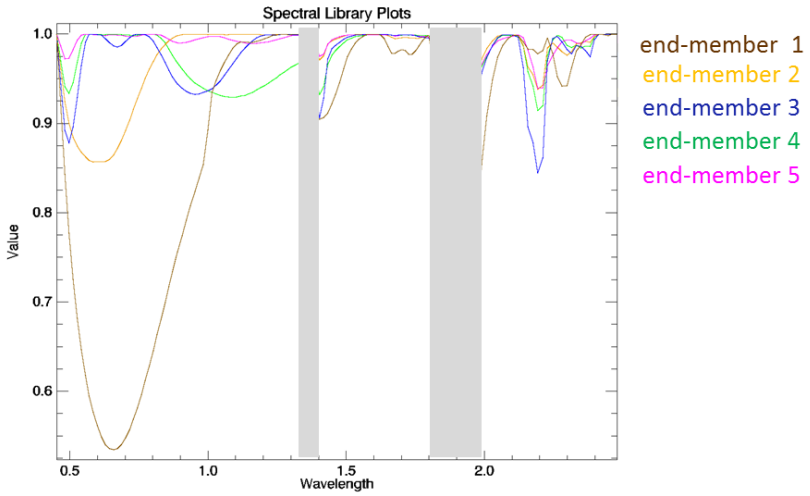

Figure 3.6: *The end-members (resampled to the HyMap data spectral resolution) used for Multi Range Spectral Feature Fitting (MRSFF).*

Table 3.2: *Different scenarios tested under the MRSFF analysis (scenario 6 achieving the best result is in bold).*

End-member	EM 1	EM2	EM3	EM4	EM5
Range	0.460-1.200 µm				
Scenario 1	x		x	x	
Range	0.460-1.200 µm; 2.080-2.400 µm				
Scenario 2	x		x	x	
Range	0.460-1.200 µm				
Scenario 3	x	x	x	x	x
Range	0.460-1.200 µm; 2.080-2.400 µm				
Scenario 4	x	x	x	x	x
Range	0.460-0.780 µm; 0.780-1.200 µm; 2.08-2.400 µm				
Scenario 5	x	x	x	x	x
Range	**0.460-0.780 µm; 0.780-1.200 µm; 1.600-1.790 µm; 2.080-2.400 µm**				
Scenario 6	**x**	**x**	**x**	**x**	**x**

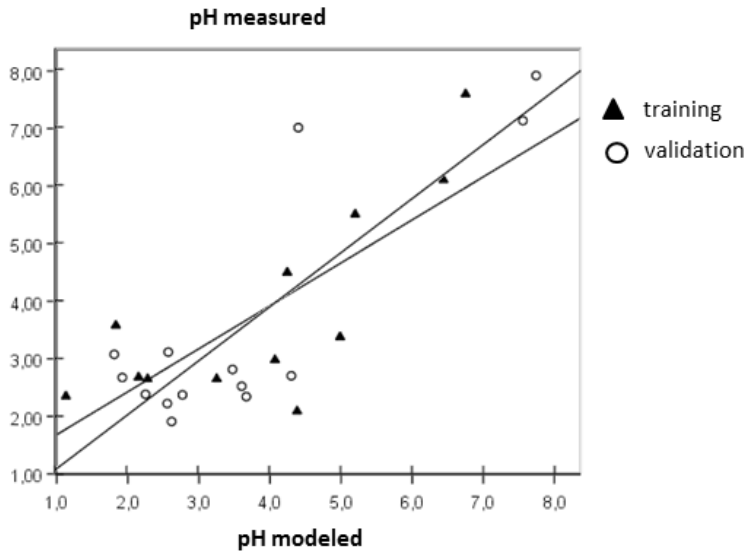

Figure.3.7: *pH training/validation regression models.*

Table 3.3: *Prediction statistics for the scenario 6 (add Tab. 3.2).*

R	R^2	Adjusted R^2	Std. Error of the Estimate	Sig.
Training				
,779	,606	,567	1,140	,003
Validation				
,873	,763	,744	1,138	,000

3.4 Discussion

In this study, the pH is quantitatively estimated using hyperspectral image data (HyMap). Good performance of hyperspectral image analysis depends on accurate atmospheric correction (Brook and Ben-Dor, 2011; Pan et al., 2013), which has a strong influence on the mineralogical spectral diagnoses (Riaza et al., 2011). Big attention was paid to this issue and the data were also corrected for the BRDF effect and radiometric rectification suggested by Brook and Ben-Dor (2011) was also implemented.

Based on the observations in this study, the minerals that reflect the specific site conditions and indicate a certain pH can be identified by assessing the subtle differences in absorption feature parameters (e.g., absorption maximum wavelength position, symmetry, depth). For jarosite and

goethite the same trend in the shift of the absorption maximum (the feature centered between 0.900-1.000 µm) is visible whether they are present individually or as mixtures. Lignite-rich material has a characteristic small slope of the spectral curve between 0.800 – 1.200 µm with an absorption maximum around 0.640 µm, and also exhibits absorptions centered at 1.700 and 2.309 µm. These characteristics also remain the same even if lignite is present in mixtures.

Using hyperspectral data for mapping purposes, the key issue still remains in selection of proper end-members. The field spectral libraries were used to map the indicative minerals. The field spectra of five fundamental mineral groups defined under the site-specific conceptual model were averaged to derive the representative end-members, which were further utilized for the MRSFF. To succeed on this, it was necessary to acquire field spectral libraries which reflect the all major mineral varieties of the site. Alternatively, the end-members could be extracted from hyperspectral images. Although diverse techniques for this extraction exist, success still depends on the proper identification of pure pixels (Zontea and Plaza, 2009). The spatial resolution of the HyMap data was 5x5 m and in such a heterogeneous environment, it can be a difficult task to derive real pure pixels. The presented approach is built on systematic field work and field data collection, so the representative field spectra can be used for image spectral mapping. In such a case no procedure to extract pure pixels is requested, moreover, the same end-members can be used if multi-date hyperspectral data are available, and thus this approach may be more universal than, for instance, partial least squares regression (PLSR).

The Multi Range Spectral Feature Fitting (MRSFF) technique was tested to identify the selected minerals or their associations defined under the conceptual model. For instance, this technique was successfully used to map diverse vegetation types in Yellowstone National Park (Kokaly et al., 2003). The vegetation also differed in the shapes and depths of absorptions present in the spectra and these were the key characteristics that enabled species mapping. Montero et al. (2005) used spectral libraries and the spectral feature technique for identification of Fe-bearing minerals, sheet and other silicates to study patterns representing the evolution of acid solutions discharged from the pyritic waste piles and the subsequent accumulation of secondary precipitates. Haest et al. (2012) employed the Multiple spectral feature fitting technique to identify and quantify minerals (iron (oxyhydr-) oxide and clay contents) in drill cores, achieving promising results (RMSE between 3,9-9.1 wt %). De Jong (2011) employed the Spectral Feature Fitting (SFF) and Linear Spectra Unmixing (LSU) techniques to map soil surface crusts and compared the results. They judged that spectral unmixing was superior to spectral feature fitting. However, the main differences between crusted and non-crusted soils were

in the overall albedo, brightness and shape and depth of the absorption feature at 2.200 µm. Unlike SFF, LSU is a method that is sensitive to albedo and color differences and this may explain why better results were obtained when this technique was employed. The wavelength of the absorption maximum centered between 0.900-1.000 µm and its shift were the key factors for mapping the indicative ferric minerals; this approach employing MRSFF, a method that is sensitive to the absorption feature parameters (shape, depth and absorption maximum wavelength), seems to be highly suitable.

The MRSFF technique yielded reliable results in identification of the selected minerals within the mineral mixtures. Fit images, where the pixel values indicate the closeness of the match between the pixel spectrum and the end-member library spectrum, could be combined into thematic maps (Fig. 3.8A) to identify, for instance, material with low pH. However, the quantitative pH map (Figs. 3.8B, 3.9) clearly has significant advantages over simple material identification. Estimating the pH via application of the regression modeling to the fit images resulting from MRSFF analysis seems to be feasible, as reliable results were obtained for both validation and training datasets (Fig. 3.7, Tab 3.3).

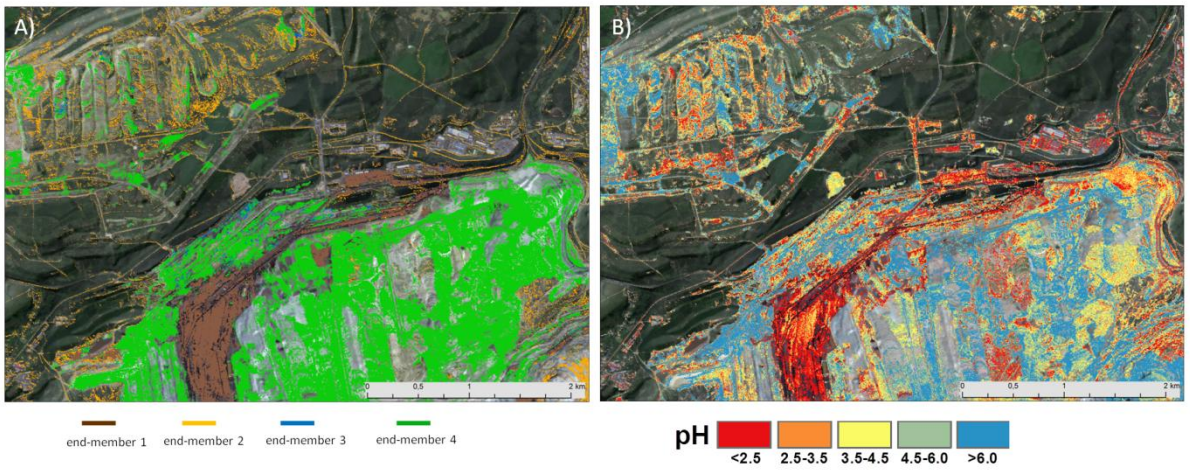

Figure 3.8: *Example of the thematic output (A: end-member fit images were thresholded to depict the pixels with the closest spectral match; B: estimated pH).*

Too few quantitative image-spectroscopy based approaches have been made in estimating the pH at mining sites. Zabcis et al. (2009) used Hymap airborne hyperspectral data to generate predictive pH maps of AMD for the Sotiel-Migollas mine complex, Southwest Spain, using PLSR analysis. Validation of the model for an independent data set results in an R^2 value of 0.71 between the actual and predicted pH values. Quenatal et al. (2013) mapped material associated with acid AMD using HyMap data and the final map displayed the mineralogical assemblage correlations $\geq$ 0.8 of variable pH indicators, particularly pinpointing a low-pH relationship to the contamination in the area. The

limited number of such studies demonstrates that quantitative pH mapping is still a challenging task and the presented approach seems to be promising.

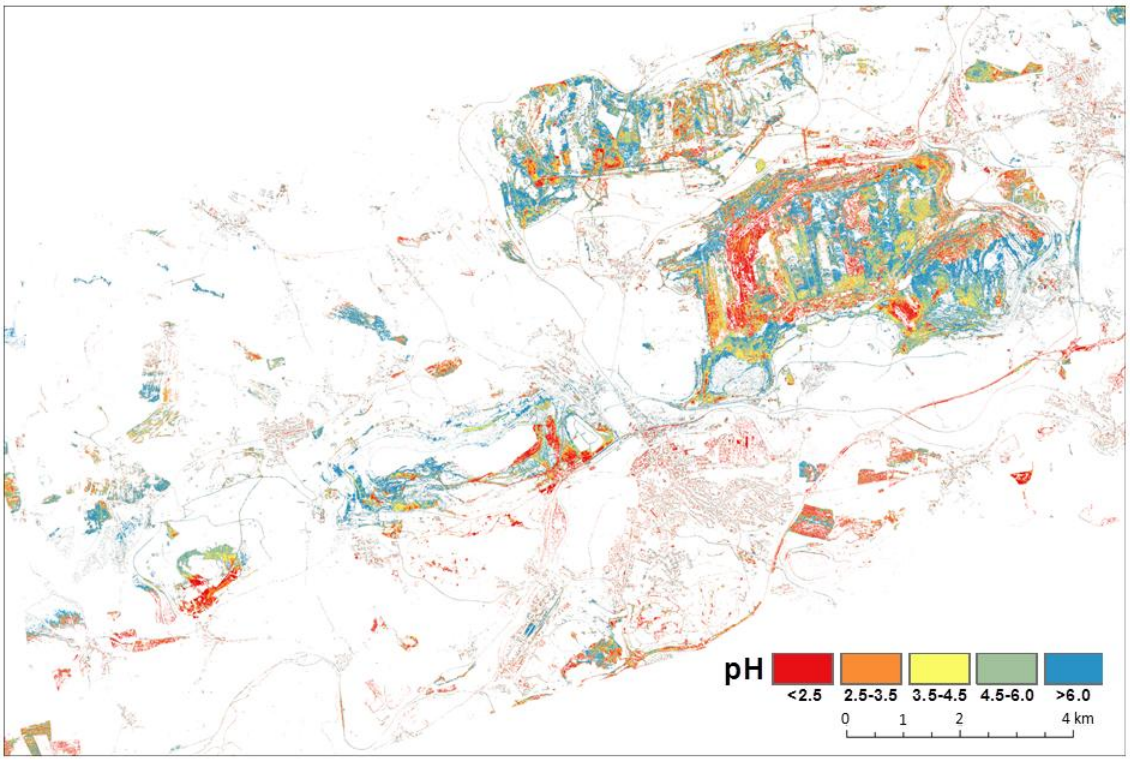

Figure 3.9: *The Sokolov lignite basin: estimated pH.*

3.5 Conclusions

The mining environment is characteristic for its high heterogeneity and complexity. Therefore, Acid Mine Drainage (AMD) mapping should be tailored to the specifics of the tested mining site. In this study, a conceptual model depicting the minerals that reflect the specific site conditions and indicate a certain pH was first defined. It was found that pH <3.0 characterized the material with the presence of pyrite, jarosite or lignite whether present individually or in mixtures. Jarosite in association with goethite indicated increased pH (3.0-6.5), while goethite alone indicated nearly neutral or higher pH (>6.5).

The spectral properties of these minerals or their mineral associations were further analyzed and common absorption feature parameters were identified. The shift to longer wavelengths of the absorption maximum centered between 0.900-1.000 µm is the main parameter allowing differentiation among Fe^{3+} secondary minerals and this trend is still visible if the minerals are part of mixtures. Lignite-rich material exhibits a characteristic small slope of the spectral curve between

0.800 – 1.200 µm with absorption maximum around 0.640 µm, and additional minor absorptions at 1.700 and 2.309 µm.

The Multi Range Spectral Feature Fitting (MRSFF) technique, allowing setting of different spectral ranges for multiple diagnostic absorptions, was successfully employed to identify and map the indicative minerals specified above using the hyperspectral images and proved to be a sufficiently sensitive method for assessing the desired spectral parameters (e.g., shape, maximum absorption wavelength position, absorption depth). A multiple regression model using the fit images, i.e. the results of MRSFF, as inputs was constructed to estimate the surface pH and a statistical significant accuracy was attained (R^2=0.61, Rv^2=0.76).

This study still represents one of the very first approaches employing image spectroscopy for quantitative pH modeling in a mining environment. As the results seem to be promising, further testing and validation using multi-temporal hyperspectral data is planned.

Acknowledgement

The present research is being undertaken within the framework of Grants No. 205/09/1989 (HypSo: grant funded by the Czech Science Foundation) and No. 244242 (EO-MINERS: FP7 grant funded by the EC). Many thanks are due to Dr. Petr Rojík (Sokolovská uhelná a.s.) for his substantial assistance with the field campaign.

References

ADAMS, J. B., SABOL, D. E., KAPOS, V., ALMEIDA, R., ROBERTS, D. A., SMITH, M. O., GILLESPIE, A. R, 1995. Classification of Multispectral Images Based On Fractions of Endmembers - Application To Land-cover Change In the Brazilian Amazon. *Remote Sensing of Environment* **52**(2), 137-154.

Adler-Golden, S. M., Matthew, M. W., Bernstein, L. S., Levine, R. Y., Berk, A., Richtsmeier, S. C., Acharya, P. K., Anderson, G. P., Felde, G., Gardner, J., Hoke, M., Jeong, L. S., Pukall, B., Ratkowski, A., Burke, H. H, 1999. Atmospheric correction for short-wave spectral imagery based on MODTRAN4. *Imaging Spectrometry V* **3753**, 61-69.

Akcil, A., Koldas, S, 2006. Acid Mine Drainage (AMD): causes, treatment and case studies, *Journal of Cleaner Production* **14**(12-13), 1139-1145.

Asner, G. P., Heidebrecht, K. B, 2002. Spectral unmixing of vegetation, soil and dry carbon cover in arid regions: comparing multispectral and hyperspectral observations. *International Journal of Remote Sensing* **23**(19), 3939-3958.

Ben-Dor, E., Chabrillat, S., Dematte, J. A. M., Taylor, G. R., Hill, J., Whiting, M. L., Sommer, S, 2009. Using Imaging Spectroscopy to study soil properties. *Remote Sensing of Environment* **113**, S38-S55.

Ben-Dor, E., Inbar, Y., Chen, Y, 1997. The reflectance spectra of organic matter in the visible near-infrared and short wave infrared region (400–2500 nm) during a controlled decomposition proces. *Remote Sensing of Environment* **61**(1), 1-15.

Boardman, J. W, 1995. Analysis, understanding and visualization of hyperspectral data as convex sets in n-space. *Imaging Spectrometry* **2480**, 14-22.

Boardman, J. W., Kruse, F. A, 1994. Automated Spectral Analysis - A Geological Example Using Aviris Data, North Grapevine Mountains, Nevada. *Proceedings of the Tenth Thematic Conference On Geologic Remote Sensing - Exploration, Environment, and Engineering, Vol I*, I407-I418.

Boardman, J, 1998. Leveraging the high dimensionality of AVIRIS data forimproved sub-pixel target unmixing and rejection of false positives: mixturetuned matched filtering, in: Summaries of the Seventh Annual JPL AirborneGeoscience Workshop, Jet Propulsion Laboratory Publication, pp. 55.

Bouska, V., Pesek, J, 1999. Quality parameters of lignite of the North Bohemian Basin in the Czech Republic in comparison with the world average lignite. *International Journal of Coal Geology* **40**(2-3), 211-235.

Brook, A., Ben Dor, E, 2011. Supervised vicarious calibration (SVC) of hyperspectral remote-sensing data. *Remote Sensing of Environment* **115**(6), 1543-1555.

Chabrillat, S., Goetz, A. F. H., Krosley, L., Olsen, H. W, 2002. Use of hyperspectral images in the identification and mapping of expansive clay soils and the role of spatial resolution. *Remote Sensing of Environment* **82**(2-3), 431-445.

Choe, E., Kim, K. W., Bang, S., Yoon, I. H., Lee, K. Y, 2009. Qualitative analysis and mapping of heavy metals in an abandoned Au-Ag mine area using NIR spectroscopy. *Environmental Geology* **58**(3), 477-482.

Choe, E., van der Meer, F., van Ruitenbeek, F., van der Werff, H., de Smeth, B., Kim, Y. W, 2008. Mapping of heavy metal pollution in stream sediments using combined geochemistry, field spectroscopy, and hyperspectral remote sensing: A case study of the Rodalquilar mining area, SE Spain. *Remote Sensing of Environment* **112**(7), 3222-3233.

CLARK, R. N., KING, T. V. V., KLEJWA, M., SWAYZE, G. A., VERGO, N, 1990. High Spectral Resolution Reflectance Spectroscopy of Minerals. *Journal of Geophysical Research-solid Earth and Planets* **95**(B8), 12653-12680.

Clark, R., Swayze, G., Gallagher, A., Gorelick, N., Kruse, F, 1991. Mapping withimaging spectrometer data using the complete band shape least-squares algo-rithm simultaneously fit to multiple spectral features from multiple materials, *in* In: Proceedings, 2nd Airborne Visible/Infrared Imaging Spectrometer (AVIRIS) workshop, JPL Publication, pp. 176–187.

Debba, P., van Ruitenbeek, F. J. A., van der Meer, F. D., Carranza, E. J. M., Stein, A, 2005. Optimal field sampling for targeting minerals using hyperspectral data. *Remote Sensing of Environment* **99**(4), 373-386.

De Jong, S. M., Addink, E. A., van Beek, L. P. H., Duijsings, D, 2011. Physical characterization, spectral response and remotely sensed mapping of Mediterranean soil surface crusts. *Catena* **86**(1), 24-35.

De Morais, M. C., Martins, P. P., Paradella, W. R, 2012. Multi-scale approach using remote sensing images to characterize the iron deposit N1 influence areas in Carajas Mineral Province (Brazilian Amazon), *Environmental Earth Sciences* **66**(7), 2085-2096.

Escribano, P., Palacios-Orueta, A., Oyonarte, C., Chabrillat, S, 2010. Spectral properties and sources of variability of ecosystem components in a Mediterranean semiarid environment. *Journal of Arid Environments* **74**(9), 1041-1051.

Gomes, M. E. P., Favas, P. J. C, 2006. Mineralogical controls on mine drainage of the abandoned Ervedosa tin mine in north-eastern Portugal. *Applied Geochemistry* **21**(8), 1322-1334.

Green, A. A., Berman, M., Switzer, P., Craig, M. D, 1988. A Transformation For Ordering Multispectral Data In Terms of Image Quality With Implications For Noise Removal. *IEEE Transactions On Geoscience and Remote Sensing* **26**(1), 65-74.

Grimalt, J. O., Ferrer, M., Macpherson, E, 1999. The mine tailing accident in Aznalcollar. *Science of the Total Environment* **242**(1-3), 3-11.

Grimalt, J. O., MacPherson, E, 1999. Special issue: The environmental impact of the mine tailing accident in Aznalcollar (south-west Spain. *Science of the Total Environment* **242**(1-3), 1-2.

Haest, M., Cudahy, T., Laukamp, C., Gregory, S, 2012. Quantitative Mineralogy from Infrared Spectroscopic Data. I. Validation of Mineral Abundance and Composition Scripts at the Rocklea Channel Iron Deposit in Western Australia. *Economic Geology* **107**(2), 209-228.

Haubrock, S. N., Chabrillat, S., Kuhnert, M., Hostert, P., Kaufmann, H, 2008. Surface soil moisture quantification and validation based on hyperspectral data and field measurements. *Journal of Applied Remote Sensing* **2**, 023552.

He, B., Oki, K., Wang, Y., Oki, T, 2009. Using remotely sensed imagery to estimate potential annual pollutant loads in river basins. *Water Science and Technology* **60**(8), 2009-2015.

Judd, C., Steinberg, S, 2007. Mapping submerged macrophytes: using multi-range spectral feature fitting to map submerged eelgrass in a turbid estuary, in: American Society for Photogrammetry and Remote Sensing – ASPRS AnnualConference, pp. 326-331.

Kemper, T., Sommer, S, 2002. Estimate of heavy metal contamination in soils after a mining accident using reflectance spectroscopy, *Environmental Science, Technology* **36**(12), 2742-2747.

Khalifa, I. H., Arnous, M. O, 2012. Assessment of hazardous mine waste transport in west central Sinai, using remote sensing and GIS approaches: a case study of Um Bogma area, Egypt. *Arabian Journal of Geosciences* **5**(3), 407-420.

Kokaly, R. F., Despain, D. G., Clark, R. N., Livo, K. E., 2003. Mapping vegetation in Yellowstone National Park using spectral feature analysis of AVIRIS data. *Remote Sensing of Environment* **84**(3), 437-456.

Kopackova, V., Chevrel, S., Bourguignon, A., Rojik, P., 2012a. Application of high altitude and ground-based spectroradiometry to mapping hazardous low-pH material derived from the Sokolov open-pit mine. *Journal of Maps* **8**(3), 220-230.

Kopackova, V., Chevrel, S., Bourguignon, A., Rojik, P., 2012b. Mapping Hazardous Low-ph Material In Mining Environment: Multispectral and Hyperspectral Approaches. *2012 IEEE International Geoscience and Remote Sensing Symposium (IGARSS),* 2695-2698.

Kopačková, V., Chevrel, S., Bourguignon, A., 2011. Spectroscopy as a tool for geochemical modeling. *Proc. SPIE* **8181**, 818106.

Kruse, F. A., Lefkoff, A. B., Boardman, J. W., Heidebrecht, K. B., Shapiro, A. T., Barloon, P. J., Goetz, A. F. H., 1993. The Spectral Image-processing System (sips) - Interactive Visualization and Analysis of Imaging Spectrometer Data. *Remote Sensing of Environment* **44**(2-3), 145-163.

Mars, J. C., Rowan, L. C., 2010. Spectral assessment of new ASTER SWIR surface reflectance data products for spectroscopic mapping of rocks and minerals. *Remote Sensing of Environment* **114**(9), 2011-2025.

Matejicek, L., Kopackova, V., 2010. Changes in Croplands as a Result of Large Scale Mining and the Associated Impact on Food Security Studied Using Time-Series Landsat Images. *Remote Sensing* **2**(6), 1463-1480.

Montero, I. C., Brimhall, G. H., Alpers, C. N., Swayze, G. A., 2005. Characterization of waste rock associated with acid drainage at the Penn Mine, California, by ground-based visible to short-wave infrared reflectance spectroscopy assisted by digital mapping. *Chemical Geology* **215**(1-4), 453-472.

Murphy, R. J., Monteiro, S. T., 2013. Mapping the distribution of ferric iron minerals on a vertical mine face using derivative analysis of hyperspectral imagery (430-970 nm). *ISPRS Journal of Photogrammetry and Remote Sensing* **75**, 29-39.

Pan, Z., Huang, J., Wang, F., 2013. Multi range spectral feature fitting for hyperspectral imagery in extracting oilseed rape planting area. *International Journal of Applied Earth Observation and Geoinformation* **25**, 21-29.

Pandit, C. M., Filippelli, G. M., Li, L., 2010. Estimation of heavy-metal contamination in soil using reflectance spectroscopy and partial least-squares regression. *International Journal of Remote Sensing* **31**(15), 4111-4123.

Plaza, A., Benediktsson, J. A., Boardman, J. W., Brazile, J., Bruzzone, L., Camps-Valls, G., Chanussot, J., Fauvel, M., Gamba, P., Gualtieri, A., Marconcini, M., Tilton, J. C., Trianni, G., 2009. Recent advances in techniques for hyperspectral image processing. *Remote Sensing of Environment* **113**, S110-S122.

Quental, L., Sousa, A. J., Marsh, S., Abreu, M. M., 2013. Identification of materials related to acid mine drainage using multi-source spectra at S. Domingos Mine, southeast Portugal. *International Journal of Remote Sensing* **34**(6), 1928-1948.

Rajchl, M., Ulicny, D., Grygar, R., Mach, K., 2009. Evolution of basin architecture in an incipient continental rift: the Cenozoic Most Basin, Eger Graben (Central Europe), *Basin Research* **21**(3), 269-294.

Riaza, A., Buzzi, J., Garcia-Melendez, E., Carrere, V., Muller, A., 2011a. Monitoring the Extent of Contamination from Acid Mine Drainage in the Iberian Pyrite Belt (SW Spain) Using Hyperspectral Imagery. *Remote Sensing* **3**(10), 2166-2186.

Riaza, A., Garcia-Melendez, E., Mueller, A,2011b. Spectral identification of pyrite mud weathering products: a field and laboratory evaluation. *International Journal of Remote Sensing* **32**(1), 185-208.

Richter, N., Jarmer, T., Chabrillat, S., Oyonarte, C., Hostert, P., Kaufmann, H., 2009. Free Iron Oxide Determination in Mediterranean Soils using Diffuse Reflectance Spectroscopy. *Soil Science Society of America Journal* **73**(1), 72-81.

Richter, N., Staenz, K., Kaufmann, H., 2008. Spectral unmixing of airborne hyperspectral data for baseline

mapping of mine tailings areas. *International Journal of Remote Sensing* **29**(13), 3937-3956.

Richter, R., 2009. Atmospheric/topographic correction for airborne imagery, DLR-German Aerospace Centre, D-82234 Wessling, Germany.

Robbins, E. I., Anderson, J. E., Cravotta, C. A., Nord, G. L., Slonecker, E. T., 2000. Remotely-sensed multispectral reflectance variations in acidic versus near-neutral contaminated coal mine drainage in Pennsylvania. *Icard 2000, Vols I and Ii, Proceedings*, 1551-1561.

Rodger, A., Laukamp, C., Haest, M., Cudahy, T., 2012. A simple quadratic method of absorption feature wavelength estimation in continuum removed spectra. *Remote Sensing of Environment* **118**, 273-283.

Rojík, P., 2004. New stratigraphic subdivision of the Tertiary in the Sokolov Basin in Northwestern Bohemia, *Journal of the Czech Geological Society* **49/3-4**, 173-185.

Schaepman-Strub, G., Schaepman, M. E., Painter, T. H., Dangel, S., Martonchik, J. V., 2006. Reflectance quantities in optical remote sensing-definitions and case studies. *Remote Sensing of Environment* **103(**1), 27-42.

Schläpfer, D., 1998. Parametric Geocoding, PARGE Using Guide, Version 2.3, ReSe Applications Schläpfer Remote Sensing Laboratories University of Zurich.

Sherman, D. M., Waite, T. D., 1985. Electronic-spectra of Fe-3+ Oxides and Oxide Hydroxides In the Near Ir To Near Uv. *American Mineralogist* **70(**11-12), 1262-1269.

Swayze, G. A., Livo, K. E., Clark, R. N., Hoefen, T. M., Higgins, C. T., Ong, C., Kokaly, R. F., Kruse, F. A., 2006. Evaluating Minerals of Environmental Concern Using Spectroscopy. *2006 IEEE International Geoscience and Remote Sensing Symposium, Vols 1-8*, 1990-1991.

Swayze, G. A., Smith, K. S., Clark, R. N., Sutley, S. J., Pearson, R. M., Vance, J. S., Hageman, P. L., Briggs, P. H., Meier, A. L., Singleton, M. J., Roth, S., 2000. Using imaging spectroscopy to map acidic mine waste. *Environmental Science, Technology* **34(**1), 47-54.

Tangestani, M. H., Jaffari, L., Vincent, R. K., Sridhar, B. B. M., 2011. Spectral characterization and ASTER-based lithological mapping of an ophiolite complex: A case study from Neyriz ophiolite, SW Iran. *Remote Sensing of Environment* **115(**9), 2243-2254.

Van der Meer, F. D., Van der Werff, H. M. A., Van Ruitenbeek, F. J. A., Hecker, C. A., Bakker, W. H., Noomen, M. F., Van der Meijde, M., Carranza, E. J. M., de Smeth, J. B., Woldai, T., 2012. Multi- and hyperspectral geologic remote sensing: A review. *International Journal of Applied Earth Observation and Geoinformation* **14(**1), 112-128.

Van der Meer, F., 2006. The effectiveness of spectral similarity measures for the analysis of hyperspectral imagery. *International Journal of Applied Earth Observation and Geoinformation* **8(**1), 3-17.

Van der Meer, F., 2004. Analysis of spectral absorption features in hyperspectral imagery. *International Journal of Applied Earth Observation and Geoinformation* **5**, 55-68.

Verrelst, J., Schaepman, M. E., Koetz, B., Kneubuhler, M., 2008. Angular sensitivity analysis of vegetation indices derived from CHRIS/PROBA data. *Remote Sensing of Environment* **112(**5), 2341-2353.

Yudovich, Y. E., Ketris, M. P., 2005. Arsenic in coal: a review. *International Journal of Coal Geology* **61(**3-4), 141-196.

Zabcic, N., Rivard, B., Ong, C., Muller, A., 2009. Using Airborne Hyperspectral Data To Characterize the Surface Ph of Pyrite Mine Tailings. *2009 First Workshop On Hyperspectral Image and Signal Processing: Evolution In Remote Sensing*, 154-157.

Ziegler, P. A., 1990. Collision Related Intra-plate Compression Deformations in Western and Central-europe. *Journal of Geodynamics* **11(**4), 357-388.

Zortea, M., Plaza, A., 2009. Spatial Preprocessing for Endmember Extraction. *IEEE Transactions On Geoscience and Remote Sensing* **47(**8), 2679-2693.

4. Utilization of hyperspectral image optical indices to assess the Norway spruce forest health status

Mišurec, J. and Kopačková, V., Lhotáková, Z., Hanuš, J., Weyermann, J., Entcheva-Campbell, P., Albrechtová, J., (2012): Utilization of hyperspectral image optical indices to assess the Norway spruce forest health status, J. Appl. Remote Sens. 6(1), 063545. doi:10.1117/1.JRS.6.063545.

Abstract

The work is concerned with assessing the health status of trees of the Norway spruce species using airborne hyperspectral (HS) data (HyMap). The study was conducted in the Sokolov basin in the western part of the Czech Republic. First, statistics were employed to assess and validate diverse empirical models based on spectral information using the ground truth data (biochemically determined chlorophyll content). The model attaining the greatest accuracy (D718/D704: RMSE = 0.2055 mg/g, R^2 = 0.9370) was selected to produce a map of foliar chlorophyll concentrations (Cab). The Cab values retrieved from the HS data were tested together with other nonquantitative vegetation indicators derived from the HyMap image reflectance to create a statistical method allowing assessment of the condition of Norway spruce. As a result, we integrated the following HyMap derived parameters (Cab, REP, and SIPI) to assess the subtle changes in physiological status of the macroscopically undamaged foliage of Norway spruce within the four studied test sites. Our classification results and the previously published studies dealing with assessing the condition of Norway spruce using chlorophyll contents are in a good agreement and indicate that this method is potentially useful for general applicability after further testing and validation.

Key words: *photosynthetic pigments, chlorophylls a and b, optical indices, Norway spruce, statistical methods, continuum removal, HyMap, actual physiological status, pre-visual damage symptoms, Sokolov basin, forest management, ICP Forests*

4.1 Introduction

Forests play an important role in regulation of the global climate via the global carbon cycle, evapotranspiration, and earth surface albedo.[1,2] Moreover, forests provide humans with the whole range of ecosystem services including provision of food and forest products, regulation of the hydrological cycle, protection of soil resources, etc.[3] Forest health and ecosystem functioning have recently been influenced by anthropogenic activities and their consequences, such as air pollution, surface mining, heavy metal contamination,4 and other biotic and abiotic stress factors such as pest invasions and soil acidification,[5] which had an especially high effect on central Europe. Therefore, large-scale monitoring of forest health and its methodologies are in the forefront of interest to scientists as well as forest managers. The condition of forests in Europe is monitored under the International Co-operative Program on Assessment and Monitoring of Air Pollution Effects on Forests (ICP Forests).[6] The monitoring consists of two levels: monitoring Level I provides an annual overview of crown condition (defoliation, discoloration, and damage visible on the trees), soil conditions, and foliar survey (contents of nutrients in soil and foliage);[7] monitoring Level II consists of 11 additional assessments (e.g., tree growth, phenology, litterfall, and others, see http://icp-forests.net/page/level-ii), which provide a better insight into the causes affecting the condition of forest ecosystems and into the effects of various stress factors. Our study aims to contribute to improving regional methods for Level II assessments, as both surveys— remote sensing and foliar chemistry—should be included in the overall evaluation.[8]

Biochemical parameters, such as foliage leaf pigments,[9] nitrogen, lignin, and contents of other polyphenols,10 reflect and determine physiological processes in plants, such as photosynthetic capacity and net primary production. On the other hand, foliar chemistry also governs other processes in the ecosystem, such as nutrient cycling and litter decomposition.11 Therefore accurate estimation of the biochemical contents of vegetation is a key factor in understanding and modeling forest ecosystem functions and dynamics. The chlorophyll content is an indicator of leaf photosynthetic activity and can be directly linked to the phenology and health status of plants.[12] Leaf chlorophyll content can be used to detect actual vegetation stress; however, as shown by Ref.[12], the chlorophyll content retrieved from Proba/CHRIS images differs according to the canopy and the leaf architecture of the examined crops. Therefore, at the canopy level, the leaf area index (LAI) and also canopy architecture should be taken into account for a particular canopy. Furthermore, chlorophyll can be used to measure vegetation stress, life stage, productivity, and CO2 sequestration. Remote sensing of the chlorophyll content has been studied extensively on both the leaf[13,14] and the canopy scales.[15–18]

Many aspects of the physiological state of trees are more or less connected with the concentrations of two main groups of leaf photosynthetic pigments: chlorophylls and carotenoids. Vegetation with a high concentration of chlorophyll is considered to be healthy, as the chlorophyll content is linked to greater light-use efficiency, photosynthetic activity, and carbon dioxide uptake.[19–21] Chlorophyll generally decreases under stress and during senescence.[20] Carotenoids play the main role in the process of incident light absorption, transportation of energy to the reaction center of the photosystems, and heat dissipation of energy in case of high irradiances.[22] The combination of the

influences of chlorophylls and carotenoids is thus connected with light-use efficiency.[23] However, higher carotenoid to chlorophyll ratios indicate vegetation stress and senescence.[22,24]

Canopy reflectance depends not only on leaf chemistry but also on vegetation type and function and canopy structure and composition.[16,25] To obtain a spatially explicit vegetation biochemical content, it is necessary to scale leaf-level biochemical measurement to canopy level. Increasing availability of airborne and spaceborne hyperspectral data has enabled the development of accurate methods for scaling of biochemical properties from the leaf to the canopy scale.[26,27]

Currently, there are three remote-sensing approaches used to scale biochemical content from the leaf to the canopy level: (i) the direct extrapolation method, (ii) the canopy-integrated method, and (iii) physical models.[10,28,29] The direct extrapolation and canopy-integration methods rely on statistical analyses to establish a relationship between the targeted biochemical parameter and a spectral parameter (e.g., spectral indices, derivatives).[30,31] The direct extrapolation method (the simplest) is based on the assumptions that all the leaves in the plant have the same biochemical content and only a fine layer of the leaves covers an entire pixel in an image. The relationships between the spectral parameter and the biochemical content are applied directly. Using the canopy-integrated method, the biochemical content is obtained by multiplying the leaf content by the corresponding canopy biophysical parameter (e.g., LAI or biomass[15,29,32]). In addition, new spectral indices taking into account species heterogeneity and non-green canopy components were developed and further tested.[15] Physical methods employ inverted radiative transfer (RT) models (e.g., PROSPECT,[29] LEAFMOD,[28] SAIL,[33] SCOPE[34]) to estimate the biochemical content at the leaf level.[35] RT modeling simulates the transfer of radiation in the canopy by computing the interaction between a plant and solar radiation.[36–38] In comparison with the direct extrapolation and the canopy-integrated approaches, inversion models offer the potential of a more generic approach to quantify the biochemical parameters of vegetation based on spectral data.

The main goal of the study was retrieval of the chlorophyll content and development of a statistical classification method allowing objective assessment of the physiological status of macroscopically undamaged foliage on a regional scale. To simplify the problem, we focused on single-species (Norway spruce) homogenous forests of a similar age and tested only the direct extrapolation and canopy-integrated methods.We did not test physical models at this stage as the computation remains time-consuming and can suffer from ill-posed problems or can lead to a bias in the retrieved biophysical parameters.[39,40]

In the Sokolov area, NW Bohemia, we selected four homogenously covered Norway spruce (*Picea abies L. Karst*) forest stands with trees of similar ages (40 to 60 years) exhibiting no visible symptoms of damage. Although these forests are situated near lignite open-pit mines, they have not been directly affected by intensive mining activities or by the massive air pollution and acid rains in the late 1990s, which were factors in the Krušné Hory Mountains, part of the heavily polluted Black Triangle region. Since 1996, the atmospheric concentrations of SO2 in Sokolov area have not exceeded 30 µg/m−3 and since 2000 have not exceeded 15 µg/m^{-3} on average (data available at Czech Hydrometeorological Institute[41]).

Statistics were employed to analyze the relationship between diverse vegetation indices and other types of spectral transformations [e.g., first derivatives, continuum removal (CR), and banddepth normalizations] and the ground truth data for the foliage sampled in stands of Norway spruce. These diverse approaches were validated, and, as a result, a map of foliar chlorophyll concentrations (Cab) was derived. The Cab values, together with another three optical parameters [the position of the inflection point on the spectral curve in the red-edge part of the spectrum (REP),[42] the photochemical reflectance index,[43] and the Structure Insensitive Pigment Index (SIPI)[44]], were then used to assess the actual health status of the Norway spruce forests.

4.2 Study Sites

The study was conducted in the Sokolov basin in the western part of the Czech Republic, in a region affected by long-term extensive mining (Fig. 1). The Sokolov basin in the Czech Republic is composed of rocks of Oligocene to Miocene age and is 8 to 9 km wide and up to 36 km long, with a total area of about 200 km2. It contains 60% volcanic ejecta originating from fissures and volcanic cones and 40% sediments.[45] The average altitude of the study region is about 470 m. Due to the fact that the basin is surrounded by the Krušné Hory Mountains, precipitation is above the average for the Czech Republic, and the local climate in the region belongs among the more extreme conditions, characterized by colder and wetter conditions.

The selected forest stands surround the lignite open pit mines in Sokolov but have not been directly affected by the mining activities. However, the soil in all of the stands exhibits low pH and high heavy metal content. We selected four research sites dominated by mature Norway spruce forests of similar age (Table 4.1; Erika, Habartov, and Studenec: 40 to 60 years; Mezihorská: 60 to 80 years). The stands were located at a maximum distance of 12 km from the active lignite open pit mines (Fig. 4.1, Table 4.1). None of the selected sites showed any severe symptoms of macroscopic damage, and they were all classified as damage class 1 with total crown defoliation not exceeding 25% and average needle retention of 8 to 10 needle age classes.

In relation to soil conditions, we assume that our four study sites are good representatives of the spruce forests in the region. The pH of the study sites (2.53 to 3.31) is slightly below the average for the Czech Republic (3.2) but in accordance with local conditions (3.0).[46] In addition to Norway spruce monocultures, mixed spruce forests (with birch or pine) are characteristic of the region. We selected study sites considering the spatial resolution of the HyMap sensor (5 ×5 m), and thus homogeneity of spruce canopy was the main criterion for site selection.

4.3 Data

4.3.1 Ground Truth Data

The source for ground truth data was foliage sampled in the Norway spruce stands. The samples of Norway spruce needles were collected in each forest stand during the ground campaign (August 27 to 30, 2009) to define statistical regression models for estimation of canopy chlorophyll content and to validate the obtained statistical models.

At each of the four test sites, 10 to 15 representative trees were selected in clearly definable groups of five (Erika: two groups A and B; Habartov: three groups C, D, and E; Mezihorská: three groups F, G, and H; and Studenec: two groups I and J). Sample branches were taken from the upper and middle portion of the sunlit canopy; the needles age classes were identified, and representative samples of the first- and third-year needles were collected. Two sample sets of the needles were generated: one for pigment determinations and one for dry matter determinations. Each set contained 200 samples (50 trees × two positions in the crown × two age classes (first and third-year needles).

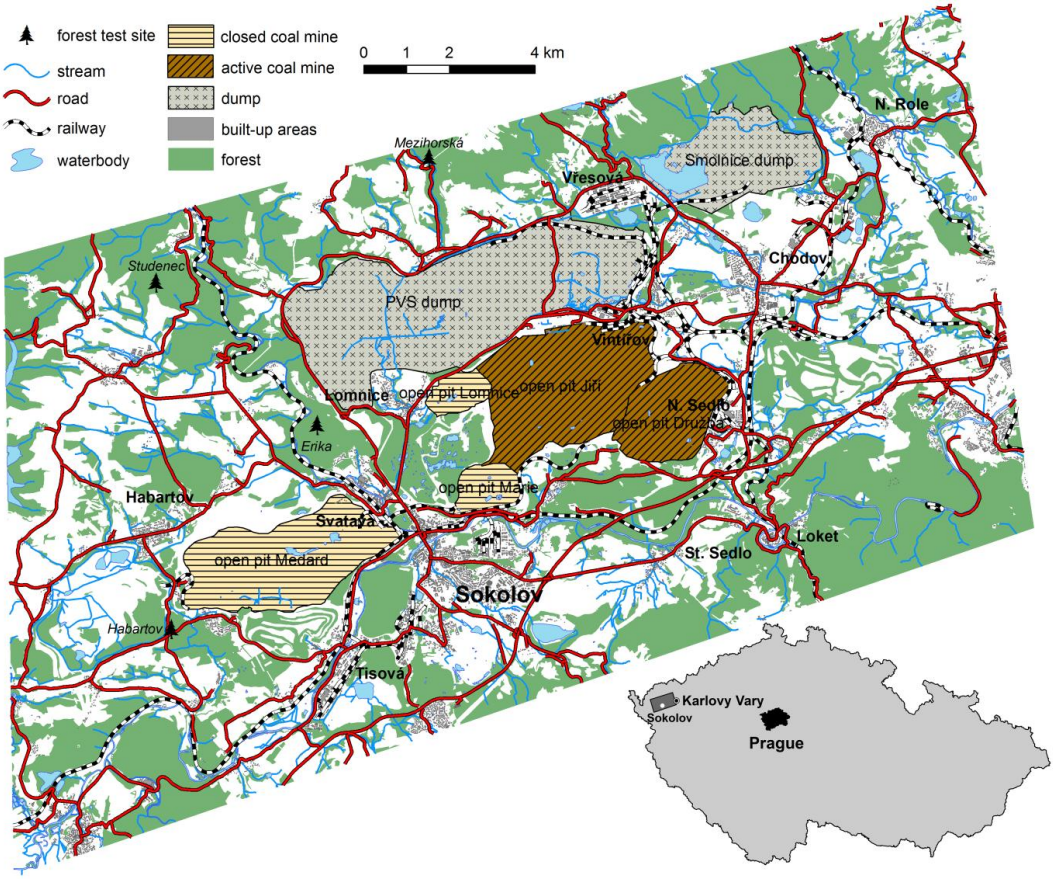

Figure 4.1: *Scheme of the Sokolov lignite basin with the four selected forest stands covered by homogenous Norway spruce (Picea abies L. Karst.) forests: Erika, Habartov, Mezihorská and Studenec.*

Photosynthetic pigments (e. g. chlorophyll a, b, and total carotenoids) were extracted following the procedure outlined by Ref. [47]. The amounts of photosynthetic pigments were determined spectrophotometrically, using equations published by Ref. [48].

In each forest stand, five representative sampling points were chosen to collect soil samples. Material was collected from four soil horizons (two organic and two lithological horizons, the depth of forest floor ranged between 0 and 40 cm). The four horizons have the following characteristics: horizon 1: organic horizon (largely undecomposed); horizon 2: organic horizon (poorly decomposed); horizon 3: mineral, mixed with humus, usually darkened; horizon 4: zone of maximum eluviation of clays and iron and aluminum oxides. The organic material was dried in the air prior to sieving

(fraction <2 mm). Ground sub-samples were analyzed for total organic carbon and nitrogen (Perkin Elmer CHN analyzer). In addition, the pH was determined in the laboratory using an ion-selective electrode in 1M KCl solution.

Table 4.1: *Norway spruce test sites and their basic characteristics*

Norway spruce test sites					
site	**latitude (N)**	**longitude (E)**	**elevation (m a.s.l.)**	**forest age (years)**	**distance from the open-pit mines (km)**
Erika	50°12'25"	12°36'17"	495	40-60	6.4
Habartov	50°09'48"	12°33'28"	477	40-60	11.2
Mezihorská	50°15'50"	12°38'17"	678	60-80	5.8
Studenec	50°14'09"	12°33'00"	722	40-60	8.5

4.3.2 High Spectral Resolution Data

4.3.2.1 HyMap airborne hyperspectral data

The hyperspectral image data was acquired on July 27, 2009, during the HyEUROPE 2009 flight campaign using the HyMap (HyVista Corp., Australia) airborne imaging spectrometer. The HyMap sensor records image data in 126 narrow spectral bands (with full-width half maximum ca. 15 nm) covering the entire spectral interval between 450 to 2500 nm. The resulting ground pixel resolution of the image data was 5 m. To cover the entire area of interest (approx. 15 × 22 km), nine cloudless flight lines were acquired in the NE-SW direction.

4.3.2.2 Supportive ground measurements

In order to successfully pre-process the hyperspectral data, a supportive calibration and validation ground campaign were organized simultaneously with the HyMap data acquisition. The ground measurements are essential to properly calibrate as well as validate the image data and to enable: (i) atmospheric correction of the airborne hyperspectral images and (ii) retrieving at surface reflectance values for the further verification. The study area was investigated in advance to find the reference targets, which must meet the following conditions: (i) spatial homogeneity for a minimum area of 5 × 5 image pixels and (ii) natural or artificial nearly Lambertian ground surfaces. Consequently, six appropriate targets with different values of the surface reflectance were chosen, covering the range of reflectivity from ca. 0 up to 70% (water pool, artificial grass, two asphalt plots, concrete, and beach-volleyball court). The hemispherical-conical reflectance factor (HCRF)[49] was measured by an ASD FielSpec-3 spectroradiometer for each reference target. Raw spectroradiometric data were transformed into the HCRF using the calibrated white spectralon panel.

In addition, Microtops II Sunphotometer (Solar Light Comp., USA) measurements were taken approximately every 30 s during the HyMap data acquisition. These data was used for estimation of the actual atmospheric conditions (aerosol optical thickness; water vapor content).

4.3.2.3 Hyperspectral image data pre-processing

The HyMap multiple flight-line data were atmospherically corrected using software (SW) package ATCOR-4 version 5.0,[50] which is based on the MODTRAN[51] radiative transfer model and enables atmospheric correction of the aerial hyperspectral images. The known reflectances of the specific reference target as well as of WV were utilized for fine-tuning of the model, as facilitated by ATCOR-4. The remaining reference targets were used for validation of the corrected image.

The orientation and geometry of the HyMap strips followed the SW-NE orientation of the lignite basin. However, this setting represented an optimal solution from the economic point of view; on the other hand, this setting (relative solar azimuth at the acquisition hour was about 73 deg) caused that the data suffered from strong cross-track illumination and bi-directional reflectance distribution function effects.[52,53] Therefore, in addition to the atmospheric correction, the data had to be further processed to minimize these effects, and semi-empirical nadir normalization using the kernel-based Ross-Li model[54] was performed for all the flight lines.

Table 4.2: *Image-derived signal-to-noise ratios (SNR) calculated for the chlorophyll absorption domain bands.*

Image derived Signal-to-noise ratio (SNR)						
Line	**SNR (646 nm)**	**SNR (660 nm)**	**SNR (675 nm)**	**SNR (690 nm)**	**SNR (704 nm)**	**SNR (718 nm)**
1	30.66	28.77	33.80	30.48	43.53	53.23
2	21.61	20.42	19.79	17.01	16.71	16.64
3	17.62	15.81	13.15	15.86	14.02	23.21
4	24.95	23.18	20.69	29.25	30.22	22.90
5	20.27	19.35	18.63	18.781	19.81	23.22
6	22.95	20.01	22.4	29.21	38.38	35.32
7	31.64	30.39	32.36	29.75	30.34	24.95
8	17.58	18.23	17.60	18.68	20.61	19.68
9	8.882	8.508	8.045	8.77	10.94	13.74

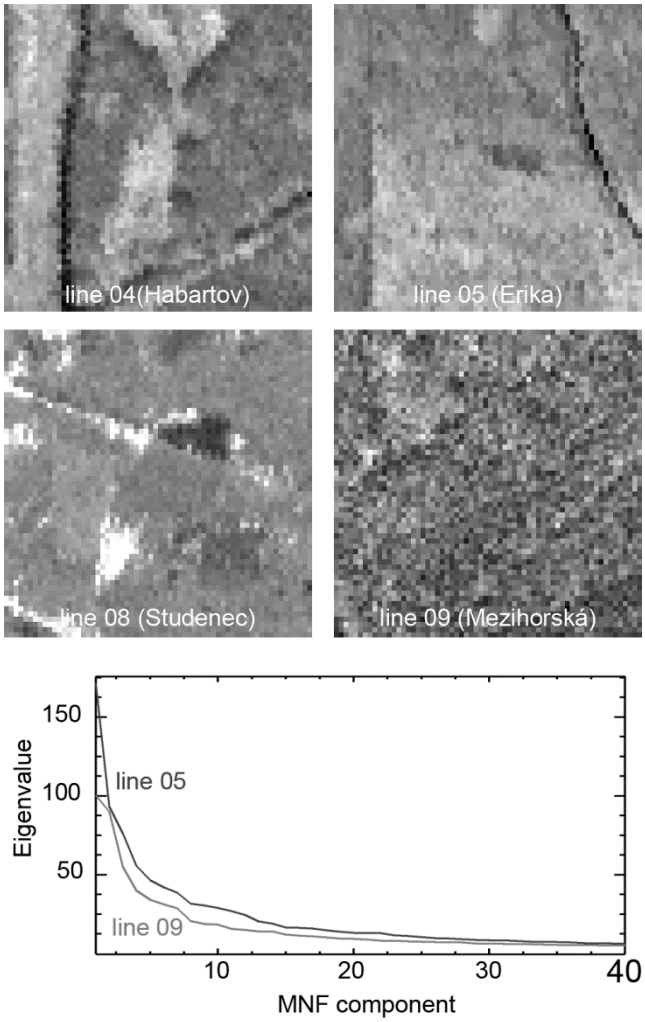

Figure 4.2 *Upper: The first MNF component of the studied localities, the high amount of noise is visible particularly for flight line No. 9. Bottom: MNF Eigenvalues calculated for the whole flight line images—flight lines numbers 05 and 09. They also show that flight line No. 9 suffers from significantly higher noise levels.*

Direct ortho-georectification was performed using the PARGE software package.[55] Data from the on-board inertial measurement unit/global positioning system unit and digital elevation model with ground resolution of 10 m were used as the input parameters for the orthogeorectification. Finally, the hyperspectral image data was georeferenced to the UTM 33N (WGS-84) coordinate system. To assess the final accuracy the ortho-rectified HyMap, the product was compared to the very high spatial resolution aerial orthophotos (pixel size ¼ 0.5 m) and a resulting standard positional accuracy of 3.7 m was defined.

Finally, we assessed the radiometric quality of each flight line by calculating the signal-to noise ratios (SNR).[56] To calculate this parameter, a dark and homogenous surface (deep clean water body) was identified for each flight line and set as a region of interest (ROI). Subsequently, the ratio of the mean radiance and the standard deviation were calculated for each ROI (Tab. 4.2). In addition, we employed the minimum noise fraction transformation[57] to assess the level of noise present in each flight line image (Fig. 4.2). Based on this assessment, we could see that two flight lines (8 and 9) had

significantly lower radiometric quality and high amounts of noise, especially flight line number 9 (Table 4.2), (Fig. 4.2).

4.4 Methods

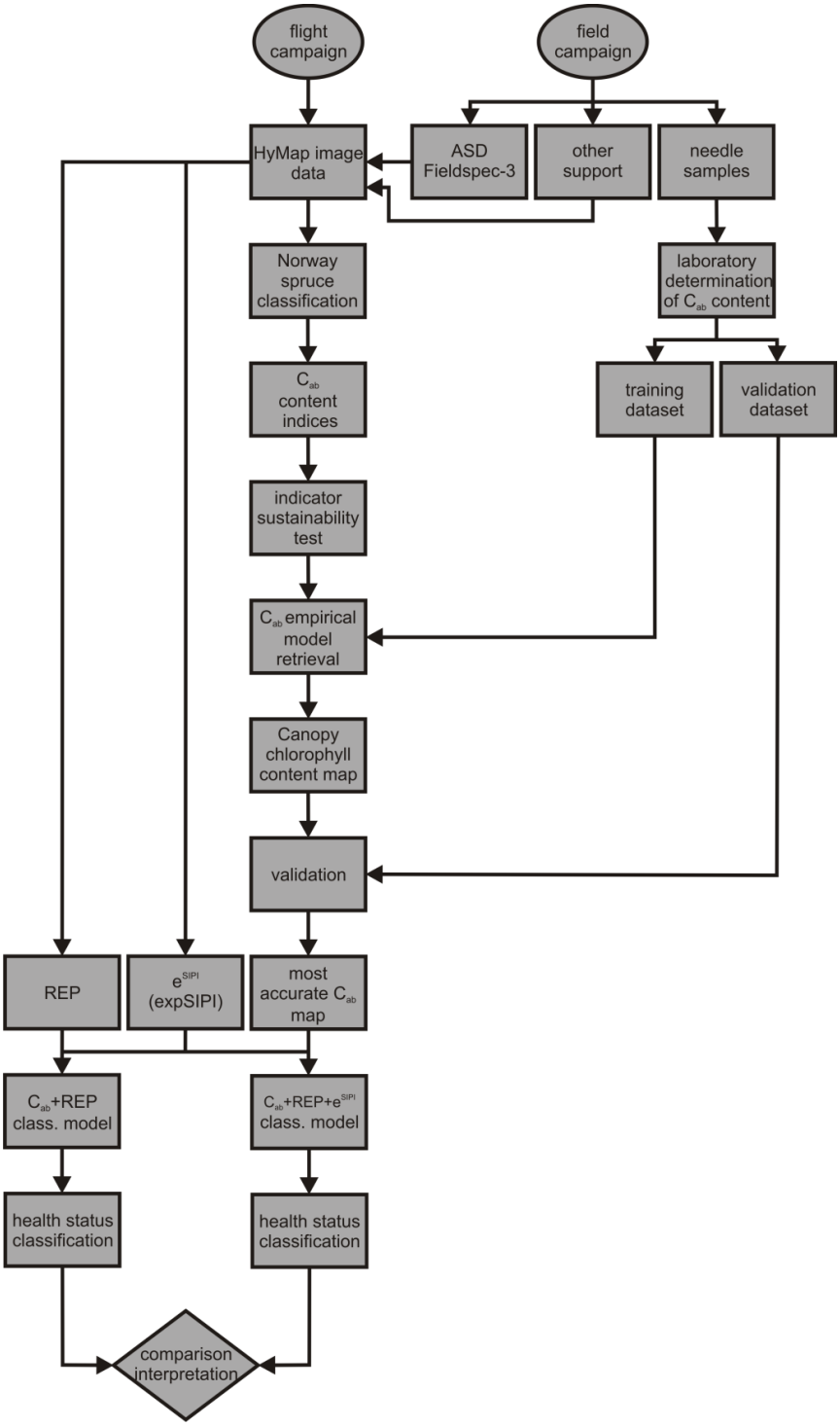

***Figure 4.3**: Data processing workflow.*

The general workflow of the completed research is outlined in Fig. 4.3. Cab was determined by testing numerous empirical models utilizing the original (nontransformed) reflectance data as well as its transformed products. Initially we defined the extent of the Norway spruce forests to which the further computation was applied. To create and validate the empirical models, we divided our ground truth data into training and validation datasets. The relationship between the predicted and measured values was described by the linear regression model and the coefficient of determination (R2 and Rv2) and root mean square errors (RMSE) were determined. To assess the vegetation health status, we also tested the following indicators: the red-edge part of spectrum (REP),[42] photosynthetic reflectance index,[43] and structure insensitive pigment index (SIPI).[44]

4.4.1 Definition of the Norway Spruce Forest Extends

We focused on homogenous Norway spruce forests, and it was thus necessary to mask out other surfaces. We used a hierarchical classification approach, which we found more efficient than simple supervised classification (Fig. 4.5). First we identified vegetated and non-vegetated areas using simple threshold classification of the red-edge normalized difference index (NDVI705 ¼ 0.3).[58] The vegetated surfaces were then classified into grasslands and forest areas using the maximum likelihood classification (MLC) applied to the first five components the results from the MNF transformation of the HyMap data. The forests were subsequently divided into coniferous and deciduous by applying the MLC method to the selected spectral ratios (R742⁄R558, R1062⁄R558, R1652⁄R558, R2192⁄R558).

To classify exclusively the Norway spruce forests, the MNF transformation and MLC were then applied again, this time only to the HyMap reflectance pixels that were previously identified as coniferous. Finally, the resultant classification was filtered using a sieve filter to remove very small clumps of pixels. The derived Norway spruce forest mask was then used for all the following calculations and transformations applied to the HyMap data.

4.4.2 Statistical Background

Although the positions of all the trees in each group were measured by a FieldMap laser rangefinder, it was not possible to distinguish individual tree crowns within the HyMap image data due to the relatively low spatial resolution (5 m). This issue needed to be resolved prior to the empirical modeling as an image pixel value could not be associated with the corresponding ground truth data value. Therefore we defined 10 tree groups as the least circumscribed rectangle defined by a cluster of trees (ROI) (Fig. 4.4). Then the average ground truth value (the average laboratory chlorophyll content calculated for each tree group) could be directly compared with the average pixel value falling within the defined group (ROI).

Basic statistics for each group defined in the following order (Erika: 2 groups A and B; Habartov: 3 groups C, D, and E; Mezihorská: 3 groups F, G, and H; Studenec: 2 groups, I and J, were calculated (Table 4.3) to ensure the proper definition of training and validation datasets. Studying the data variability within each group and spatial variability within each site, we defined the following two datasets required for further statistical treatment:

- The training dataset that was used to define the regression models: groups A, C, D, F, G, and I.
- The validation dataset that was used to validate the obtained models for Cab: groups B, E, H, and J.

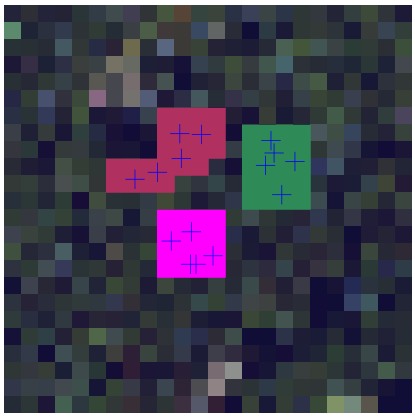

***Figure 4.4**: Examples of the defined ROIs.*

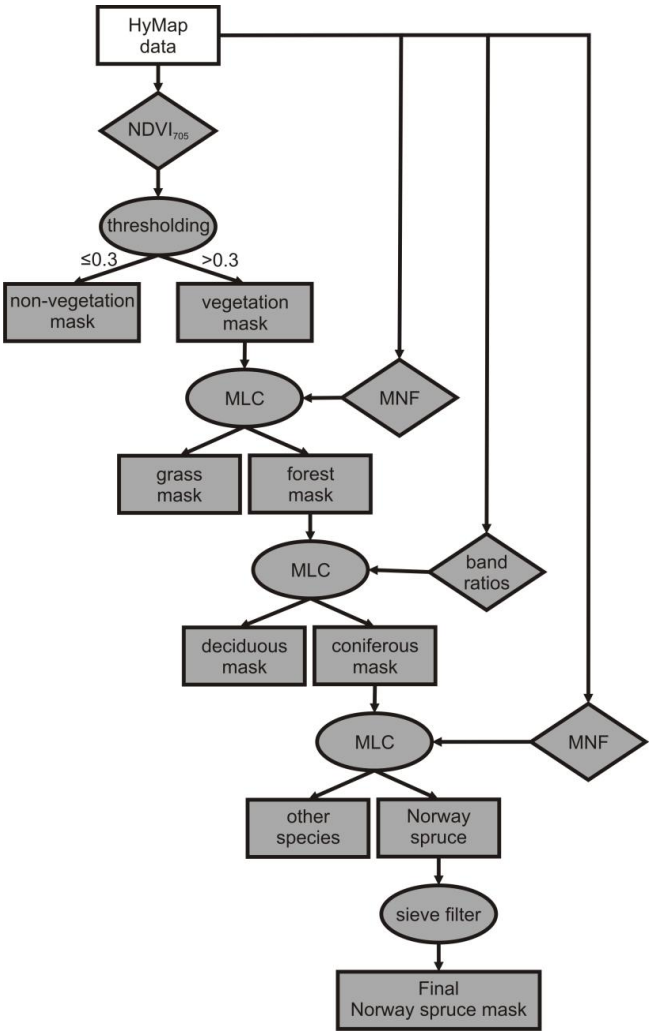

***Figure 4.5:** HyMap data classification workflow. MNF-minimum noise fraction, MLC-maximum likelihood classifier.*

4.4.3 Retrieval of the Chlorophyll Content

For the further empirical modeling of chlorophyll content (Cab), we used the spectral transformations as follows:

- Vegetation indices.
- Stepwise multiple regression (SMR) models.
- Ratio indices derived from the first-derivative spectra.
- Normalized reflectance models.

4.4.3.1 Vegetation indices

The vegetation indices models are based on the simple linear relationship between the chlorophyll content concentration and the vegetation index. The first group of vegetation indices is based on the (normalized) ratios of a few selected bands. We selected the NDVI705 [58] and a simple ratio Vogelmann red-edge index (VOG).[59] Furthermore, we calculated the position of the inflection point of the spectral reflectance curve in red-edge part of the spectra red-edge position (REP)[42] as it allows assessing the shape of the spectral curve in chlorophyll absorption in the red-edge domain. The calculated point separates the convex and concave parts of the spectral curve (in the red-edge part of the spectrum) and lies on the part with the maximum slope. Therefore it also identifies a point where the first derivative of the spectrum exhibits a maximum. To calculate the position of the red-edge inflection point, we used the four-point interpolation technique described in Ref. [60].

Besides the well-known indices, we tested a new index "chlorophyll absorption depth normalized area under curve between 543 and 760 nm (CADAC543–760)" to retrieve the chlorophyll content of the Norway spruce based on similar principles as the ANMB650–725 index.[61] The CADAC543–760 index also utilizes the continuum-removed spectrum and is defined as the area under the reflectance curve between 543 and 760 nm, while each band within this interval is normalized to the maximum depth of the chlorophyll absorption feature (at 675 nm) (Fig. 4.6):

$$CADAC_{543\text{–}760} = 0.5 \cdot \sum_{j=1}^{n-1} \left(\lambda_{j+1} - \lambda_j\right) \cdot \left(\frac{BD_{j+1}}{BD_{675}} + \frac{BD_j}{BD_{675}}\right) \quad \text{[eq. 6]}$$

where: $\lambda_j \ldots \lambda_{n-1}$ refers to the central wavelength of the absorption feature between 543-760 nm and $BD_j \ldots BD_{n-1}$ is the band depth of continuum removed reflectance.

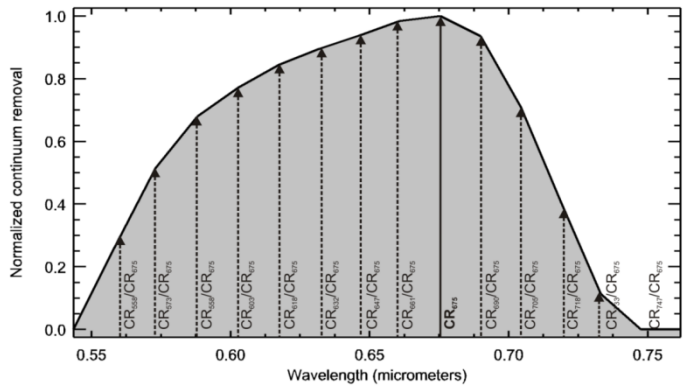

***Figure 4.6**: Chlorophyll absorption and depth normalized area under the curve between 543 to 760 nm (CADAC543–760).*

***Table 4.3**: Description statistics of the laboratory chlorophyll content values.*

Training and validation chlorophyll content laboratory values						
group	locality	use	C_{ab} (min) [mg/g]	C_{ab} (max) [mg/g]	C_{ab} (mean) [mg/g]	C_{ab} (std) [mg/g]
A	Erika	calibration	1.7260	3.4439	2.7146	0.6251
C	Habartov	calibration	2.1862	3.5375	2.8805	0.4930
D	Habartov	calibration	2.0755	3.1775	2.6008	0.3646
F	Mezihorská	calibration	1.8657	2.3356	2.1417	0.1699
G	Mezihorská	calibration	1.6008	2.3668	2.0292	0.2780
I	Studenec	calibration	2.3670	3.2668	2.9070	0.3121
calibration (the whole dataset)			*1.6008*	*3.5375*	*2.5456*	*0.5373*
B	Erika	validation	2.0485	3.3826	2.5832	0.4995
E	Habartov	validation	1.8710	2.9022	2.1765	0.3738
H	Mezihorská	validation	1.5004	2.7110	2.3043	0.4260
J	Studenec	validation	2.6293	3.2483	2.8959	0.2321
validation (the whole dataset)			*1.5004*	*3.3826*	*2.4899*	*0.4949*

4.4.3.2 Stepwise multiple regression models

In addition to the vegetation indices, we tested two multivariate approaches that utilize the bands between 543 to 760 nm to estimate the chlorophyll content.[62] We used SMR[63] to construct a model defining a relationship between the chlorophyll content and (i) spectral derivatives: the first derivatives of the image spectra between 543 and 760 nm, (ii) BD normalization: the continuum-removal transformation[64] was applied to the spectrum between 543 and 760 nm, and then the BD of each spectral band was divided by the depth maximum of the chlorophyll absorption (675 nm for the HyMap data).

4.4.3.3 Ratio indices derived from the first-derivative spectra

We used two spectral derivative indices based on the ratios of the transformed (first derivation) reflectance D718⁄D704 and D718⁄D747.[65]

4.4.3.4 Normalized reflectance models

Another tested approach was based on the normalization of the reflectance to the reflectance minimum at 675 nm (maximal absorption of the chlorophyll) and to the reflectance maximum at 744 nm.[65]

4.4.4 Statistical Assessment of the Relationship Between the Canopy Chlorophyll Content and the Spectral Indices Calculated from the HyMap Data

To test if there is a linear relationship between the chlorophyll content determined in the laboratory for the collected needle samples and the spectral indices derived from the HyMap data, we calculated Pearson's correlation coefficient (see Sec. 4.5.1) using the training dataset of the group trees (A, C, D, F, G and I). All the independent variables (see 4.3) as well as the dependent variable (laboratory chlorophyll content, Cab) have passed the Shapiro-Wilk normality test[66] (p-value > 0.05) and proved to have normal distributions (Table 4.4).

Table 4.4: *Shapiro-Wilk normality test: Results of the Shapiro-Wilk normality test for chlorophyll content (C_{ab}) values (laboratory determined) and the spectral indices of the C_{ab} content (image derived). p-value – significance, W – Shapiro-Wilk test statistic.*

Shapiro-Wilk normality test (α=0.05)		
variable	**p-value**	**W**
C_{ab}	0.1862	0.8936
$NDVI_{705}$	0.4348	0.9287
VOG	0.4745	0.9327
REP	0.1667	0.8893
$CADAC_{543-760}$	0.3900	0.9238
Continuum removal BD normalization model	0.1877	0.8939
D_{718}/D_{701}	0.6273	0.9465
D_{718}/D_{747}	0.7430	0.9563
N_{690}	0.0599	0.8512
N_{704}	0.2197	0.9001
N_{718}	0.2393	0.9035
N_{733}	0.5920	0.9435

After the normal distribution of all the variables was demonstrated, we could test whether the value of the correlation coefficient was large enough to reject the zero-value hypothesis stating the correlation coefficient is equal to 0. By rejecting this hypothesis, we demonstrated that the spectral indicators and the chlorophyll content are not independent. The confidence level was set at 98.5%. Following the statistical testing described above, the linear regression models were then applied to the spectral indices data to predict the canopy chlorophyll content.

Using the training dataset (tree groups A, C, D, F, G, and I), the coefficient of determination (R2) between each spectral index and the Cab content was calculated (Tab. 4.5), describing the amount of data variability explained. The validation dataset (tree groups B, E, H, and J) was then used to validate the accuracy and consistency of the chlorophyll prediction models by calculating the RMSE and coefficients of determination of predicted versus measured Cab values (Rv^2) (Tab. 4.6).

Table 4.5: *Training dataset: Pearson's correlation coefficient (r_{xy}), coefficient of determination (R^2) and the t-test results.*

Correlation between the tested spectral indices and canopy chlorophyll content				
spectral indicator	**r_{xy} (Pearson)**	**critical value (α=0.05)**	**t**	**R^2**
$NDVI_{705}$	0.8517	2.776	3.2509	0.7254
VOG	0.9085	2.776	4.3494	0.8255
REP	0.9397	2.776	5.4932	0.8830
$CADAC_{543-760}$	0.8899	2.776	3.9026	0.7920
SMR spectral derivative model[1]	-0.9225 -0.6931 0.2558	X	X	0.99998
continuum removal BD normalization model	0.9398	2.776	5.5003	0.8831
D_{718}/D_{704}	0.9555	2.776	6.4782	0.9131
D_{718}/D_{747}	-0.8807	2.776	3.7186	0.7756
N_{690}	-0.9013	2.776	4.1612	0.8124
N_{704}	-0.9306	2.776	5.0847	0.8660
N_{718}	-0.9563	2.776	6.5413	0.9146
N_{733}	-0.8914	2.776	3.9337	0.7946
[1]partial correlation coefficients between canopy chlorophyll content and each variable of the multivariate regressions				

Table 4.6: *Validation dataset: Validation of the total canopy chlorophyll content retrieved from the HyMap image data. RMSE – Root Mean Square Error, Rv^2 – coefficient of determination of the predicted vs. measured values of the chlorophyll content.*

Canopy chlorophyll content retrieval validation		
spectral indicator	**RMSE (mg/g)**	**Rv^2**
$NDVI_{705}$	0.2278	0.8960
VOG	0.2269	0.9340
REP	0.3840	0.9050
$CADAC_{543\text{-}760}$	0.3395	0.9114
SMR spectral derivative model	0.7962	$1 \cdot 10^{-5}$
continuum removal BD normalization model	0.2832	0.9328
D_{718}/D_{704}	0.2055	0.9370
D_{718}/D_{747}	0.2456	0.9880
N_{690}	0.4305	0.8254
N_{704}	0.2833	0.9293
N_{718}	0.2664	0.9440
N_{733}	0.2736	0.9905

4.4.5 Vegetation Health Status Classification Method

The main aim of the study was to develop a statistical method allowing qualitative classification of the forest stands based on their health status. We selected four indicators of vegetation health that are based on the plant/forest spectral property:

1. Total canopy chlorophyll content (Cab) (D718⁄D704)[65]

2. Position of the inflection point of the spectral curve in the red-edge part of spectrum (REP)[42]

3. Photosynthetic reflectance index (PRI)[43]

4. Structure insensitive pigment index (SIPI)[44]

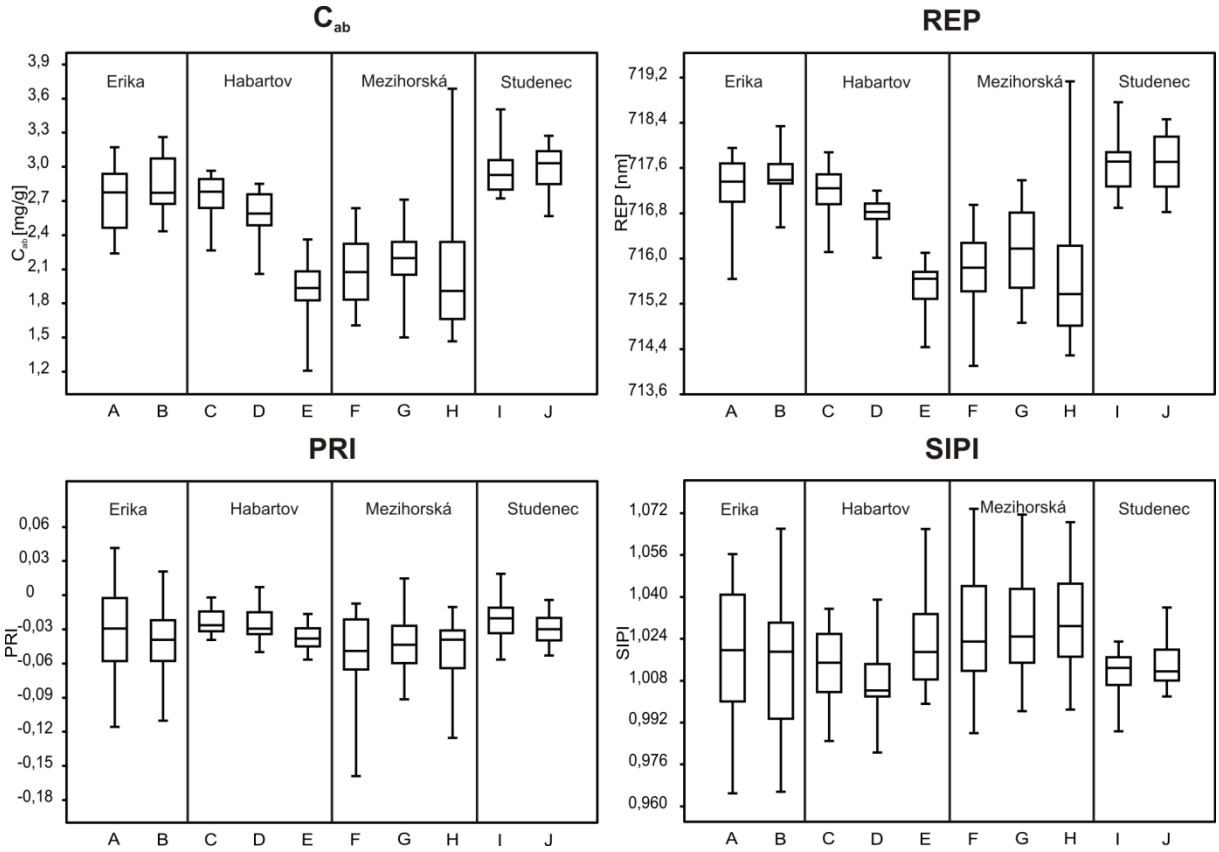

Figure 4.7: *The selected indicator variability within the studied test sites/groups of trees. C_{ab} – content of chlorophyll a+b, REP – position of the inflection point of the spectral curve in the red-edge part of the spectrum, PRI – Photochemical Reflectance Index, SIPI – Structure Insensitive Pigment Index, A – J 10 groups of 5 sampled trees.*

The canopy chlorophyll content was estimated using the empirical model that yielded the best results after the validation (see Results, part 5.1). The amount of green biomass and canopy chlorophyll content primarily determine the position of the inflection point of the spectral curve in the red-edge region. Increasing chlorophyll concentration causes broadening of the major chlorophyll absorption feature around 675 nm and thus causes a shift in the inflection point towards longer wavelengths.[67–71] On the other hand, vegetation stress (e.g., the presence of heavy metals in the soil) might cause a shift in the inflection point to shorter wavelengths.[72] Therefore we also included REP (described in 4.3.1) in the further statistics, as it can serve as an indicator of the vegetation stress.[42,71,73,74] The PRI was originally defined by Ref. [43] and proposed as an indicator of the de-epoxidation of the carotenoids—xanthophyll pigments; they are related to light-absorption mechanisms and closely linked with light use efficiency and carbon dioxide uptake;[43,75] and Refs. [76] and [77] propose to use this index as an indicator of water stress. The SIPI was designed by Ref. [44] to maximize the sensitivity of the index to the ratio of bulk carotenoids to chlorophyll while decreasing sensitivity in the canopy structure. Due to the relative low dynamic range of the SIPI values, we used its exponential transformation (expSIPI) in further analysis.

We must emphasize that, except for the canopy chlorophyll content, none of these indices give direct quantitative information on any particular vegetation biochemical parameter. Instead, they are intended to map only relative amounts, which can be further interpreted in terms of the condition of

the ecosystem. The statistical relationship between the estimated canopy chlorophyll content and the selected indicators (e.g., REP, PRI, and SIPI) was assessed (Fig. 4.7).We found that the value of PRI did not change much for the Norway spruce in the entire area of interest and thus didn't show high enough variability. In addition, the direct relationship of PRI to the chlorophyll content was also relatively weak. Therefore we decided to exclude the PRI index from further investigations. The values of the three selected indices were transformed into standardized z-scores (Tab. 4.7) to ensure their comparability and independence of their physical dimensions (units). Z-scores generally express how far from the mean the particular value is in terms of the standard deviations (σ). Two products were created using the obtained normalized z-score values. First the map of chlorophyll content was classified into five classes defined by the following threshold values (Fig. 4.8):

Class 1: values < mean − 1.0σ

Class 2: mean − 1.0σ < values < mean − 0.5σ

Class 3: mean − 0.5σ < values < mean þ 0.5σ

Class 4: mean − 0.5σ < values < mean þ 1.0σ;

Class 5: values > mean þ 1.0σ.

Table 4.7: *Threshold values of selected indicators (see abbreviation list and chapter 2) used for the further health status assessment. Mean (μ) and Standard Deviation (σ).*

Threshold values of the selected indicators					
health status indicator	-1.0σ	-0.5σ	+0.5σ	-1.0σ	μ
C_{ab} [mg/g]	1.914	2.219	2.828	3.132	2.523
REP [nm]	715.508	716.107	717.306	717.905	716.706
SIPI	0.944	0.980	1.053	1.090	1.017
expSIPI	2.683	2.724	2.806	2.847	2.765

In addition to the classified chlorophyll content map, we created another raster product that combined the information from both indicators REP and expSIPI. REP has the same directly proportional relationship with the vegetation health as the chlorophyll content, and REP was therefore classified identically. On the other hand, expSIPI needed to be classified in the reverse order as the higher values reflect higher carotenoid-to-chlorophyll contents and thus worse vegetation health (in this case Class 1 was calculate as values > mean + 1.0σ; ….., Class 5 as values < mean − 1.0σ). To create the final raster combining the information from REP and expSIPI, they were both summarized and one raster ranging from 2 to 10 was obtained. These values were finally linearly reclassified into the 1 to 5 range to make this output comparable with the Cab raster (Fig. 4.9). As a result, in both maps (Cab and REP þ exp SIPI) the Class 1 indicates worse health status for the trees without visible damage symptoms and Class 5 represents the values indicating the healthiest trees.

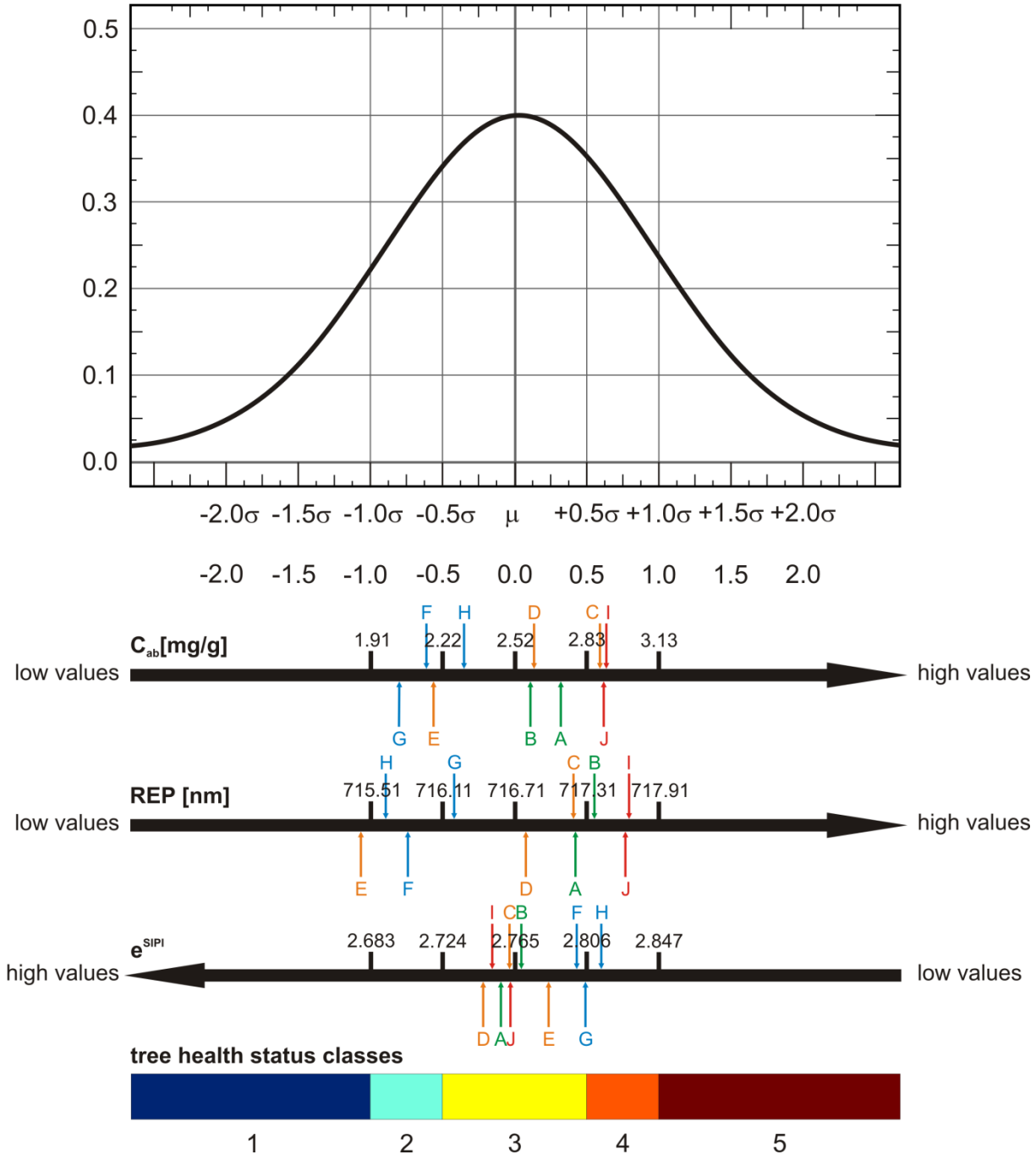

Figure 4.8: *Scheme showing how the suggested statistical method was constructed. The z-normalized values of all the three selected indicators are classified into classes 1-5 using the standard deviation (σ) classification method. The studied groups of trees (A-J) are projected on an absolute scale for each indicator. The colors correspond to the locations of the studied groups of trees (green A, B = Erika, orange C, D, E = Habartov, blue H, G = Mezihorská and red I, J = Studenec).* C_{ab} *– content of chlorophyll a+b, REP – Position of the inflection point of spectral curve in red-edge part of spectrum,* e^{SIPI} *– exponentially transformed Structure Insensitive Pigment Index.*

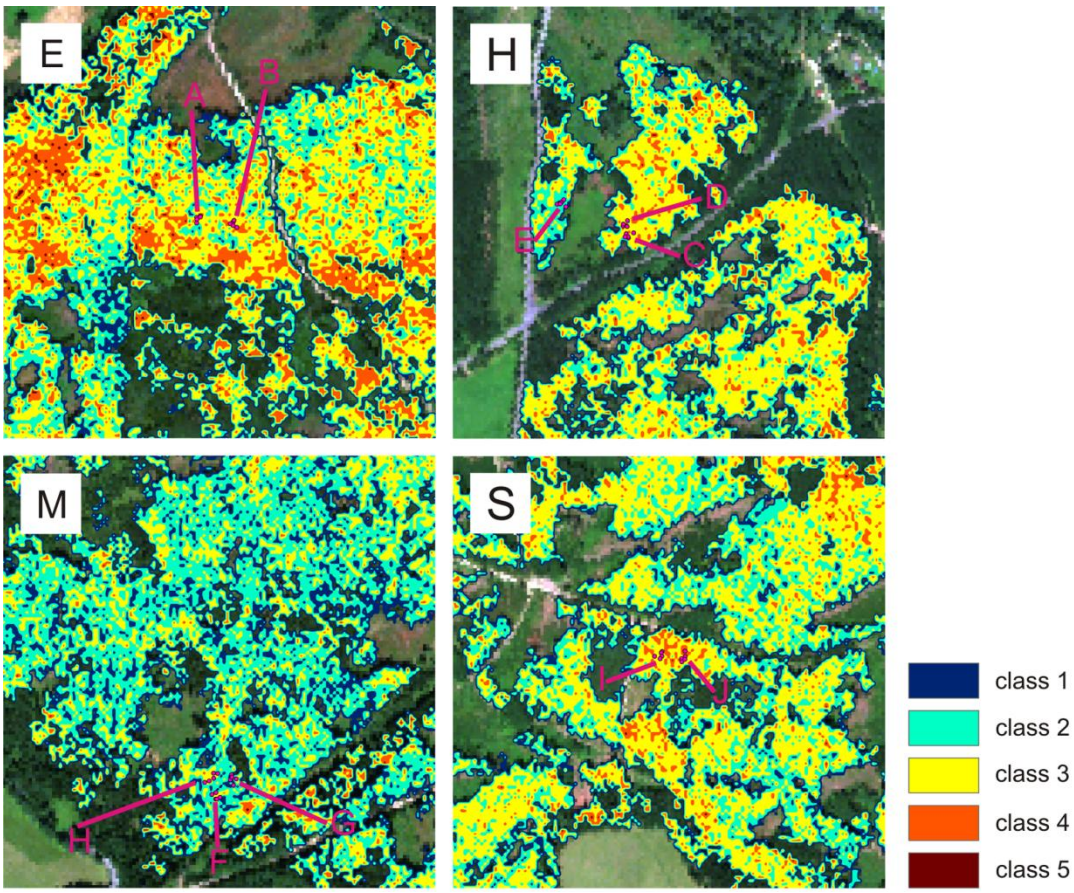

***Figure 4.9**: Statistical classification of the Norway spruce health status by integrating the Cab, REP, and expSIPI. E ¼ Erika; H ¼ Habartov; M ¼ Mezihorská; S ¼ Studenec study sites; A through J;10 defined tree groups. Color scale 1 through 5—health status classes for the trees without visible damage symptoms; 1 = the worst and 5 = the best result (see Fig. 4.7).*

4.5 Results and Discussion

4.5.1 Validation and Prediction of the Canopy Chlorophyll Content (Cab)

In both multivariate approaches, the SMR spectral derivative and the continuum removal BD normalization models, the null hypothesis was tested. As a result, three different derivative variables (the derivative of the bands with central wavelengths 632, 661, and 544 nm) and only one normalized band ($RCR_{norm705}$) passed this test and where further used (Tab. 4.5).

Using the training dataset (A, C, D, F, G, and I), we obtained the models that all attained rxy high enough to pass the initial t-test (Tab. 4.5). For the validation dataset (groups B, E, H, and J), the statistical parameters, Rv2 and RMSE (Tab. 4.6), were used to test how well the linear models can predict the chlorophyll content, and the image average values were compared with the average values of the chlorophyll content obtained in the laboratory (ground truth).

In general, we obtained rather high coefficients of determination for the linear models calculated between the tested spectral indices and the ground truth dataset (canopy chlorophyll content) on both the training and the validation datasets (R2, Rv2). These results confirmed the assumption of a

strong dependence between the selected spectral indicators and the canopy chlorophyll contents. The scatterplots between ground (laboratory) chlorophyll content value and selected image derived spectral indices are shown in Fig. 4.10. For the training dataset (Tab. 4.5), the highest correlation coefficients (strongest linear relationship) were obtained for the normalized reflectance (N718) and the derivative ratio (D718⁄D704) models. The weakest correlation was found for the NDVI705 index. The strong negative correlations between the canopy chlorophyll content and the normalized reflectances (N690, N704, N718, and N733) are in accordance with the theoretical background. The higher the chlorophyll concentration, the higher is the absorption of radiation and the lower is the observed reflectance. SMR analysis found a valid result only for the multiple linear regression of spectral derivatives. For this particular case, we were able to calculate only the partial correlation coefficients between each independent variable (spectral index) and the dependent variable chlorophyll content (chlorophyll content). Therefore the general coefficient (rxy) was not defined for this model.

Comparing R2 (Tab.4. 5) to RMSE (Tab. 4.6) indicates that the model exhibiting the highest R2 does not necessarily give the best result. This can be demonstrated on the example of the multiple linear model calculated from the spectral derivatives. Despite the very high value of R^2 (R^2 = 0.99998), the model has the highest RMSE (RMSE = 0.7962 mg⁄g, relative RMSE = 32%). We assume this is due to the rather high noise level, which was multiplied by calculating the first derivatives from the image spectrum. The variability and the dynamic range of the predicted values for the chlorophyll contents were compared with the ground truth dataset using box plot diagrams. The box plots constructed for the predicted Cab values (D718⁄D708) and the ground truth Cab data (Fig. 4.11) exhibit good agreement for the Studenec and Erika sites. In contrast, a worse match was found for the Mezihorská test site, where extremely high variability of the predicted values can be observed. This can be explained by the low radiometric quality of the HyMap line (line No. 9) where the site is located. This particular line No. 9 suffers from a very high noise level compared with the other HyMap lines acquired in 2009 (see Chap. 4.3, Table 4.2, Fig. 4.2).

The best result taking in account R2, Rv2, and RMSE was obtained using the model based on the D718⁄D708 ratios (R2 = 0.9131, Rv2 = 0.9370, RMSE = 0.2055 mg⁄g, and relative RMSE = 8%). Therefore the D718⁄D708 model was applied to the all HyMap image data (lines 1 through 9) to retrieve the map of the canopy chlorophyll content (Fig. 4.12). This output was further used to assess the canopy health status.

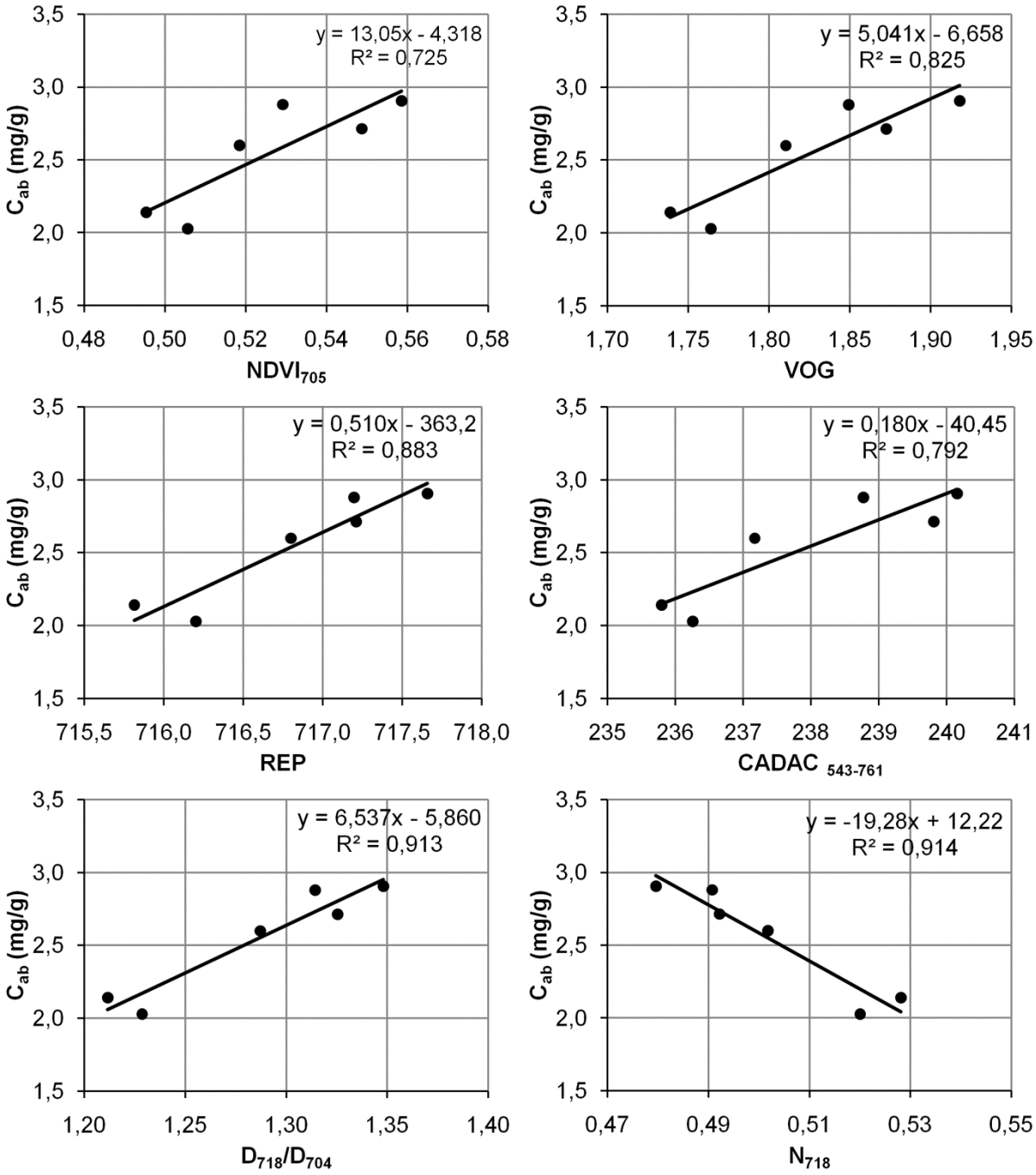

***Figure 4.10**: Scatterplots between ground (laboratory) measured chlorophyll content and selected image derived hyperspectral indices.*

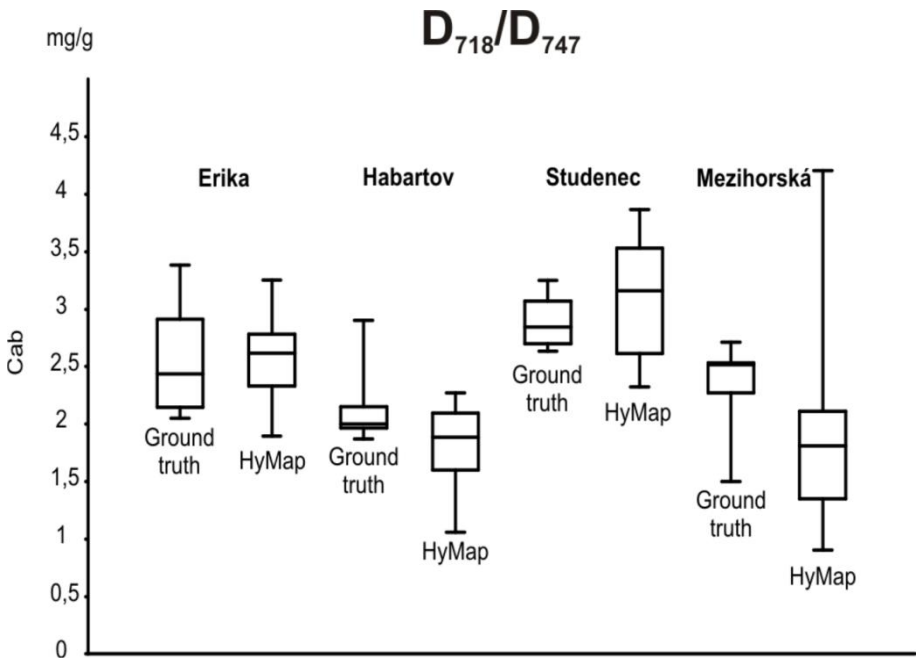

***Figure 4.11**: Box plots of the Measured (ground truth) and the predicted (HyMap) canopy chlorophyll contents for the derivative ratio index (D_{718}/D_{708}). C_{ab} – content of chlorophyll a+b (g of pigment related to dry mass).*

1.1.1 Assessment of the Norway spruce Health Status

Two statistical scenarios, Cab and REP þ exp SIPI, were tested to assess and classify the Norway spruce health status (see Chap. 4.5). Both scenarios were applied to all the pixels classified as homogenous Norway spruce forest in the HyMap image data (lines 1 through 9) (Fig. 4.9).

In both cases, Cab and REP þ exp SIPI, the frequency histograms (Figs. 4.13 and 4.14) show rather symmetrical distribution that is close to the Gaussian normal distribution. However, the histograms computed for each test site (Erika, Habartov, Mezihorská, and Studenec) show significant asymmetries. At the Erika site, we can identify slight asymmetry toward the higher-class values, indicating the higher frequencies of average and above-average values. On the other hand, for the Habartov site we can observe slight asymmetry toward the lower-class numbers, indicating the higher frequencies of average and below-average values. For the Mezihorská site, a very strong asymmetry can be observed. The majority (almost 75%) of the pixels were classified into the Classes 1 and 2, while Classes 4 and 5 have very low frequencies. The opposite situation can be observed for the Studenec site, where a strong asymmetry toward the high classes can be observed.

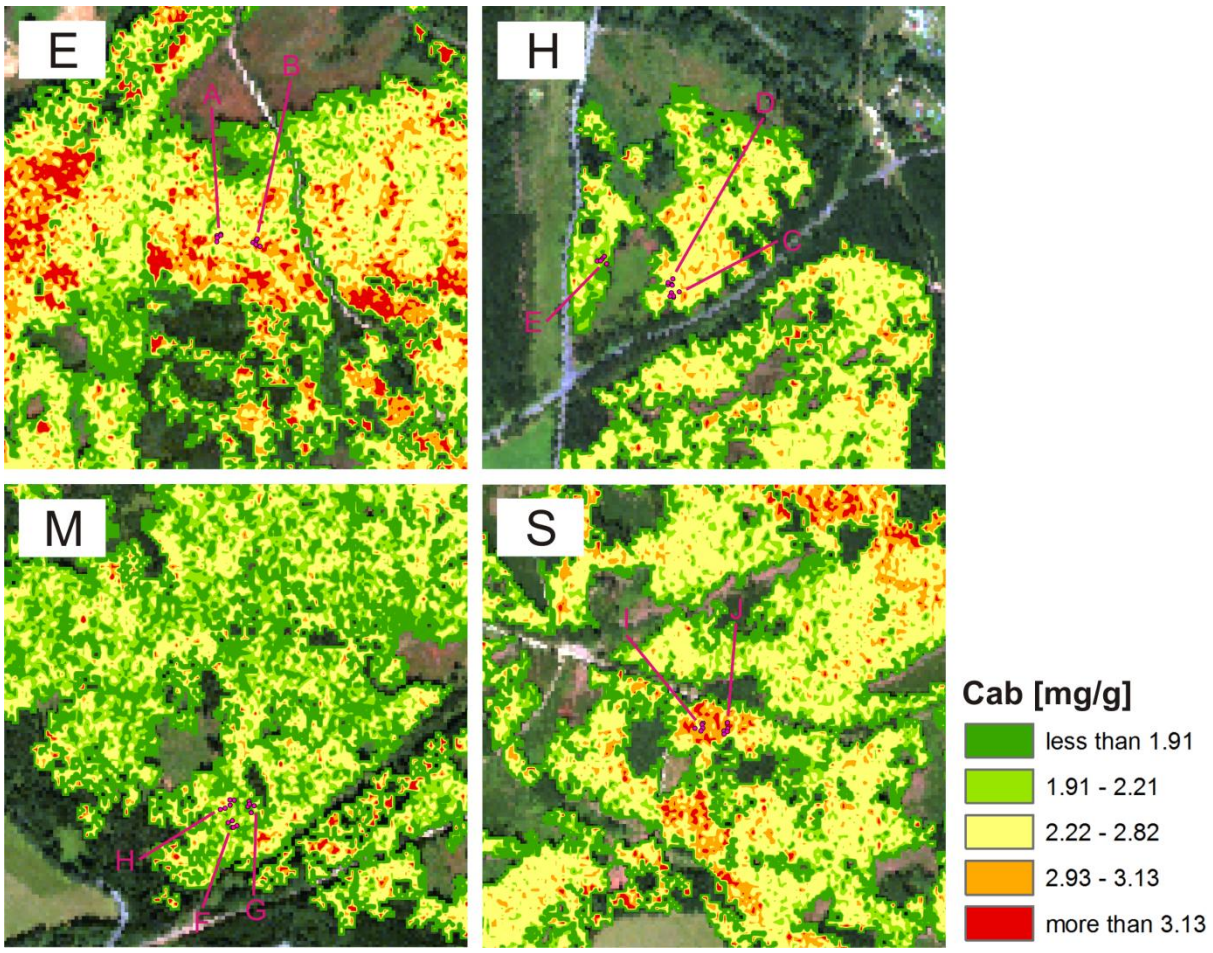

***Figure 4.12**: Map of the Norway spruce canopy chlorophyll content derived by applying the D_{718}/D_{704} regression model. E – Erika, H – Habartov, M – Mezihorská, S – Studenec. C_{ab} – content of chlorophyll a+b (g of pigment related to dry mass), A-J – 10 groups of 5 sampled trees.*

Erika, Habartov, Mezihorská, and Studenec (below). Comparing the two tested classification scenarios (Cab and REP þ exp SIPI), the Cab method shows higher data variability. The Cab scenario has higher frequencies of extreme values (Class 1 and Class 5) in contrast with the REP þ exp SIPI scenario, where the values are more frequently classified in the average Class 3. This can be explained by the higher variability of the Cab values compared with the expSIPI values. The laboratory analysis of the Norway spruce needles, collected during the project described in Ref.[61], indicated that higher needle chlorophyll content is not automatically connected with a better health status. Therefore the chlorophyll content itself cannot be the only indicator of damage to the Norway spruce. To take in account this fact, the expSIPI index was used as a correcting factor in the selected model. If the Norway spruce stands have very high Cab and REP values, and the expSIPI values don't indicate any health damage, the pixels fall into average Class 3 instead of being classified in Class 4 or 5.

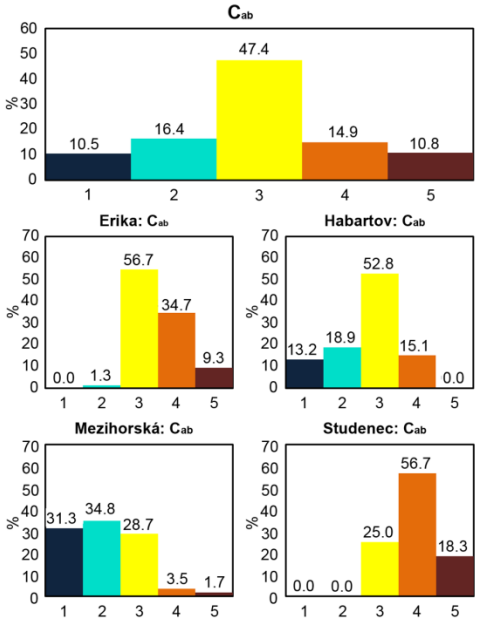

Figure 4.13: *Relative frequencies (%) of the Norway spruce health status classes obtained for the Cab classification scenario. The entire Sokolov lignite basin area (top) and the individual sites Erika,Habartov, Mezihorská, and Studenec (below).*

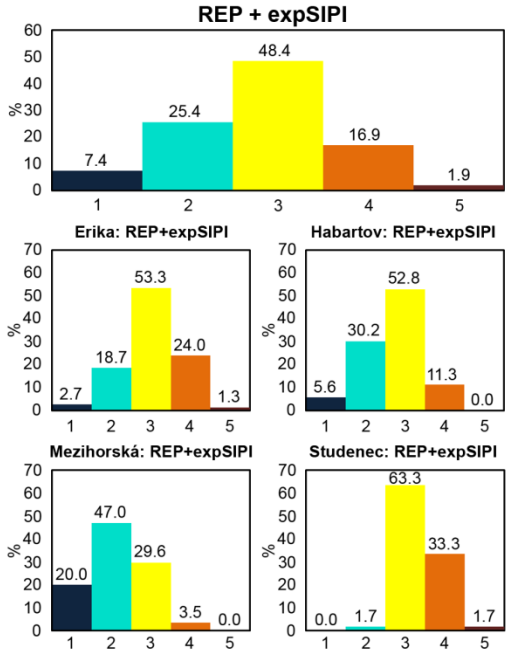

Figure 4.14: *Relative frequencies (%) of the Norway spruce health status classes obtained by the statistical scenario REP þ expSIPI. The entire Sokolov lignite basin area (top) and the individual sites.*

All the studied sites exhibited soil solution pH values under 3.5 (Tab. 4.8), which correspond to low pH threshold for forest soils in the Czech Republic.[46] We assume that soil acidity is the main stress factor in the studied locality. This finding is supported by the fact that Central Europe and Denmark were considered to be the areas with the highest exceeding of limits for soil acidification indicators, pH and base cations-to-Al ratios in 2010.[79] Soil conditions, especially nutrient availability and balance,

determine the physiological status of forest trees. Nutrient imbalances and deficiencies may result in increased susceptibility to a number of stress factors, such as weather extremes or pest invasions.[79] Thus determination of the health status of trees should include evaluation of numerous parameters and should also take into account other factors such as soil pH and the base cations-to-Al ratios, used to estimate the risk of damage to the vegetation from acidified soil (ICP Forests Executive Report, 2010). High values of the organic horizon C:N ratios (above 22) also imply the possibility of lower nitrification[11] and thus slower nutrient turnover or misbalance.

Table 4.8: *The soil solution pH (in KCl) and C:N ratio for the two organic top horizons. One-way ANOVA, * significant difference at 0.05, ** significant difference at 0.01. Different letters indicate significant differences between sites according to the Turkey-Kramer multiple comparison test.*

pH and C:N ratio in two organic horizons						
Site	**pH (KCl)**			**C:N ratio**		
	upper horizont	lower horizont	both horizonts	upper horizont	lower horizont	both horizonts
Erika	2.55^{b**}	2.50^{d**}	2.53^{d**}	28.06^{ac*}	27.10^{ns}	28.40^{ns}
Habartov	3.18^{ad**}	3.43^{a**}	3.31^{a**}	26.68^{b*}	31.80^{ns}	29.24^{ns}
Mezihorská	2.87^{c**}	2.76^{c**}	2.81^{c**}	28.65^{abc*}	27.24^{ns}	27.65^{ns}
Studenec	3.33^{a**}	2.99^{b**}	3.16^{b**}	29.70^{a*}	26.80^{ns}	27.73^{ns}

1.2 Conclusions

According to the ICP Forest methodologies, the main indicators for forest health assessment at Level I consists in evaluation of crown defoliation and foliage discoloration; however several limitations of these indicators have been discussed recently.[6] Although the chlorophyll content could serve as a relevant quantitative forest health indicator, it is not included either in the foliage chemistry indicators of the ICP Forest manual[80] or in the US Forest Service's Forest Inventory and Analysis program.[81] This could be explained by the fact that large-scale assessment of the chlorophyll content could be problematic due to laboriousness and high costs of the needle sampling and biochemical analyses. At the present time, hyperspectral technologies provide an opportunity to retrieve a reliable continuous chlorophyll model while requiring only a reasonable number of samples.

Although the chlorophyll content in foliage is quite often declared to be an indicator of plant physiological status,[82] the uniform classification of chlorophyll contents for Norway spruce needles is not yet very well established. To date, no fixed threshold values of needle chlorophyll content for determination exact classes of forest health status exists. The actual chlorophyll content in the needles of coniferous trees depends on the local and microclimatic conditions, including geographical factors such as latitude and altitude.[83] Particularly the altitude correspond with a combination of several environmental factors, such as irradiance,[17,18] temperature, water, and nutrient availability, which are all factors that influence the chlorophyll content in foliage.[83,84]

Oleksyn et al.[83] reported that seedlings of high-altitude Norway spruce populations in colder regions contained higher chlorophyll concentrations in needles than trees at low elevations. According to Ref. [85], the chlorophyll content in needles of healthy mature (60 years and older) Norway spruce (altitude 840 m) ranges between 2.2 to 2.7 mg per gram of dry mass and other authors state even higher chlorophyll contents: 3.21±0.30 mg per gram of dry mass (altitude 400 m)[62] or 4.30±1.06 mg per gram of dry mass (altitude 700 m).[86] Therefore it is necessary in each case to adjust the threshold values of the chlorophyll content to local conditions. We assume that our model could be applied to other spruce or coniferous species, but at least minimal ground truth calibration and laboratory analyses of pigment contents are advisable. It appears that local environmental conditions affect the chlorophyll content even more strongly than the difference between two spruce species. According to Barsi et al.,[84] the difference in chlorophyll content in needles of early succession black spruce (1.6 mg per gram of dry mass) and late succession red spruce (1.44 mg per gram of dry mass), both grown under the same controlled conditions, was on average only 10%.

We evaluated the numerous approaches to determine the chlorophyll content empirically. The individual models were statistically assessed using the ground truth training/validation datasets and the best model based on the spectral derivative ratio (D718⁄D704, RMSE = 0.2055 mg⁄g, R2 = 0.9370) was chosen to estimate the chlorophyll (Cab) content for the Norway spruce species using the HyMap multiflight line data. Then we developed a new statistical method to assess the physiological status of macroscopically undamaged foliage of Norway spruce. As the chlorophyll content alone may not correspond sufficiently well to the physiological/health status, the suggested method utilizes three indicators (Cab, REP, expSIPI). Thus the suggested method takes in account the two major biochemical parameters that are closely connected with photosynthetic functions (chlorophylls and carotenoids), and it allows assessing of the vegetation stress in a more objective way. Based on our z-score classification of the needle chlorophyll content, the medium health status class of trees lacking visible damage symptoms (Class 3, chlorophyll content 2.22 to 2.83 mg per gram dry mass) corresponds well with the chlorophyll values reported by Ref. [84]. This accordance suggests the possibility of the general applicability of our model after further testing and validation.

Acknowledgments

The research is being undertaken as part of a larger HYPSO scientific research project within the framework of grant No. 205/09/1989 funded by the Czech Science Foundation. Many thanks belong to Dr. Jan Frouz for his technical support of the field campaign and to all the students who participated in sample collection.

References

1. R. B. Jackson et al., “Protecting climate with forests,” En. Re. Lett. 3(4), 044006 (2008), http://dx.doi.org/10.1088/1748-9326/3/4/044006.

2. G. B. Bonan, “Forest and climate change: forcing, feedbacks and their climate benefits of forests,” Science 320(5882), 1444–1449 (2008), http://dx.doi.org/10.1126/science.1155121.

3. R.Hassan and N. Scholes, Eds., Ecosystems and Human Well-being: Current State and Trends, p. 815, Island Press, Washington, DC (2005).

4. J. C. Aznar et al., “Lead exclusion and copper translocation in black spruce needles,” Water Air Soil Poll. 203(1–4), 139–145 (2009), http://dx.doi.org/10.1007/s11270-009-9997-8.

5. P. Šebesta et al., “Acidification of primeval forests in the Ukraine Carpathians: vegetation and soil changes over six decades,” Forest Ecology Manag. 262(7), 1265–1279 (2011), http://dx.doi.org/10.1016/j.foreco.2011.06.024.

6. J. Johnson and M. Jacob, “Monitoring the effects of air pollution on forest condition in Europe: is crown defoliation an adequate indicator?” iForest 3, 86–88 (2010), http://dx.doi.org/10.3832/ifor0538-003.

7. Large scale forest condition. [on-line], http://icp-forests.net/page/largescale-forest-condition.

8. ICP forest assessment—level II. [on-line], http://icp-forests.net/page/level-ii.

9. S. L. Ustin et al., “Retrieval of foliar information about plant pigment systems from high resolution spectroscopy,” Re. Sens. Envir. 113, S67–S77 (2009), http://dx.doi.org/10.1016/j.rse.2008.10.019.

10. R. F. Kokaly et al., “Characterizing canopy biochemistry from imaging spectroscopy and its application to ecosystem studies,” Re. Sens. Envir. 113, S78–S91 (2009), http://dx.doi.org/10.1016/j.rse.2008.10.018.

11. S. V. Ollinger et al., “Regional variation in foliar chemistry and N cycling among forests of diverse history and composition,” Ecology 83(2), 339–355 (2002), http://dx.doi.org/10.2307/2680018.

12. J. S. Delegido et al., “Estimating chlorophyll content of crops from hyperspectral data using a normalized area over reflectance curve (NAOC),” Inter. J. App. Earth Ob. Geoinfo. 12(3),165–174 (2010), http://dx.doi.org/10.1016/j.jag.2010.02.003.

13. D. H. Card, D. L. Peterson, and P. A. Matson, “Prediction of leaf chemistry by the use of visible and near infrared reflectance spectroscopy,” Re. Sens. Envir. 26(3), 123–147 (1988), http://dx.doi.org/10.1016/0034-4257(88)90092-2.

14. D. L. Peterson et al., “Remote sensing of forest canopy and leaf biochemical contents,” Re. Sens. Envir. 24, 85–108 (1988), http://dx.doi.org/10.1016/0034-4257(88)90007-7.

15. A. Gitelson et al., “Remote estimation of canopy chlorophyll content in crops,” Geophys. Re. Lett. 32, 4–7 (2005), http://dx.doi.org/10.1029/2005GL022688.

16. B. Datt, “A new reflectance index for remote sensing of chlorophyll content in higher plants: tests using eucalyptus leaves,” J. Plant Phy. 154(1), 30–36 (1999), http://dx.doi.org/10.1016/S0176-1617(99)80314-9.

17. A. D. Richardson, G. P. Berlyn, and T. G. Gregoire, “Spectral reflectance of Picea rubens(Pinaceae) and Abies balsama (Pinaneae) needles along an elevational gradient, MoosilaukeMt.,New Hampshire,” 1. Am. J.Botany 88(4), 667–676 (2001), http://dx.doi.org/10.2307/2657067.

18. A. D. Richardson, J. B. Reeves, and T. G. Gregoire, “Multivariate analyses of visible/near infrared (VIS/NIR) absorbance spectra reveal underlying spectral differences among dried, ground conifer needle samples from different growth environments,” New Phytologist

161(1), 291–301 (2004), http://dx.doi.org/10.1046/j.1469-8137.2003.00913.x.

19. P. J. Kramer, “Carbon dioxide concentration, photosynthesis and dry matter production,” BioScience 31(1), 29–33 (1981), http://dx.doi.org/10.2307/1308175.

20. G. A. Blackburn, “Hyperspectral remote sensing of plant pigments,” J. Exper. Botany 58(4), 855–867 (2007), http://dx.doi.org/10.1093/jxb/erl123.

21. C. Wu et al., “Estimating chlorophyll content from hyperspectral vegetation indices: modeling and validation,” Agr. Forest Meteorol. 148(8–9), 1230–1241 (2008), http://dx.doi.org/10.1016/j.agrformet.2008.03.005.

22. B. Demming-Adams and W. W. Adams, “The role of xanthophyll cycle carotenoids in the protection of photosynthesis,” Trends Plant Sci. 1(1), 21–26 (1996), http://dx.doi.org/10.1016/S1360-1385(96)80019-7.

23. J. J. Landsberg et al., “Energy conversion and use in forest: an analysis of forest production in terms of radiation utilization efficiency,” H. L.Gholz, K. Nakane, and H. Shimoda, Eds., The Use of Remote Sensing in the Modeling of Forest Productivity, pp. 273–298, Kluver Academic Publishers, Dordrecht, The Netherlands(1996).

24. A. Young and G. Britton, “Carotenoids and stress,” R. G.Alscher and J. R. Cummings, Eds., Stress Responses in Plants: Adaptation and Aclimation Mechanisms, pp. 87–112, Willey-Liss, New York (1990).

25. Z. Malenovský et al., “Scaling dimensions in spectroscopy of soil and vegetation,” Internat. J. App. Earth Ob. Geoinfo. 9(2), 137–164 (2007), http://dx.doi.org/10.1016/j.jag.2006.08.003.

26. R. Pu, P. Gong, and Q. Yu, “Comparative analysis of EO-1 ALI and Hyperion, and Landsat ETMþ data for mapping forest crown closure and leaf area index,” Sensors 8(6), 3744–3766 (2008), http://dx.doi.org/10.3390/s8063744.

27. D. R. Peddle et al., “Physically-based inversion modeling for unsupervised cluster labeling, independent forest classification and LAI estimation using MFM-5-scale,” Can. J. Re. Sens. 33(3), 214–225 (2007), http://dx.doi.org/10.5589/m07-026.

28. B. D. Ganapol et al., “LEAFMOD: a new within-leaf radiative transfer model,” Re. Sens. Envir. 63(2), 182–193 (1998), http://dx.doi.org/10.1016/S0034-4257(97)00134-X.

29. S. Jacquemoud and F. Baret, “PROSPECT: a model of leaf optical properties spectra,” Re. Sens. Envir. 34(2), 75–91 (1990), http://dx.doi.org/10.1016/0034-4257(90)90100-Z.

30. C. S. T. Daughtry et al., “Estimating corn leaf chlorophyll concentration from leaf and canopy reflectance,” Re. Sens. Envir. 74(2), 229–239 (2000), http://dx.doi.org/10.1016/S0034-4257(00)00113-9.

31. D. Haboudane et al., “Integrated narrow-band vegetation indices for prediction of cropchlorophyll content for application to precision agriculture,” Re. Sens. Envir. 81(2–3), 416–426 (2002), http://dx.doi.org/10.1016/S0034-4257(02)00018-4.

32. R. A. Jago, M. E. Cutler, and P. J. Curran, “Estimating canopy chlorophyll concentration from field and airborne spectra,” Re. Sens. Envir. 68(3), 217–224 (1999), http://dx.doi.org/10.1016/S0034-4257(98)00113-8.

33. W. Verhoef, “Light-scattering by leaf layers with application to canopy reflectance modeling–the SAIL model,” Re. Sens. Envir. 16(2), 125–141 (1984), http://dx.doi.org/10.1016/0034-4257(84)90057-9.

34. C. van der Tol et al., “An integrated model of soil-canopy spectral radiance observations,

photosynthesis, fluorescence, temperature and energy balance,” Biogeosciences Disc. 6, 6025–6075 (2009), http://dx.doi.org/10.5194/bgd-6-6025-2009.

35. V. Demarez and J. P. Gastellu-Etchegorry, “A modeling approach for studying forest chlorophyll content,” Re. Sens. Envir. 71(2), 226–238 (2000), http://dx.doi.org/10.1016/S0034-4257(99)00089-9.

36. S. Jacquemoud, “Inversion of the PROSPECT þ SAIL canopy reflectance model from AVIRIS equivalent spectra: theoretical study,” Re. Sens. Envir. 44(2–3), 281–292 (1993), http://dx.doi.org/10.1016/0034-4257(93)90022-P.

37. S. Chaurasia and V. K. Dadhwal, “Comparison of principal component inversion with VIempirical approach for LAI estimation using simulated reflectance data,” Inter. ReJ. Sens. 25(14) 2881–2887 (2004), http://dx.doi.org/10.1080/01431160410001685018.

38. R. Houborg and E. Boegh, “Mapping leaf chlorophyll and leaf area index using inverse and forward canopy reflectance modeling and SPOT reflectance data,” Re. Sens. Envir. 112(1) 186–202 (2008), http://dx.doi.org/10.1016/j.rse.2007.04.012.

39. C. Atzberger, “Object-based retrieval of biophysical canopy variables using artificial neural nets and radiative transfer models,” Re. Sens. Envir. 93(2–3), 53–67 (2004), http://dx.doi.org/10.1016/j.rse.2004.06.016.

40. C. Atzberger et al., “Retrieval of wheat bio-physical attributes from hyperspectral data and SAILH þ PROSPECT radiative transfer mode,” M.Habermayer, A. Müller, and S. Holzwarth, Eds., in Proc. of the 3rd EARSeL Workshop on Imaging Spectroscopy, pp. 473–482, Herrchnig, Germany (2003).

41. Annual Tabular Overview, Air Quality Protection Division, Czech Hydrometeorological Institute, [on-line], http://portal.chmi.cz/files/portaldocs/uoco/tab_roc_CZ.html

42. P. J. Curran, W. R. Windham, and H. L. Gholz, “Exploring the relationship between reflectancered edge and chlorophyll concentration in slash pine leaves,” Tree Physiology 15(3),203–206 (1995).

43. J. A. Gamon, J. Peñuelas, and C. B. Field, “A narrow-wave band spectral index that trackdiurnal changes in photosynthetic efficiency,” Re. Sens. Envir. 41(1), 35–44 (1992), http://dx.doi.org/10.1016/0034-4257(92)90059-S.

44. J. Peñuelas, F. Baret, and I. Fiella, “Semi-empirical indices to assess carotenoids/chlorophyll-a ratio from leaf spectral reflectance,” Photosynthetica 31(2), 221–230 (1995).

45. P. Rojík, “New stratigraphic subdivision of the tertiary in the Sokolov Basin in Northwestern Bohemia,” J. Czech Geological Society 49(3–4), 173–186 (2003).

46. P. Fabiánek, Forest Condition and Monitoring in the Czech Republic 1984–2003, Ministry of Agriculture of the Czech Republic and Forestry and Game Management Research Institute, ELAN spol. s.r.o., Přerov, Czech Republic, p. 431 (2004).

47. R. Porra, W. Thompson, and P. Kriedemann, "Determination of accurate extinction coefficientsand simultaneous equations for assaying chlorophylls a and b extracted with four different solvents: verification of the concentration of chlorophyll standards by atomic absorption spectroscopy," Biochimica et Biophysica Acta 975(3), 384–394 (1989), http://dx.doi.org/10.1016/S0005-2728(89)80347-0.

48. A.Welburn, "The spectral determination of chlorophyll-a and chlorophyll-b, as well as total carotenoids, using various solvents with spectrophotometers of different resolution," J. Plant Phys. 144(3), 307–313 (1994), http://dx.doi.org/10.1016/S0176-1617(11)81192-2.

49. G. Schaepman-Strub et al., "Reflectance quantities in optical remote sensing—definitionsand case studies," Re. Sens. Envir. 103(1), 27–42 (2006), http://dx.doi.org/10.1016/j.rse.2006.03.002.

50. R. Richter, "Atmospheric/topographic correction for airborne imagery," ATCOR-4 User Guide, Version 5.0, January 2009, DLR-German Aerospace Centre, D-82234 Wessling, Germany, p. 168 (2009). 51. A. Berk, G. P. Anderson, and L. S. Bernstein, "MODTRAN-4 radiative transfer modeling for atmospheric correction, optical spectroscopic techniques and instrumentation for atmospheric and space research III book series," Proc. SPIE 3756, 348–353 (1999).

52. J. Weyermann, A. Damm, and M. Schaepman, "Comparing empirical and semi-empirical approaches for brdf correction in airborne imaging," (in preparation) 53. J. Verrelst et al., "Angular sensitivity analysis of vegetation indices derived from CHRIS/PROBA data," Re. Sens. Envir. 112(5), 2341–2351 (2008), http://dx.doi.org/10.1016/j.rse.2007.11.001.

54. C. B. Schaaf et al., "First operational BRDF, albedo nadir reflectance products from MODIS," Re. Sens. Envir. 83(1–2), 135–148 (2002), http://dx.doi.org/10.1016/S0034-4257(02)00091-3.

55. D. Schläpfer, "Parametric Geocoding, PARGE Using Guide," Version 2.3, ReSe Applications Schläpfer & Remote Sensing Laboratories University of Zurich, PDF/CD-ROM Edition, Wil SG, p. 195

56. F. van der Meer and S. de Jong, "Quality control: signal to noise characterization," chapter 2, part 9, in Imaging Spectrometry: Basic Principles and Prospective Application, International Institute for Geo-information Science and Earth Observation (ITC), pp. 1922 (2002).

57. A. A. Green et al., "A transformation for ordering multispectral data in terms of image quality with implications for noise removal," IEEE Trans. Geosci. Re. Sens. 26(1), 65–74 (1988), http://dx.doi.org/10.1109/36.3001.

58. D. A. Sims and J. A. Gamon, "Relationships between leaf pigment content and spectral reflectance across a wide range of species, leaf structures and developmental stages," Re. Sens. Envir. 81(2–3), 337–354 (2002), http://dx.doi.org/10.1016/S0034-4257(02)00010-X.

59. E. Vogelmann, B. N. Rock, and D. M. Moss, "Red edge spectral measurements from sugar maple leaves," Inter. J. Re. Sens. 14(8), 1563–1575 (1993), http://dx.doi.org/10.1080/01431169308953986.

60. J. G. P. Guyot and F. Baret, "Utilisation de la heute resolution spectrale pour suivre l'état des couverts végétaux," Proceedings of the 4th International colloquium on spectral signatures of object in remote sensing, ESA SP-287, Assois, France, 279–286 (1988).

61. Z. Malenovský et al., “A New hyperspectral index for chlorophyll estimation of a forest canopy: area under curve normalized to maximal band depth between 650–725 nm,”EARSel eProceedings 5(2), 161–172 (2006).

62. M. Schlerf et al., “Retrieval of chlorophyll content and nitrogen in Norway spruce (Picea abies KarstL.) using imaging spectroscopy,” Inter. J. Appl. Earth Ob. Geoinfo. 12(1), 17–26 (2010), http://dx.doi.org/10.1016/j.jag.2009.08.006.

63. R. I. Jennrich, “Stepwise regression,” K.Enslein, A. Ralston, and S. Wilf, Eds., Statistical Methods for Digital Computers, pp. 76–90, Wiley, New York (1977).

64. R. N. Clark and T. L. Roush, “Reflectance spectroscopy: quantitative analysis techniques for remote sensing appélications,” J. Geo. Re. 89(B7), 6329–6340 (1984),http://dx.doi.org/10.1029/JB089iB07p06329.

65. P. K. Entcheva-Campbell et al., “Detection of initial damage in Norway spruce canopies using hyperspectral airborne data,” Inter. J. Re. Sens. 25(24), 5557–5583 (2004), http://dx.doi.org/10.1080/0143116041000172605.

66. S. S. Shapiro and M. B. Wilk, “An analysis of variance test for normality (complete samples),”Biometrika 52(3–4), 591–611 (1965), http://dx.doi.org/10.1093/biomet/52.3-4.591.

67. D. M. Gates et al., “Spectral properties of plants,” Appl. Optic. 4(1), 11–20 (1965).68. W. Collins, G. L. Raines, and F. C. Canney, “Airborne spectroradiometer discrimination of vegetation anomalies over sulphide mineralization–a remote sensing technique,” in 90thAnnual Meeting problems and Abstracts, Geological Society of America Seattle, Vol. 9, pp. 932–933, Washington, DC (1977).

69. N. H. Horler, J. Barber, and A. R. Barringer, “Effects of heavy metals on the absorbance andreflectance spectra of plants,” Inter. J. Re. Sens. 1(2), 121–136 (1980), http://dx.doi.org/10.1080/01431168008547550.

70. F. Boochs et al., “Shape of the red edge as vitality indicator for plants,” Inter. J. Re. Sens. 11(10), 1741–1753 (1990), http://dx.doi.org/10.1080/01431169008955127.

71. G. P. W. Clevers et al., “Derivation of the red edge index using MERIS standard band setting,”Inter. J. Re. Sens. 23(16), 3169–3184 (2002), http://dx.doi.org/10.1080/01431160110104647.

72. B. N. Rock, T. Hoshizaki, and J. R. Miller, “Comparison of in situ and airborne spectralmeasurement of the blue shift associated with forest decline,” Re. Sens. Envir. 24(1),

109–127 (1988), http://dx.doi.org/10.1016/0034-4257(88)90008-9.

73. D. N. H. Horler,M. Dockray, and J. Barber, “The red edge of plant leaf reflectance,” Inter. J Re. Sens. 4(2), 279–288 (1983), http://dx.doi.org/10.1080/01431168308948546.

74. S. H. Chang andW. Collins, “Confirmation of the airborne biogeophysical mineral exploration technique using laboratory methods,” Econ. Geol. Bull. Soc. Econ. Geol. 78(4), 723–736 (1983), http://dx.doi.org/10.2113/gsecongeo.78.4.723.

75. J. A. Gamon, L. Serrano, and J. S. Surfus, “The photochemical reflectance index: an optical indicator of photosynthetic radiation use efficiency across species, functional types and nutrient levels,” Oecologia 112(4), 492–501 (1997), http://dx.doi.org/10.1007/s004420050337.

76. F. Thenot, M. Méthy, and T. Winkel, “The Photochemical Reflectance Index (PRI) as a water stress index,” Inter. J. Re. Sens. 23(23), 5135–5139 (2002), http://dx.doi.org/10.1080/01431160210163100.

77. L. Súarez et al., “Modeling PRI for water stress detection using radiative transfer models,” Re. Sens. Envir. 113(4), 730–744 (2009), http://dx.doi.org/10.1016/j.rse.2008.12.001.

78. C. Y. Kramer, “Extension of multiple range test to group means with unequal number of replications,” Biometrics 12(3), 307–310 (1956), http://dx.doi.org/10.2307/3001469.

79. ICP Forests Executive Report 2010, [on-line], http://icp-forests.net/page/icp-forestsexecutive-report

80. ICP Forests Manual, part XII Sampling and Analysis of Leaves and Needles, [on-line], http://icp-forests.org/pdf/FINAL_Foliage.pdf

81. C. W. Woodal et al., “Status and future of the forest health indicators program of the USA,” Environ. Monit. Assess. 177(1–4), 419–436 (2011), http://dx.doi.org/10.1007/s10661-010-1644-8.

82. J. Soukupová, B. N. Rock, and J. Albrechtová, “Comparative study of two spruce species in a polluted mountainous region,” New Phytologist 150(1), 133–145 (2001), http://dx.doi.org/10.1046/j.1469-8137.2001.00066.x.

83. J. Oleksyn et al., “Growth and physiology of Picea abies populations from elevational transects: common garden evidence for altitudinal ecotypes and cold adaptation,” Funct. Ecol. 12(4), 573–590 (1998), http://dx.doi.org/10.1046/j.1365-2435.1998.00236.x.

84. D. Barsi et al., “Generic variation and control of chloroplast pigment concentrations an related needle-level traits in Picea rubens, Picea marina and their hybrids: moisture and light environmental effects,” Trees—Struct. Funct. 23(3), 555–571 (2009), http://dx.doi.org/10.1007/s00468-008-0301-0.

85. D. Siefermannharms, “Light and temperature control of season-dependent changes in the alphacarotene and beta-carotene content of spruce needles,” J. Plant Phys. 143(4–5), 488–494 (1994).

86. C. Atzberger and W. Werner, “Needle reflectance of healthy and diseased Spruce stands,” 1st EARSeL Workshop on Imaging Spectroscopy, pp. 271–283, Remote Sensing Laboratories, University of Zurich, Impression Dumas, Saint-Etiene rance (1998).

5. Using multi-date high spectral resolution data to assess physiological status of macroscopically undamaged foliage on a regional scale

Kopačková, V., Mišurec, J., Lhotáková, Z., Oulehle, F., Albrechtová, J., (submitted for International Journal of Applied Earth Observation and Geoinformation): Using multi-date high spectral resolution data to assess the physiological status of macroscopically undamaged foliage on a regional scale, Forest Ecology and Management.

Abstract

Forests play an important role in regulation of the global climate; moreover, they provide human beings with a whole range of ecosystem services. Forest health and ecosystem functioning have been influenced by anthropogenic activities and their consequences, such as air pollution, surface mining, heavy metal contamination, and other biotic and abiotic stress factors, which had an especially serious effect on central Europe. Many aspects of the physiological state of trees are more or less related to the concentrations of two main groups of leaf photosynthetic pigments: chlorophylls and carotenoids. Therefore, their contents can be used as non-specific indicators of the actual tree physiological status, stress and the pre-visible tree damage. Variations in leaf biochemical composition affect foliar optical properties and can be assessed remotely using high spectral resolution data (hyperspectral data). These data were successfully used in earlier studies to detect vegetation stress and damage. However, only a few approaches have dealt with the use of hyperspectral remote sensing to assess vegetation physiological status on a regional scale. Moreover, little or no research has been done on assessing vegetation health while utilizing multi-date hyperspectral images.

In this study, the method for assessing forest health conditions using optical indices retrieved from hyperspectral data was applied to the two temporal HyMap date sets acquired in 07/2009 and 08/2010 to detect stress for the Norway spruce forests in Sokolov, NW Bohemia, a region affected by long-term extensive mining. The classification results were validated by ground truth data (total chlorophyll - Cab, carotenoids - Car and carotenoid to chlorophyll ratio - Car/Cab) and were associated with the geochemical conditions of the forest stands. Both biochemical analysis of the sampled foliage and classification of 2009 and 2010 hyperspectral image identified the same sites affected by vegetation stress. In addition to higher Car/Cab, which enabled detection of the stressed trees using hyperspectral image data, these sites showed critically low pH and lower values for the macronutrient parameters in both organic horizons and, in addition, both sites exhibit critically low base cation to aluminum ratios (Bc/Al) for lower organic and top mineral (0-20 cm) soil horizons. The results of this study demonstrate (i) the potential application of hyperspectral remote sensing as a rapid method of identifying tree stress prior to symptom expression, and (ii) the added value of multi-temporal approaches for hyperspectral data and its further potential for monitoring forest ecosystems.

Key words: *foliar biochemistry, forest monitoring, image spectroscopy, chlorophyll, carotenoids, tree stress*

5.1 Introduction

Forests play an important role in regulation of the global climate via the global carbon cycle, evapotranspiration, and earth surface albedo (Bonan, 2008; Jackson et al., 2008). Moreover, forests provide humans with a whole range of ecosystem services including provision of food and forest products, regulation of the hydrological cycle, protection of soil resources, etc. (Hassan and Scholes, 2005). Forest health and ecosystem functioning have recently been influenced by anthropogenic activities and their consequences, such as air pollution, surface mining, heavy metal contamination (Aznar et al., 2009), and other biotic and abiotic stress factors such as pest invasions and soil acidification (Šebesta et al., 2011), which had an especially high effect on central Europe. Therefore, large-scale monitoring of forest health and its methodologies are in the forefront of interest for scientists as well as forest managers.

Many aspects of the physiological state of trees are more or less connected with the concentrations of two main groups of leaf photosynthetic pigments: chlorophylls and carotenoids (Ustin et al., 2009). Vegetation with a high concentration of chlorophyll is considered to be healthy, as the chlorophyll content is linked to greater light-use efficiency, photosynthetic activity and carbon dioxide uptake (Blackburn, 2007; Kramer, 1981; Wu et al., 2008). Chlorophyll generally decreases under stress and during senescence (Blackburn, 2007). Carotenoids play the main role in the process of incident light absorption, transportation of energy to the reaction center of the photosystems, and heat dissipation of energy in case of high irradiation (Demmig-Adams and Adams, 1996). Combination of the influences of chlorophylls and carotenoids is thus connected with light-use efficiency (Landsberg et al., 1997). However, higher carotenoid to chlorophyll ratios indicate vegetation stress and senescence (Demmig-Adams and Adams, 1996; Young and Britton, 1990).

Therefore, the content of biochemical compounds such as photosynthetic pigments can be used as non-specific indicators of the actual tree physiological status, stress and the pre-visible tree damage. Moreover, the contents of photosynthetic pigments are closely related to photosynthetic performance and can serve as non-specific stress indicators in a very early stage, when the needles do not yet show any microscopic or macroscopic damage symptoms (Lepedus et al., 2005; Soukupová et al., 2000; Tzvetkova and Hadjiivanova, 2006). When dealing with photosynthetic pigments as vegetation stress indicators, seasonal dynamics in pigment contents in evergreen conifers must be taken into account. Changes in pigment levels reflect the normal physiological responses in the plant as well as the responses to environmental stress (Gamon and Surfus, 1999;

Gitelson et al., 2001, 2002, Grisham et al. 2010).The chlorophyll content in needles increases in the spring (from May/June) and during the summer (July-September) and then remains relatively constant until October, when it again decreases during the frost hardening process (Öquist and Huner, 2003). Some of the carotenoids (e.g. lutein, β-carotene) exhibit stable contents during the seasons in contrast to several groups of xanthopylls (e.g. antheraxanthin, zeaxanthin; Yatsko et al., 2011), which increase significantly during the winter and serve as effective protection of the photosynthetic apparatus under conditions of high irradiance and low temperature during the winter and spring (Maslova, 2009). The total carotenoid to total chlorophyll ratio decreases in parallel with the chlorophyll increase in the spring (Martz et al., 2007).

Conventional laboratory analyses of leaf biochemical parameters can be very precise, although they have a number of disadvantages (e.g., limited number of samples, high labor and cost demands). It has been demonstrated that variations in leaf biochemical composition affect foliar optical properties (Carter and Knapp, 2001; Kokaly et al., 2009; Sims and Gamon, 2002; Ustin et al., 2009). The spectral reflectance characteristics of plant canopies are influenced by the chemical composition, internal leaf structure and spatial distribution of the leaves (Asner, 1998; Ollinger, 2011; Zwiggelaar, 1998). Leaf pigments are well positioned to absorb incident light and can be assessed with spectral reflectance. The more important absorption pigments and their characteristic absorption wavelengths/wavebands were reviewed by Zwiggelaar (1998).

Modern remote sensing has become a novel tool not only for detecting target materials and also for monitoring dynamic processes and physical-property induced changes. The use of multispectral imagery has been demonstrated to effectively map the distribution of ecosystem types and vegetation systems (Everitt et al., 2002; Gould, 2000; Knorn et al., 2009; Lamb and Brown, 2001; Vogelmann et al., 2012); however, the low spectral resolution of multispectral imagery is a major limitation. On the other hand, imagery with higher spectral resolution (e.g., hyperspectral) provides sufficient spectral resolution to describe diagnostic absorption signatures and allows sufficiently detailed species discrimination and biochemical differentiation (Aspinall et al., 2002; Feret and Asner, 2013; Kokaly, 2009; Lass and Prather, 2004; Majeke et al., 2008; Odagawa & Okada, 2009; Underwood et al., 2003; Ustin et al., 2004; Zhao et al., 2013).

Data with very high spectral resolution – also referred to as imaging spectroscopy (IS) data, which is also known in the remote sensing community as hyperspectral data – has been successfully used in earlier studies to detect vegetation stress and damage (Campbell et al., 2004, 2007; Hamzeh et al.,

2013; Hernandez-Clemente et al., 2011; Pu et al., 2008; Romer et al., 2012). In the forestry context, most published precedents used IS data as a basis for identification of stress-sensitive wavelengths (e.g. Ahern, 1988), for development of stress-sensitive vegetation indices (e.g. Carter and Miller, 1994; Carter and Knapp 2001) and for integrating stress-sensitive indices in more complex models (e.g. Pontius et al., 2008; Shafri et al., 2012; Zarco-Tejada et al., 2004; Zhao et al., 2013).

In contrast, only a few approaches (Asner and Martin, 2009; Kampe et al., 2010) have dealt with the use of hyperspectral remote sensing (image spectroscopy) to assess vegetation physiological status on a regional scale. Moreover, little or no research has been done on assessing vegetation health utilizing multi-date hyperspectral image data, as a time-series of hyperspectral data and reliable methods to extract change/stress information for remotely sensed data analysis are still lacking.

We recently proposed a new method for assessing forest health condition via statistical integration of optical indices retrieved from HS image data (Mišurec, Kopačková et al., 2012). To assess subtle changes in the physiological status of macroscopically undamaged foliage of Norway spruce, this method integrated the following HyMap derived parameters: quantitative retrieval of chlorophyll concentrations (Cab); Red-Edge Position (REP) (Curran et al., 1995) – the inflection point of the spectral curve in the red-edge region, which is shifted to shorter wavelengths under vegetation stress (e.g., the presence of heavy metals in the soil) (Chang and Collins, 1983; Clevers et al., 2002; Curran et al., 1995; Horler et al., 1983; Rock et al., 1988); and the Structure Insensitive Pigment Index (SIPI) (Peñuelas et al., 1995) which is sensitive to the ratio of bulk carotenoids to chlorophyll. Although reliable results were obtained, further testing and validation was requested to confirm the general applicability of this method.

Therefore, in this study the same method (Mišurec, Kopačková et al., 2012) was employed while using two temporal HS image data sets (HyMap 2009 and 2010 image data) in order to:

- validate the new method using an additional temporal HS image dataset
- study the forest Norway Spruce variations in biochemical parameters while comparing the foliar pigment content from the samples collected in two subsequent growing seasons 2009 (28^{th}-29^{th} July) and 2010 (2^{nd}-3^{rd}September)
- assess vegetation stress within the selected Norway spruce sites while putting together information on forest stand geochemical conditions, foliar biochemistry (pigment contents) and the temporal differences detected by classifying the two HS image datasets acquired one year apart

5.2 Material and methods

5.2.1 Test site

The study was performed in the Sokolov basin in the western part of the Czech Republic, in a region affected by long-term extensive lignite mining (Fig. 5.1). Due to the mining activities and coal burning power plants that were built in the immediate vicinity of the mined area, this region is one of the most contaminated areas of the Czech Republic where high abundances of trace elements have been detected (Suchara et al., 2011). The average altitude of the study region is about 470 m. Because the basin is surrounded by the Krušné Hory Mountains, precipitation is above the average for the Czech Republic and the local climate in the region is subject to more extreme weather, characterized by colder and wetter conditions. According to the data of the meteorological station situated nearby (Karlovy Vary, 606 m a.s.l.), long-term (1962-2006) annual temperature and precipitation were 6.7°C and 589 mm, respectively.

The Sokolov basin in the Czech Republic is composed of rocks of Oligocene to Miocene age and is 8 - 9 km wide and up to 36 km long, with a total area of about 200 km^2. The basement of the Sokolov Basin is formed of Variscan and pre-Variscan metamorphic complexes of the Eger, Erzgebirge, Slavkov Forest, Thuring-Vogtland Crystalline Units, and granitoids of the Karlovy Vary Pluton (Fig. 5.1). The basal late Eocene Staré-Sedlo-Formation is formed of well-sorted fluvial sandstones and conglomerates and is overlain by a volcano-sedimentary complex up to 350 m thick, which contains three lignite seams (Rojík, 2004). The brown coal (lignite) contains 5 to 8% sulfur (S), and belongs among coal seams enriched in As (Yudovich and Ketris, 2005) and other heavy metals, such as Cd, Ni, Cu, Zn, Pb (Bouška and Pešek, 1999). Due to the presence of S in the coal, the lignite mines both still active and abandoned, are largely affected by acid mine drainage (AMD) (Kopačková et al., 2012).

The selected forest stands surround the lignite open pit mines in Sokolov, but have not been directly affected by the mining activities. However, the soil in all of the stands exhibits low pH, additionally Al and As were identified as toxic elements with high bio-availability (Kopačková, under review). Norway spruce was selected as it represents the predominant forest species in this region; in addition, spruce needles were confirmed to be well-suited for detection of contamination (Suchara et al., 2011). We selected four research sites dominated by mature Norway spruce forests of similar age (Tab. 1); this was important criteria as the stand age is the most important factor for defoliation. The stands were located at a maximum distance of 12 km from the active lignite open-pit mines (Fig.

Tab. 5.1). None of the selected sites exhibited any severe symptoms of macroscopic damage and they were all classified as damage class 1 with total crown defoliation not exceeding 25% and average needle retention of 8-10 needle age classes.

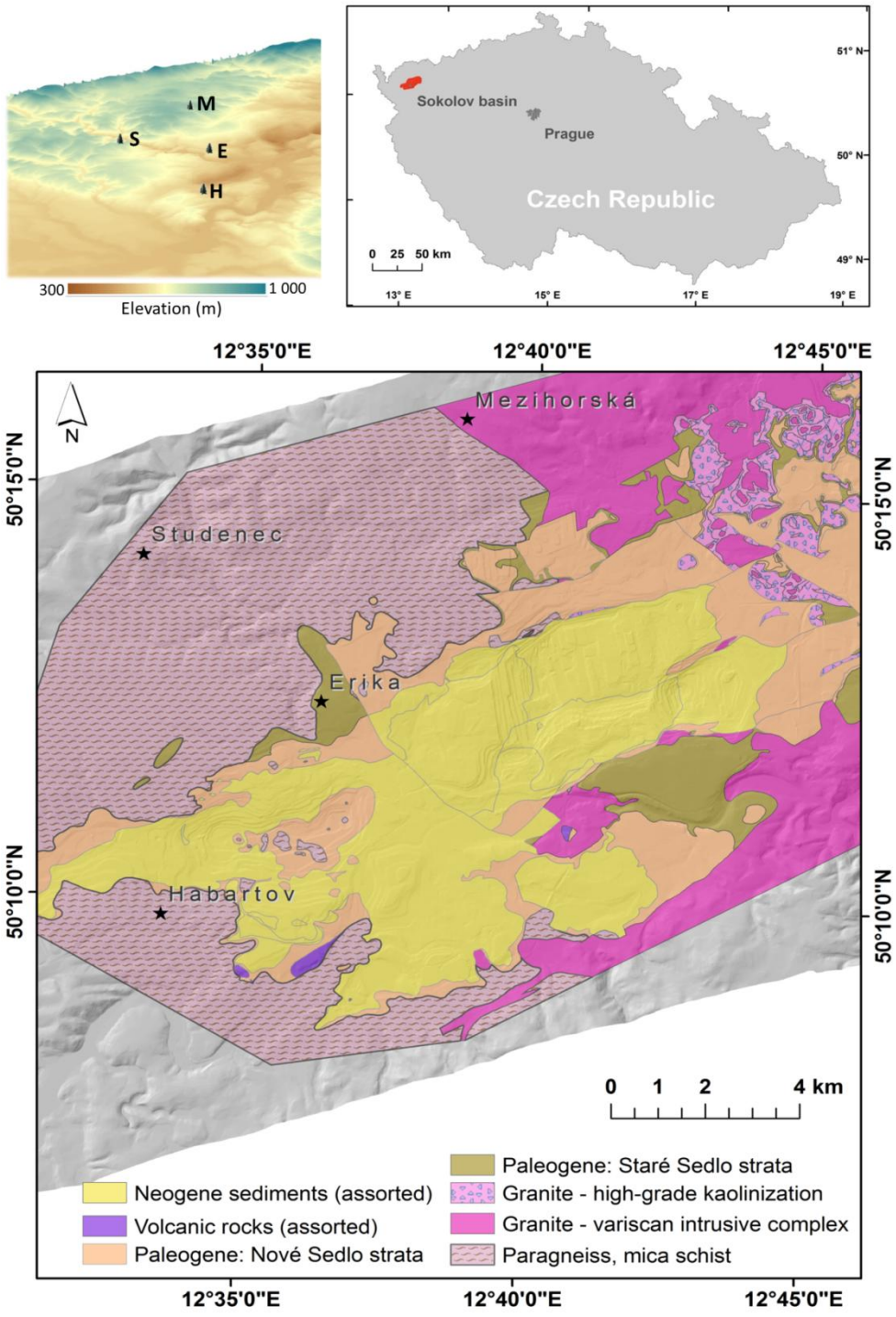

Figure 5.1: *Scheme showing the topography and simplified geological situation of the studied area.*

Table 5.1: *Norway spruce test sites.*

Site	Latitude (N)	Longitude (E)	Elevation (m a.s.l.)	Forest age (years)	Distance from the open-pit mines (km)	Geological unit
Erika	50°12'25"	12°36'17"	495	40-60	6.4	Staré Sedlo sandstones
Habartov	50°09'48"	12°33'28"	477	40-60	11.2	paragneiss, mica shist
Mezihorská	50°15'50"	12°38'17"	678	60-80	5.8	Granite
Studenec	50°14'09"	12°33'00"	722	40-60	8.5	paragneiss, mica shist

5.2.2 Field data

5.2.2.1 Foliar sampling

In 2009 Norway spruce needle samples were obtained in the week when the HyMap flight campaign (27th July 2009) was performed under unchanged weather conditions (27th –30th July). In 2010 due to the heavy rain the needles from the same trees were samples approximately 2 weeks after the HyMap data acquisition (21st August 2010). At each of the 4 test sites, 10-15 representative trees were selected in clearly definable groups of five (Erika: 2 groups (E_1, E_2), Habartov: 3 groups (H_1, H_2, H_3), Mezihorská: 3 groups (M_1, M_2, M_3) and Studenec: 2 groups (S_1, S_2)). Sample branches were taken from the sun-exposed (sunlit) and transitive portion of the canopy by tree climbers, the needles age classes were identified, and representative samples of the 1st and 3rd year needles were collected. Each set then contained 200 samples (50 trees x 2 positions in the crown x 2 age classes (1st and 3rd year needles). The samples were placed in plastic Eppendorf vials in a portable freezer (at 0° C), and transported within 2 hours to a nearby laboratory for further processing. The dry matter of the needles was acquired after drying in an oven for 48 hours at 80°C.

Photosynthetic pigments (e. g. chlorophyll a, b and total carotenoids) were extracted in dimethylforamide (DMF) for 7 days at 4°C under dark conditions, following the procedure outlined by (Porra et al., 1989). The amounts of photosynthetic pigments were determined spectrophotometrically, using equations published by (Welburn et al., 1994). The pigment concentrations were then expressed as weight of pigment per gram of needle dry matter (mg/g).

***Figure 5.2**: Foliage sampling scheme.*

5.2.2.2 Soil sampling

In each forest stand, five representative sampling pits were chosen to collect soil samples. Material was collected from four soil horizons (two organic and two mineral). The sampled horizons have the following characteristics: horizon 1 – organic horizon (Ol+Of); horizon 2 – organic horizon (Oa); horizon 3 – mineral soil 0–10cm, mixed with humus, usually darkened ($A_{0\text{-}10}$); horizon 4 – mineral soil 10–20cm ($A_{10\text{-}20}$). The total depth of mineral soil (20 cm) was chosen to reflect the majority of tree root distribution. The collected material was dried in the air prior to sieving. Exchangeable cations and selected trace elements were determined in all four horizons. Exchangeable cations (Ca, Mg, K) and Al were analyzed in 0.1 M $BaCl_2$-extracts by the AAS method. To measure selected trace elements (Cu, Zn, As, Hg), samples were sieved (<5 mm for Ol, Of and Oa; and <2 mm for mineral soil) and homogenized using a portable Innov-x Alpha RFA spectrometer. Furthermore, for the first two horizons, the pH, total exchangeable acidity (TEA) and total C and N were measured. Taking in

account the character of the parent lithologies together with the fact that total C was analyzed only for two organic horizons, in our case the total C can be entirely related with organic carbon (Corg). Soil pH was determined in distilled water and in 1 M KCl. To measure TEA BaCl2-extracts were titrated by 0.025 M NaOH to pH = 7.8. Total C and N were determined simultaneously using a Carlo-Erba Fisons 1108 analyzer.

Cation exchange capacity (CEC) was calculated as the sum of exchangeable base cations (Bc=Ca+Mg+K+Na) and TEA. Base saturation (BS) was determined as the fraction of CEC associated with BC.

5.2.3 Aerial HS image datasets

The hyperspectral image data was acquired in 2009 (July 27) and in 2010 (21st August 2010) during the HyEUROPE 2009 and 2010 flight campaigns using the HyMap (HyVista Corp., Australia) airborne imaging spectrometer. The HyMap sensor records image data in 126 narrow spectral bands (with full-width half maximum ca. 15 nm) covering the entire spectral interval between 450 to 2500 nm. The resulting ground pixel resolution of the image datasets was 5 m. In order to successfully pre-process the hyperspectral data, a supportive calibration and validation ground campaigns were organized simultaneously with the HyMap data acquisition in 2009 and 2010. At the selected homogenous targets the ground measurements were acquired by the ASD FielSpec-3 spectroradiometer to properly calibrate as well as validate the image data and to enable: (i) atmospheric correction of the airborne hyperspectral images and ii) retrieving at surface reflectance values for the further verification. The selected targets meet the following conditions: (i) spatial homogeneity for a minimum area of 5x5 image pixels and (ii) natural or artificial nearly Lambertian ground surfaces. The hemispherical-conical reflectance factor (HCRF) (Schaepman-Strub et al., 2006) was measured for each reference target. Raw spectroradiometric data were transformed into the HCRF using the calibrated white spectralon panel. In addition, Microtops II Sunphotometer (Solar Light Comp., USA) measurements were taken approximately every 30 seconds during the HyMap data acquisition. Data acquired by the Sunphotometer was used for estimation of the actual atmospheric conditions (AOT - aerosol optical thickness, WV- water vapor content).

5.2.4 Image data preprocessing

The 2009 and 2010 HyMap multiple flight line data were atmospherically corrected using software (SW) package ATCOR-4 version 5.0 (Richter, 2009). This SW is based on MODTRAN radiative transfer

model (Adler-Golden et al., 1999) and enables atmospheric correction of the aerial hyperspectral images. The aerosol optical thickness (AOT) estimated by the Sunphotometer measurements was used as an input parameter for the model. The known reflectances of the specific reference target as well as of water vapor (WV) were utilized for fine tuning of the model, as facilitated by ATCOR-4. The remaining reference targets were used for validation of the corrected image.

The orientation and geometry of the HyMap strips followed the SW-NE orientation of the lignite basin. However, this setting represented an optimal solution from the economic point of view; on the other hand, this setting (relative solar azimuth at the acquisition hour was about 73°) caused that the data suffered from strong cross track illumination and BRDF effects (Verrelst et al., 2008). Therefore, in addition to the atmospheric correction, the 2009 and 2010 reflectance data had to be further processed to minimize these effects employing semi-empirical nadir normalization using the kernel-based Ross-Li model (Schaaf et al., 2002).

Direct ortho-georectification was performed using the PARGE software package (Schläpfer et al, 1998). Data from the on-board Inertial measurement unit/GPS (IMU/GPS) unit and digital elevation model (DEM) with ground resolution of 10 m were used as the input parameters for the ortho-georectification. Misalignment angles between the IMU/GPS unit and the HyMap sensor were determined specifically for the Sokolov site. Finally, the hyperspectral image data were georeferenced to the UTM 33N (WGS-84) coordinate system.

5.2.5 Hyperspectral data processing: Vegetation health classification and change detection

The processing workflow for both image datasets followed the method described by Mišurec, Kopačková et al. (2012). A general description is given in this section. Initially, the extent of the Norway spruce forests was defined by employing a hierarchical classification approach combining thresholding of the normalized difference vegetation index (NDVI) and the maximum likelihood classification (MLC), which was applied to the first five components, and the results from the MNF transformation of the HyMap data. The canopy chlorophyll content (Cab) was estimated using the empirical model based on the derivative indices (D_{718}/D_{708}). To validate the 2009 and 2010 empirical models, ground truth biochemical data were divided into training and validation datasets. The relationship between the predicted and measured values was described by the linear regression model and coefficient of determination (training: R^2 and validation: Rv^2, respectively) and the root mean square errors (RMSE) were determined. In addition, to assess the vegetation health status, two

selected indicators of vegetation health (REP and SIPI) were calculated from the HS 2009 and 2010 image datasets. Due to the relative low dynamic range of the SIPI values, we used its exponential transformation (expSIPI) in further analysis.

The Cab, Rep and expSIPI were further statistically classified. The values of the three selected indices were transformed into standardized z-scores to ensure their comparability and the independence of their physical dimensions (units) and further classified into five classes defined by the threshold values given in Tab. 5.5. Two products were created using the obtained normalized z-score values: the map of chlorophyll content (histograms in Fig. 5.7) and a raster combining the information from REP and expSIPI (both were summarized and then linearly reclassified into 5 classes, however expSIPI needed to be classified in the reverse order as the higher values reflect higher carotenoid-to-chlorophyll contents and thus worse vegetation health; Figs 5.8, 5.9). For both products a relative classification was used based on the histogram dynamic ranges, averages and standard deviations. Consequently, no hard threshold values were required. The only condition to be fulfilled was normal distribution of all the data classified (entire scene) (Figs. 5.7, 5.8). In both maps, Class 1 indicates worse health status for the trees without visible damage symptoms and Class 5 corresponds to the values indicating the healthiest trees (Figs. 5.7, 5.8, 5.9).

The difference image was calculated to enable comparison of the 2009 and 2010 class values and to detect changes in health status. To minimize the effect of miss-rectification errors, the input classified data were resampled to 15x15 m spatial resolution (3x3 original pixel size). This made it possible to compute an image showing the class change. Fig. 5.10 depicts negative changes in the following manner: class 1 (1-class decreases), class 2 (2-class decreases) and class 3 (3-class decreases and higher).

5.3 Results

5.3.1 Site soil characteristics

The soil chemistry at all the sites was characterized by low exchangeable pH in both organic (Ol+Of, Oh) and mineral soils ($A_{0\text{-}10}$,$A_{10\text{-}20}$) (Fig. 5.3). However, the mineral soil chemistry reflected the composition of the parent material. Erika, the most acidic site, is underlain by sandstone and quartzite characterized by extremely low base cation contents. As a consequence, the lowest base saturation (2-2.5%) and Bc/Al ratio (0.04-0.06) were measured in the top mineral soil (0-20 cm). Slightly higher pH in the organic horizons (Fig. 5.3) and higher BS were measured at Mezihorská. This

site is underlain by granite with a low content of base cations and low weathering rate. A higher concentration of base cations, compared to Erika, is reflected in slightly higher BS in the mineral soil (3.3-3.9%). Both sites, Erika and Mezihorská, had higher total exchangeable acidity compared to Habartov and Studenec. The latter two sites, Habartov and Studenec, are both underlain by more easily weathered mica schist which is, however, low in base cations. Both sites were characterized by higher exchangeable pH in both the organic and mineral soils, with significantly higher BS in the mineral soil (Fig. 5.3) compared to Erika and Mezihorská. Higher concentration of base cations led to more favourable Bc/Al ratios (0.19-0.26) (Fig. 3) which were, however, still below the critical threshold of 1 (Cronan and Grigal, 1995). Regarding the content of trace metals (Tab. 5.2), two toxic elements, Al and As, were detected as mobile in the studied soils (Kopačková et al., under review).

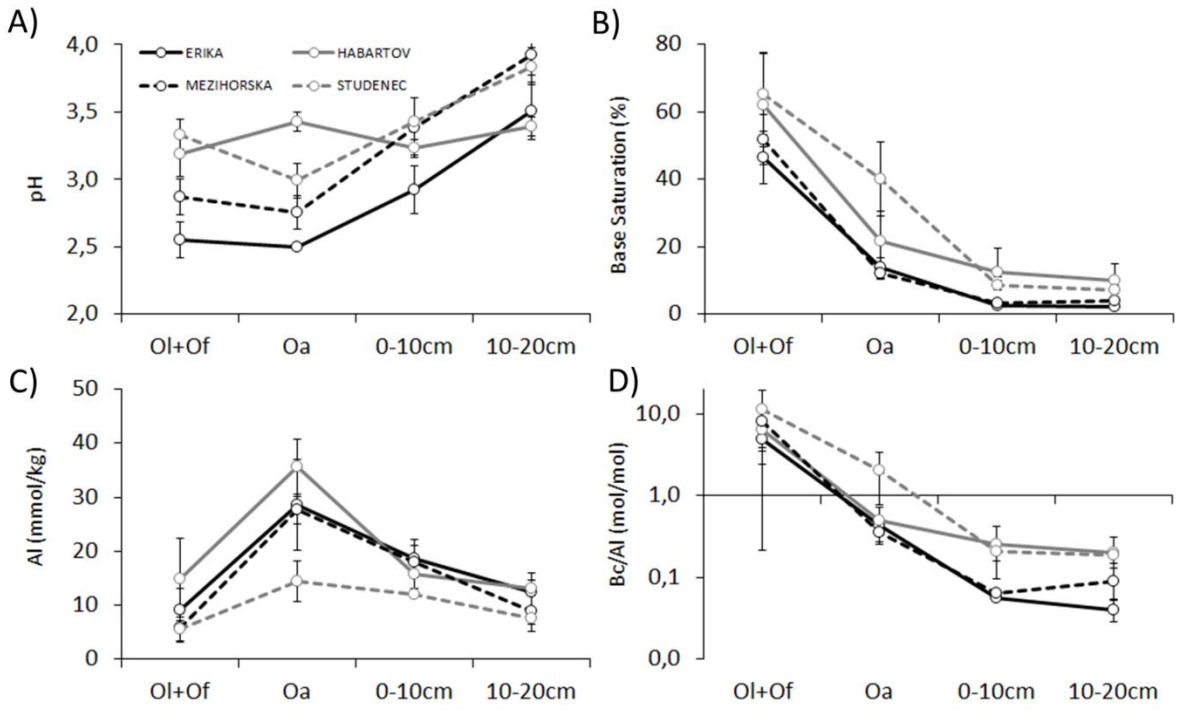

Figure 5.3: *Average soil characteristics and standard deviations of exchangeable pH (a), base saturation (b), exchangeable aluminium (c) and Bc/Al ratio (d) across sites.*

5.3.2 Biochemical characteristics

Table 5.2: *Average ± standard deviation of soil characteristics across all sites.*

	pH_{KCl}	Ca	Mg	Al	TEA	BS	Bc/Al
		$mmol_{(+)}\ kg^{-1}$	$mmol_{(+)}\ kg^{-1}$	$mmol\ kg^{-1}$	$mmol_{(+)}\ kg^{-1}$	%	$mol\ mol^{-1}$
Erika							
Ol+Of	2,55 ± 0,14	43 ± 6,8	13 ± 1,9	9,2 ± 3,8	80 ± 20	46 ± 7,8	4,94 ± 2,5
Oa	2,50 ± 0,01	9,5 ± 3,0	5,2 ± 0,80	29 ± 8,4	131 ± 31	14 ± 3,0	0,43 ± 0,1
0-10 cm	2,92 ± 0,18	0,5 ± 0,0	0,6 ± 0,2	19 ± 3,6	72 ± 14	2,5 ± 0,2	0,06 ± 0,00
10-20 cm	3,51 ± 0,21	0,2 ± 0,2	0,2 ± 0,1	12 ± 3,4	46 ± 9,2	2,0 ± 0,6	0,04 ± 0,01
Habartov							
Ol+Of	3,18 ± 0,16	99 ± 34	12 ± 4,2	15 ± 7,7	69 ± 21	62 ± 15,2	6,46 ± 6,2
Oa	3,43 ± 0,07	26 ± 14	3,6 ± 1,0	36 ± 5,1	117 ± 16	22 ± 9,0	0,49 ± 0,2
0-10 cm	3,24 ± 0,06	6,4 ± 5,4	1,1 ± 0,8	16 ± 2,7	56 ± 8,4	12 ± 7,3	0,26 ± 0,2
10-20 cm	3,39 ± 0,07	3,7 ± 2,9	0,7 ± 0,5	13 ± 1,5	47 ± 5,1	9,8 ± 5,2	0,20 ± 0,1
Mezihorská							
Ol+Of	2,87 ± 0,14	38 ± 3,8	11 ± 1,4	5,7 ± 2,7	61 ± 16	52 ± 7,5	8,08 ± 4,2
Oa	2,76 ± 0,12	4,6 ± 1,0	4,3 ± 0,5	28 ± 2,5	110 ± 8,6	12 ± 1,9	0,35 ± 0,1
0-10 cm	3,38 ± 0,23	0,5 ± 0,0	0,7 ± 0,2	18 ± 3,0	65 ± 11	3,3 ± 0,4	0,06 ± 0,01
10-20 cm	3,93 ± 0,16	0,4 ± 0,2	0,3 ± 0,1	8,7 ± 3,7	35 ± 11	3,9 ± 1,1	0,09 ± 0,04
Studenec							
Ol+Of	3,33 ± 0,11	70 ± 23	13 ± 3,9	5,5 ± 2,3	46 ± 8,0	65 ± 12	11,5 ± 8,0
Oa	2,99 ± 0,13	36 ± 11	8,1 ± 2,1	14 ± 3,8	72 ± 13	40 ± 11	2,06 ± 1,3
0-10 cm	3,42 ± 0,02	2,2 ± 0,5	1,1 ± 0,1	12 ± 0,5	48 ± 1,3	8,4 ± 1,3	0,21 ± 0,05
10-20 cm	3,84 ± 0,14	1,4 ± 0,2	0,5 ± 0,1	7,6 ± 1,1	34 ± 3,2	7,1 ± 1,1	0,19 ± 0,04

	C	N	C/N	Cu	Zn	Hg	As
	%	%	$g\ g^{-1}$	$mg\ kg^{-1}$	$mg\ kg^{-1}$	$mg\ kg^{-1}$	$mg\ kg^{-1}$
Erika							
Ol+Of	31 ± 3,0	1,06 ± 0,03	30 ± 3,7	31 ± 5,2	69 ± 6,7	1,0 ± 0,1	30 ± 6,7
Oa	26 ± 2,5	0,95 ± 0,08	27 ± 2,1	36 ± 4,0	50 ± 4,2	2,6 ± 0,3	53 ± 4,6
0-10 cm	N.D. ± N.D.	N.D. ± N.D.	N.D. ± N.D.	23 ± 4,6	27 ± 2,8	1,0 ± 0,3	27 ± 3,2
10-20 cm	N.D. ± N.D.	N.D. ± N.D.	N.D. ± N.D.	25 ± 2,1	38 ± 7,9	0,8 ± 0, 6	18 ± 2,5
Habartov							
Ol+Of	32 ± 3,6	1,21 ± 0,13	27 ± 1,2	95 ± 47	78 ± 8,9	1,8 ± 0,3	69 ± 19
Oa	23 ± 2,6	0,74 ± 0,10	32 ± 2,4	166 ± 20	47 ± 3,5	2,5 ± 0,4	84 ± 5,3
0-10 cm	N.D. ± N.D.	N.D. ± N.D.	N.D. ± N.D.	23 ± 3,5	24 ± 3,9	1,1 ± 0,4	19 ± 4,6
10-20 cm	N.D. ± N.D.	N.D. ± N.D.	N.D. ± N.D.	21 ± 1,2	25 ± 6,0	1,0 ± 0,1	11 ± 3,9
Mezihorská							
Ol+Of	34 ± 2,4	1,21 ± 0,05	28 ± 1,2	29 ± 11	60 ± 6,2	0,7 ± N.D.	13 ± 3,4
Oa	23 ± 2,5	0,86 ± 0,09	27 ± 3,7	47 ± 10	73 ± 6,8	1,4 ± 0,3	38 ± 6,3
0-10 cm	N.D. ± N.D.	N.D. ± N.D.	N.D. ± N.D.	18 ± 0,0	94 ± 20	0,9 ± 0,1	21 ± 6,1
10-20 cm	N.D. ± N.D.	N.D. ± N.D.	N.D. ± N.D.	23 ± 2,8	107 ± 7,8	1,2 ± 0,2	14 ± 3,5
Studenec							
Ol+Of	29 ± 4,7	1,01 ± 0,15	29 ± 0,7	29 ± 4,4	227 ± 40	0,9 ± 0,1	31 ± 10
Oa	24 ± 3,5	0,92 ± 0,14	27 ± 4,3	32 ± 2,6	213 ± 45	1,0 ± 0,1	36 ± 3,8
0-10 cm	N.D. ± N.D.	N.D. ± N.D.	N.D. ± N.D.	33 ± 14	377 ± 64	1,2 ± N.D.	40 ± 9,5
10-20 cm	N.D. ± N.D.	N.D. ± N.D.	N.D. ± N.D.	29 ± 5,0	477 ± 191	1,1 ± 0,1	31 ± 7,9

As the Norway spruce needle samples were collected from two different years, statistics were employed to test whether there are statistically significant differences in the biochemical properties of the samples taken in 07/ 2009 and 09/2010. First the Shapiro-Wilk test (Shapiro and Wilk, 1965) was employed to test the normal distribution. For Car and Cab, the normally distributed parameters, analysis of variance (ANOVA) was used to test whether there are statistically significant differences.

For Car/Cab, as this parameter was not normally distributed, the two-sample Kolmogorov-Smirnov (K-S) non-parametric test was employed (Tab. 5.3).The increasing trend with increasing needle age in foliar photosynthetic pigment contents was observed. The Cab and Car contents did not exhibit significant deviations between the 2009 and 2010 seasons (Tab. 5.3) but, in general, the chlorophyll content was slightly higher and the carotenoid content slightly lower in July 2009. Assessing differences among the sites, the lowest Cab and Car values are characteristic for the Mezihorská site (Figs. 5.4 and 5.5). This site also exhibits the largest changes between the 2009 and 2010 chlorophyll (position L3) and carotenoid contents (position U1) (Tab. 5.3). Erika exhibits higher carotenoid contents and higher variability in both pigment contents. Additionally, the trees at Erika exhibit statistically significant changes between the 2009 and 2010 current-year needles at both positions (U1 and L1, Tab. 3). Except for these cases, there are no significant changes in the photosynthetic pigment contents at the studied sites.

Larger differences can be observed in the Car/Cab ratios (Fig. 5.6, Tab. 5.3). Clearly, higher values characterize the samples taken in 09/2010. In most of the cases, the Car/Cab ratios significantly differ for the 2009 and 2010 samples (Tab.5.3), where the largest differences were exhibited by the current-year needles (L1 and U1). Erika exhibits the highest Car/Cab for both years followed by the Mezihorská site, which has higher Car/Cab values mainly for 2010. Moreover, the Erika site had the smallest variations in its gradients among all the positions and years sampled. In 07/2009, the higher Car/Cab values are characteristic for the older needles (L3, U3) but the trend was the opposite in 09/2010, where the current year needles (U1, U1) have higher Car/Cab values than the older once (U3, L3).

Table 5.3: *statistically tested differences in the biochemical properties between the samples taken in 07/ 2009 and 09/2010; statistically significant differences are in bold; (K-S: two-sample Kolmogorov-Smirnov test); (H: habartov, E: Erika, M: Mezihorská, S: Studenec; U and L refer to upper and lower level of the production part respectively; 1 and 3 refer to the first- and third-year needles).*

ANOVA Cab		**ANOVA Cab** Sig.	**ANOVA Car** Sig.	**K-S Car/Cab** Sig. (2-tailed)
H U1	Between 2009-10	,855	**,011**	**,000**
H U3	Between 2009-10	,224	,349	,076
H L1	Between 2009-10	,910	**,006**	**,000**
H L3	Between 2009-10	,241	,288	,076
E U1	Between 2009-10	,618	,637	,055

E U3	Between 2009-10	,432	,845	**,001**
E L1	Between 2009-10	,143	,330	**,001**
E L3	Between 2009-10	,535	,656	**,000**
M U1	Between 2009-10	,625	**,041**	**,000**
M U3	Between 2009-10	,935	,596	,097
M L1	Between 2009-10	,466	,078	**,000**
M L3	Between 2009-10	**,023**	,173	**,001**
S U1	Between 2009-10	,565	,216	**,003**
S U3	Between 2009-10	,127	,449	**,015**
S L1	Between 2009-10	,522	,485	**,001**
S L3	Between 2009-10	,282	,500	,164

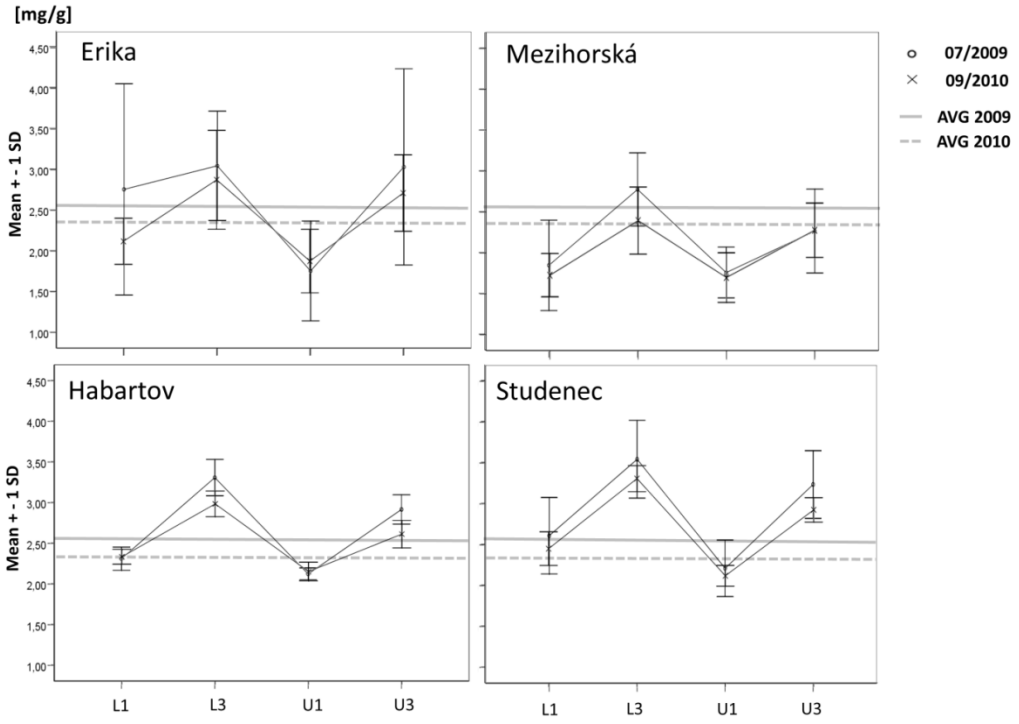

Figure 5.4: *Cab foliage content for 07/2009 and 09/2010 – Means and Standard Deviations are displayed per each site (U and L refer to upper and lower level of the production part respectively while 1 and 3refer to the first- (1) and third-year (3) needles. AVG 2009: overall average for 2009, AVG 2010: overall average for 2010.*

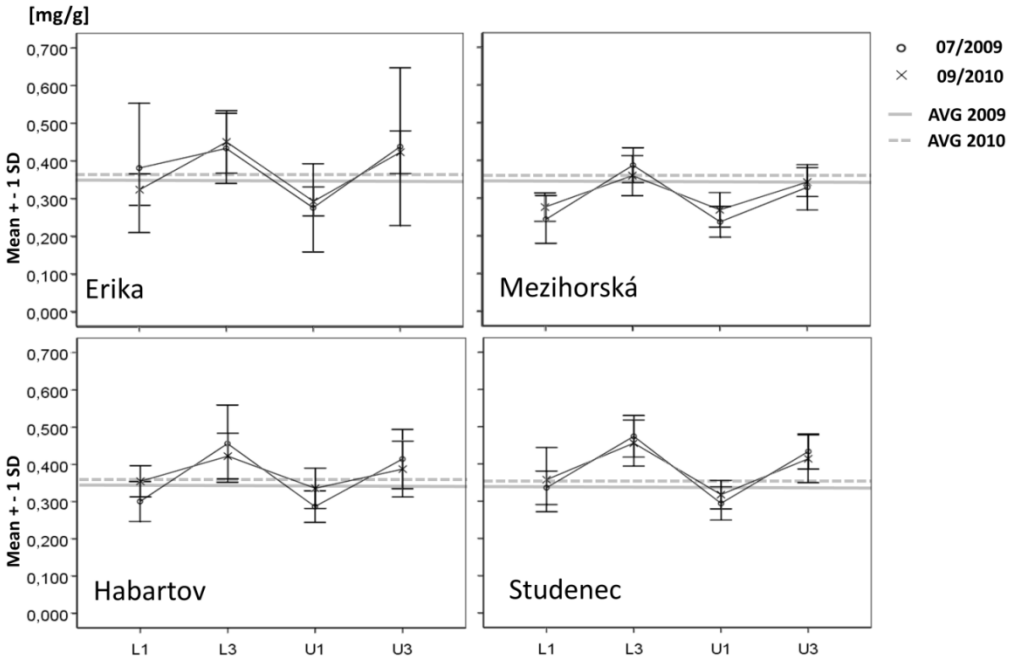

Figure 5.5: *Car foliage content for 07/2009 and 09/2010 – Means and Standard Deviations are displayed per each site (U and L refer to upper and lower level of the production part respectively while 1 and 3refer to the first- (1) and third-year (3) needles. AVG 2009: overall average for 2009, AVG 2010: overall average for 2010.*

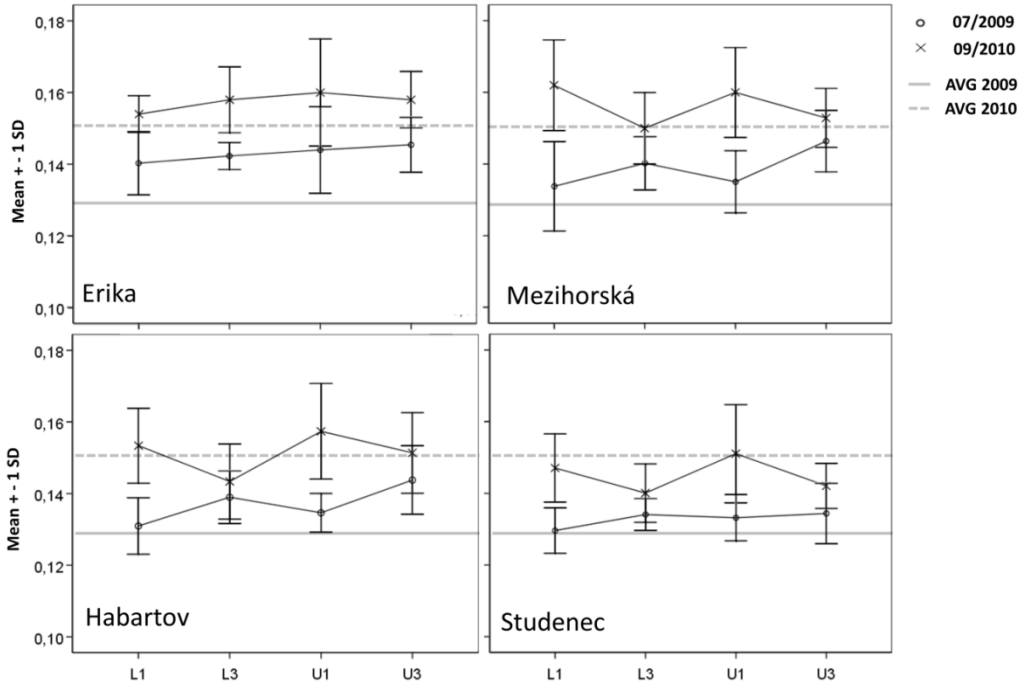

Figure 5.6: *Car/Cab ratio – Means and Standard Deviations are displayed per each site (U and L refer to upper and lower level of the production part respectively. 1 and 3refer to the first- (1) and third-year (3) needles. AVG 2009: overall average for 2009, AVG 2010: overall average for 2010.*

5.3.3 Vegetation health: site differences between HyMap 2009 and 2010 classifications

The chlorophyll content estimation achieved higher accuracy using the 2009 datasets (Tab. 5.4). This can be explained by the longer period between the HS data acquisition and the tree sampling in 2010, as unfavorable weather conditions (heavy rains) developed immediately after the acquisition day and the trees were sampled approximately two weeks after the HS image data were acquired.

Identifying the most significant changes between 2009 and 2010, the places where the trees were cut down can be easily identified, where these areas fall in the class 1 (worse vegetation health) of the vegetation health map (Fig. 9), or in classes 2 or 3 (decreases about 2 classes and more) of the change detection map (Fig. 10). To detect less visible changes, both the chlorophyll content and the vegetation health class histograms can be compared and the class frequencies and asymmetries calculated can be studied for each site.

Table 5.4: *Chlorophyll content estimation: regression models (measured vs. predicted).*

Chlorophyll content estimation model (linear regression)		
	2009	**2010**
R^2 (training)	0,9131	0,5340
RMSE (mg/g)	0,2055	0,2174
Rv^2 (validation)	0,9370	0,7305

Table 5.5: *Threshold values used for image classifications.*

Threshold values						
indicator (year)	**μ**	**σ**	**-1.0σ**	**-0.5σ**	**+0.5σ**	**+1.0σ**
Cab (2009)	2.5996	0.6126	1.9871	2.2934	2.9059	3.2122
Cab (2010)	2.4394	0.3944	2.0450	2,2422	2.6366	2.8338
REP (2009)	716.8650	1.2242	715.6409	716.2530	717.4772	718.0893
REP (2010)	717.5770	1.2673	716.3097	716.9434	718.2107	718.8443
expSIPI (2009)	2.7668	0.0967	2.6701	2.7185	2.8152	2.8635
expSIPI (2010)	2.7137	0.1200	2.5937	2.6532	2.7738	2.8338

Tab. 5.6: *Descriptive statistics on optical indices retrieved from hyperspectral image data.*

Optical indices			
	Cab (mg/g)	**REP (nm)**	**expSIPI**
2009			
Erika	***mean:*** *2.5980* ***std.:*** *0.5597* ***range:*** *5.9681*	***mean:*** *716.9967* ***std.:*** *1.1122* ***range:*** *15.2957*	***mean:*** *2.5980* ***std.:*** *0.1087* ***range:*** *2.0174*
Habartov	**mean:** 2.4606 **std.:** 0.4259 **range:** 4.6724	**mean:** 716.5647 **std.:** 0.8615 **range:** 9.0443	**mean:** 2.7461 **std.:** 0.0977 **range:** 2.2605
Mezihorská	**mean:** 2.4465 **std.: 0.**6840 range: 6.8480	**mean:** 716.5236 **std.:** 1.3648 **range:** 12.2448	**mean:** 2.7898 **std.:** 0.1226 **range:** 5.5991
Studenec	**mean:** 2.4807 **std.:** 0.6277 **range:** 5.1922	**mean:** 716.6943 **std:** 1.2707 **range:** 12.2448	**mean:** 2.8021 **std:** 0.1842 **range:** 6.5375
entire scene	**mean:** 2.5996 **std.:** 0.6126 **range:** 9.7289	**mean:** 716.8650 **std.:** 1.2242 **range:** 99.2157	**mean:** 2.7668 **std.:** 0.0967 **range:** 8.8227
2010			
Erika	**mean:** 2.2108 **std.:** 0.2987 **range:** 3.3349	**mean:** 716,8093 **std.:** 0.9755 **range:** 11.2010	**mean:** 2.7187 **std.:** 0.1558 **range:** 3.4459
Habartov	**mean:** 2.3387 **std.:** 0.2950 **range:** 3.6363	**mean:** 717.1238 **std.:** 0.9389 **range:** 13.7618	**mean:** 2.6335 **std.:** 0.1088 **range:** 1.8463
Mezihorská	**mean:** 2.2488 **std.:** 0.4166 **range:** 3.7887	**mean:** 716.9843 **std.:** 1.3637 **range:** 13.1354	**mean:** 2.7902 **std.:** 0.2066 **range:** 3.7386
Studenec	**mean:** 2.4392 **std:** 0.4177 **range:** 3.3104	**mean:** 717.5986 **std:** 1.2890 **range:** 10.9415	**mean:** 2.7146 **std:** 0.1393 **range:** 2.5776
entire scene	**mean:** 2.4394 **std.:** 0.3944 **range:** 7.1953	**mean:** 717.5770 **std.:** 1.2673 **range:** 88.2487	**mean:** 2.7137 **std.:** 0.1200 **range:** 6.4288

Comparing the HyMap indices statistics (Tab. 5.6), the chlorophyll content decreased slightly for the entire scene in 2010, but there were no other significant differences. However, if each site is assessed separately, Erika is the site with the largest decreases in Cab content and largest increases in the SIPI index, followed by the Mezihorská site (Tab. 5.6, Figs. 5.7 and 5.8). These trends can be easily depicted on the basis of the classified maps (Fig. 5.9), as health classes 1 and 2 were more populated for Erika and Mezihorská in 2010 than in 2009. In addition, these two sites exhibit frequent negative changes in their health status (Fig. 5.10). On the other hand, the Studenec site is the most stable site of all, as the 2009 and 2010 histograms of the chlorophyll content and heath class status (Figs. 5.7 and 5.8) look almost the same. In terms of the negative changes (decreases in health class) in health status for the Studenec site, mainly class 1, indicating smallest changes in tree health, is present and sparsely distributed (Fig. 5.10).The Habartov site was partially covered by clouds in 2010 (Fig. 5.9), However, similarly as the Studenec site, the cloudless parts available for the analysis exhibit very similar histograms of the chlorophyll content and health classes for 2009 and 2010 (Figs. 5.7 and 5.8) and sparse health change patterns (Fig. 5.10).

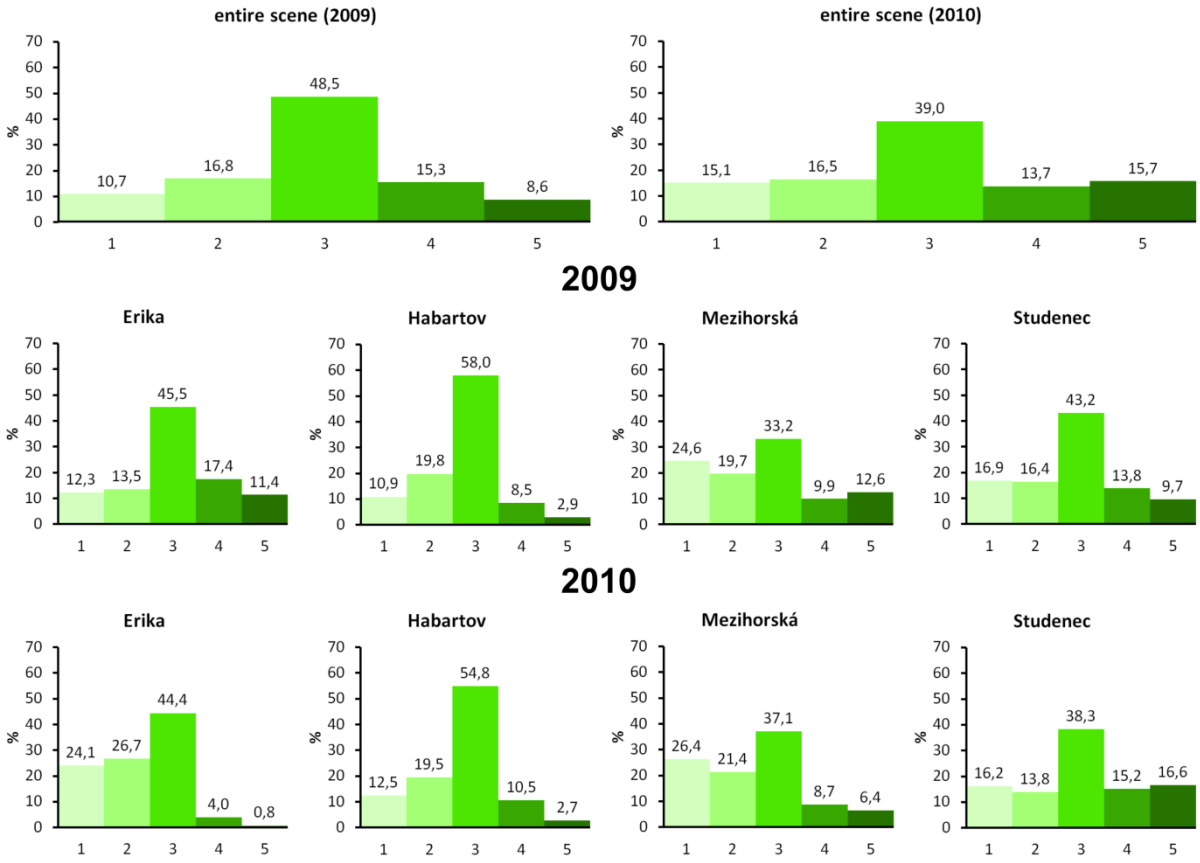

***Figure 5.7**: chlorophyll content retrieved from the HyMap data: Relative frequencies (%) compared for 2009 and 2010.*

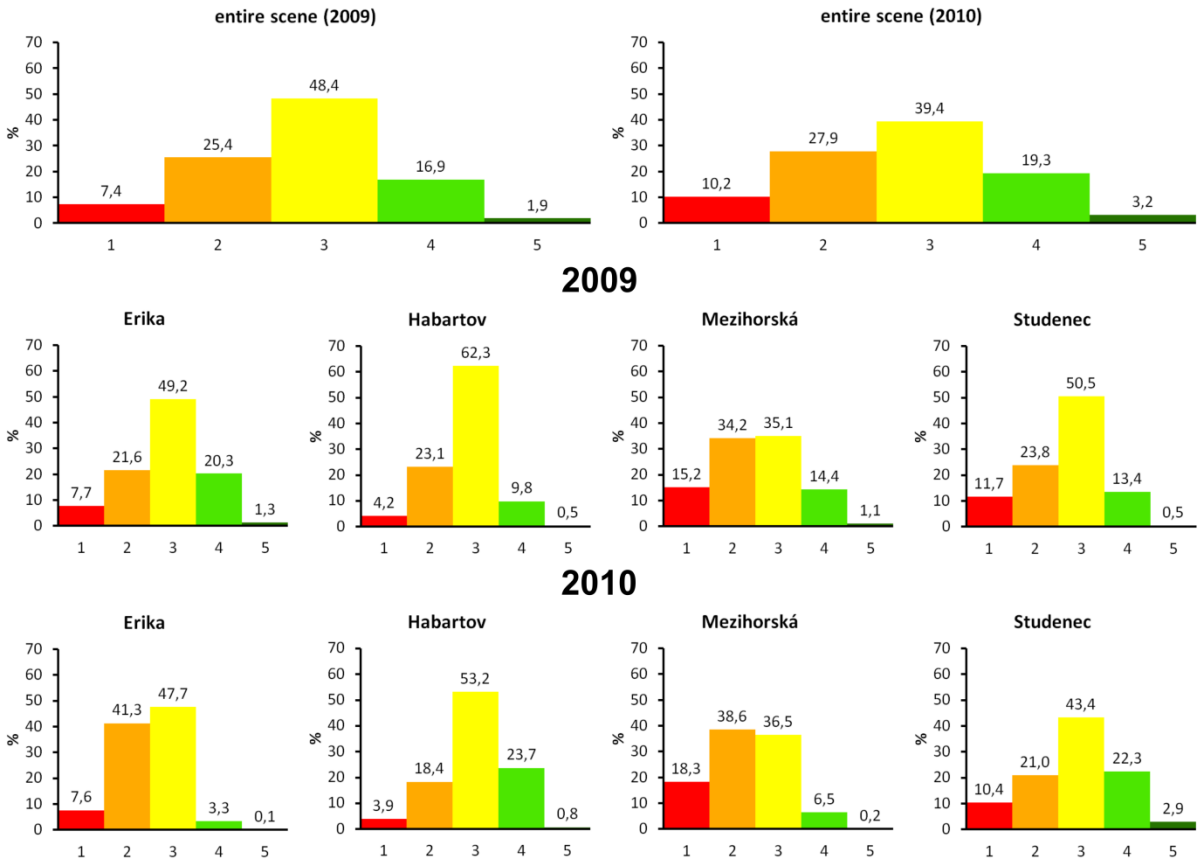

***Figure 5.8**: Norway spruce health status classes: Relative frequencies (%) compared for 2009 and 2010.*

6 Discussion

All the sites are located in the vicinity of the Sokolov basin, an area with historically high emissions of acidifying compounds (SO_2, NO_x). Unfavourable low Bc/Al ratios across all the sites might be connected to the high deposition of S and N in the past and subsequently to the anthropogenic acidification of forest soils in this region (Krám et al., 1997; Oulehle et al., 2006). Soil acidification promotes leaching of base cations and mobilization of aluminium (Kram et al., 2009). Thus, anthropogenic acidic deposition, spruce forest plantations and naturally acidic parent bedrock promoted acidification of forest soils across the investigated sites. The C/N ratios in organic horizons were similar at all the sites, ranging from 27 to 32 in the Oa horizon. Based on the close relationship between the C/N ratio in the forest floor and N leaching in catchments across the Czech Republic (Oulehle et al,. 2008) we can expect relatively low N leaching as the C/N ratio of the organic soil is above the critical threshold of approx. 25 when N leaching could be expected. In general, soils with

the lowest base cation nutrient availability and low Bc/Al ratios are found at Erika and Mezihorská, where the soils are underlain by the most acidic bedrocks (sandstone/quartzite and granite, respectively).

In accordance with the previously published results (Albrechtová et al., 2008; Homolová et al., 2013) the content of photosynthetic pigments (Cab and Car) increased with the needle age of the sampled foliage. The chlorophyll content in mature coniferous foliage is known to be relatively constant or increases moderately during the summer (July-September) (Kirchgessner et al., 2003; Thomas et al., 2009). The first-year needles (U1 and L1) also exhibit minimal changes in chlorophyll a and b contents after June after the needles gain their final length and fresh weight (Silkina et al., 2009), and thus the slightly shifted sampling dates in 2009 (end of June) and 2010 (early September) should not affect the needle chlorophyll contents.

In contrast to the pigment contents alone, Car/Cab values exhibit more dynamic changes during the growing season, and are positively correlated in the majority of cases with the intensity of photosynthetically active radiation and negatively are correlated with the temperature (Kirchgessner et al., 2003). The significant increase in the average Car/Cab values between the 2009 and 2010 seasons may reflect the season-specific weather conditions or canopy microclimate. The carotenoids in needles play a dual role: on the one hand they are important for light-harvesting, but on the other hand they protect the pigment-protein complexes from photodamage (Demmig-Adams, 1998). The average monthly temperature and monthly sum of sunlight hours during the months of the sampling were higher in 2009 than in 2010 (16.2°C and 180 sunlight hours; 15.0°C and 140 sunlight hours respectively, data from the nearby meteorological station at Karlovy Vary, www.chmi.cz). Thus it appears that the lower temperature in August 2010 compared to July 2009 could be the predominant factor causing the higher Car/Cab ratio in the 2010 season. The increase in the Car/Cab ratio mainly due to chlorophyll degradation may indicate the onset of leaf senescence in deciduous trees (Garcia-Plazaola et al., 2001). However, for the long-lived foliage of evergreen conifers, in relation to one- or three-year old needles, we do not think that senescence could explain the above-discussed changes in Car/Cab.

The opposite effect of needle age on Car/Cab in two studied seasons may be explained by the different response speed of first-year and older needles to the environmental conditions, particularly irradiance, as shown by Kirchgessner et al. (2003), who observed the fast-type response (<20days) in changes in the chlorophyll a to b ratio in last year's needles in comparison with the slow-type change

(>30days) in the current-year needles of Norway spruce. The total carotenoid pool in coniferous needles is represented by several chemical species, including, e.g., lutein and β-carotene, rather stabile pigments during the growing season (Yatsko et al., 2011) and a dynamic pool of xanthophyll cycle carotenoids (Kirchgessner et al., 2003; Yatsko et al., 2011). Thus, the adjustment of carotenoid composition may be more relevant parameter than the size of total carotenoid pool (Demmig-Adams, 1998).

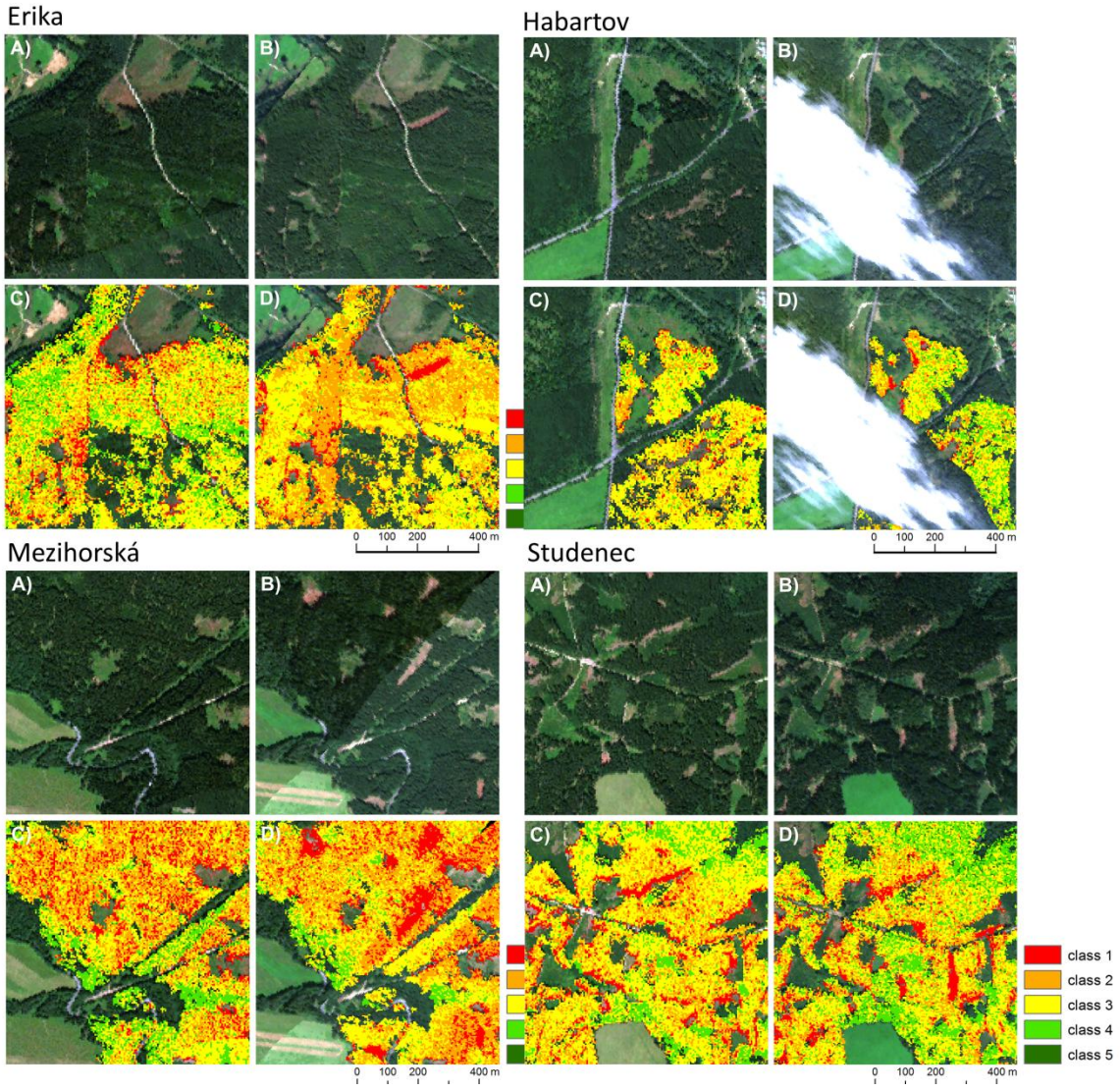

Figure 5.9: *Studied sites— HyMap true color combination showing the actual situation of the site A) 2009 and B) 2010. Statistical classification of the Norway spruce health status C) classification of 2009 data, D) classification of 2010 data; color scale 1 through 5—health status classes; 1 - the worst and 5 - the best result.*

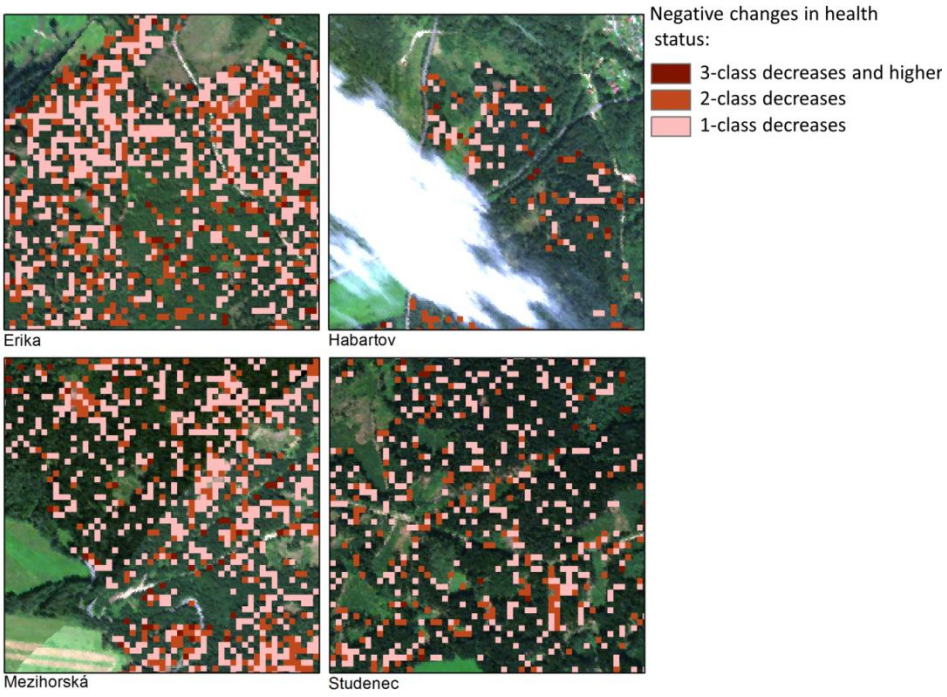

Figure 5.10: *Depicted negative changes (2009-2010): class 1 (1-class decreases), class 2 (2-class decreases) and class 3 (3-class decreases and higher).*

The foliar laboratory results show that the chlorophyll content (Car) should not be the only indicator considered when assessing forest health. The absolute carotenoid contents (Car) alone also do not reflect the differences among the studied sites. On the other hand, the Car/Cab ratio allowed site sorting by comparison with the mean annual values for all the sites, as is shown in Fig. 5.6 and was consistent for all the sites in both years in the following order (sorted from least to most healthy): Erika, Mezihorská, Habartov and Studenec.

The same sorting was depicted using the HyMap 2009 and 2010 classification products, while the differences among the sites are considered the best in the map of the health status (Fig. 5.9). This map combines the two indices - REP (sensitive to vegetation stress) and index SIPI (sensitivity to the ratio of bulk carotenoids to chlorophyll) - and also supports the idea that, in addition to the chlorophyll content, it is important to take into account the carotenoid content when assessing forest health. The increased Car/Cab content of first-year needles (U1, L1) (Fig. 5.6) sampled at the beginning of September 2010 may have enabled better detection of forest health status using the 2010 HS dataset, as the difference among the sites are more pronounced in 2010. These needles contribute the most to the total foliage area (Porté et al., 2000; Weiskittel et al., 2006), the area that can be sensed from the sky.

To summarize the results, both biochemical analysis of the sampled tree needles and hyperspectral image data have been shown to reflect the soil chemistry. Higher Car/Cab ratios in spruce needles and lower health status derived from HyMaps were related to the lowest Bc/Al ratio in mineral soil. The strong linkage between soil chemistry and parent bedrock indicated that bedrock geochemical reactivity (Chuman et al., in press) should be considered to be important factor in the assessment of forest health status.

7 Conclusions

In this study, the recently proposed method for assessing forest health conditions using optical indices retrieved from HS data (Mišurec, Kopačková et al. 2012) was applied to the two temporal HyMap date sets acquired in 07/2009 and 08/2010 for detecting stress in Norway spruce forests on a regional scale. The classification results were validated by ground truth data (foliar biochemistry: Cab, Car and Car/Cab) and were associated with the geochemical conditions of the forest stands (pH, macronutrient parameters, base saturation, exchangeable aluminium, Bc/Al ratio). The method proved suitable as the HyMap classification results were in accordance with the statistical assessment of the biochemical properties of the sampled trees as well as with the geochemical properties of the forest sites. It is apparent that, in both years, differences detected by biochemical and hyperspectral methods remained consistent among spruce stands and only mild changes in the physiological condition of the stands under study were detected by both approaches. This finding supports the validity of the previously presented model.

Both the biochemical analysis of the sampled foliage and classification of the 2009 and 2010 hyperspectral image data indicate that Erika and Mezihorská are sites with higher vegetation stress. In addition to higher Car/Cab, which enabled the detection of stressed trees using hyperspectral image data, these sites exhibited critically low pH and lower values for the macronutrient parameters in the organic horizons (Ol+Of and Oh). Moreover, both sites exhibit critically low Bc/Al ratios for the organic and top soil mineral horizons (Ol+Of, Oh, A_{0-10},A_{10-20}).

The results of this study demonstrate: (i) the potential application of hyperspectral remote sensing as a rapid method of identifying tree stress prior to symptom expression and (ii) the added value of multitemporal approaches for hyperspectral data and its further potential for monitoring forest ecosystems. These distance methods could be the most cost-effective long-term tool available for

forest management in the future, when the space-born HS missions (e.g., EnMap or PRISMA) will be in operation.

Acknowledgements

The present research is being undertaken within the framework of Grants No. 205/09/1989 (HypSo: grant funded by the Czech Science Foundation) and No. 244242 (EO-MINERS: FP7 grant funded by the EC). Many thanks are due to Dr. Petr Rojík (Sokolovská uhelná a.s.) for his substantial assistance with the field campaign.

References

A.R. Weiskittel, D. M. & Garber, S. (2006), 'Influence of Swiss needle cast on foliage age-class structure and vertical foliage distribution in Douglas-fir plantations in north coastal Oregon', *Can. J. For. Res.* **36**, 1497-1508.

Adler-Golden, S. M.; Matthew, M. W.; Bernstein, L. S.; Levine, R. Y.; Berk, A.; Richtsmeier, S. C.; Acharya, P. K.; Anderson, G. P.; Felde, G.; Gardner, J.; Hoke, M.; Jeong, L. S.; Pukall, B.; Ratkowski, A. & Burke, H. H. (1999), 'Atmospheric correction for short-wave spectral imagery based on MODTRAN4', *Imaging Spectrometry V* **3753**, 61-69.

AHERN, F. J. (1988), 'The Effects of Bark Beetle Stress On the Foliar Spectral Reflectance of Lodgepole Pine', *International Journal of Remote Sensing* **9**(9), 1451-1468.

Albrechtova, J.; Seidl, Z.; Aitkenhead-Peterson, J.; Lhotakova, Z.; Rock, B. N.; Alexander, J. E.; Malenovsky, Z. & McDowell, W. H. (2008), 'Spectral analysis of coniferous foliage and possible links to soil chemistry: Are spectral chlorophyll indices related to forest floor dissolved organic C and N?', *Science of the Total Environment* **404**(2-3), 424-432.

Asner, G. P. (1998), 'Biophysical and biochemical sources of variability in canopy reflectance', *Remote Sensing of Environment* **64**(3), 234-253.

Asner, G. P. & Martin, R. E. (2009), 'Airborne spectranomics: mapping canopy chemical and taxonomic diversity in tropical forests', *Frontiers In Ecology and the Environment* **7**(5), 269-276.

Aspinall, R. J. (2002), 'Use of logistic regression for validation of maps of the spatial distribution of vegetation species derived from high spatial resolution hyperspectral remotely sensed data', *Ecological Modelling* **157**(2-3), 301-312.

Aznar, J. C.; Richer-Lafleche, M.; Begin, C. & Begin, Y. (2009), 'Lead Exclusion and Copper Translocation in Black Spruce Needles', *Water Air and Soil Pollution* **203**(1-4), 139-145.

Blackburn, G. A. (2007), 'Hyperspectral remote sensing of plant pigments', *Journal of Experimental Botany* **58**(4), 855-867.

Bonan, G. B. (2008), 'Forests and climate change: Forcings, feedbacks, and the climate benefits of forests', *Science* **320**(5882), 1444-1449.

Bouska, V. & Pesek, J. (1999), 'Quality parameters of lignite of the North Bohemian Basin in the Czech Republic in comparison with the world average lignite', *International Journal of Coal Geology* **40**(2-3), 211-235.

Campbell, P. K. E.; Middleton, E. M.; McMurtrey, J. E.; Corp, L. A. & Chappelle, E. W. (2007), 'Assessment of vegetation stress using reflectance or fluorescence measurements', *Journal of Environmental Quality* **36**(3), 832-845.

Campbell, P. K. E.; Rock, B. N.; Martin, M. E.; Neefus, C. D.; Irons, J. R.; Middleton, E. M. & Albrechtova, J. (2004), 'Detection of initial damage in Norway spruce canopies using hyperspectral airborne data', *International Journal of Remote Sensing* **25**(24), 5557-5583.

Carter, G. A. & Knapp, A. K. (2001), 'Leaf optical properties in higher plants: Linking spectral characteristics to stress and chlorophyll concentration', *American Journal of Botany* **88**(4), 677-684.

CARTER, G. A. & MILLER, R. L. (1994), 'Early Detection of Plant Stress By Digital Imaging Within Narrow Stress-sensitive Wavebands', *Remote Sensing of Environment* **50**(3), 295-302.

CHANG, S. H. & COLLINS, W. (1983), 'Confirmation of the Airborne Biogeophysical Mineral Exploration

Technique Using Laboratory Methods', *Economic Geology* **78**(4), 723-736.

Chuman T, Hruška J, O. F. e. a. (in press), 'Does stream water chemistry reflect watershed characteristics?', *Environmentla Monitoring and Assessment*.

Clevers, J. G. P. W.; De Jong, S. M.; Epema, G. F.; Van der Meer, F. D.; Bakker, W. H.; Skidmore, A. K. & Scholte, K. H. (2002), 'Derivation of the red edge index using the MERIS standard band setting', *International Journal of Remote Sensing* **23**(16), 3169-3184.

CRONAN, C. S. & GRIGAL, D. F. (1995), 'Use of Calcium Aluminum Ratios As Indicators of Stress In Forest Ecosystems', *Journal of Environmental Quality* **24**(2), 209-226.

CURRAN, P. J.; WINDHAM, W. R. & GHOLZ, H. L. (1995), 'Exploring the Relationship Between Reflectance Red Edge and Chlorophyll Concentration In Slash Pine Leaves', *Tree Physiology* **15**(3), 203-206.

Demmig-Adams, B. (1998), 'Survey of thermal energy dissipation and pigment composition in sun and shade leaves', *Plant and Cell Physiology* **39**(5), 474-482.

DemmigAdams, B. & Adams, W. W. (1996), 'The role of xanthophyll cycle carotenoids in the protection of photosynthesis', *Trends In Plant Science* **1**(1), 21-26.

Everitt, J. H.; Yang, C.; Escobar, D. E.; Lonard, R. I. & Davis, M. R. (2002), 'Reflectance characteristics and remote sensing of a riparian zone in south Texas', *Southwestern Naturalist* **47**(3), 433-439.

Feret, J. B. & Asner, G. P. (2013), 'Tree Species Discrimination in Tropical Forests Using Airborne Imaging Spectroscopy', *Ieee Transactions On Geoscience and Remote Sensing* **51**(1), 73-84.

Gamon, J. A. & Surfus, J. S. (1999), 'Assessing leaf pigment content and activity with a reflectometer', *New Phytologist* **143**(1), 105-117.

Garcia-Plazaola, J. & Becerril, J. M. (2001), 'Seasonal changes in photosynthetic pigments and antioxidants in beech (Fagus sylvatica) in a Mediterranean climate: implications for tree decline diagnosis', *Australian Journal of Plant Physiology* **28**(3), 225-232.

Gitelson, A. A.; Merzlyak, M. N. & Chivkunova, O. B. (2001), 'Optical properties and nondestructive estimation of anthocyanin content in plant leaves', *Photochemistry and Photobiology* **74**(1), 38-45.

Gitelson, A. A.; Zur, Y.; Chivkunova, O. B. & Merzlyak, M. N. (2002), 'Assessing carotenoid content in plant leaves with reflectance spectroscopy', *Photochemistry and Photobiology* **75**(3), 272-281.

Gould, W. (2000), 'Remote sensing of vegetation, plant species richness, and regional biodiversity hotspots', *Ecological Applications* **10**(6), 1861-1870.

Grisham, M. P.; Johnson, R. M. & Zimba, P. V. (2010), 'Detecting Sugarcane yellow leaf virus infection in asymptomatic leaves with hyperspectral remote sensing and associated leaf pigment changes', *Journal of Virological Methods* **167**(2), 140-145.

Hamzeh, S.; Naseri, A. A.; AlaviPanah, S. K.; Mojaradi, B.; Bartholomeus, H. M.; Clevers, J. G. P. W. & Behzad, M. (2013), 'Estimating salinity stress in sugarcane fields with spaceborne hyperspectral vegetation indices', *International Journal of Applied Earth Observation and Geoinformation* **21**, 282-290.

Hernandez-Clemente, R.; Navarro-Cerrillo, R. M.; Suarez, L.; Morales, F. & Zarco-Tejada, P. J. (2011), 'Assessing structural effects on PRI for stress detection in conifer forests', *Remote Sensing of Environment* **115**(9), 2360-2375.

Homolova, L.; Lukes, P.; Malenovsky, Z.; Lhotakova, Z.; Kaplan, V. & Hanus, J. (2013), 'Measurement methods and variability assessment of the Norway spruce total leaf area: implications for remote sensing', *Trees-*

structure and Function **27**(1), 111-121.

HORLER, D. N. H.; DOCKRAY, M. & BARBER, J. (1983), 'The Red Edge of Plant Leaf Reflectance', *International Journal of Remote Sensing* **4**(2), 273-288.

Jackson, R. B.; Randerson, J. T.; Canadell, J. G.; Anderson, R. G.; Avissar, R.; Baldocchi, D. D.; Bonan, G. B.; Caldeira, K.; Diffenbaugh, N. S.; Field, C. B.; Hungate, B. A.; Jobbagy, E. G.; Kueppers, L. M.; Nosetto, M. D. & Pataki, D. E. (2008), 'Protecting climate with forests', *Environmental Research Letters* **3**(4), 044006.

Kampe, T. U.; Asner, G. P.; Green, R. O.; Eastwood, M.; Johnson, B. R. & Kuester, M. (2010), 'Advances in Airborne Remote Sensing of Ecosystem Processes and Properties - Toward High-Quality Measurement on a Global Scale', *Remote Sensing and Modeling of Ecosystems For Sustainability Vii* **7809**, 78090J.

Kirchgessner, H. D.; Reichert, K.; Hauff, K.; Steinbrecher, R.; Schnitzler, J. P. & Pfundel, E. E. (2003), 'Light and temperature, but not UV radiation, affect chlorophylls and carotenoids in Norway spruce needles (Picea abies (L.) Karst.)', *Plant Cell and Environment* **26**(7), 1169-1179.

Knorn, J.; Rabe, A.; Radeloff, V. C.; Kuemmerle, T.; Kozak, J. & Hostert, P. (2009), 'Land cover mapping of large areas using chain classification of neighboring Landsat satellite images', *Remote Sensing of Environment* **113**(5), 957-964.

Kokaly, R. F.; Asner, G. P.; Ollinger, S. V.; Martin, M. E. & Wessman, C. A. (2009), 'Characterizing canopy biochemistry from imaging spectroscopy and its application to ecosystem studies', *Remote Sensing of Environment* **113**, S78-S91.

Kopackova, V.; Chevrel, S.; Bourguignon, A. & Rojik, P. (2012), 'Application of high altitude and ground-based spectroradiometry to mapping hazardous low-pH material derived from the Sokolov open-pit mine', *Journal of Maps* **8**(3), 220-230.

Kopackova, V.; Lhotakova, Z. & Oulehle, F. Jand Albrechtova, J. (under review), 'Assessing forest health via linking the geochemical properties of a soil profile with the biochemical vegetation parameters', *International Journal of Environmental Science and Technology*.

Kram, P.; Hruska, J.; Driscoll, C. T.; Johnson, C. E. & Oulehle, F. (2009), 'Long-term changes in aluminum fractions of drainage waters in two forest catchments with contrasting lithology', *Journal of Inorganic Biochemistry* **103**(11), 1465-1472.

Kram, P.; Hruska, J.; Wenner, B. S.; Driscoll, C. T. & Johnson, C. E. (1997), 'The biogeochemistry of basic cations in two forest catchments with contrasting lithology in the Czech Republic', *Biogeochemistry* **37**(2), 173-202.

KRAMER, P. J. (1981), 'Carbon-dioxide Concentration, Photosynthesis, and Dry-matter Production', *Bioscience* **31**(1), 29-33.

Lamb, D. W. & Brown, R. B. (2001), 'Remote-sensing and mapping of weeds in crops', *Journal of Agricultural Engineering Research* **78**(2), 117-125.

Landsberg, J.; Prince, S.; Jarvis, P.; McMurtrie, R.; Luxmoore, R. & Medlyn, B. (1997), Energy Conversion and Use in Forests: An Analysis of Forest Production in Terms of Radiation Utilisation Efficiency (É›), *in* Haruhisa Shimoda; HenryL. Gholz & Kaneyuki Nakane, ed., 'Forestry Sciences', Springer Netherlands, , pp. 273-298-.

Lass, L. W. & Prather, T. S. (2004), 'Detecting the locations of Brazilian pepper trees in the everglades with a hyperspectral sensor', *Weed Technology* **18**(2), 437-442.

Lepedus, H.; Viljevac, M.; Cesar, V. & Ljubesic, N. (2005), 'Functioning of the photosynthetic apparatus under low and high light conditions in chlorotic spruce needles as evaluated by in vivo chlorophyll fluorescence', *Russian Journal of Plant Physiology* **52**(2), 165-170.

Majeke, B.; van Aardt, J. A. N. & Cho, M. A. (2008), 'Imaging spectroscopy of foliar biochemistry in forestry environments', *Southern Forests* **70**(3), 275-285.

Martz, F.; Sutinen, M. L.; Derome, K.; Wingsle, G.; Julkunen-Tiitto, R. & Turunen, M. (2007), 'Effects of ultraviolet (UV) exclusion on the seasonal concentration of photosynthetic and UV-screening pigments in Scots pine needles', *Global Change Biology* **13**(1), 252-265.

Maslova, T. G.; Mamushina, N. S.; Sherstneva, O. A.; Bubolo, L. S. & Zubkova, E. K. (2009), 'Seasonal Structural and Functional Changes in the Photosynthetic Apparatus of Evergreen Conifers', *Russian Journal of Plant Physiology* **56**(5), 607-615.

Misurec, J.; Kopackova, V.; Lhotakova, Z.; Hanus, J.; Weyermann, J.; Entcheva-Campbell, P. & Albrechtova, J. (2012), 'Utilization of hyperspectral image optical indices to assess the Norway spruce forest health status', *Journal of Applied Remote Sensing* **6**, 063545.

Odagawa, S. & Okada, K. (2009), 'Tree Species Discrimination Using Continuum Removed Airborne Hyperspectral Data', *2009 First Workshop On Hyperspectral Image and Signal Processing: Evolution In Remote Sensing* , Ieee, 243-246.

Ollinger, S. V. (2011), 'Sources of variability in canopy reflectance and the convergent properties of plants', *New Phytologist* **189**(2), 375-394.

Oquist, G. & Huner, N. P. A. (2003), 'Photosynthesis of overwintering evergreen plants', *Annual Review of Plant Biology* **54**, 329-355.

Oulehle, F.; Hofmeister, J.; Cudlin, P. & Hruska, J. (2006), 'The effect of reduced atmospheric deposition on soil and soil solution chemistry at a site subjected to long-term acidification, Nacetin, Czech Republic', *Science of the Total Environment* **370**(2-3), 532-544.

Oulehle, F.; McDowell, W. H.; Aitkenhead-Peterson, J. A.; Kram, P.; Hruska, J.; Navratil, T.; Buzek, F. & Fottova, D. (2008), 'Long-term trends in stream nitrate concentrations and losses across watersheds undergoing recovery from acidification in the Czech Republic', *Ecosystems* **11**(3), 410-425.

PENUELAS, J.; BARET, F. & FILELLA, I. (1995), 'Semiempirical Indexes To Assess Carotenoids Chlorophyll-a Ratio From Leaf Spectral Reflectance', *Photosynthetica* **31**(2), 221-230.

Pontius, J.; Martin, M.; Plourde, L. & Hallett, R. (2008), 'Ash decline assessment in emerald ash borer-infested regions: A test of tree-level, hyperspectral technologies', *Remote Sensing of Environment* **112**(5), 2665-2676.

PORRA, R. J.; THOMPSON, W. A. & KRIEDEMANN, P. E. (1989), 'Determination of Accurate Extinction Coefficients and Simultaneous-equations For Assaying Chlorophyll-a and Chlorophyll-b Extracted With 4 Different Solvents - Verification of the Concentration of Chlorophyll Standards By Atomic-absorption Spectroscopy', *Biochimica Et Biophysica Acta* **975**(3), 384-394.

Porté, A., B. A. C. I. & Loustau, D. (2000), 'Estimating the foliage area of Maritime pine (Pinus pinaster Ait.) branches and crowns with application to modelling the foliage area distribution in the crown', *Ann. For. Sci.* **57**, 73-86.

Pu, R. L.; Kelly, M.; Anderson, G. L. & Gong, P. (2008), 'Using CASI hyperspectral imagery to detect mortality and vegetation stress associated with a new hardwood forest disease', *Photogrammetric Engineering and Remote Sensing* **74**(1), 65-75.

Richter, R. (2009), 'Atmospheric/topographic correction for airborne imagery', DLR-German Aerospace Centre, D-82234 Wessling, Germany.

ROCK, B. N.; HOSHIZAKI, T. & MILLER, J. R. (1988), 'Comparison of Insitu and Airborne Spectral Measurements of the Blue Shift Associated With Forest Decline', *Remote Sensing of Environment* **24**(1), 109-127.

Rojík, P. (2004), 'New stratigraphic subdivision of the Tertiary in the Sokolov Basin in Northwestern Bohemia', *Journal of the Czech Geological Society* **49/3-4**, 173-185.

Romer, C.; Wahabzada, M.; Ballvora, A.; Pinto, F.; Rossini, M.; Panigada, C.; Behmann, J.; Leon, J.; Thurau, C.; Bauckhage, C.; Kersting, K.; Rascher, U. & Plumer, L. (2012), 'Early drought stress detection in cereals: simplex volume maximisation for hyperspectral image analysis', *Functional Plant Biology* **39**(10-11), 878-890.

Schaaf, C. B.; Gao, F.; Strahler, A. H.; Lucht, W.; Li, X. W.; Tsang, T.; Strugnell, N. C.; Zhang, X. Y.; Jin, Y. F.; Muller, J. P.; Lewis, P.; Barnsley, M.; Hobson, P.; Disney, M.; Roberts, G.; Dunderdale, M.; Doll, C.; d'Entremont, R. P.; Hu, B. X.; Liang, S. L.; Privette, J. L. & Roy, D. (2002), 'First operational BRDF, albedo nadir reflectance products from MODIS', *Remote Sensing of Environment* **83**(1-2), 135-148.

Schaepman-Strub, G.; Schaepman, M. E.; Painter, T. H.; Dangel, S. & Martonchik, J. V. (2006), 'Reflectance quantities in optical remote sensing-definitions and case studies', *Remote Sensing of Environment* **103**(1), 27-42.

Schläpfer, D. (), 'Parametric Geocoding, PARGE Using Guide, Version 2.3,', ReSe Applications Schlдpfer & Remote Sensing Laboratories University of Zurich.

Sebesta, J.; Samonil, P.; Lacina, J.; Oulehle, F.; Houska, J. & Bucek, A. (2011), 'Acidification of primeval forests in the Ukraine Carpathians: Vegetation and soil changes over six decades', *Forest Ecology and Management* **262**(7), 1265-1279.

Shafri, H. Z. M.; Hamdan, N. & Anuar, M. I. (2012), 'Detection of stressed oil palms from an airborne sensor using optimized spectral indices', *International Journal of Remote Sensing* **33**(14), 4293-4311.

SHAPIRO, S. S. & WILK, M. B. (1965), 'An Analysis of Variance Test For Normality (complete Samples)', *Biometrika* **52**, 591-.

Silkina, O. V. & Vinokurova, R. I. (2009), 'Seasonal dynamics of chlorophyll and microelement content in developing conifer needles of Abies sibirica and Picea abies', *Russian Journal of Plant Physiology* **56**(6), 780-786.

Sims, D. A. & Gamon, J. A. (2002), 'Relationships between leaf pigment content and spectral reflectance across a wide range of species, leaf structures and developmental stages', *Remote Sensing of Environment* **81**(2-3), 337-354.

Soukupova, J.; Cvikrova, M.; Albrechtova, J.; Rock, B. N. & Eder, J. (2000), 'Histochemical and biochemical approaches to the study of phenolic compounds and peroxidases in needles of Norway spruce (Picea abies)', *New Phytologist* **146**(3), 403-414.

Suchara, I.; Sucharova, J.; Hola, M.; Reimann, C.; Boyd, R.; Filzmoser, P. & Englmaier, P. (2011), 'The performance of moss, grass, and 1- and 2-year old spruce needles as bioindicators of contamination: A comparative study at the scale of the Czech Republic', *Science of the Total Environment* **409**(11), 2281-2297.

Thomas, V.; McCaughey, J. H.; Treitz, P.; Finch, D. A.; Noland, T. & Rich, L. (2009), 'Spatial modelling of photosynthesis for a boreal mixedwood forest by integrating micrometeorological, lidar and hyperspectral remote sensing data', *Agricultural and Forest Meteorology* **149**(3-4), 639-654.

Tzvetkova, N. & Hadjiivanova, C. (2006), 'Chemical composition and biochemical changes in needles of Scots pine (Pinus sylvestris L.) stands at different stages of decline in Bulgaria', *Trees-structure and Function* **20**(4), 405-409.

Underwood, E.; Ustin, S. & DiPietro, D. (2003), 'Mapping nonnative plants using hyperspectral imagery', *Remote Sensing of Environment* **86**(2), 150-161.

Ustin, S. L.; Gitelson, A. A.; Jacquemoud, S.; Schaepman, M.; Asner, G. P.; Gamon, J. A. & Zarco-Tejada, P. (2009), 'Retrieval of foliar information about plant pigment systems from high resolution spectroscopy',

Remote Sensing of Environment **113**, S67-S77.

Ustin, S. L.; Roberts, D. A.; Gamon, J. A.; Asner, G. P. & Green, R. O. (2004), 'Using imaging spectroscopy to study ecosystem processes and properties', *Bioscience* **54**(6), 523-534.

Verrelst, J.; Schaepman, M. E.; Koetz, B. & Kneubuhler, M. (2008), 'Angular sensitivity analysis of vegetation indices derived from CHRIS/PROBA data', *Remote Sensing of Environment* **112**(5), 2341-2353.

Vogelmann, J. E.; Xian, G.; Homer, C. & Tolk, B. (2012), 'Monitoring gradual ecosystem change using Landsat time series analyses: Case studies in selected forest and rangeland ecosystems', *Remote Sensing of Environment* **122**, 92-105.

Welburn, A. (1994), 'The spectral determination of chlorophyll-a and chlorophyll-b, as well as total carotenoids, using various solvents with spectrophotometers of different resolution', *J. Plant Phys.* **144(3)**, 307–313.

Wu, C. Y.; Niu, Z.; Tang, Q. & Huang, W. J. (2008), 'Estimating chlorophyll content from hyperspectral vegetation indices: Modeling and validation', *Agricultural and Forest Meteorology* **148**(8-9), 1230-1241.

Yatsko, Y. N.; Dymova, O. V. & Golovko, T. K. (2011), 'Violaxanthin cycle pigment de-epoxidation and thermal dissipation of light energy in three boreal species of evergreen conifer plants', *Russian Journal of Plant Physiology* **58**(1), 169-173.

Yudovich, Y. E. & Ketris, M. P. (2005), 'Arsenic in coal: a review', *International Journal of Coal Geology* **61**(3-4), 141-196.

Zarco-Tejada, P. J.; Miller, J. R.; Morales, A.; Berjon, A. & Aguera, J. (2004), 'Hyperspectral indices and model simulation for chlorophyll estimation in open-canopy tree crops', *Remote Sensing of Environment* **90**(4), 463-476.

Zhao, K. G.; Valle, D.; Popescu, S.; Zhang, X. S. & Mallick, B. (2013), 'Hyperspectral remote sensing of plant biochemistry using Bayesian model averaging with variable and band selection', *Remote Sensing of Environment* **132**, 102-119.

Zwiggelaar, R. (1998), 'A review of spectral properties of plants and their potential use for crop/weed discrimination in row-crops', *Crop Protection* **17**(3), 189-206.

6. Assessing forest health via linking the geochemical properties of a soil profile with the biochemical vegetation parameters

Kopačková, V., Lhotáková, Z., Oulele, F., Albrechtová, J., (under review): Assessing forest health via linking the geochemical properties of a soil profile with the biochemical vegetation parameters, International Journal of Environmental Science and Technology.

Abstract

The transfer of chemical elements/compounds within the soil–plant chain is a part of the biochemical cycling and this system is controlled by biotic and abiotic factors which determine the final mobility and availability of chemical variables. Heavy metal contamination and low pH are stress factors that lead to changes in the contents of important foliage compounds, which can be used as non-specific indicators of plant stress. In this study, Norway spruce forests in the Sokolov region, being a part of the "Black Triangle", were selected to assess geochemical and biochemical interactions in the natural soil/plant system. The authors studied the relationship between soil and spruce needle contents of macronutrients and potentially toxic elements and tested whether the soil parameters and their vertical distribution within a soil profile (two organic and two mineral horizons) affect foliage biochemical parameters (contents of photosynthetic pigments, phenolic compounds and lignin). Factor analysis was used to identify underlying variables that explained the pattern of correlations within and between the biochemical and geochemical datasets. Al and As were identified as toxic elements with high bio-availability for spruce trees and both were taken up by trees and translocated to the foliage. The correlations between two toxic element contents in needles (aluminum (Al) and arsenic (As)) and the contents of soluble phenolic compounds and total carotenoid to chlorophyll (Car/Cab) ratio suggest that these latter two biochemical parameters, which both proved to be sensitive to the soil geochemical conditions, can serve as suitable non-specific stress markers.

Keywords: Norway spruce (Picea abies L. Karst) health; non-specific stress markers; heavy metal stress; factor analysis; phenolic compounds; photosynthetic pigments

6.1 Introduction

The transfer of trace elements within the soil–plant continuum is a part of the biogeochemical cycling of chemical elements. Plant species vary in their ability to withstand exposure to heavy metals from hyperaccumulation known for phytoextraction species to prevention of uptake characteristic for phytostabilisation species (Salt et al. 1998; Nwoko 2010; Mani et al. 2012a and 2012b). Heavy metal contamination and other negative physio-chemical changes under soil conditions, such as low pH are often a consequence of long-term industrial pollution (Lepedus et al. 2005; Tuzhilkina 2009).

Changes in the contents of important plant compounds can be used as non-specific indicators of plant stress; these include the contents of photosynthetic pigments, phenolic compounds and lignin, as shown for coniferous trees by many authors (e.g. Soukupova et al. 2000; Lepedus et al. 2005; Tzvetkova and Hadjiivanova 2006). Additionally, these parameters can be monitored by the means of hyperspectral (HS) remote sensing and enable large-scale monitoring of forest health (Campbell et al. 2004; Mišurec, Kopačková et al. 2012; Kupková et al. 2012).

Limited work has been performed under field conditions exploring the effects of accumulated sediment/soil-borne metals on biochemical processes in plant tissues and assessment of their suitability as potential biomarkers of metal stress (MacFarlane 2002; Bialonska et al. 2007). Additionally, the contents of available macronutrients (Ca^{2+}, Mg^{2+}, K^{+}) can also play an essential role in the tree physiology. Therefore, there is an urgent need for the development of methodologies for assessing the sub-lethal effects of trace elements in conjunction with macronutrient availability and the way in which these soil characteristics affect leaf biochemical parameters in situ.

The biochemical composition of spruce needles with their longevity and exposure to environmental conditions is often used as a bioindicator of soil or air contamination (Ollerová et al. 2010; Tuzhilkina 2009). Particularly the contents of photosynthetic pigments are closely related to photosynthetic performance and can serve as early-warning symptoms of plant stress, before macroscopic changes are detected (e.g. Lepedus et al. 2005; Soukupová et al. 2000). The chlorophyll content of needles generally decreases under stress conditions, including nutrient deficiency and the presence of heavy metals (Huang and Tao 2004; Ivanov et al. 2011; Maestri et al. 2010). In general, conifers allocate relatively high ratios (7.3–12.3%) of the whole-tree carbon to foliar phenolics (Aspinwall et al. 2011). Phenolic compounds represent a very heterogeneous group playing a role in defense mechanisms against pathogenes and herbivores (Klepzig et al. 1996) and environmental stress conditions, often serving as a non-specific stress marker. Tannins are involved in chelating heavy metals in plant cells

(Lavid et al. 2001); in addition, polyphenols such as tannins not only inhibit decay of soil organic matter, but they may also impede soil N mineralization–immobilization reactions (Northup et al. 1998; Yu et al. 2003). Lignin is a structural compound of polyphenolic nature and its content in foliage plays an important role in litter decomposition and nutrient cycling (Ushio et al. 2009). Thus changing the content of phenolics in litter may alter wider biogeochemical carbon cycling in forest soils.

In this study, Norway spruce forests in the Sokolov region, the north-western part of the Czech Republic, were selected to assess geochemical and biochemical interactions in the natural soil/plant system. This region is exceptional for its long-term excessive lignite mining history and was also greatly affected by air pollution and soil acidification during the second half of the 20th century (Moldan and Schnoor 1992). Even today, this part of the country with its open-pit lignite mining is considered to be one of the most polluted regions in the Czech Republic. Norway spruce (*Picea abies L. Karst*) is a dominant species in the silviculturally managed coniferous forests in Central Europe and particularly in the Czech Republic. However, this tree species has proven to be prone to environmental stresses. Long-term industrial pollution resulted in large-scale spruce forest dieback observed in many regions of Central Europe, particularly in the area of the so-called Black Triangle (Moldan and Schnoor 1992), the well know region in Europe heavily polluted in the second half of the 20th century. Therefore, monitoring of the health condition of spruce forests remains important for forest management in Central Europe. Particularly the response of tree species to adverse soil conditions (e.g., contents of trace elements, basic cations depletion, and acidification) is of great importance.

The authors analyzed a wide range of biochemical parameters in the Norway spruce needles serving as non-specific stress markers (biochemical dataset): photosynthetic pigments, soluble phenolic compounds, lignin and water content. Furthermore, around the sampled-trees the contents of selected macronutrients, which are present in the form of exchangeable cations (Ca^{2+}, Mg^{2+}, K^{+}) and Al as well as selected heavy metals (e.g., Zn, Cu, As and Hg) were determined in the corresponding soil profiles (geochemical dataset). Ca has a signaling role and structural involvement, Mg is a central atom of the chlorophyll molecule and K is a principal cation in establishing cell turgor and maintaining cell electroneutrality. Zn and Cu are classified as micronutrients involved in redox reactions in plant cells, while As and Hg are considered to be non-essential, potentially very toxic metals for plants affecting plant water status (Javot and Maurel 2002; Czech et al. 2010).

Mobilization of ionic Al under acid conditions may have negative effects on Ca and Mg uptake by trees (Schröder et al. 1988; de Wit et al. 2010).

In addition to basic statistics, factor analysis was used to identify underlying variables or factors, that explain the pattern of correlations within and between the biochemical and geochemical sets of the variables described above. Factor analysis was previously successfully employed using environmental data and was particularly tested for the purposes of mineral exploration (Harraz et al. 2012) and to interpret diverse geochemical datasets (Tripathi 1979; Ijmker et al. 2012) as well as water or soil chemical data (Fitzpatrick et al. 2007). The authors assume this method is also well suited to studying relationships and chemical/biochemical interactions in the soil/plant system and, to our knowledge, has not yet been used for this purpose.

As the present study quantitatively correlates a wide range of spruce needle biochemical parameters with macronutrient and accumulated heavy metal contents determined for four soil horizons in the polluted region, the aims have been to:

- Determine macronutrient/heavy metal abundances and their associations present in four different soil horizons (including organic and mineral soil horizons).
- Investigate whether these associations and their vertical distribution within a soil profile affect the accumulation of the same chemical elements in foliage.
- Assess the applicability of using selected needle biochemical parameters (photosynthetic pigment contents, phenolic and lignin contents, and selected nutritional and trace element contents) as biological indicators of adverse soil conditions (low pH, high concentrations of trace elements) in Norway spruce forest ecosystems.

This work was carried out at the Czech Geological Survey and at the Faculty of Science (Charles University in Prague) within 2009-2011.

6.2 Material and methods

6.2.1 Test site

General description on the test site is given in the chapter 5.2.1.

6.2.2 Soil samples

General description on the test site is given in the chapter 5.2.2.2.

6.2.3 Norway spruce samples

At each of the four test sites, 10 to 15 representative trees were selected. A tree-climber cut branches from the production part of the crown, which means that all the sampled branches were sunlit and contributed significantly to the photosynthetic production of the tree. One branch was sampled in the upper level of the production part (U) of the crown almost at the boundary with the most upper juvenile part of the crown and the second branch in the lower level of the production crown part (L). Needles of the first- (1) and third-year (3) were sampled from each branch for subsequent chemical and biochemical analyses.

Photosynthetic pigments (chlorophyll a and b: Cab, total carotenoids: Car) were extracted in dimethyl formamide according to (Porra et al. 1989) and determined spectrophotometrically based on equations from (Wellburn 1994). Soluble phenolic compounds were determined according to (Singleton 1965). Frozen needles were homogenized in liquid nitrogen. Phenolics (FFW = fresh weight, FDW = dry weight) were extracted in 80% methanol (v/v) in a water bath (50°C) and the concentrations were determined spectrophotometrically at a wavelength of 750 nm using a Helios α spectrophotometer (Unicam, Cambridge, UK) with Folin-Ciocalteau phenol reagent and gallic acid as a standard (for details see Soukupová et al. 2000).

The lignin (Lig) content was determined by thioglycolate solubilization according to (Lange et al. 1995) and the amount of lignin was determined spectrophotometrically at a wavelength of 280 nm using hydrolytic lignin (Aldrich Chemical Company, USA; [8672-93-3]) as a standard.

Analyses of Ca, K, Mg, Al, Cu, Zn, As and Hg were performed for the first-year needles sampled from the lower production part of the crown (L1). Needle samples were slowly combusted (550°C) and then digested in concentrated HF (40%, p.a., 15ml) and $HClO_4$ (70%, p.a., 2 ml) on a hot plate. The following evaporation residue was digested in 5ml of HCl (37%, p.a.). Destiled water was used to make a 100 ml solution which was used for cations measurements at AAS (Perkin-Elmer AAnalyst 100). Hg was determined by AAS after pyrolysis of the samples and As was analyzed using HGAAS (hydride generation of arsenic species coupled with atomic absorption).

The overall statistics of the needle properties were further statistically assessed and are presented in the Appendix: Tabs 3 and 5.

6.2.4 Statistical methods

First the Shapiro-Wilk test (Shapiro and Wilk 1965) was employed to test the normal distribution of both the geochemical and biochemical datasets and some of the variables were not normally distributed according to this test (Appendix: Tabs 1 and 5). However, since the ratios between the maximum and minimum measurement concentrations are generally high enough, log-transformation was employed to squeeze/stretch the values on the logarithmic (loge) scale with the exception of the pH, as this parameter is already log-transformed and exhibits normal distribution. After this transformation, distributions with skewnesses varied between -0.8 and 0.8, or with kurtosis between -3 and 3 for all of the geochemical and most of the biochemical parameters. Such datasets more or less behave like normally distributed (Ijmker et al. 2012). However, the water content at both levels (L1, L3) and Hg content at level L1 did not fulfill this condition and this fact was taken into consideration when interpreting the results. Further statistics was applied to the log-transformed data.

As the Norway Spruce needle samples were collected from two different crown positions (U-upper, L-lower) and needle ages (1-3 years old), analysis of the variance (two-way ANOVA) was employed to test whether there are statistically significant differences in the biochemical properties of the Norway Spruce needles with regard to their position within a crown and their age. In further statistical assessments (PCA and factor analysis), only the age effect was considered (L1 and L3 samples were statistically assessed), because the needle age significantly influenced all the examined biochemical characteristics (Appendix: Table 4).

The relationships between (i) the geochemical parameters within the four soil horizons, (ii) the biochemical parameters (photosynthetic pigment contents, phenolic and lignin contents) conducted for two different needle ages (1-3 years old) from position L and (iii) biochemical parameters including selected nutritional and trace element content of the sampled trees (1st year needles, lower position: L1) were assessed using the Pearson correlation coefficient. The bivariate correlation was attained at a 95% confidence level (2-tailed). As a great number of soil parameters were assessed, the Pearson correlation coefficients were transformed into the form of color-coded correlation matrix (Figs. 2, 5, 6) for easer interpretation.

Afterwards, factor analysis was employed. In our case, factor analysis was employed on the sets of variables that represented (i) chemical variables uncounted for each soil horizon, (ii) the common chemical variables determined for both soil horizons and the tree needles (macronutrients and

selected heavy metals) and (iii) biochemical variables determined for the Norway spruce needles (macronutrients and selected heavy metals). Factor analysis of the soil parameters enabled study of the correlations between elements, forming groups with similar behavior (natural associations) in each horizon and of how these associations change with soil depth (Appendix: Tabs. 8 and 9, Fig. 6.2). The approach comparing the abundances of the common chemical variables, which were determined for all the four soil horizons as well as for the tree needle samples, enabled the authors to study which chemical elements present in the soil have been taken up by the vegetation and thus have the most significant impact on the vegetation health and physiological functions (Appendix: Tabs. 10 and 11, Fig. 6.4). Finally, factor analysis of the biochemical parameters allowed determination of the correlating biochemical parameters that can affect specific physiological functions of the trees (Appendix: Tabs. 12 and 13).

Factor analysis produces factor loadings that represent the correlation of a variable (in our case geochemical and biochemical) with a factor. It calculates a factor score for every single observation, showing the weight of a specific factor for that specific observation. Factor analysis was performed by the SPSS program (version 14.0). Principle Component Analysis was used to extract the factors and to form uncorrelated linear combinations of the observed variables. An orthogonal rotation method (varimax), which is the most common orthogonal rotation criterion (Davis 2002), was employed to rotate the factors. The varimax rotation fits the axes to the maximum direction of variance, thereby spreading the explained variance more evenly over the different factors (Hartmann and Wünnemann 2009). This rotation method minimized the number of variables that have high loadings on each factor and in that way simplified the interpretation of the factors.

New data were derived from these linear combinations, forming the principal components, (PC) which can be displayed as scores and weights. The first PC, or factor, accounts for the greatest variability in the data, and there can be an infinite number of new factors, with each accounting for less data variability than the previous one (Webster 2001). Factor loadings are correlation coefficients between the original variables and factors and are intended to investigate the processes that control data variability. A loading on one variable close to ±1 indicates a strong correlation between the variable and the factor. Similarly to Hu et al. (2012), the authors considered the variables that exhibited a loading of >0.4 or <-0.4 to be statistically significant.

6.3 Results and discussion

6.3.1 Geochemical properties and their changes across the soil profile

The pH of the sampled soils was low (2.96-3.65) with a slight increase towards deeper mineral soils (Appendix: Table 1). According to Kabata-Pendias (2004) several trace metals (especially Cd, Zn, Co, Cu and Ni) are readily mobile in such acid soils, which are generally characterized by oxidizing conditions, and are available to plants. In addition, low pH is also a serious problem as it facilitates the release of aluminium (Al) from Al-containing minerals into the soil solution forming toxic conditions for forest vegetation or downstream aquatic organisms (Krám et al. 2009). In particular, it is a matter of concern that soil acidification caused by acid deposition, together with the consequent depletion of labile pools of nutrient cations (e.g. Ca^{2+}, Mg^{2+}) and enhancing leaching of Al from the soil, could contribute to forest dieback (Driscoll et al. 2001; Juice et al. 2006). To assess the possible aluminium mobilization via using the Ca/Al ratio (Hruška and Krám 1994), the molar concentrations were calculated for Ca and Al (Appendix: Tabs 2). Only in the most top horizon (Ol+Of) did the Ca/Al ratios fall above the critical value = 1, previously reported to be the threshold for damage to plant roots (Matzner and Prenzel 1992).

For each soil horizon, the concentration ranges (min., max.), mean values and standard deviations are shown in Appendix: Table 1. As regards the exchangeable cations, Ca was the most abundant cation in all four horizons, followed by Al, K, Mg. Comparing the total concentrations of trace elements, Zn was the most abundant metal, followed by Cu, As and Hg. The basic statistics also show that elements such as Mg, Ca, K and As have significantly higher concentrations in the topmost horizon (Ol+Of) and their abundances decrease with increasing soil depth. On the other hand, the abundances of Zn increase with increasing soil depth and this indicates that this element is most probably of lithological origin. Elements such as Al, Cu and Hg exhibit the highest abundances in the second horizon (Oa) as does the TEA parameter. High concentrations of Cu, Hg and As in the humus-rich horizons point to strong binding of these elements to the soil organic matter (Blaser et al. 2000; Mani and Kumar 2005).

The measured concentrations of exchangeable cations and trace elements (organic horizons together (Ol+Of and Oa), A0-10 and A10-20) were compared with the

mean values classified and published for the Czech Republic (Fabiánek 2004). In general, the cation concentrations were found to correspond to low values on the scale for the Czech Republic.

The contents of exchangeable Ca were low in the organic horizons (Ol+Of and Oa: 1307.4 and 379.5 mg/kg) or rather low in A0-10 and A10-20. Exchangeable K in all the studied horizons was estimated as low and corresponded to the lowest values found in the Czech Rep. The mean contents of exchangeable Mg in mineral horizons were low, but in accordance with the mean values (A0-10: 10.5 mg/kg), or close to the minimum values found in the Czech Republic (A10-20: 5.6 mg/kg). Considering the C/N ratio, there are no significant differences between the two organic horizons. The average C/N ratio in the studied forest stands ranged between 24.9 and 35.0 in Ol+Of and between 21.8 and 34.4 in Oa.

In terms of the trace element gradients, the organic horizons contained moderate amounts of Cu (50.1 and 78.9 mg/kg, respectively) and Zn (102.7 and 89.3 mg/kg). In both organic horizons and in A0-10 the contents of As exceeded the limit value given by the regulations issued by the Ministry of the Environment of the Czech Republic (382/2001 Sb.). Additionally, high contents of Hg were detected across the whole soil profile (max in Oa: 1.63 mg/kg).

Analysis of the color-coded matrix (Fig. 6.1) reflects strong positive correlations across the entire soil profiles for Zn, indicating that this element is of lithological origin. This corresponds to the results published by Borůvka et al. (2005) as they found that most topsoil and subsoil Zn was bound in silicates. Naturally, significant positive correlations for all four horizons exist between Al –TEA, as Al cation content is one of the parameters contributing to TEA, and for Mg-Ca; enrichment in these two elements is a result of organic material decomposition. On the other hand, a generally significant negative correlation exists between Zn-TEA.

Factor analysis is a powerful tool for identifying relationships that are not readily evident from simple correlation analysis. Therefore, further statements are formulated, interpreting together both the results of the correlation matrix and also the results of factor analysis (Fig. 6.1, Appendix: Tabs 8 and 9). Factor analysis was conducted for each soil horizon separately; they represent different material/mineral compositions and physical-chemical conditions; therefore, the authors expected to find different element associations. The result of the factor analysis shows that, after varimax rotation, the first three components explain the majority of the variance in the studied soil variables (Appendix: Tab. 8). Statistically significant variables which exhibited loading of >0.4 or <-0.4 are shown in bold (positive- black, negative-white), the closer numbers of loadings correspond to the closest relationships between studied variables.

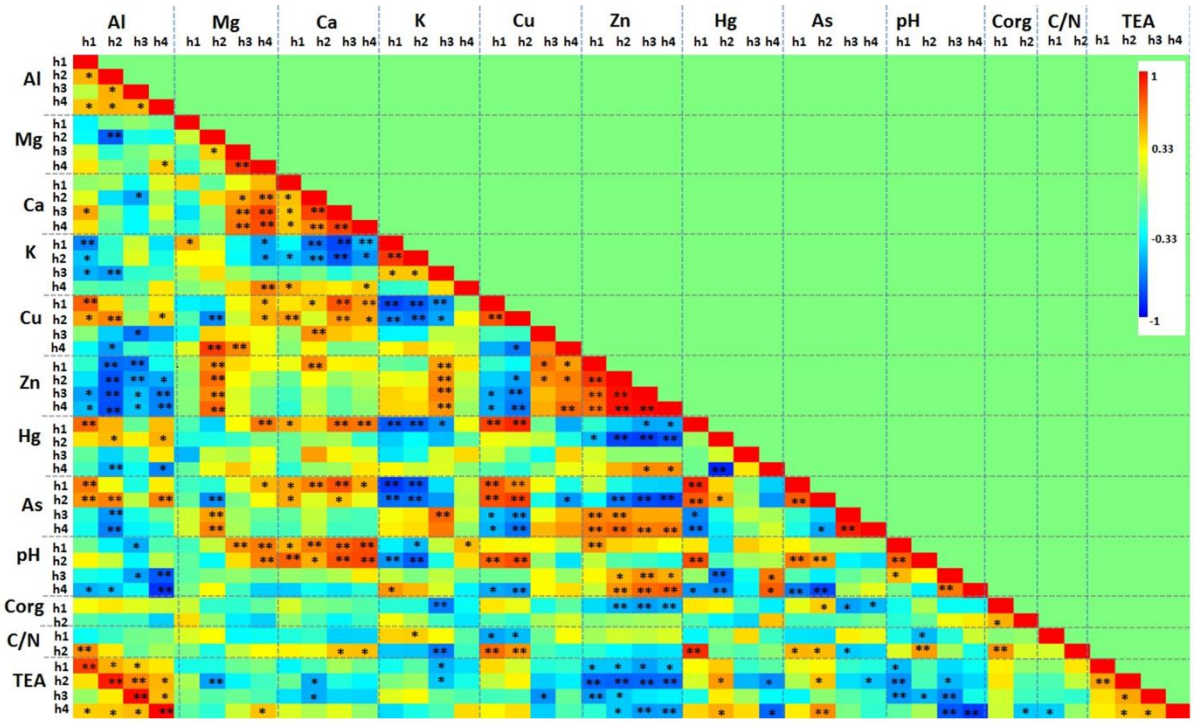

Figure 6.1: *Pearson correlation color coded matrix (the values were $\log_e$ transformed): Soil profile geochemical properties; the coefficients were assigned colors according to their values (color scale from dark blue (correlation= -1) to dark red (correlation= 1)). (** Correlation is significant at the 0.01 level, * Correlation is significant at the 0.05 level).*

Horizon 1 (Ol+Of)

Factor 1 accounts for 42% of the data variability. There are two associations of this factor: Al-As-Hg-Cu (high positive loadings above 0.750) representing mainly toxic elements, and the correlation between Ca and the pH (positive loadings around 0.460). Factor 2 accounts for 22% of the data variability and, in this case, a strong relationship was found between Zn and pH as well as between Al-TEA-Corg. Factor number 3 covered about 19% of the data variability and correlation between the C/N and Mg-Ca association was identified, corresponding to parameters that have their origin in the organic material and related decomposition processes.

Horizon 2 (Oa)

Factor 1 accounts for 44% of the data variability. One main association, Ca-Cu-As, characterizes this factor and correlates with the C/N ratio and the pH. Surprisingly, Ca fell into this group and the authors assume that Ca originates mainly from the decomposition of organic material coming from the litter. The affinity of Cu and As for soil organic matter and the stability of organic complexes were demonstrated by Berthelsen et al. (1994) and by Yudovich and Kertris (2005), respectively. However, as Cu and As correlate with C/N but not with the organic matter content (Corg) by itself, we assume

these elements in this horizon originate mainly from poorly decomposed organic material, which is typically characterized by a high C/N ratio (Egli et al. 2010). Two major associations were identified in factor 2 (27% of the data variability), a group of mainly toxic elements (Al-Hg-As-Cu) correlating with TEA and the Mg-Ca-Zn association. Ca and Mg correspond to nutrients and Zn is also an essential element if not present in high concentrations (Pallardy 2008). Factor 3 (9% of the data variability) is explained mainly by the variability in Hg (high positive loadings) and Corg (high negative loadings) and has not allowed any other associations to be identified.

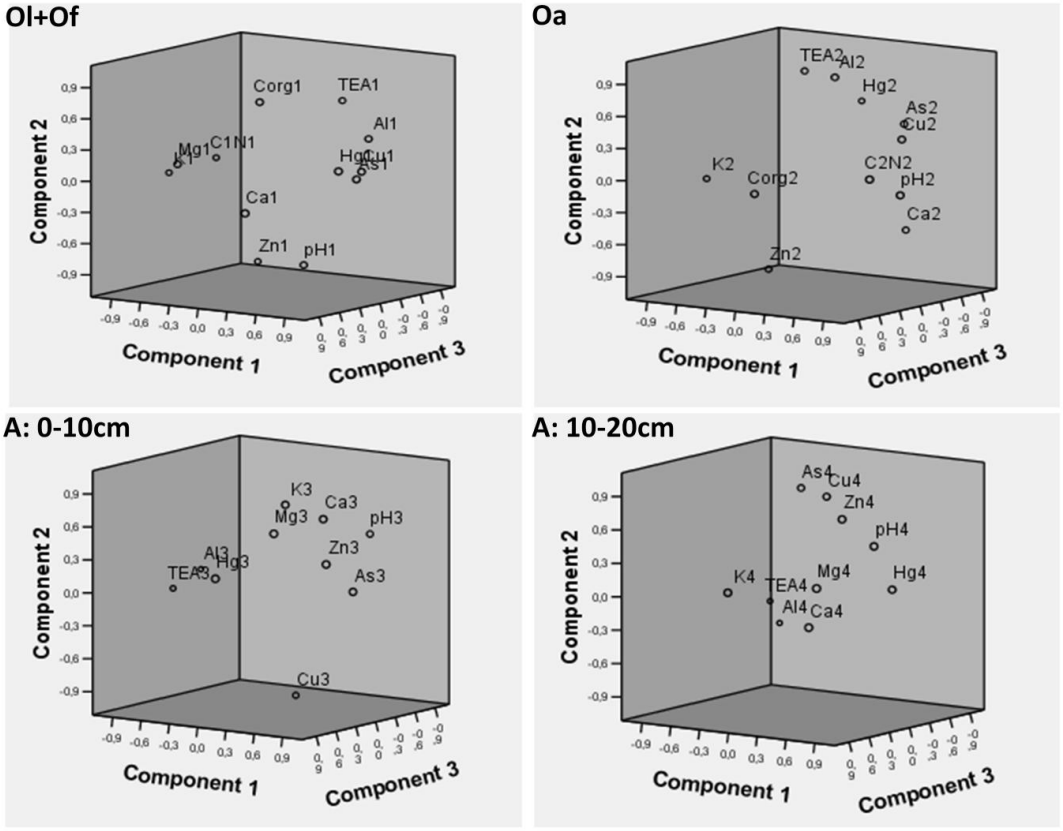

Figure 6.2: *Factor analysis: 3D plot of the first three components calculated for the four different horizons.*

Horizon 3 (A0-10)

Factor 1 accounts for 65% of the data variability and two major groups were found; the Mg-Ca-K and Zn-As associations, which have a strong relationship to the soil pH. The authors assume that both associations are products of the weathering of diverse minerals (e.g., alluminosilicates, feldspars, biotite). Factor 2 (22% of the data variability) indicated a relationship between Mg-Ca-K, nutrient association that most likely has organic origin. A correlation between Mg-Hg, the elements with the same charge, was identified in factor 3 (13% of the data variability).

Horizon 4 (O10-20)

The lithology of the parent rock material affects this horizon more when the overlying horizons described above, in this profile the mineral products of weathering, have common occurrence. Factor 1 accounts for 61% of the data variability and one major group – Mg-Ca-Zn and Hg – correlating with the pH – explains this factor. The major Zn-Cu-As associations was identified in factor 2 (19% of the data variability) and, also in this group, correlated with the pH. The relationship between Mg-Ca-K was identified in factor 3 (12% of the data variability), the same nutrient association detected in the overlying horizon A0-10.

6.3.2 Linking chemical properties of the soil and Norway spruce

To link the gradients of the same nutrients/heavy metals in the soil and their contents in needles was a key aspect as the total abundances of these chemical constituents/elements cannot, in itself, predict their uptake by tree roots and the potential risk they represent for plants (Bussinow et al. 2008; Aznar et al. 2009). The authors assumed that, if a statistically significant relationship is found between the soil and needle abundances of the same chemical elements, transfer exists between the soil and the root systems. These elements should be further considered as mobile in the soil, with high potential bioavailability.

Principle component 1 (49% of the data variability) indicated relationships between soil and needle element contents for Al, Hg and As (Fig. 6.3, Appendix: Tabs 10 and 11): (i) the amounts of Al in needles correlated positively with the soil contents in all four soil horizons, (ii) Hg in the needles had a strong correlation with Hg abundances in the two organic horizons, although it needs to be taken in account that Hg in the sampled needles did not exhibit normal distribution and optimally this result should be further tested using a new dataset. However to support the relationship, a similar distribution of Hg in the soil profile and foliage was also described by (Obrist et al. 2012) in Douglas fir and red alder stands. These results can be explained by a strong affinity of Hg for the soil organic matter, as reported by Kolka et al. (1999) or Mani and Kumar (2005). Nevertheless, it is still not clear whether Hg is taken up by the trees preferentially from the upper soil horizons and transported to the needles or whether it accumulates in the needles and surface soil profile from atmospheric deposition, as mentioned, e.g., by (Brun et al. 2010). Hg is reported to be immobile in soils (Adriano 2001); thus the authors assume that Hg is loaded into the upper soil profile mainly by atmospheric deposition, (iii) the As content in the needles correlated with the As contents in A0-10 and A10-20, the mineral horizons already influenced by the parent rock material. This was in accordance with

findings that roots take up As mainly in inorganic forms (arsenate and arsenite) and As is transported to the above-ground organs in the form of arsenite (Zhao et al. 2010). Similarly, a study of the spatial distribution of trace elements in Norway spruce stands showed that As is mainly associated with the mineral horizons in Norway spruce forest soil (Brun et al. 2010).

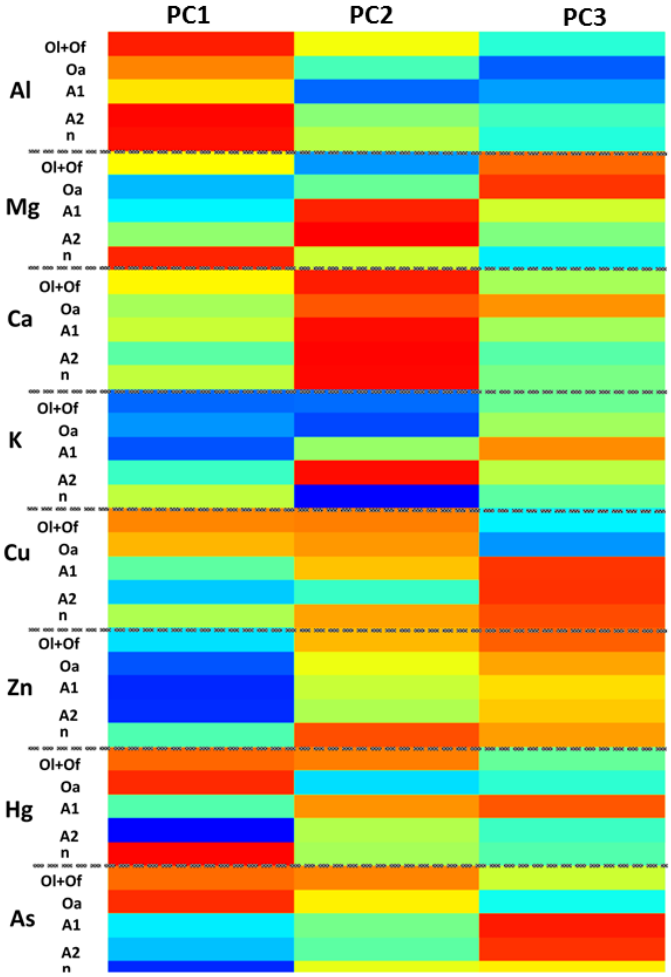

Figure 6.3: *Color-coded matrix of the loading factors for the first free components: Element abundances in the soil horizons (organic horizons: Ol+Of and Oa, A1: mineral soil 0-10 cm, A2: mineral soil 10-20 cm) and the Norway spruce needles (marked as n).*

Principle component 2 (39% of the data variability) identified the following relationships (Fig. 6.3, Appendix: Tabs 10 and 11): (i) Ca: correlations between the needle contents and the abundances in all four soil horizons, (ii) K: the abundances in needles correlate with the abundances in the first two organic horizons, as K is enriched in the forest floor horizons through the decomposition of K-rich litter. During the decomposition of organic matter (OM) monovalent ions are released relatively quickly and are thus available for uptake by trees. The high turnover rate of K between the forest

floor and foliage is thus responsible for the close relationship, (iii) Zn: correlation between the needle content and the Zn content in the first soil horizon was detected, (iv) Cu: a relationship was found between the needle content and the Cu abundances in the Ol+ Of, Oa and A1-10 soil horizons. This result demonstrates that, in acid soils, the Cu content is more often related to organic matter pools (Egli et al. 2010).

Component 3 (12% of the data variability) additionally allowed identification of a relationship between the needle abundances of Cu and mainly the lower mineral horizons (A0-10 and A10-20).

6.3.3 Variability of biochemical parameters according to the needle position in a crown and the age

In general, the mean pigment contents of the sampled trees (2.6 ± 0,8 mg/g DW of chlorophyll a+b: Cab) correspond to healthy Norway spruce (Siefermannharms 1994). Assessing vertical gradients, only the contents of photosynthetic pigments and their ratio depended on the needle position within the production crown part, while the other biochemical parameters (soluble phenolics and water/ lignin contents) were independent of the needle vertical position (Appendix: Tab. 4). The needles from the lower position of the production part of the crown received less direct radiation and tend to have higher pigment concentrations like the needles from the „transition" canopy level (Homolová et al. 2012). Similarly, in this case needles sampled from the lower position (L) exhibited higher pigment contents. In contrast to the needle crown position, the needle age had a significant effect for all the investigated biochemical parameters. Therefore, the authors decided to keep the different needle age classes separated regardless of the needle vertical position in further statistical assessments.

The first component (31% of the data variability, Appendix: Tabs. 6 and 7) is explained mainly by the variances in the water (W), chlorophyll (Cab) and carotenoid (Car) contents of the L1 needles (higher production crown part, younger needles). Similarly, component 2 (18% of the data variability) is explained mainly by the variance in the Cab and Car values in the L3 needles (lower production crown part, older needles). The same relationship shows the correlation color-coded matrix (Fig. 6.4). A strong positive correlation between the contents of chlorophylls and carotenoids was expected, as both types of pigments cooperate in light harvesting in primary photosynthetic reactions (Demmig-Adams and Adams 1996). Although the first-year needles are assumed to be mature at the time of sampling (late July), the contents of Cab and Car in these needles usually increase in the subsequent one or two seasons (Albrechtová et al. 2008) and the water content decreases (Homolová 2012), which may both change the strength of the relationships between these

biochemical parameters and explain the stronger correlation between photosynthetic pigments and needle water contents in L1. Additionally, the Car/Cab ratio is influenced by needle age: in the first-year needles, the pigment ratio was more dependent on the carotenoid content in comparison with 3rd year needles, where the value of the Car/Cab ratio was driven by increasing chlorophyll content (Fig. 6.4).

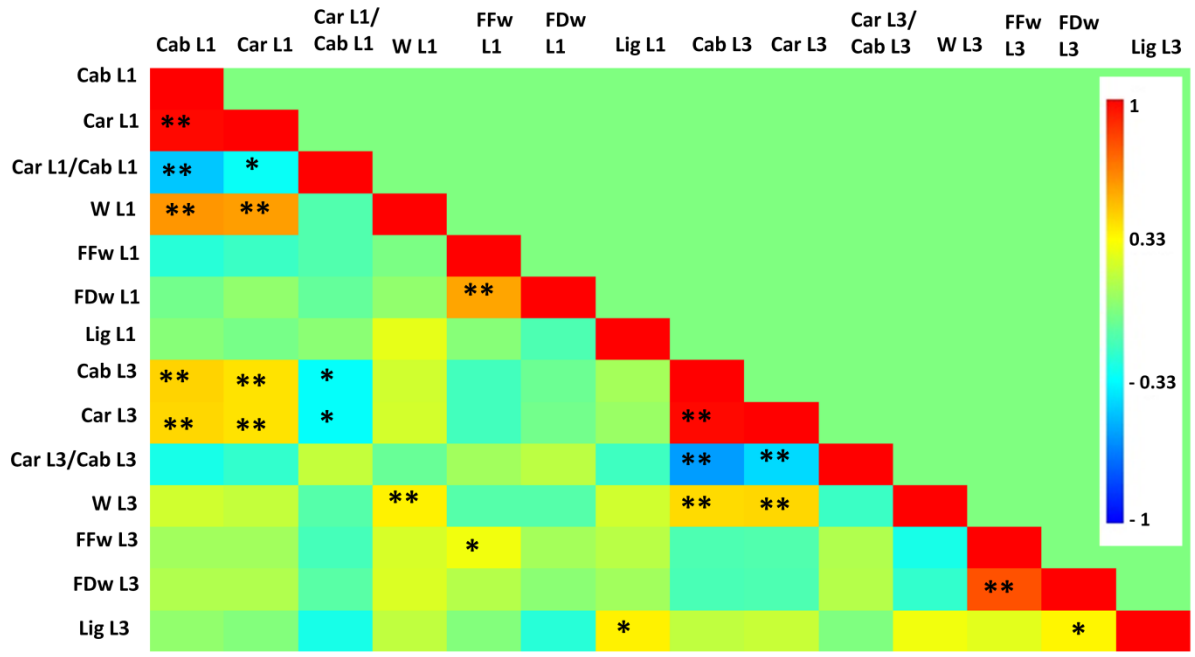

Figure 6.4: *Pearson correlation color-coded matrix (values were log_e transformed): chemical and biochemical properties of the Norway Spruce at the position of L1, the coefficients were assigned colors according to their values (color scale from dark blue (correlation= -1) to dark red (correlation= 1)). (** Correlation is significant at the 0.01 level, * Correlation is significant at the 0.05 level).*

Component 3 (13% of the data variability) indicated a relationship between Car/Cab ratio and soluble phenolic contents (both L1 position). In addition to the accessory light-harvesting function, carotenoids protect photosynthetic membranes and chlorophyll from reactive oxygen species (Pallardy 2008), and thus the Car/Cab ratio may increase under oxidative stress caused by excessive light (Tauzs et al. 2007) or heavy metal stress (Martinez-Penalver et al. 2012). Similarly phenolic compounds play a protective role due to their antioxidant properties (Bialonska et al. 2007). The synergic effect in scavenging reactive oxygen species may explain the positive loading of both the Car/Cab ratio and soluble phenolics in component 3.

Component 4 (11% of the data variability) as well as color coded matrix (Fig. 6.4) identified the relationship between lignin and soluble phenolic compounds for the L3 position. Lignin and soluble

phenolic compounds are both important protective secondary metabolites (Moura et al. 2010), although soluble phenolics are more connected with non-specific stress reactions and defense (being synthetized much faster after stressor effects), while lignin tends rather to play a structural role (less mobile).

The last component (8% of the data variability) identified the relationship between the water and lignin contents in both positions (L1, L3), as both the water and lignin contents decrease with needle age if related to the total needle dry mass. Further testing is necessary also in this case, as the water content data didn't follow a normal distribution.

6.3.4 Chemical and biochemical properties of Norway spruce

Although the Sokolov region is considered to be one of the most heavily contaminated in the country in terms of the wide range of metals, the studied trees did not exhibit either visible damage caused by metal contamination or high accumulation of trace elements in the needles (Appendix: Tabs. 3 and 5). The medians of Ca, Cu, K and Hg in the first-year spruce needles corresponded well with the values presented by Suchara et al. (2011), while the medians of Mg and Zn were higher. Assessing the contents of selected mineral elements (Mg, Ca and K), the first-year Norway spruce needles exhibited moderate values with no signs of deficiency (Fabiánek 2004). In relation to potentially toxic elements, the As content in almost half of the needle samples was below the detection limit. It seems that Norway spruce tend rather to accumulate As in the roots, as shown by Brun et al. (2010), while As was almost undetectable in the wood, green needles and litter. The critical loads of Al in plant tissues have not been generally established, however the content of Al in needles in our study (87mg/kg) was higher than that described by Suchara et al. (2011) and comparable with other studies on Norway spruce conducted in polluted areas, e.g. 30-120 mg/kg Al (Jonard et al. 2012) and 30-200 mg/kg (Bussinow et al. 2008).

The correlation matrix (Fig. 6.5) shows that there are statistically significant positive correlations between Zn-Cu, which are both essential for many enzymatic functions and similarly both are required in very small quantities. The next positive association was found between Ca-Mg-Al and Zn-Ca-Mg. A significant negative linear relationship was found between K-Zn and K-Ca. The chlorophyll content exhibits a positive correlation with Cu and Zn, which suggest that Cu and Zn do not play the role of contaminants here but are a suitable source of micronutrients. Further statements are based on analyzing the results of both correlation matrix (Fig. 6.5) and factor analysis (Appendix: Tabs. 12 and 13).

The second component (13% of the data variability) identified the relationship between the K content and phenolic compounds in the wet matter (both negative loadings) and between Zn-Al (positive loadings). The third component (13% of the data variability) depicted the relationship among the contents of As, phenolic compounds (dry and wet matter) and Car/Cab ratios. Component 4 (10% of the data variability) indicated the relationship between Cu-Zn and confirmed the relationship among the Al concentrations and the contents of phenolic compounds and the Car/Cab ratios. Thus, components 3 and 4 identified the most sensitive biochemical parameters –phenolic compounds and Car/Cab ratios – both were positively correlating with As and Al, the elements considered to be toxic for coniferous forests (Zhao et al. 2010; Collignon et al. 2012). Component 5 (8% of the data variability) can be explained mainly by the data variability of Hg (high positive loadings) and lignin (high negative loadings).

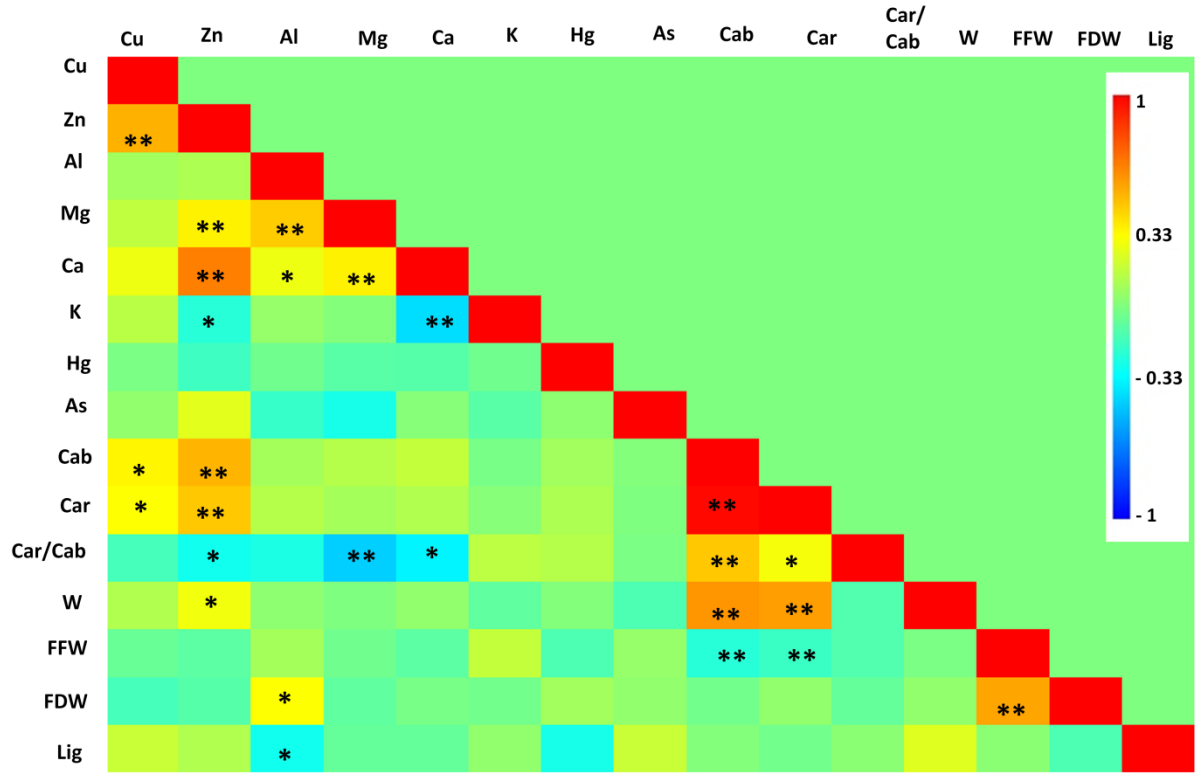

Figure 6.5: *Pearson correlation color-coded matrix (the values were log_e transformed): chemical and biochemical properties of the Norway at the positions of L1 and L3, the coefficients were assigned colors according to their values (color scale from dark blue (correlation= -1) to dark red (correlation= 1 (** Correlation is significant at the 0.01 level, * Correlation is significant at the 0.05 level).*

6.4 Conclusions

The studied spruce sites can be generally characterized by low-pH soils depleted of exchangeable cations with moderate concentrations of Zn and Cu and rather high contents of Hg and As. In spite of the low Ca/Al ratios, moderate contents of selected nutrients (Mg, Ca and K) in the first-year needles are high enough and the chlorophyll needle content proves that their availability in such acidified soils is still sufficient for Norway spruce, pointing out that the Ca/Al ratio alone might be a weak predictor of the foliage nutrient status. High concentrations of Al in the first-year needles are in accordance with acid soil conditions that facilitate Al uptake by the roots.

Using factor analysis, the authors were able to determine diverse nutrient/heavy metal associations that characterize the four studied horizons; among them, the Al-As-Hg-Cu association of mainly toxic elements was identified in both organic horizons (Ol+Of and Oa). For two mineral horizons (A0-10 and A10-20), similar associations depending on the soil pH, Zn-As and Zn-As-Cu were identified. Considering the potentially toxic elements, the authors found correlations between soil and tree concentrations for Al (needle Al content correlated with the Al concentrations in all four horizons), As (needle As content correlated with the As concentrations in the mineral horizons (A0-10 and A10-20) and Cu in the organic horizons (Ol+Of and Oa).

For Al and As, the elements detected as mobile in the studied soils, a correlation between concentrations in the Norway spruce tissues and the two biochemical parameters –soluble phenolic compounds and Car/Cab ratios was found. This finding shows that the production of phenolic compounds in the biomass could be stimulated and subsequently affect litter decomposition and overall soil carbon balance in regions with current or historic acidification and consequent mobilization of toxic elements (Al and As). Soluble phenolic compounds and the Car/Cab ratio appeared to be the most sensitive biochemical parameters of all those assessed and the authors suggest that they can serve as suitable non-specific stress markers.

In addition to the statements formulated above, the study contributes to better understanding of the relationships between soil and foliar chemistries, particularly in coniferous forests affected by anthropogenic pollution.

Acknowledgements

This research is being undertaken as part of a HYPSO scientific research project within the framework of grant No. 205/09/1989 funded by the Czech Science Foundation. Many thanks are due to Dr. Petr Rojík (Sokolovská uhelná a.s.) for his substantial assistance with the field campaign, to all the students who participated in sample collection and to Mgr. Drahomíra Bartáková who helped with biochemical assessments of phenolic compounds and lignin.

References

Adriano D (2001) Trace Elements in Terrestrial Environments — Biogeochemistry Bioavailability and Risks of Metals. Springer Verlag, New York

Albrechtova J, Seidl Z, Aitkenhead-Peterson J, Lhotáková Z, Rock BN, Alexander JE et al (2008) Spectral analysis of coniferous foliage and possible links to soil chemistry: Are spectral chlorophyll indices related to forest floor dissolved organic C and N? [Article; Proceedings Paper]. Science of the Total Environment 404(2-3): 424-432. doi: 10.1016/j.scitotenv.2007.11.006

Aspinwall MJ, King JS, Booker FL, McKeand SE (2011) Genetic effects on total phenolics condensed tannins and non-structural carbohydrates in loblolly pine (Pinus taeda L.) needles. Tree Physiology 31(8): 831-842. doi: 10.1093/treephys/tpr073

Aznar JC, Richer-Lafleche M, Begin C, Begin Y (2009) Lead Exclusion and Copper Translocation in Black Spruce Needles. Water Air and Soil Pollution 203(1-4): 139-145. doi: 10.1007/s11270-009-9997-8

Berthelsen BO, Ardal L, Steinnes E, Abrahamsen G, Stuanes AO (1994) Mobility of heavy-metals in pine forest soils as influenced by experimental acidification. Water Air and Soil Pollution 73(1-4): 29-48. doi: 10.1007/bf00477974

Bialonska D, Zobel AM, Kuras M, Tykarska T, Sawicka-Kapusta K (2007) Phenolic compounds and cell structure in bilberry leaves affected by emissions from a Zn-Pb smelter. Water Air and Soil Pollution 181(1-4): 123-133doi: 10.1007/s11270-006-9284-x

Blaser P, Zimmermann S, Luster J, Shotyk W (2000) Critical examination of trace element enrichments and depletions in soils: As Cr Cu Ni Pb and Zn in Swiss forest soils. Science of the Total Environment 249(1-3): 257-280. doi: 10.1016/s0048-9697(99)00522-7

Borůvka L, Vacek O, Jehlička J (2005) Principal component analysis as a tool to indicate the origin of potentially toxic elements in soils. Geoderma 128(3-4): 289-300. doi: 10.1016/j.geoderma.2005.04.010

Bouška V, Pešek J (1999) Quality parameters of lignite of the North Bohemian Basin in the Czech Republic in comparison with the world average lignite. International Journal of Coal Geology 40(2-3): 211-235. doi: 10.1016/s0166-5162(98)00070-6

Brun CB, Peltola P, Astrom ME, Johansson MB (2010) Spatial distribution of major trace and ultra trace elements in three Norway spruce (*Picea abies*) stands in boreal forests Forsmark Sweden. Geoderma 159(3-4): 252-261. doi: 10.1016/j.geoderma.2010.07.018

Bussinow M, Sarapatka B, Dlapa P (2008) Effect of old mining acitivities on nutrient and toxic elements concentration in the biomass of Norway spruce (Picea abies LKarst.) and European Birch (*Betula pendula L.*). International Journal of Environment and Pollution 33(2-3): 235-247. doi: 10.1504/ijep.2008.019396

Campbell PKE, Rock BN, Martin MEm Neefus CD, Irons JR, Middleton EM et al (2004) Detection of initial damage in Norway spruce canopies using hyperspectral airborne data. International Journal of Remote Sensing *25*(24): 5557-5583. doi: 10.1080/01431160410001726058

Collignon C, Boudot JP, Turpault MP (2012) Time change of aluminium toxicity in the acid bulk soil and the rhizosphere in Norway spruce (*Picea abies (L.) Karst.*) and beech (*Fagus sylvatica L.*) stands. Plant and Soil

357(1-2): 259-274. doi: 10.1007/s11104-012-1154-2

Czech V, Cseh E, Fodor F (2010) Arsenate induces water stress. Journal of Plant Nutrition 34(1): 60-70. doi: 10.1080/01904167.2011.531359

Davis J (2002) Statistics and Data Analysis in Geology (third ed.) John Wiley Sons Inc., New York

de Wit HA, Eldhuset TD, Mulder J (2010) Dissolved Al reduces Mg uptake in Norway spruce forest: Results from a long-term field manipulation experiment in Norway. Forest Ecology and Management 259(10): 2072-2082. doi: 10.1016/j.foreco.2010.02.018

Demmig-Adams B, Adams WW (1996) The role of xanthophyll cycle carotenoids in the protection of photosynthesis. Trends in Plant Science 1(1) 21-26

Driscoll CT, Lawrence GB, Bulger AJ, Butler TJ, Cronan CS, Eagar C, Lambert KF, Likens GE, Stoddard JL, Weathers KC (2001) Acidic deposition in the northeastern United States: Sources and inputs ecosystem effects and management strategies. Bioscience 51(3): 180-198. doi: 10.1641/0006-3568(2001)051

Egli M, Sartori G, Mirabella A, Giaccai D, Favilli F, Scherrer D et al (2010) The influence of weathering and organic matter on heavy metals lability in silicatic Alpine soils. Science of the Total Environment 408(4): 931-946. doi: 10.1016/j.scitotenv.2009.10.005

Fabiánek P (2004) Forest Condition and Monitoring in the Czech Republic 1984–2003, Ministry Of Agriculture of the Czech Republic and Forestry and Game Management Research Institute, ELAN spol. s.r.o., Přerov, Czech Republic

Fitzpatrick ML, Long DT, Pijanowski BC (2007) Exploring the effects of urban and agricultural land use on surface water chemistry across a regional watershed using multivariate statistics. Applied Geochemistry 22(8): 1825-1840. doi: 10.1016/j.apgeochem.2007.03.047

Harraz HZ, Hamdy MM, El-Mamoney MH (2012) Multi-element association analysis of stream sediment geochemistry data for predicting gold deposits in Barramiya gold mine Eastern Desert Egypt. Journal of African Earth Sciences 68*:* 1-14. doi: 10.1016/j.jafrearsci.2012.03.009

Hartmann K, Wunnemann B (2009) Hydrological changes and Holocene climate variations in NW China inferred from lake sediments of Juyanze palaeolake by factor analyses. Quaternary International 194*:* 28-44. doi: 10.1016/j.quaint.2007.06.037

Homolová L, Lukeš P, Malenovský Z, Lhotáková Z, Kaplan V, Hanuš J (2013) Measurement methods and variability assessment of the Norway spruce total leaf area: implications for remote sensing. Trees-Structure and Function 27(1): 111-121. doi: 10.1007/s00468-012-0774-8

Hruška J, Krám P (1994) Aluminum chemistry of the root-zone of forest soil affected by acid deposition at the lysina catchment czech-republic. Ecological Engineering 3(1): 5-16. doi: 10.1016/0925-8574(94)90007-8

Hu S, Luo T, Jing C (in print) Principal component analysis of fluoride geochemistry of groundwater in Shanxi and Inner Mongolia China. Journal of Geochemical Exploration(0) doi: http://dx.doi.org/10.1016/j.gexplo.2012.08.013

Huang Y, Tao S (2004) Influences of excessive Cu on photosynthesis and growth in ectomycorrhizal Pinus sylvestris seedlings. Journal of Environmental Sciences-China 16(3): 414-419

Ijmker J, Stauch G, Hartmann K, Diekmann B, Dietze E, Opitz S et al (2012) Environmental conditions in the Donggi Cona lake catchment NE Tibetan Plateau based on factor analysis of geochemical data. Journal of Asian Earth Sciences 44*:* 176-188. doi: 10.1016/j.jseaes.2011.04.021

Ivanov YV, Savochkin YV, Kuznetsov VV (2011) Scots pine as a model plant for studying the mechanisms of conifers adaptation to heavy metal action: Effects of continuous zinc presence on morphometric and physiological characteristics of developing pine seedlings. Russian Journal of Plant Physiology 58(5): 871-878. doi: 10.1134/s1021443711050104

Javot H, Maurel C (2002) The role of aquaporins in root water uptake [Review]. Annals of Botany 90(3): 301-313. doi: 10.1093/aob/mcf199

Jonard M, Legout A, Nicolas M, Dambrine E, Nys C, Ulrich E et al (2012) Deterioration of Norway spruce vitality despite a sharp decline in acid deposition: a long-term integrated perspective. Global Change Biology 18(2): 711-725. doi: 10.1111/j.1365-2486.2011.02550.x

Juice SM, Fahey TJ, Siccama TG, Driscoll CT, Denny EG, Eagar C, Cleavitt NL, Minocha R, Richardson AD (2006) Response of sugar maple to calcium addition to northern hardwood forest. Ecology 87(5): 1267-1280

Kabata-Pendias A (2004) Soil-plant transfer of trace elements - an environmental issue. Geoderma 122(2-4) 143-149. doi: 10.1016/j.geoderma.2004.01.004

Klepzig KD, Smalley EB, Raffa KF (1996) Interactions of ecologically similar saprogenic fungi with healthy and abiotically stressed conifers. Forest Ecology and Management 86(1-3): 163-169. doi: 10.1016/s0378-1127(96)03777-2

Kolka RK, Nater EA, Grigal DF, Verry ES (1999) Atmospheric inputs of mercury and organic carbon into a forested upland bog watershed. Water Air and Soil Pollution 113(1-4): 273-294. doi: 10.1023/a:1005020326683

Kopačková V, Chevrel S, Bourguignon A (2011) Spectroscopy as a tool for geochemical modeling. Proc. SPIE 8181, 818106. doi: 10.1117/12.898404

Kopačková V, Chevrel S, Bourguignon A. Rojík P (2012) Application of high altitude and ground-based spectroradiometry to mapping hazardous low-pH material derived from the Sokolov open-pit mine. Journal of Maps 8(3): 220-230. doi: 10.1080/17445647.2012.705544

Krám P, Hruška J, Driscoll CT, Johnson CE, Oulehle F (2009) Long-term changes in aluminum fractions of drainage waters in two forest catchments with contrasting lithology. Journal of inorganic biochemistry 103(11): 1465-1472. doi: 10.1016/j.jinorgbio.2009.07.025

Kupková L, Potůčková M, Buřičová M, Kopačková V, Lhotáková Z, Albrechtová J et al (2012) Determination of lignin content in norway spruce foliage using nir spectroscopy and hyperspectral data. 2012 Ieee International Geoscience and Remote Sensing Symposium (Igarss) 4190-4193

Lange BM, Lapierre C, Sandermann H (1995) Elicitor-induced spruce stress lignin - structural similarity to early developmental lignins. Plant Physiology 108(3): 1277-1287

Lavid N, Schwartz A, Yarden O, Tel-Or E (2001) The involvement of polyphenols and peroxidase activities in heavy-metal accumulation by epidermal glands of the waterlily (Nymphaeaceae). Planta 212(3): 323-331. doi: 10.1007/s004250000400

Lepedus H, Viljevac M, Cesar V, Ljubesic N (2005) Functioning of the photosynthetic apparatus under low and high light conditions in chlorotic spruce needles as evaluated by in vivo chlorophyll fluorescence. Russian Journal of Plant Physiology 52(2): 165-170. doi: 10.1007/s11183-005-0024-7

MacFarlane GR (2002) Leaf biochemical parameters in Avicennia marina (Forsk.) Vierh as potential biomarkers of heavy metal stress in estuarine ecosystems. Marine Pollution Bulletin 44(3): 244-256. doi: 10.1016/s0025-326x(01)00255-7

Maestri E, Marmiroli M, Visioli G, Marmiroli N (2010) Metal tolerance and hyperaccumulation: Costs and trade-offs between traits and environment. Environmental and Experimental Botany 68(1): 1-13. doi: 10.1016/j.envexpbot.2009.10.011

Mani D, Kumar C (2005) Study of the heavy metals mobility in different soils affecting vegetation. National Academy Science Letters 28(7-8): 251-258

Mani, D, Sharma, B, Kumar, C, Pathak, N, Balak, S (2012a) Phytoremediation potential of helianthus annuus l in sewage-irrigated indo-gangetic alluvial soils. International Journal of Phytoremediation 14(3): 235-246. doi: 10.1080/15226514.2010.498844

Mani D, Sharma B, Kumar C, Balak S (2012b) Depth-wise distribution mobility and naturally occurring glutathione based phytoaccumulation of cadmium and zinc in sewage-irrigated soil profiles. International Journal of Environmental Science and Technology 1-14. doi: 10.1007/s13762-012-0121-z

Martinez-Penalver A, Grana E, Reigosa MJ, Sanchez-Moreiras AM (2012) The early response of Arabidopsis thaliana to cadmium- and copper-induced stress. Environmental and Experimental Botany 78*:* 1-9. doi: 10.1016/j.envexpbot.2011.12.017

Matzner E, Prenzel J (1992) acid deposition in the german soiling area - effects on soil solution chemistry and al mobilization. Water Air and Soil Pollution 61(3-4): 221-234. doi: 10.1007/bf00482606

Merilo E, Tulva I, Räim O, Kükit A, Sellin A, Kull O. (2009) Changes in needle nitrogen partitioning and photosynthesis during 80 years of tree ontogeny in in Picea abies. Trees - Structure and Function 23(5): 951-958

Mišurec J, Kopačková V, Lhotáková Z, Hanuš J, Weyermann J, Entcheva-Campbell P et al (2012) Utilization of hyperspectral image optical indices to assess the Norway spruce forest health status. Journal of Applied Remote Sensing 6: 063545. doi: 10.1117/1.jrs.6.063545

Moldán B, Schnoor JL (1992) Czechoslovakia - examining a critically ill environment. Environmental Science Technology 26(1): 14-21. doi: 10.1021/es00025a001

Moura JCMS, Bonine CAV, Viana JDF, Dornelas MC, Mazzafera P (2010) Abiotic and Biotic Stresses and Changes in the Lignin Content and Composition in Plants. Journal of Integrative Plant Biology 52(4): 360-376

Northup RR, Dahlgren RA, McColl JG (1998) Polyphenols as regulators of plant-litter-soil interactions in northern California's pygmy forest: A positive feedback?. Biogeochemistry 42(1-2): 189-220. doi: 10.1023/a:1005991908504

Nwoko CO (2010) Trends in phytoremediation of toxic elemental and organic pollutants. African Journal of Biotechnology 9(37): 6010-6016

Obrist D, Johnson DW, Edmonds RL (2012) Effects of vegetation type on mercury concentrations and pools in two adjacent coniferous and deciduous forests. Journal of Plant Nutrition and Soil Science 175(1): 68-77. doi: 10.1002/jpln.201000415

Ollerová H, Marusková A, Kontrisová O, Pliestiková L (2010) Mercury Accumulation in Picea abies (L.) KarstNeedles with Regard to Needle Age. Polish Journal of Environmental Studies 19(6): 1401-1404

Pallardy S (2008) Physiology of Woody Plants. Elsevier, London

Porra RJ, Thompson WA, Kriedemann PE (1989) Determination of accurate extinction coefficients and simultaneous-equations for assaying chlorophyll-a and chlorophyll-b extracted with 4 different solvents - verification of the concentration of chlorophyll standards by atomic-absorption spectroscopy. Biochimica Et Biophysica Acta 975(3): 384-394. doi: 10.1016/s0005-2728(89)80347-0

Rojík P (2004) New stratigraphic subdivision of the Tertiary in the Sokolov Basin in Northwestern Bohemia. Journal of the Czech Geological Society 49(3-4): 173-185

Salt DE, Smith RD, Raskin I (1998) Phytoremediation. Annual Review of Plant Physiology and Plant Molecular Biology 49*:* 643-668

Schroder WH, Bauch J, Endeward R (1988) Microbeam analysis of Ca exchange and uptake in the fine roots of spruce: influence of pH and aluminum. Trees-Structure and Function 2(2): 96-103

Shapiro SS, Wilk MB (1965) An analysis of variance test for normality (complete samples) Biometrika 52(3–4): 591–611

Siefermannharms D (1994) Light and Temperature Control of Season-Dependent Changes in the Alpha-Carotene and Beta-Carotene Content of Spruce Needles. Journal of Plant Physiology 143(4-5): 488-494

Simon L, Hally J (1984) Rychlé stanovení arsenu v hnědém uhlí SHR — Quick determination of arsenic in coal of the North-bohemian brown coal distrikt. Acta Montana 68*:* 253-263

Singleton VL (1965) Colorimetry of total phenolics and phosphomolybdicphosphotungistic acid reagents In Rossi VA (Ed.): American Journal of Enolology and Viticulture 16: 144-158

Soukupová J, Cvikrová M, Albrechtová J, Rock BN, Eder J (2000) Histochemical and biochemical approaches to the study of phenolic compounds and peroxidases in needles of Norway spruce (Picea abies*). New Phytologist 146*(3): 403-414. doi: 10.1046/j.1469-8137.2000.00666

Suchara I, Sucharová J, Holá M,Reimann C, Boyd R, Filzmoser P et al (2011) The performance of moss grass and 1- and 2-year old spruce needles as bioindicators of contamination: A comparative study at the scale of the Czech Republic. Science of the Total Environment 409(11): 2281-2297. doi: 10.1016/j.scitotenv.2011.02.003

Tausz M, Landmesser H, Posch S, Monschein S, Grill D, Wienhaus O (2007) Multivariate patterns of antioxidative and photoprotective defence compounds in spruce needles at two central European forest sites of different elevation. Environmental Monitoring and Assessment 128(1-3): 75-82. doi: 10.1007/s10661-006-9416-1

Tripathi VS (1979) Factor-analysis in geochemical-exploration. Journal of Geochemical Exploration 11(3): 263-275. doi: 10.1016/0375-6742(79)90004-9

Tuzhilkina VV (2009) Response of the pigment system of conifers to long-term industrial air pollution. Russian Journal of Ecology 40(4): 227-232. doi: 10.1134/s1067413609040018

Tzvetkova N, Hadjiivanova C (2006) Chemical composition and biochemical changes in needles of Scots pine (*Pinus sylvestris L.*) stands at different stages of decline in Bulgaria. Trees-Structure and Function 20(4): 405-409. doi: 10.1007/s00468-006-0052-8

Ushio M, Miki T, Kitayama K (2009) Phenolic Control of Plant Nitrogen Acquisition through the Inhibition of Soil Microbial Decomposition Processes: A Plant-Microbe Competition Model. Microbes and Environments 24(2): 180-187. doi: 10.1264/jsme2.ME09107

Webster R (2001) Statistics to support soil research and their presentation. European Journal of Soil Science 52(2): 331-340. doi: 10.1046/j.1365-2389.2001.00383.x

Wellburn AR (1994) The spectral determination of chlorophyll-a and chlorophhyll-b as well as total carotenoids using various solvents with spectrophotometers of different resolution. Journal of Plant Physiology 144(3): 307-313

Yu ZS, Kraus TEC, Dahlgren RA, Horwath WR, Zasoski RJ (2003) Mineral and dissolved organic nitrogen dynamics along a soil acidity-fertility gradient. Soil Science Society of America Journal 67(3): 878-888

Yudovich YE, Ketris MP (2005) Arsenic in coal: a review. International Journal of Coal Geology 61(3-4): 141-196. doi: 10.1016/j.coal.2004.09.003

Zhao FJ, McGrath SP, Meharg AA (2010) Arsenic as a Food Chain Contaminant: Mechanisms of Plant Uptake and Metabolism and Mitigation Strategies. Annual Review of Plant Biology 61: 535-559

Zirlewagen D, Raben G, Weise M (2007) Zoning of forest health conditions based on a set of soil topographic and vegetation parameters. Forest Ecology and Management 248(1-2): 43-55. doi: 10.1016/j.foreco.2007.02.038

7. Synthesis

7.1 Research findings

The main purpose of this thesis was to use Image Spectroscopy as a tool to monitor the environmental conditions in a region affected by anthropogenic activities via estimating both geochemical and biochemical parameters on a regional scale. The thesis was divided into two thematic parts. First part was devoted to applications of Image Spectroscopy into Acid Mine Drainage mapping and its related issues while in the second part Image Spectroscopy was applied into monitoring of vegetation stress.

Major research findings relevant to the specific research objectives defined in section 1.3 are described below:

To formulate mineral spectroscopy-based techniques allowing identification of acidity sources and surface pH estimation for exposed surfaces in extremely heterogeneous environments characteristic for mining sites.

- In chapter 2, high-altitude spectroradiometry (ASTER - Advanced Spaceborne Thermal Emission and Reflection Radiometer satellite data) together with ground-based spectroradiometry were employed in order to identify the locations of the most significant sources of Acid Mine Drainage (AMD) discharge at the Sokolov lignite open-pit mines. The equivalent mineral end-members were successfully derived from the ASTER image data (Advanced Spaceborne Thermal Emission and Reflection Radiometer satellite data) and a sub-pixel method (Linear Spectral Unmixing, LSU) was employed to relatively estimate the selected end-member abundances and to identify low-pH zones. The sub-pixel method (LSU) was selected due to the the extreme heterogeneity of the Sokolov surfaces and diverse material mixing level present in the ASTER pixels (VNIR: 15 m, SWIR: 30 m). The LSU analysis was a sufficient first order approximation to constrain the mineralogy as the absolute abundances of the indicative minerals were not required. The map with the low pH zones delineated achieved sufficient overall accuracy (75%).
- In the following study (chapter 3) pH was estimated on the basis of mineral and image spectroscopy. First, a geochemical conceptual model of the site was defined. Diagnostic minerals of very low pH (<3.0) as well as increased pH (3.0-6.5) and nearly neutral or higher pH (>6.5) were identified. In heterogeneous environment characterizing mining sites, the pixel reflectance (in this case HyMap pixel size was 5x5 m) has a significant mixing problem. Therefore, it was necessary to identify such absorption feature parameters which are

common for individual minerals as well as mineral mixtures and select a mapping technique/method which is robust enough to identify the targeting minerals even if present as part of mixtures. The Multi Range Spectral Feature Fitting (MRSFF) technique was found to be sensitive enough to assess differences in the desired spectral parameters (e.g., absorption maximum wavelength position, absorption depth) and to be scalable in the way that field spectra end-members were successfully used for the HS image mapping. Furthermore, the multiple regression model using the fit images, the results of MRSFF, as inputs was constructed to estimate the surface pH and statistical significant accuracy was attained (R^2=0.61, Rv^2=0.76). This study represents one of the very first approaches employing image spectroscopy for quantitative pH modeling in a mining environment and the achieved results demonstrate the potential application of hyperspectral remote sensing as an efficient method for environmental monitoring.

To formulate a HS remote sensing technique allowing early detection of vegetation stress on a regional scale.

- A new statistical method was developed to assess the physiological status of macroscopically undamaged foliage of Norway spruce (*chapter 4*). As the chlorophyll content alone may not correspond sufficiently well to the physiological/health status, the suggested method utilized three indicators (Cab, REP, expSIPI). Two products were created using HyMap 2009 multi-flight line data: the map of chlorophyll content (Cab) and a raster combining the information from REP (sensitive to vegetation stress) and expSIPI (sensitivity to the ratio of bulk carotenoids to chlorophyll). For both products a relative classification (normalized z-scores) was used based on the histogram dynamic ranges, averages and standard deviations. Consequently, no hard threshold values were required. The only condition to be fulfilled was a normal distribution of the classified data. In both maps, Class 1 indicates worse health status for the trees without visible damage symptoms and Class 5 corresponds to the values indicating the healthiest trees. As this method takes in account the two major biochemical parameters that are closely connected with photosynthetic functions, it allows assessing of the vegetation stress in a more objective way. However it is necessary to emphasize that this method is suitable for one-species (monoculture) forests. Norway spruce was selected as it represents the predominant forest species in the studied region; in addition, spruce needles were confirmed to be well-suited for detection of contamination.

To validate one of the latter techniques using an additional temporal HS image dataset.

- In the following study (*chapter 5*) the same method described above was employed and validated while using additional temporal HS image data set (HyMap 2010 data) in order to (i) validate the new method (*chapter 4*), (ii) study the forest Norway Spruce variations in biochemical parameters while comparing the foliar pigment content from the samples collected in two subsequent growing seasons, (iii) assess vegetation stress within the selected Norway spruce sites while putting together information on forest stand geochemical conditions, foliar biochemistry (pigment contents) and the temporal differences detected by classifying the two HS image datasets acquired one year apart. To summarize the results, both biochemical analysis of the sampled tree needles and hyperspectral image data have been shown to reflect the soil chemistry. Higher Car/Cab ratios in spruce needles and lower health status derived from HyMaps were related to the lowest Bc/Al ratio in mineral soil. The strong linkage between soil chemistry and parent bedrock indicated that bedrock geochemical reactivity should be considered to be important factor in the assessment of forest health status.
- The method proved suitable as the HyMap classification results were in accordance with the statistical assessment of the biochemical properties of the sampled trees as well as with the geochemical properties of the forest sites. Apparently, in both years, differences detected by biochemical and hyperspectral methods remained consistent among spruce stands and only mild changes in the physiological condition of the stands under study were detected by both approaches. This finding supports the validity of the previously presented model.

To assess the applicability of using diverse needle biochemical parameters as biological indicators of adverse soil condition parameters and select the most sensitive ones with the greatest potential for future HS Remote Sensing monitoring.

- *In chapter 6* the relationship between soil and spruce needle contents of macronutrients and potentially toxic elements was studied and tested whether the soil parameters and their vertical distribution within a soil profile (two organic and two mineral horizons) affect foliage biochemical parameters (contents of photosynthetic pigments, phenolic compounds and lignin). Factor analysis identified Al and As as toxic elements with high bio-availability for spruce trees, whereas acid soil conditions facilitate the heavy metal uptake by the roots. For these toxic elements detected as mobile in the studied soils, a correlation between concentrations in the Norway spruce tissues and the two biochemical parameters – soluble

phenolic compounds and Car/Cab ratios was found. This finding suggests that these latter two biochemical parameters, which both proved to be sensitive to the soil geochemical conditions, can serve as suitable non-specific stress markers. The results demonstrated in *chapters 4 and 5* also point out that Car/Cab is more suitable indicator of forest health than using just absolute contents of both photosynthetic pigments.

7.2 Conclusions and future remarks

The presented studies demonstrate the potential application of hyperspectral remote sensing as an efficient method for environmental monitoring. The presented research resulted in the following overall conclusions:

- Good performance of hyperspectral image analysis depends on accurate atmospheric correction, which has a strong influence on the spectral diagnoses. If multi-flight line and multi-date hyperspectral data are used, additional corrections for the BRDF effect may need to be implemented; esecialy if sensors with wide field of view are utilized. To minimize the BRDF effect flight lines should follow the N-S directions. Although this thesis doesn't address this issue, the HS image data were corrected for the atmospheric and BRDF effects.
- The mining environment is characteristic for its high heterogeneity and complexity. Therefore, Acid Mine Drainage (AMD) mapping should be tailored to the specifics of the tested mining site and a simplified concept needs to be set out first. A conceptual model depicting the minerals that reflect the specific site conditions and indicate a certain pH needs to be defined prior spectral mapping.
- Even high-spatial-resolution (5-m pixel) images have contributions from multiple sub-pixel-scale components. Based on these findings, the most efficient and valid methods are those taking in account the spectral mixture models or methods which are scalable as a pixel is represented by an area on the ground whereas a sample is a point on the ground.
- The shift to longer wavelengths of the absorption maximum centered between 0.90-1.00 µm was found to be the main parameter that allows differentiation among the Fe^{3+} secondary minerals even if they are present as mixtures. Alternatively, other techniques which allow absorption feature wavelength estimation (e.g., derivative analysis, quadratic method) should be tested and results compared.
- The Multi Range Spectral Feature Fitting (MRSFF) technique was employed for mineral mapping and was found to be sensitive enough to assess differences in the desired spectral parameters (e.g., absorption maximum wavelength position, absorption depth). Additionally,

this technique was found to be scalable as the field spectra of fundamental mineral end-members were successfully utilized for mineral mapping within the HS image data.

- Physiological status of macroscopically undamaged foliage can be assessed by the means of image spectroscopy and stress can be detected prior the symptoms are visually expressed. The suggested method to classify health status of the Norway spruce forests proved suitable as the HyMap classification results were in accordance with the statistical assessment of the biochemical properties of the sampled trees as well as with the geochemical properties of the forest sites. If Multi-date HS data are utilized, this method has further potential for monitoring of forest ecosystems.
- Too few studies have been devoted to estimation of phenolics for forest canopy but the published results show that these compounds are detectable by means of optical remote sensing as they were successfully predicted using PLSR. Therefore further research should be done in this field to investigate how phenolics could be estimated and further used for detecting forest stress using imaging spectroscopy.

8. Appendix

8.1 Mathematical expression for the spectral mapping techniques used in this thesis

The linear spectral mixture modeling (e.g., Linear Spectral Unmixing, *chapter 2*) framework can be mathematically expressed:

$$R_i(\lambda) = \sum_{j=1}^{n} F_j R_f(\lambda)_i + \varepsilon_i \quad \text{(Eq. 1)}$$

$$0 \leq \sum_{j=1}^{0} F_j \leq 1 \quad \text{(Eq. 2)}$$

Where R_i is the composite reflectance of the mixed spectrum in band *i*, F_j the fraction of end-member (*j*) in the mixture, R_f is the reflectance of that end-member in band *i*, *n* the number of end-members, ε the error in the sensor band *i* and λ is the wavelength. Eq. (2) constraints the fractions allowed to be between 0 and 1. Implicit in the above equations is the assumption that each cover type contributes linearly to pixel reflectance, and thus non-linear interactions between end-members are negligible.

The spectral feature fitting (*chapter 3*) expresses the relationship between image spectra and end-member spectra for each band by the linear function y = ax + b, in the form of a vector. In a sense of least squares problem the mathematical description is described below (Eq. 3):

$$x_{ij} = \left(x_{ij}(1), x_{ij}(2), \ldots, x_{ij}(n)\right)$$

$$x_{ij}(n) = \begin{bmatrix} x_{11}(n) & x_{12}(n) & \ldots & x_{1j}(n) \\ x_{21}(n) & x_{22}(n) & \ldots & x_{2j}(n) \\ \vdots & \vdots & \ddots & \vdots \\ x_{i1}(n) & x_{i2}(n) & \ldots & x_{ij}(n) \end{bmatrix}$$

$$y_1 = ax(1) + b$$
$$y_2 = ax(2) + b \quad \text{(Eq. 3)}$$
$$\vdots$$
$$y_n = ax(n) + b$$
$$E^2 = (y_1 - \hat{y}_1)^2 + (y_2 - \hat{y}_2)^2 + \ldots + (y_n - \hat{y}_n)^2$$

Where x_{ij} represents a hyperspectral dataset, $x_{ij}(n)$ is a single band in an image, y is estimated pixel value based on the regression function, $\hat{y}$ is the reference spectra or actual observation value, n is

the band number of the image, and i and j correspond to a band's row and column, respectively. Parameters a and b are the fitting coefficients of a single band, respectively.

8.2 Descriptive statistics for the chapter 6

***Table 1**: Descriptive statistics of soil properties calculated for each horizon (numbers 1-4 refer to the relevant soil horizon: 1- the topmost, 4- the deepest).*

	N	Minimum	Maximum	Mean	Std. Deviation	p (Sh-W)	Kurtosis $\log_e$	Skewness $\log_e$	Units
Al_1	19	73,00	703,00	249,84	165,68	0,01	-0,62	0,15	
Al_2	19	240,00	1112,00	**744,11**	246,95	0,05	1,56	-1,17	mg/kg
Al_3	19	308,00	635,00	436,68	94,92	0,05	-1,05	0,06	
Al_4	19	123,00	408,00	288,21	92,65	0,05	-0,33	-0,87	
Ca_1	19	660,00	2890,00	**1307,37**	672,70	-	-1,32	0,49	
Ca_2	19	60,00	1020,00	379,47	306,40	0,01	-1,54	0,00	mg/kg
Ca_3	19	10,00	270,00	54,74	77,92	-	-0,43	0,87	
Ca_4	19	1,00	140,00	32,32	43,37	-	-0,48	-0,44	
Mg_1	19	66,00	223,00	**149,95**	36,51	0,01	2,95	-1,30	
Mg_2	19	29,00	130,00	61,47	25,13	0,01	0,28	0,42	mg/kg
Mg_3	19	4,00	30,00	10,53	5,82	-	0,81	0,55	
Mg_4	19	1,00	19,00	5,58	4,06	-	0,84	-0,14	
K_1	19	123,00	619,00	**364,84**	136,10	0,05	0,00	-0,81	
K_2	19	61,00	276,00	146,63	59,78	0,05	-0,70	-0,35	mg/kg
K_3	19	12,00	45,00	21,58	7,82	-	0,77	0,72	
K_4	19	8,00	23,00	15,37	4,18	0,05	0,05	-0,45	
Cu_1	19	16,00	168,00	50,05	40,15	-	0,34	0,97	
Cu_2	19	29,00	203,00	**78,89**	61,82	-	-1,41	0,69	mg/kg
Cu_3	19	18,00	53,00	16,18	14,78	-	3,03	1,54	
Cu_4	19	20,00	36,00	15,79	12,88	-	0,81	0,77	
Zn_1	19	49,00	271,00	102,74	68,70	-	0,42	1,34	
Zn_2	19	43,00	265,00	89,32	69,08	-	0,19	1,25	mg/kg
Zn_3	19	20,00	455,00	117,16	143,66	-	-1,03	0,70	
Zn_4	19	19,00	758,00	**144,58**	195,75	-	-0,70	0,69	
Hg_1	19	0,00	2,20	0,95	0,71	0,05	-1,35	0,37	
Hg_2	19	0,00	**3,00**	**1,68**	0,83	0,05	-0,71	-0,43	mg/kg
Hg_3	19	0,00	1,50	1,03	0,26	-	-0,85	0,65	
Hg_4	19	0,00	1,30	0,97	0,51	-	-0,38	0,66	
As_1	19	8,00	97,00	37,84	25,38	0,05	-0,83	-0,14	
As_2	19	32,00	90,00	**55,16**	21,43	-	-1,54	0,28	mg/kg
As_3	19	13,00	50,00	25,53	9,90	0,05	-0,46	0,29	
As_4	19	7,00	38,00	17,53	8,87	0,01	-0,33	0,17	
pH_1	19	2,36	3,43	3,00	0,32	0,05	-	-	
pH_2	19	2,49	3,53	2,96	0,37	0,01	-	-	-
pH_3	19	2,75	3,66	3,25	0,23	0,05	-	-	
pH_4	19	3,33	4,09	**3,65**	0,27	0,01	-	-	
$Corg_1$	19	22,13	19,84	**31,90**	3,68	0,05	2,74	-1,46	%
$Corg_2$	19	36,38	28,77	24,04	2,70	0,05	-0,99	-0,04	%
C_1/N_1	19	24,87	34,99	28,09	2,09	-	-0,97	-0,10	
C_1/N_2	19	21,83	34,42	**28,54**	3,69	0,05	-0,78	-0,30	-
TEA_1	19	37,80	102,10	64,25	19,84	0,05	1,33	0,03	
TEA_2	19	53,80	175,50	**108,81**	26,61	0,05	1,66	-0,78	mmol/kg
TEA_3	19	43,60	90,80	59,98	12,80	0,05	-0,73	0,42	
TEA_4	19	23,20	52,50	40,65	9,26	0,05	0,05	-0,37	

***Table 2**: Descriptive statistics of Ca/Al ratio calculated for each horizon (numbers 1-4 refer to the relevant soil horizon: 1- the topmost, 4- the deepest).*

	N	Minimum	Maximum	Mean
Ca_1/Al_1	19	0,79	14,02	3,64
Ca_2/Al_2	19	0,05	1,15	0,33
$Ca3/Al_3$	19	0,01	0,37	0,04
Ca_4/Al_4	19	0,03	4,64	0,04

***Table 3**: Descriptive statistics of the Norway spruce biochemical parameters (all samples together: U1-U3 and L1-L3), FW = fresh weight, DW = dry weight.*

	N	Min.	Max.	Median	Mean	Std. Deviation	Units
Water content	200	20,57	78,80	55,71	55,51	8,10	% FW
Chlorophyll a	197	0,45	4,21	1,85	1,91	0,61	$mg.g^{-1}$ DW
Chlorophyll b	197	0,14	1,48	0,62	0,65	0,22	$mg.g^{-1}$ DW
Chlorophyll a+b	197	0,59	5,69	2,46	2,56	0,83	$mg.g^{-1}$ DW
Total carotenoids	197	0,08	0,92	0,34	0,35	0,11	$mg.g^{-1}$ DW
Phenolics-FW	200	48,38	293,14	96,22	100,02	30,23	$mg.g^{-1}$ FW
Phenolics-DW	200	114,79	1082,76	351,97	365,56	115,63	$mg.g^{-1}$ DW
Lignin	157	29,73	62,56	44,43	44,87	7,40	$mg.g^{-1}$ DW

Table 4**: ANOVA: Effect of needle crown position and needle age on needle biochemical parameters. Three-way ANOVA, F-ratios and significance are shown. Significance at: 0.05 *, 0.01**, 0.001.*

Biochemical parameter	Effect	
	Crown position (U,L)	**Needle Age (1,3)**
Chlorophyll a+b (Cab, mg/g DW)	9.84 **	68.17 ***
Carotenoids (Car, mg/g DW)	6.32 *	99.83 ***
Carotenoids / Chlorophylls (Car/Cab)	9.84 **	326.80 ***
Water content	1.47 ns	18.03 ***
Phenolics (FW)	0.02 ns	221.06 ***
Phenolics (DW)	0.04 ns	90.66 ***
Lignin (mg/g DW)	2.90 ns	117.30 ***

***Table 5**: Descriptive statistics of the Norway spruce biochemical parameters. L1 and L3, FW = fresh weight, DW = dry weight.*

	N	Min.	Max.	Median	Mean	Std. Deviation	p (Sh-W)	Kurtosis log_e	Skewness log_e	Units
L1										
Water content	50	25,46	78,80	60,03	59,79	8,04	-	**15,41**	**-3,30**	% FW
Chlorophyll a+b	50	0,59	4,89	2,29	2,32	0,81	-	2,45	-0,90	mg,g^{-1} DW
Total carotenoids	50	0,08	0,67	0,30	0,37	0,10	-	3,28	-0,79	mg,g^{-1} DW
Phenolics-FW	50	48,38	103,37	78,05	79,33	13,73	0,05	-0,39	-0,29	mg,g^{-1} FW
Phenolics-DW	50	114,79	435,59	293,42	299,87	75,66	0,01	1,20	-1,01	mg,g^{-1} DW
Lignin	50	35,76	62,56	79,63	50,77	5,74	0,05	0,28	-0,23	mg,g^{-1}

										DW
Al	50	49	175	87	88,76	24,74	-	-0,12	-0,01	mg/kg
Mg	50	0,87	1,53	1,13	1,15	0,15	0,05	-0,37	0,30	mg/kg
Ca	50	1,34	7,51	3,62	3,92	1,63	0,05	-0,77	-0,31	mg/kg
K	50	2,89	8,13	6,03	5,81	1,26	0,01	1,26	0,24	mg/kg
Cu	50	2,3	3,9	3,1	3,10	0,41	0,05	-0,68	-0,06	mg/kg
Zn	50	17,2	60,3	35,45	36,35	11,12	0,05	-0,95	-0,23	mg/kg
Hg	50	0,014	0,05	0,02	0,02	0,01	-	**19,75**	**4,31**	mg/kg
As	22	0,10	0,81	0,11	0,15	0,15	0,01	2,63	1,10	mg/kg
L3										
Water content	50	20,57	60,65	54,20	52,80	6,37	-	**22,52**	**-4,41**	% FW
Chlorophyll a+b	50	1,23	4,71	3,19	2,32	0,70	0,01	2,72	-1,14	mg,g-1 DW
Total carotenoids	50	0,17	0,61	0,43	0,31	0,10	-	2,73	-1,55	mg,g-1 DW
Phenolics-FW	50	75,32	192,00	119,57	119,73	23,30	0,05	0,17	-0,01	mg,g-1 FW
Phenolics-DW	50	208,84	753,56	434,65	436,69	105,05	0,05	0,59	-0,43	mg,g-1 DW
Lignin	50	30,90	51,65	39,43	39,90	4,84	0,05	-0,36	0,15	mg,g-1 DW

***Table 6**: Explained total variance of the studied biochemical variables for L1 and L3 .*

	Initial Eigenvalues		
Component	Total	% of Variance	Cumulative %
1	4,275	30,533	30,533
2	2,548	18,200	48,733
3	1,781	12,718	61,451
4	1,479	10,563	72,014
5	1,138	8,129	**80,143**

***Table 7**: Biochemical variables (L1 and L3): rotated Component Matrix (h1= horizon 1, …, h4=horizon 4), statistically significant variables that exhibited a loading>0.4 or <-0.4 are given in bold (positive-black, negative-white).*

	Component				
	1	2	3	4	5
Cab_{L1}	**0,926**	0,273	-0,125	0,046	0,026
Car_{L1}	**0,926**	0,248	-0,029	0,040	-0,047
Car_{L1}/Cab_{L1}	-0,369	-0,238	**0,523**	-0,060	-0,372
W_{L1}	**0,693**	-0,049	0,065	0,176	**0,528**
FFW_{L1}	-0,168	-0,118	**0,860**	0,229	0,087
FDW_{L1}	0,108	-0,056	**0,920**	0,017	-0,060
Lig_{L1}	-0,057	0,188	0,107	0,237	**0,807**
Cab_{L3}	0,194	**0,953**	-0,119	-0,028	0,109
Car_{L3}	0,193	**0,916**	-0,123	0,025	0,073
Car_{L3}/Cab_{L3}	-0,102	-0,638	0,044	0,250	-0,213
W_{L3}	0,324	0,190	-0,151	-0,280	0,**733**
FFW_{L3}	0,101	-0,055	0,225	**0,859**	0,090
FDW_{L3}	0,105	-0,149	0,022	**0,884**	0,030
Lig_{L3}	-0,132	0,098	-0,331	**0,495**	**0,544**

***Table 8**: Factor analysis: Explained total variance of soil variables (h1= horizon 1, …, h4=horizon 4).*

Component	Initial Eigenvalues		
	Total	% of Variance	Cumulative %
h1: Ol+Of			
1	5,075	42,292	42,292
2	2,654	22,118	64,410
3	2,301	19,176	**83,586**
h2: Oa			
1	5,386	44,880	44,880
2	3,185	26,542	71,421
3	1,421	11,843	**83,264**
h3: A_{0-10}			
1	6,509	65,088	65,088
2	2,197	21,971	87,059
3	1,294	12,941	**100,000**
h4: A_{10-20}			
1	6,161	61,607	61,607
2	1,905	19,047	80,654
3	1,145	11,453	**92,107**

***Table 9**: Soil variables: rotated Component Matrix (h1= horizon 1, …, h4=horizon 4), statistically significant variables that exhibited a loading>0.4 or <-0.4 are given in bold (positive-black, negative-white).*

	Component			Component		
	1	2	3	1	2	3
	Ol+of			**Oa**		
Al	**0,778**	**-0,429**	-0,287	0,191	**0,925**	0,119
Mg	-0,288	0,038	**0,847**	-0,328	**-0,824**	0,186
Ca	**0,469**	**0,462**	**0,713**	**0,700**	**-0,541**	0,390
K	-0,847	0,062	0,374	**-0,870**	-0,108	-0,264
Cu	**0,925**	-0,094	-0,125	**0,823**	**0,439**	0,137
Zn	-0,197	**0,788**	-0,108	-0,172	**-0,835**	-0,399
Hg	**0,969**	-0,038	0,174	0,009	**0,517**	**0,764**
As	**0,933**	-0,008	-0,066	**0,704**	**0,512**	0,358
pH	**0,466**	**0,831**	-0,067	**.0,951**	-0,021	-0,089
Corg	0,268	**-0,634**	**0,577**	-0,058	-0,014	**-0,744**
C/N	-0,233	-0,158	**0,707**	**0,768**	0,076	-0,189
TEA	0,374	**-0,789**	-0,310	-0,161	**0,900**	0,203
	A_{0-10}			**$A1_{0-20}$**		
Al	**-0,953**	0,027	-0,301	**-0,657**	**-0,436**	**-0,591**
Mg	**0,467**	**0,627**	**0,624**	**0,612**	0,185	**0,671**
Ca	**0,677**	**0,716**	0,174	**0,579**	-0,160	**0,740**
K	**0,401**	**0,845**	0,354	-0,107	0,116	**0,966**
Cu	0,195	-0,976	-0,099	0,287	**0,888**	0,057
Zn	**0,854**	0,352	0,384	**0,599**	**0,747**	0,274
Hg	0,089	0,229	**0,969**	0,**935**	0,110	0,007
As	**0,983**	0,083	0,162	0,008	**0,935**	0,039
pH	**0,754**	**0,502**	-0,424	0,**820**	**0,503**	0,113
TEA	**-0,993**	-0,099	0,065	**-0,745**	-0,245	**-0,574**

***Table 10**: Explained total variance of the common chemical variables determined for both soil horizons and the tree needles at L1.*

	Initial Eigenvalues		
Component	Total	% of Variance	Cumulative %
1	19,533	48,833	48,833
2	15,595	38,988	87,821
3	4,872	12,179	100,000

Table 11: Common chemical variables determined for both soil horizons and the tree needles at L1: rotated Component Matrix (h1= horizon 1, …, h4=horizon 4), statistically significant variables that exhibited a loading>0.4 or <-0.4 are given in bold (positive-black, negative-white).

	Component				Component		
	1	2	3		1	2	3
Al_1	**0,925**	0,314	-0,216	Cu_1	0,653	**0,671**	-0,351
Al_2	**0,658**	-0,136	-0,741	Cu_2	0,530	**0,607**	-0,593
Al_3	**0,410**	-0,713	-0,569	Cu_3	-0,079	**0,496**	**0,865**
Al_4	**0,987**	0,036	-0,157	Cu_4	-0,456	-0,174	**0,873**
Al_n	**0,960**	0,157	-0,231	Cu_n	0,133	**0,577**	**0,806**
Mg_1	0,343	-0,583	0,736	Zn_1	-0,398	**0,521**	**0,755**
Mg_2	-0,497	-0,050	0,866	Zn_2	-0,763	0,294	**0,575**
Mg_3	-0,342	0,913	0,222	Zn_3	-0,882	0,198	**0,428**
Mg_4	0,055	0,998	0,008	Zn_4	-0,867	0,134	**0,480**
Mg_n	0,909	0,204	-0,363	Zn_n	-0,117	**0,797**	**0,593**
Ca_1	0,359	**0,927**	0,111	Hg_1	**0,735**	0,675	-0,058
Ca_2	0,110	**0,778**	0,619	Hg_2	**0,893**	-0,403	-0,203
Ca_3	0,200	**0,974**	0,105	Hg_3	-0,107	0,620	0,777
Ca_4	-0,084	**0,992**	-0,093	Hg_4	-0,976	0,142	-0,163
Ca_n	0,182	**0,983**	-0,003	Hg_n	**0,988**	0,112	-0,108
K_1	-0,713	**-0,700**	-0,043	As_1	0,723	0,658	0,209
K_2	-0,594	**-0,798**	0,099	As_2	0,886	0,374	-0,276
K_3	-0,766	0,074	0,639	As_3	**-0,410**	-0,020	0,931
K_4	-0,169	0,971	0,167	As_4	**-0,482**	-0,082	0,873
K_n	0,179	**-0,980**	-0,082	As_n	**-0,880**	0,283	0,382

***Table 12**: Explained total variance of the studied biochemical variables at L1.*

Component	Initial Eigenvalues		
	Total	% of Variance	Cumulative %
1	4,204	28,024	28,024
2	2,707	18,048	46,072
3	2,007	13,380	59,452
4	1,534	10,227	69,678
5	1,181	7,872	**77,550**

***Table13**: Biochemical variables (L1): rotated Component Matrix (h1= horizon 1, …, h4=horizon 4), statistically significant variables that exhibited a loading>0.4 or <-0.4 are given in bold (positive-black, negative-white).*

	Component				
	1	2	3	4	5
Cu	0,292	0,140	-0,108	**0,720**	0,030
Zn	0,222	**0,538**	-0,263	**0,659**	-0,156
Al	0,221	**0,555**	-0,136	**-0,657**	0,050
Mg	-0,029	0,113	**-0,817**	0,057	0,074
Ca	-0,096	0,**860**	**-0,624**	0,211	-0,036
K	0,048	**-0,909**	-0,048	0,047	0,012
Hg	0,108	0,023	0,097	0,065	**0,841**
As	-0,481	0,065	**0,644**	0,243	0,118
Cab	**0,956**	-0,078	-0,056	0,208	0,037
Car	**0,956**	-0,136	0,039	0,144	0,090
Car/Cab	-0,208	-0,321	**0,564**	**0,414**	0,307
W	**0,858**	0,228	-0,125	-0,037	-0,160
FFW	-0,108	**0,435**	**0,573**	-0,058	-0,240
FDW	0,181	0,103	**0,577**	**0,457**	0,227
Lig	0,312	0,083	0,189	0,405	**0,688**

Curriculum Vitae

Veronika Kopačková

Education

1999-2001: MSc., Master's degree in Environmental Studies, Faculty of Science, Charles University

1998-2000: MSc. program in geochemistry, Faculty of Science, Charles University

1996-1998: Bc., Bachelor's degree in geology, Faculty of Science, Charles University

Professional training courses

2005: Pecomines II training course, JRC Ispra - "Use of remote sensing for mapping and evaluating of mining waste anomalies" – training at JRC, Ispra

2008: Certificate for successful training participation Course Atmospheric Correction over Land using ATCOR. (4-day training), DLR, Germany

2008: 2nd HYPER-I-NET Summer School: Earth Science and Applications using Imaging Spectroscopy, Wageningen University, Holland.

2009: 3rd HYPER-I-NET Summer School "Hyperspectral data: from images to information" Pavia, Italy.

2010: Distance course in Hyperspectral Remote Sensing. ITC/Faculty of Geo-Information Science and Earth Observation of the University of Twente. 144 hours equivalent to 5 ECTS. Grade: Excellent.

2011: Distance course in Learning IDL for Building Expert and Earth Observation (2011). ITC/Faculty of Geo-Information Science and Earth Observation of the University of Twente. 144 hours equivalent to 5 ECTS. Certificate (95%).

2011: Summer School on Practical Methods for Modeling Soil Spectral Information (DePeMossi): Under N4EWG – Expert Working Group: Soil spectroscopy activity and leadership ISPRS WGV11/3 Information Extracted from Hyperspectral Data GFZ, Potsdam August 29-31/2011.

Employment record

2001-2003: GIS specialist, Dept. of Informatics, Czech Environmental Institute, Prague

Since 2003: Remote Sensing and GIS specialist, Informatics, Czech Geological Survey

Since 2006: Coordiantor of the Remote Sensing Unit (Czech Geological Survey)

Since 2009: External lector at the Charles University in Prague (Faculty of Science)

Research interests

Remote Sensing and GIS applications into geosciences: Image Spectroscopy, Optical and Thermal

remote sensing, Slope instability modeling, Integration of RS techniques into diverse environmental studies

Scientific Projects - Primary Investigator

2007-2009: Observation des effets d´exploitation á ciel ouvert fondé sur la spectroscopie optique et thermique, bilateral cooperation ČGS-BRGM.

2009-2012: Assessment of Mining Related Impacts Based on Utilization of ARES Airborne Hyperspectral Sensor. GAČR No. 205/09/1989, Czech Science Foundation.

2010-2012: Czech Coordiantor for the FP7 project: EO-MINERS-Earth Observation for Monitoring and Observing Environmental and Societal Impacts of Mineral Resources Exploration and Exploitation.

2011-2014: Czech Coordiantor for the FP7 project: PANGEO: Enabling access to geological information in support of GMES.

2011: DeMinTIR: Detection of Mineral Surface Parameter and Vegetation status from Airborne Thermal Infrared Imaginery (EUFAR)

2013-2014: HyperAlgo: Development of algorithms and computing techniques for data mining of spectral-based information for ecological and soil mapping, Czech Ministry of Education, Czech-Israel cooperation.

Scientific Projects - Co-investigator

2009 - 2011: Recent deglaciation of the northern part of James Ross Island, Antarctica. GAČR No. 205/09/1876

2004-2009: Geological studies of natural hazards, El Salvador (Foreign development aid of the Czech Rep.

2004-2010: Natural hazards in the central and upper catchment's areas of the Chira and Puira rivers, NW Peru (Foreign development aid of the Czech Republic.

2005-2007: Hydrogeology & balneology feasibility studies - Cajamarca and Churín, Peru (Foreign development aid of the Czech Republic, in collaboration with Aquatest.

Peer-reviewed papers coming out of this thesis

Kopačková, V., Chevrel, S., Bourguignon, A., & Rojík, P., (2012): Application of high altitude and ground-based spectroradiometry to mapping hazardous low-pH material derived from the Sokolov open-pit mine, Journal of Maps, DOI:10.1080/17445647.2012.705544.

Kopačková, V., (submitted for International Journal of Applied Earth Observation and Geoinformation): Using multiple spectral feature analysis for quantitative pH mapping in a mining environment.

Mišurec, J. and Kopačková, V., Lhotáková, Z., Hanuš, J., Weyermann, J., Entcheva-Campbell, P.,Albrechtová, J., (2012): Utilization of hyperspectral image optical indices to assess the Norway spruce forest health status, J. Appl. Remote Sens. 6(1), 063545. doi:10.1117/1.JRS.6.063545.

Kopačková, V., Mišurec, J., Lhotáková, Z., Oulehle, F., Albrechtová, J., (submitted for International Journal of Applied Earth Observation and Geoinformation): Using multi-date high spectral resolution data to assess the physiological status of macroscopically undamaged foliage on a regional scale.

Kopačková, V., Lhotáková, Z., Oulele, F., Albrechtová, J., (under review): Assessing forest health via linking the geochemical properties of a soil profile with the biochemical vegetation parameters, International Journal of Environmental Science and Technology.

Other peer-rewied papers

Kupková L, M Potůčková, K Zachová, Z Lhotáková, V Kopačková & J Albrechtová, (2012): Chlorophyll determination in Silver Birch and Scots Pine foliage from heavy metal polluted regions using spectral reflectance data. EARSeL eProceedings, 11(1): 64-73.

Kopačková, V., Rapprich, V., Zelenková, K., Šebesta, J.: Slope dependent morphometric analysis as a tool contributing to reconstruction of volcano evolution, (2011): In Dar I.A: Earth and Environmental Sciences, s. 220-240. – InTech Open Access, ISBN 978-953-307-468-9.

Kopačková, V., Rajchl, M. , Harbula, J. , Laufek, F. , Nývlt, D. , Hroch, T. , Hanuš, J. (2010): Detection of ENSO-induced changes based on analyses of multitemporal earth observation data: a study from NW Peru. PHOTO-INTERPRÉTATION EUROPEAN JOURNAL OF APPLIED REMOTE SENSING, 2, 64-78, 95-101.

Matějíček, L., Kopačková, V. (2010): Changes in Croplands as a Result of Large Scale Mining and the Associated Impact on Food Security Studied Using Time-Series Landsat Images. Remote Sensing 2, 6, 1463-1480. ISSN 1424-8220. DOI 10.3390/rs2061463.

Rapprich, V., Erban, V., Fárová, K., Kopačková, V., Bellon, H. , Hernández, W. (2010): Volcanic history of the Conchagua Peninsula (eastern El Salvador). Journal of Geosciences 55, 2, 95-112. ISSN 1802-6222. DOI: 10.3190/jgeosci.069.

Peer-rewied proceedings

Kopačková, V., Chevrel, S., Bourguignon, A., (2011): "Spectroscopy as a tool for geochemical modeling" in Earth Resources and Environmental Remote Sensing/GIS Applications II, edited by Ulrich Michel, Daniel L. Civco, Proceedings of SPIE Vol. 8181 (SPIE, Bellingham, WA 2011) 818106, DOI:10.1117/12.898404.

Harbula, J., Kopačková, V., (2011): "Air pollution detection using MODIS data" in Earth Resources and Environmental Remote Sensing/GIS Applications II, edited by Ulrich Michel, Daniel L. Civco, Proceedings of SPIE Vol. 8181 (SPIE, Bellingham, WA 2011) 81811E, DOI:10.1117/12.898107.

Kopačková, V. , Bourguignon, A., Chevrel, S., Koubová, M., Rojík, P., (2009): Effect of mineralogical and geochemical properties on reflectance properties of waste from Sokolov open pit lignite mine, Czech Republic, Mine Closure 2009 - A.B. Fourie, M. Tibbett (eds), Australian Centre for Geomechanics, Perth, pp 569-580, ISBN: 978-0-9804185-9-0.

Chevrel, S., Kopačková, V., Bourguignon,A., Rojík, P., Metelka, V., (2008): Monitoring Hazardous Wastes Using Space-borne and Ground-based Spectroradiometry - Sokolov Lignite Mines : Czech Republic, Mine Closure 2008, proceedings 3rd International Seminar on Mine Closure, 14-18 October 2008, Johannesburg, South Africa, Fourrier A., Tibbet M., Weiersbye I., Dye P. Eds, Australian Centre for Geomatics, Perth, pp 651- 662, ISBN: 978-0-9804185-6-9.

Selected presentations at international conferences

Veronika KOPAČKOVÁ, Daniel NÝVLT and Michal RAJCHL, (2012): Utilization of ASTER VIS/SWIR/TIR time series data for mapping dynamics of desert sediments, 34th International Geological Congress, Brisbane, Australia, 5-10 August, 2012.

Veronika KOPAČKOVÁ, Jan MIŠUREC, Kateřina ZELENKOVÁ, Stephane CHEVREL, Anne BOURGUIGNON, Anna BROOK, Eyal BEN-DOR, Christoph EHRLER, Christian FISCHER (2012): Application of mineral and image-based spectroscopy to mapping surface pH at open pit lignite mines: Multi-temporal approach, 34th International Geological Congress, Brisbane, Australia, 5-10 August, 2012.

Veronika Kopačková, Stéphane Chevrel, Anne Bourguignon (2012): MAPPING HAZARDOUS LOW-PH MATERIAL IN MINING ENVIRONMENT: MULTISPECTRAL AND HYPERSPECTRAL APROACHES. IEEE International Geoscience and Remote Sensing Symposium "Remote Sensing for a Dynamic Earth", IGARSS 2012 proceedings, 2695-2698, ISBN: 978-1-4673-1159-5.

Lucie Kupková, Markéta Potůčková, Michaela Buřičová, Veronika Kopačková, Zuzana Lhotáková, Jana Albrechtová (2012): DETERMINATION OF LIGNIN CONTENT IN NORWAY SPRUCE FOLIAGE USING NIR SPECTROSCOPY AND HYPERSPECTRAL DATA. IGARSS 2012 proceedings, 4190-4193, ISBN: 978-1-4673-1159-5.

Veronika Kopačková, Jan Franěk, Kryštof Verner, Karel Martínek, Michal Tesař, (2011): Structural approach combining ALOS PALSAR linear feature extraction with field structural and geophysical investigations, Geological Remote Sensing Group Workshop: Advances in Geological Remote Sensing (Including the Oil and Gas Earth Observation Group Workshop), 7-9 December 2011, ESA/ESRIN, Frascati, Italy.

Mišurec J., Kopačková V., Lhotáková Z., Albrechtová J., Hanuš J., Weyermann J. (2011): A comparison of different approaches to empirical modeling for retrieval of leaf pigments content of Norway spruce canopies from HyMap airborne hyperspectral image data. 1st Workshop on Forestry, Abstract book,2nd-3rd June 2011, Prague, Czech Republic, s. 8-9. European Association of Remote Sensing Laboratories.

Mišurec J., Kopačková V., Lhotáková Z., Albrechtová J., Hanuš J. (2011): Estimation of biochemical and geochemical variables in Norway spruce forest stands from hyperspectral image data. 7th EARSeL Workshop of the Special Interest Group in Imaging Spectroscopy, 11th - 13th April 2011, University of Edinburgh, Scotland, UK, s. 71. European Associtation of Remote Sensing Laboratories. Edinburgh, United Kingdom.

Veronika Kopačková, Stephane Chevrel, Anna Burginon, Petr Rojík, (2011): Quantitative determination of selected geochemical variables from hyperspectal data: a case study from Sokolov open pit lignite mine. 4th EARSeL SIG Workshop on Land Use Land Cover, Prague. June 01-03, 2011.

V. Kopačková, S. Chevrel, A. Bourguignon (2011): EFFECTS OF HEAVY METAL ABUNDANCE AND SPECIATION ON REFLECTANCE PROPERTIES OF POLY-PHASE MATERIAL OF WASTE ROCK DUMPS, 7 th EARSeL Workshop of the Special Interest Group in Imaging Spectroscopy 11 th to 13 th April 2011 University of Edinburgh, Scotland, UK

Kopačková, V. , Albrechtová, J. , Lhotáková, Z. , Hanuš, J. , Malenovský, Z. , Jung, A. , Glasser, C. , Chevrel, S. , Burginon, A. , Salbach, C. (2010): HYPSO (HYPERSPECTRAL SOKOLOV): A MULTIDISCIPLINARY HYPERSPECTRAL PROJECT ASSESSING MINING RELATED IMPACTS BY MEANS OF IMAGE SPECTROSCOPY. In Lacoste-Francis H.: Proceedings of Hyperspectral 2010 Workshop, svazek SP-683. s. 1-7. ESA Communications, ESTEC. Noordwijk. ISBN 978-92-9221-247-6.

Nývlt D., Kopačková V., Láska K. and Engel Z. (2010): Recent changes detected on two glaciers at the northern part of James Ross Island, Antarctica, Geophysical Research Abstracts, Vol. 12, EGU2010-8102, 2010.

Nývlt, D., Láska, K., Kopačková, V., Engel, Z. (2009): Glacio-meteorological measurements on two glaciers at the northern part of James Ross Island, Antarctica. In Barták, M., Hájek, J., Váczi, P.: Structure and function of Antarctic Terrestrial Ecosystems. Oct. 22-23, Book of Abstracts and Contributed Papers, s. 7-8. Masarykova Univerzita, Brno. Brno. ISBN 978-80-210-4987-1.

Kopačková, V., Chevrel, S., Bourguignon, A., Rajch, M., (2008): Spectral mineral mapping utilizing high altitude and ground-based spectroradiometry: Case studies from Sokolov open-pit mine, Czech Republic, and Sechura desert, Peru, 33rd International Geological congress, Oslo, August 6-14, 2008, presentation at session: GTR-04 Hyperspectral remote sensing and image spectroscopy, CD-ROM

Kopačková, V., Rajchl, M., Nývlt, D., Šebesta, J., Hroch, T., Vít,. J., (2008): Detection of changes in the Chira and Piura lower - catchment's areas, Sechura desert - Peru, based on spatial and spectral analyses of multitemporal Earth observation data. Geological mapping using satellite techniques, 33rd IGC Congress in Oslo 6. August 2008, CD-ROM

Bourguignon, A., Chevrel, S., Kopačková, V., (2008): Utilisation couplée d'ENVI et d'ArcMap pour l'évaluation de l'impact environnemental des mines de lignite de Sokolov (République Tcheque), SIG2008, Conférence francophone ESRI, Versailles, 1-2 octobre 2008, CD-ROM

Rajchl, M. , Nývlt, D., Kopačková, V. , Šebesta, J. , Vít, J. , Hroch, T. (2008): GEOMORPHOLOGICAL EVOLUTION OF THE PIURA RIVER FLUVIAL FAN, NORTHERN PERU, PRELIMINARY STUDY. Abstract Volume, XIII Latin-American Geological Congress, XIV Peruvian Geological Congress.

Chevrel, S., Kopačková, V., Bourguignon, A., Rojík, P., Metelka, V., (2008): Application of high altitude and ground-based spectroradiometry in the monitoring of hazardous waste derived from Sokolov open-pit mine, proceedings 10th International Mine Water Association congress, Karlovy Vary, June 2- 5, 2008, Rapantova N & Hrkal Z. Eds, Technical University of Ostrava publisher, pp 371 – 374

Kopačková, V., Rambousek, P., (2007): Mining remote sensing and its role in implementation of Czech and EU directives - a case study for Sokolov open pit mine. Extractive Industry and the Environment in the Central Europe EIECE 2007 - Conference Proceedings, pp. 1-5. ISSN 1802-5870.

Kopačková, V. - Nývlt, D. - Šebesta, J. (2006): Building the Information System of Geohazards in Peru. In ESRI, Redlands: ESRI Map Book, pp. 76. ESRI PRESS. USA, California. ISBN 1-58948-133-X.

Text books, teaching courses

Martínek, K. - Kopačková, V. - Štych, P. - Bravený, L. (2007): "GIS a DPZ pro geology/GIS and Remote Sensing for geologist" 150 s/150 p. Czech Space Office, o. p. s.. Kateřinská 10, 128 00 Prague 2.

Kopačková, V., (2008): Statistical landslide susceptibility zonation - a case study in the northern part of El Salvador: In Van Westen, C. et al.: Curso sobre Alertamiento y Evaluación de Riesgos por Deslizamientos en Centro América. Antigua, Guatemala, 2. - 6. 6. 2008, CD-ROM. ITC, Holland.